Characterization of ammonium minerals in the alteration halos of the Favona, Martha, and Wharekirauponga (WKP) low sulfidation epithermal gold-silver deposits in New Zealand

Nikolas Kristoffersen

Thesis submitted to the University of Ottawa
in partial fulfillment of the requirements for
Master of Science Earth Sciences

Department of Earth and Environmental Science
University of Ottawa

uOttawa

Acknowledgments

I would like to take a moment to show my appreciation for all those who have been there to help throughout this project. First, I would like to thank Keiko Hattori for all her hard work guiding me through this research as well as all the knowledge I have gained from her guidance as a thesis supervisor and a professor. I could not be at this moment today with her and all that I have learned from my professors at the University of Ottawa who have looked out for and guided me throughout my university career. I would also like to thank all my friends and peers who have worked together to ensure school was the perfect place to learn while enjoying my time spent here.

This project was made possible by Shannon Richards and Lorrance Torckler at OceanaGold who allowed us to conduct this research as well as all of those who aided in collecting samples. A special thank you to Mark Simpson from GNS Science, Wairakei who not only provided samples and data but guidance throughout the project. This project would not be possible without him.

I would also like to thank all the technicians at the University of Ottawa who aided with sample preparation and analysis throughout this project. I would like to thank Alain Mauviel for all his help with thin section preparation and rock sample preparation. Paul Middlestead and the rest of the technicians at the Ján Veizer Stable Isotope Laboratory for their help acquiring ammonium contents and nitrogen isotope data. Glenn Poirier for his assistance with the SEM-EDS. Jeffrey Ovens for his help with the XRD at the uOttawa X-Ray Laboratories. Nimal De Silva and Smita Mohanty for their help with ICP-ES / MS at the uOttawa Geochemistry Laboratory. Finally, I would like to thank Jeffrey Hedenquist for his input and feedback throughout the project.

Abstract

Ammonium has been detected in and around several epithermal Au-Ag deposits, including those in Nevada, Japan, Argentina, Mexico, and New Zealand, using short-wave infrared (SWIR) reflectance spectroscopy. This study examined the distribution and occurrence of ammonium in three epithermal low-sulfidation vein-type deposits in the Hauraki goldfield of New Zealand: Martha (>6.7Moz Au, >42.1Moz Ag), Favona (>0.6Moz Au, >2.36Moz Ag), and the recently discovered Wharekirauponga (WKP; 0.42Moz Au, 0.8Moz Ag) deposit. The Martha and Favona auriferous quartz-adularia veins are hosted by late Miocene to Pliocene andesite, whereas auriferous veins at WKP are hosted by late Miocene to Pliocene rhyolite. The wallrock of all three deposits is altered to form quartz, illite, smectite, adularia, chlorite, and pyrite +/- kaolinite. Ammonium contents are enriched (>137 ppm) in wallrock samples from all three deposits and low (<94 ppm) in vein samples. Ammonium contents are higher at Favona (<10,675 ppm) than at Martha (<192 ppm) and WKP (<2,783 ppm). Leaching experiments using a 2N KCl solution show that most ammonium is in mineral structures (>90% at Favona, >80% at Martha, >70% at WKP). There is a positive correlation of ammonium contents with LOI (0.6 – 16.3 wt%) and with K_2O (1.3 – 8.0 wt%) in all samples which suggest a hydrous potassium mineral as the major host of the ammonium. This is supported by the SWIR data obtained by previous workers of these samples where they show an absorption at ~1410 nm due to OH. At Favona, samples with high ammonium (>990 ppm) are reported to have significant absorption at ~2000 nm and ~2100 nm in the SWIR spectra likely due to ammonium. High ammonium contents (990 – 10,675 ppm) are found in rocks less than ~100m from the Favona vein which occur within an ammonium-bearing zone identified by previous workers based on SWIR. Samples outside of this zone contain low ammonium (107 – 301 ppm) with the smectite altered samples being the lowest. Ammonium contents within the hangingwall (1,827 – 10,675 ppm) of the Favona vein tend to be higher than in the footwall (990 – 4,301 ppm) and are highest within the most intensely illite altered rocks. At WKP, the intensely adularia +/- minor illite altered samples within 100m of the main East-Graben (EG) vein contain low ammonium (<200 ppm). The intensely illite altered samples away from the EG vein (>100m) have higher ammonium contents (200 – 800 ppm). This relationship of high ammonium contents to high illite abundance confirms illite as the major host of ammonium in these deposits. $\delta^{15}N$ values for all samples (n=54) including near and far from auriferous veins range from +0.5 to +7.9 ‰, suggesting the derivation of most of the ammonium from the Jurassic greywacke basement or sediments intercalated within the volcanic rocks.

Résumé

L'ammonium a été détecté dans et autour de plusieurs gisements épithermaux Au-Ag, y compris ceux du Nevada, du Japon, de l'Argentine, du Mexique et de la Nouvelle-Zélande, en utilisant la spectroscopie de réflectance infrarouge à ondes courtes (SWIR). Cette étude a examiné la distribution et la présence d'ammonium dans trois gisements épithermiques de type filonien à faible sulfuration dans le champ aurifère de Hauraki en Nouvelle-Zélande: Martha (>6.7Moz Au, >42.1Moz Ag), Favona (>0.6Moz Au, >2.36Moz Ag), et le gisement récemment découvert de Wharekirauponga (WKP; 0.42Moz Au, 0.8Moz Ag). Les veines de quartz-adularia aurifères de Martha et Favona sont encaissées dans une andésite de la fin du Miocène au Pliocène, tandis que les veines aurifères de WKP sont encaissées dans une rhyolite de la fin du Miocène au Pliocène. Les parois rocheuses des trois gisements sont altérées en quartz, illite, smectite, adulaire, chlorite et pyrite. Les teneurs en ammonium sont enrichies (>137 ppm) dans les échantillons de roche de paroi des trois gisements et faibles (<94 ppm) dans les échantillons de veine. Les teneurs en ammonium sont plus élevées à Favona (<10 675 ppm) qu'à Martha (<192 ppm) et WKP (<2 783 ppm). Les expériences de lixiviation utilisant une solution de KCl 2N montrent que la plupart de l'ammonium se trouve dans les structures minérales (>90% à Favona, >80% à Martha, >70% à WKP). Il existe une corrélation positive entre la teneur en ammonium et le LOI (0,6 - 16,3 % en poids) et le K2O (1,3 - 8,0 % en poids) dans tous les échantillons, ce qui suggère qu'un minéral potassique hydraté est le principal hôte de l'ammonium. Ceci est confirmé par les données SWIR obtenues par des chercheurs précédents sur ces échantillons, qui montrent une absorption à ~1410 nm due à OH. À Favona, les échantillons à forte teneur en ammonium (>990 ppm) présentent une absorption significative à ~2000 nm et ~2100 nm dans le spectre SWIR, probablement due à l'ammonium. On trouve des teneurs élevées en ammonium (990 - 10 675 ppm) dans des roches situées à moins de 100 m du filon de Favona, à l'intérieur d'une zone d'ammonium identifiée par les chercheurs précédents sur la base du SWIR. Les échantillons situés en dehors de cette zone contiennent peu d'ammonium (107 - 301 ppm), les échantillons altérés par la smectite étant les plus pauvres. Les teneurs en ammonium dans l'éponte supérieure (1 827 - 10 675 ppm) du filon de Favona ont tendance à être plus élevées que dans l'éponte inférieure (990 - 4 301 ppm) et sont plus élevées dans les roches les plus intensément altérées par l'illite. A WKP, les échantillons intensément altérés en adulaire +/- illite mineure dans un rayon de 100m de la veine principale East-Graben (EG) contiennent peu d'ammonium (<200 ppm). Les échantillons intensément altérés par l'illite et éloignés de la veine EG (>100m) ont des teneurs en ammonium plus élevées (200 - 800 ppm). Cette relation entre les teneurs élevées en ammonium et la forte abondance d'illite confirme que l'illite est le principal hôte de l'ammonium dans ces gisements. Les valeurs de δ15N pour tous les échantillons (n=54), y compris ceux situés à proximité et loin des veines aurifères, varient de +0,5 à +7,9 ‰, ce qui suggère que la plupart de l'ammonium provient du socle de grauwacke du Jurassique ou de sédiments intercalés dans les roches volcaniques.

Table of Contents

List of Figures

List of Tables

Chapter 1 | Introduction

1.1 Preamble

Since the discovery of buddingtonite by Erd et al., 1964 ammonium (NH_4^+) minerals have been discovered in a variety of hydrothermal / geothermal environments. Ammonium minerals such as buddingtonite ($NH_4Al_3SiO_8$ an ammonium feldspar) or tobelite ($[NH_4,K]Al_2[AlSi_3O_{10}][OH]_2$ an ammonium mica; Higashi 1982) have been reported based on spectroscopic data within the alteration haloes of low sulfidation epithermal deposits around the world (Figure 1; e.g., Favona, New Zealand (Simpson, 2015), Esquel, Argentina (Soechting et al., 2008)). The NH_4^+ molecule substitutes for the K^+ cation in the crystal lattice of minerals such as adularia (Erd et al., 1964) and illite (Ruiz Cruz and Sanz de Galdeano, 2009). NH_4^+ is commonly detected by short-wave infrared (SWIR) spectrometry during mapping of the alteration halos of these epithermal systems. Ammonium detected in SWIR has been shown to have potential to aid in the discovery of mineralization by narrowing the alteration footprint in epithermal vein systems (Simpson & Mauk, 2007). Ammonium can be detected using a handheld SWIR reflectance spectrometer (Felzer et al., 1964; Ridgway et al., 1991) on outcrop or in drill core or through airborne geophysical methods (Rowan et al., 2003). Ammonium minerals have been identified by SWIR reflectance spectroscopy at multiple deposits in the Hauraki goldfield e.g., Favona, Simpson (2015); Wharekirauponga (WKP), Simpson (2018). The discovery of ammonium minerals by Simpson (2015) at the Favona deposit in part prompted this thesis to better understand the occurrence of ammonium at Favona; comparing the results to deposits elsewhere in the Hauraki goldfield.

1.1.1 Objectives

This thesis aims to answer questions about ammonium-bearing minerals in the alteration halos of low sulfidation epithermal gold deposits. Firstly (1), what is the main mineral that hosts the ammonium? Second (2), why are ammonium minerals identified in some systems but not all? Third (3), how are ammonium minerals distributed around the mineralized Au-Ag veins? Four (4), what is the source of the ammonium? To answer these questions a study of the Martha, Favona, and Wharekirauponga (WKP) Au-Ag low sulfidation epithermal deposits in Hauraki goldfield of New Zealand has been undertaken.

Figure 1. *Map showing reported occurrences of ammonium minerals detected by reflectance spectroscopy in low sulfidation epithermal systems around the world. Esquel, Argentina (Soechting et al., 2008), Don Sixto, (Mugas Lobos et al., 2018), Chapi Chiara, Peru (Carrino et al., 2018), Banderas, Guatemala (Harlap, 2008), El Zapote, Mexico (Hattori et al., 2019), Acoculco, Mexico (Canet et al., 2015), Jerritt Canyon, USA (Mateer, 2010), Hollister, USA (Smith, 2014), Hakuryu & Hishikari, Japan (Kristoffersen, 2019), Leven Star, Australia (Travers & Wilson, 2015), Favona (Simpson, 2015).*

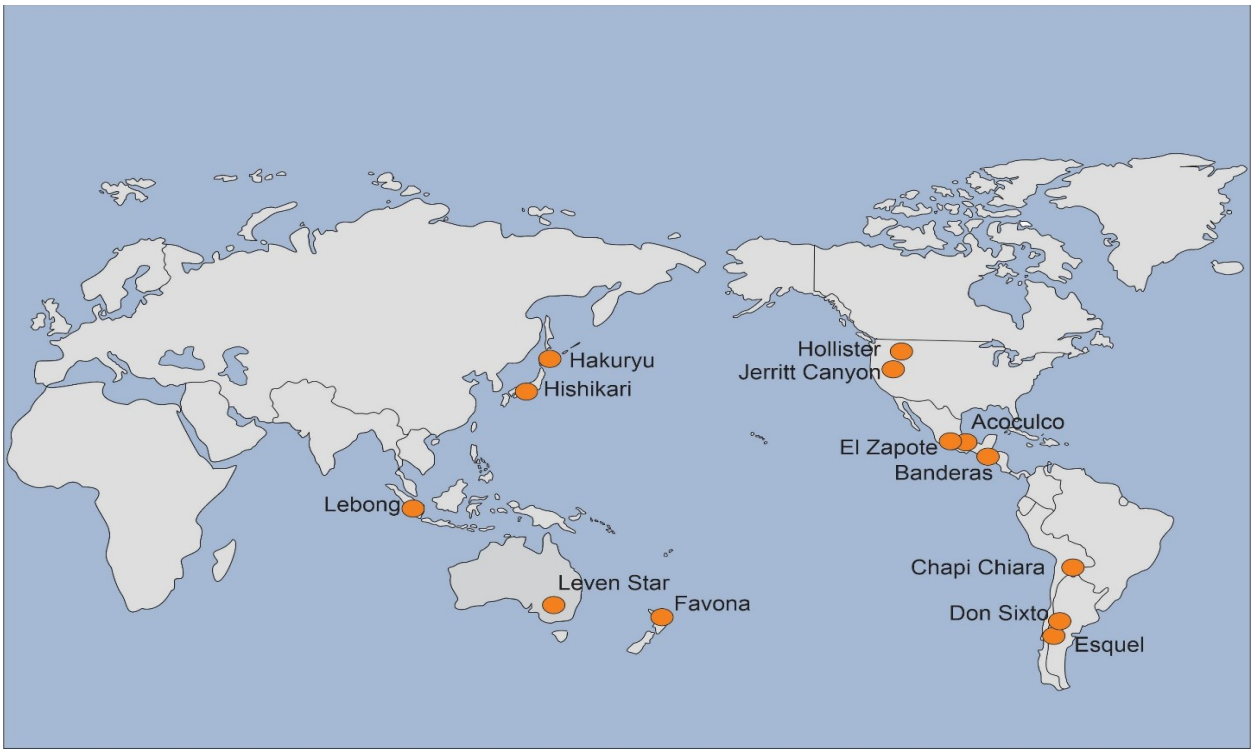

Figure 2. *Cross-section of the Favona deposit from Simpson & Mauk, 2007 and Simpson, 2015. Shows the distribution of illite, mixed layer illite-smectite, and smectite as well as a halo of ammonium (blue dashed line) surrounding the Favona vein identified by SWIR reflectance spectroscopy.*

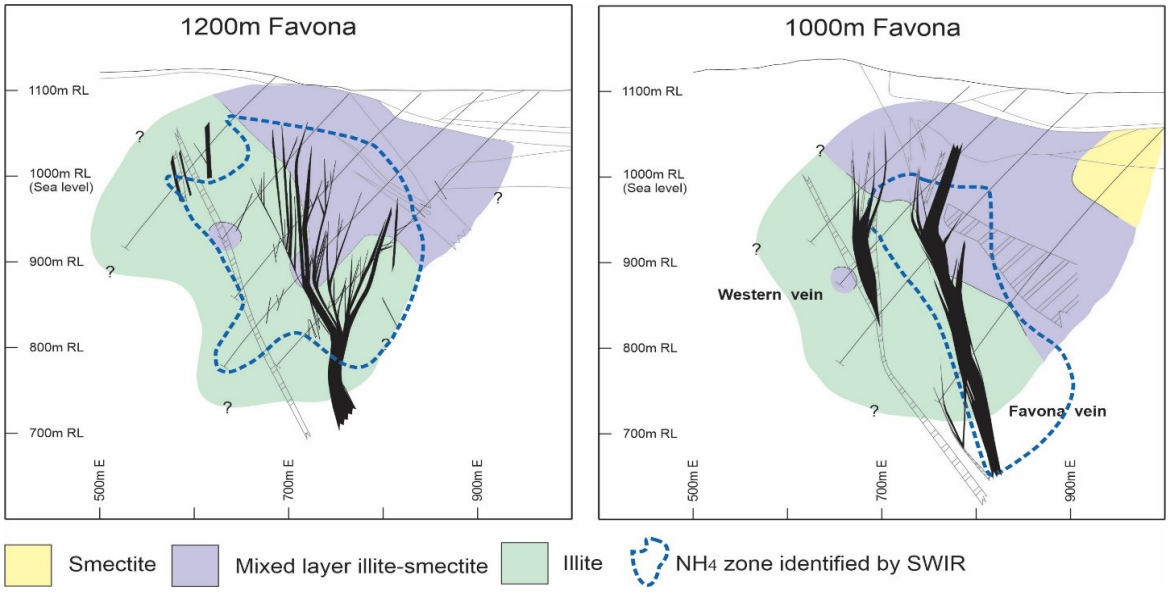

1.1.2 Area of Study

This study area was chosen because of the Hauraki goldfield's long history of low sulfidation epithermal Au-Ag mining and exploration. Favona represents a non-eroded low sulfidation epithermal vein system including the overlaying silica sinter and hydrothermal breccia pipe which will help to demonstrate the distribution of ammonium around a complete vertical section of the deposit. Furthermore, ammonium minerals have been found at the Favona deposit (Simpson, 2015) but have never been reported at Martha. This comparison provides an opportunity to evaluate the causes why ammonium minerals are not found in all deposits. Next, the comparison of Favona and Martha with WKP offers the opportunity to evaluate the influence of host rock composition on the formation of ammonium minerals as the latter is hosted in predominately rhyolitic rocks and the former two are hosted in andesitic rock.

This research measured ammonium content of bulk rock samples. The data will be used alongside petrographic and geochemical analysis such as thin section microscopy, X-Ray diffraction, and nitrogen isotope compositions to answer the above questions and form a better understanding of ammonium minerals associated with low sulfidation epithermal gold deposits.

1.2 Related Previous Work

The author examined ammonium contents in and around several low sulfidation epithermal deposits such as Hishikari, Fuke, and Kago in Japan as his BSc Honour's thesis (Kristoffersen, 2019).

In New Zealand in 2007, Mark Simpson and Jeffrey Mauk characterized the hydrothermal alteration of the wallrock at the Favona deposit utilizing X-Ray diffraction (XRD). They identified varying distributions of adularia, illite, smectite, and chlorite. Illite was found to occur primarily within the footwall and mixed layer illite-smectite within the hanging wall of the Favona vein (Figure 2). Within the mixed layer illite-smectite zone, they showed the ratio of illite to smectite to gradually become more smectite rich towards the surface away from the Favona vein. Chlorite was shown to be restricted primarily to the footwall. Adularia is common throughout. SWIR reflectance data on their samples was presented by Mark Simpson in 2015 at the AusIMM New Zealand Branch Annual Conference where he identified a 50 - 100m halo of ammonium minerals surrounding the Favona vein (Figure 2). Mark Simpson also presented a SWIR reflectance study of the Wharekirauponga (WKP) deposit at the AusIMM New Zealand Branch Annual Conference in 2018. He identified widespread occurrences of illite and significant kaolinite as well as ammonium illite and buddingtonite. Some of the samples from these studies were examined in this thesis.

1.3 Contributions of the Author

This thesis cumulates the original research completed by Nikolas Kristoffersen from 2019 - 2022 under the supervision of Dr. Keiko Hattori at the University of Ottawa. The following outlines the contributions of the author:

1. Wrote all chapters and produced all figures and tables.
2. Collected WKP and Martha core samples were collected at the OceanaGold office in Waihi with Dr. Keiko Hattori
3. Conducted cobaltinitrite staining of thin section cut-offs.
4. Pulverized samples at the University of Ottawa.
5. Measured loss on ignition at the University of Ottawa.
6. Conducted thin section and hand sample petrography
7. Did leaching of ammonium using potassium chloride
8. Weighed samples for ammonium content analysis and nitrogen isotope analysis. Analysis was completed by Paul Middlestead at the Jan Veizer lab.
9. Conducted SEM-EDS at the University of Ottawa with the assistance of Glenn Poirier.
10. Powdered samples for XRD of Martha and WKP samples. XRD was completed at the University of Ottawa X-Ray lab with help of Jeffrey Ovens.
11. Packing samples to ship to ActLabs for major and trace element data

Several aspects of the data written in this thesis have been reported as conference abstracts and presented orally. All abstracts are in Appendix E.

1. Kristoffersen, N.K., Hattori, K., Simpson, M.P. (2021). Ammonium Minerals in the Alteration Halos of Epithermal Gold-Silver Deposits in the Hauraki Goldfield, New Zealand. Geological Society of America Abstracts with Programs. Vol 53, No. 6, 2021.

2. Kristoffersen, N.K., Hattori, K., Simpson, M.P. (2022). Ammonium associated with the Favona epithermal gold deposit in the Coromandel peninsula, New Zealand: its distribution and source. Society of Geology Applied to Mineral Deposits 16th Biennial Meeting Rotorua.

Chapter 2 | Geological Setting of the Study Area

2.1 Regional Geology

The Hauraki goldfield is a district rich in low sulfidation epithermal gold-silver deposits in the Coromandel peninsula (Figure 3). It is comprised of a sequence of Miocene to Pliocene subaerial volcanic rocks of Coromandel Volcanic Zone (CVZ) overlying a late Jurassic graywacke basement. The CVZ is bordered to the south by the Taupo Volcanic Zone (TPZ) and to the west by the Hauraki graben. The Quaternary volcanic rocks of the TPZ overly those of the CVZ to the south. To the west, the 1-2Ma sediments within the Hauraki graben overlie the volcanic rocks of the CVZ. Faulting occurs throughout the CVZ commonly propagating from the Hauraki graben (Christie et al., 2007).

The CVZ is composed of two main phases of volcanism. The Coromandel group andesites and dacites (18 - 3Ma) make up a majority (61%) of the exposed rock on the peninsula whereas 30% of the coverage is composed of the Whitianga group rhyolites and rhyodacites (9 - 6Ma). The remaining exposures are a very small amount of basalts of the Kerikeri group and minor exposed Jurassic greywacke basement to the north (Figure 3b; Christie et al., 2007). This exposure of the basement rock in the north is due to a gradual tilt of the graywacke basement dipping to the south. Volcanism progressed from north to south resulting in a southern younging of the sequence. Therefore, there is a gradual thickening of the volcanic sequence to the south overlying the tilted Jurassic basement (Skinner, 1986).

The Coromandel group is composed of calc-alkaline, medium K, andesites and dacites which are subdivided into five subgroups separated by periods of quiescence. Pyroxene andesites make up most of the Coromandel group but some subgroups contain hornblende-pyroxene andesite to dacites. The Whitianga group is primarily found along the central and eastern portion of the CVZ and is composed of primarily calc-alkaline to alkaline felsic lavas and volcaniclastics that are associated with flow-domes and caldera complexes. Throughout the northern and central parts of the peninsula there are local porphyritic andesite dikes, stocks, and plugs. Minor quartz diorite to granodiorite plutons are also found locally. These intrude the Jurassic basement occasionally extending into the overlying volcanic rocks (Christie et al., 2007). Throughout the CVZ are numerous north-northwest and north-northeast faults; a few of which transect the entire Coromandel peninsula. Many faults in the overlying volcanic rocks are believed to be the result of reactivation of block faulting in the greywacke basement (Skinner, 1995). Some faults are however related to the Hauraki graben to the west (Gadsby et al, 1990).

Figure 3. *A). Map of the Coromandel peninsula showing zones of hydrothermal alteration as well as epithermal veins. Shows the location of the Martha, Favona, and WKP deposits. B) Geology map of the coromandel peninsula. Shows location of the Waihi district (Martha-Favona) which is hosted in andesite as well as WKP which is hosted in rhyolite. Modified from Simpson & Christie, 2019.*

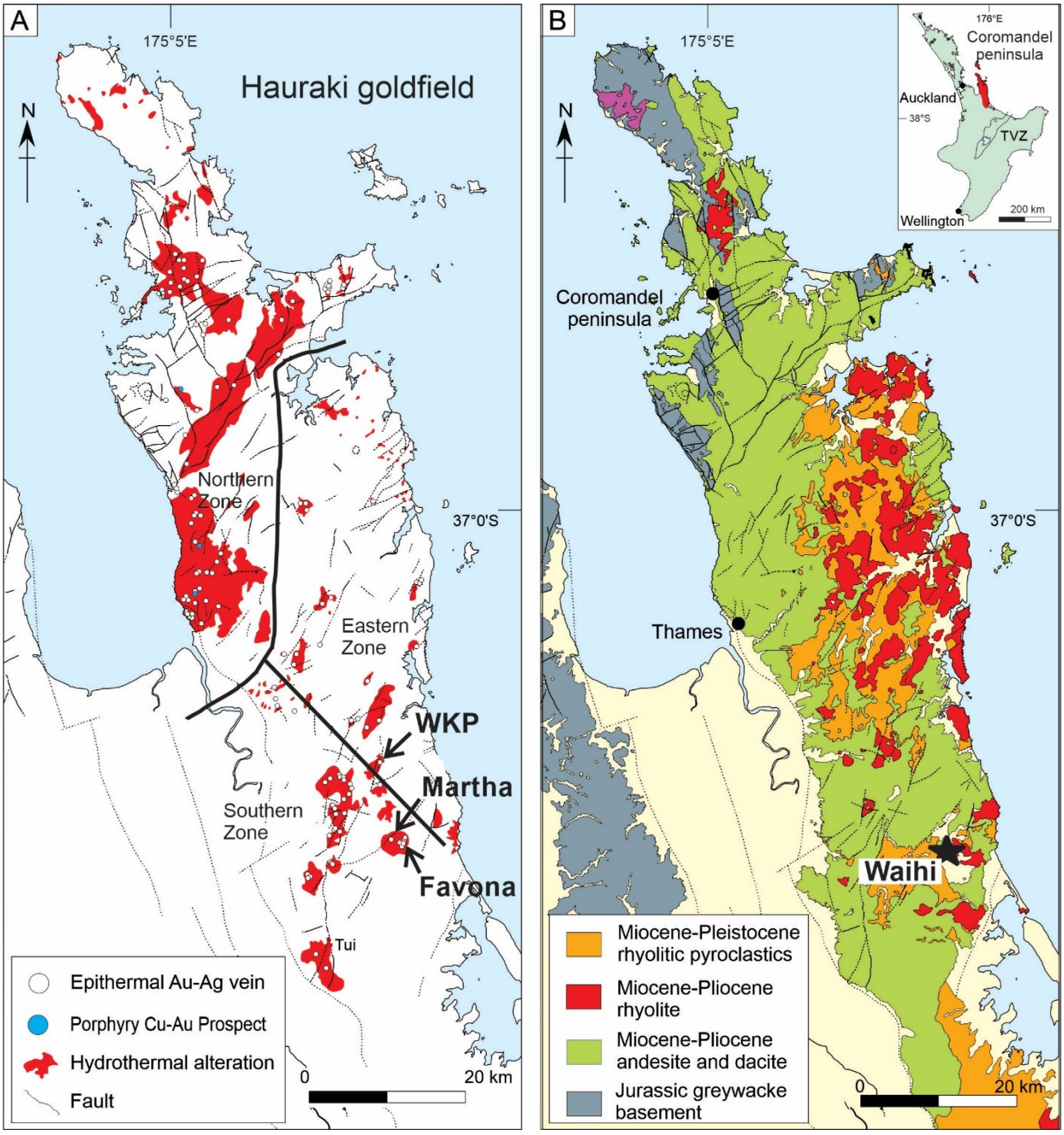

2.1.1 Mineralization in the Hauraki goldfield

Low sulfidation epithermal quartz-adularia veining makes up most of the mineralization in the Hauraki goldfield. However, in the northern zone, there are small porphyry copper prospects associated with quartz diorite plutons (Figure 3a). Low sulfidation epithermal deposits consist of quartz +/- adularia, calcite, illite veins which fill high-angle fractures (Christie et al., 2007). Veins in the northern zone predominately strike north to north-northwest with ^{40}Ar-^{39}Ar mineralization ages of vein adularia ranging from 16.3Ma in the most northern tip of the peninsula to 11Ma in the mid-west (Christie et al., 2007). Veins in the southern zone, which includes the Martha and Favona veins, generally strike north-northeast and range in age from 7 - 6Ma having been formed during a period of strong regional extension (Mauk et al., 2006). This southern zone is by far the largest producer in the area and includes the world class Waihi mine.

2.2 Geology of the Studied Au-Ag deposits

2.2.1 Waihi (Martha & Favona)

The Waihi district consists of a network of auriferous quartz-adularia veins which occur over ~2km^2 area within a ~12km^2 demagnetized zone due to hydrothermal alteration (Figure 4a; Simpson & Christie, 2019). The district is divided into four main deposits: the Martha, Favona, Correnso, and Trio deposits with over a dozen auriferous veins between them (Figure 4). The Martha deposit was mined underground from 1883-1952 and open pit mined since 1988. Current drilling at Martha is focused on the remaining mineralization below the historic mine workings deemed the Martha Underground project. The Favona deposit is located about 2km east of the Martha deposit and saw underground mining from 2006-2013. The Trio and Correnso deposits are found between the Favona and Martha deposits, Trio being mined from 2012-2014 and Correnso from 2015 to 2020. Overall, the Waihi mine has produced over 8Moz of Au and 45.5Moz of Ag; the Martha deposit accounting for most of this production (Torckler et al, 2016).

Quartz-adularia veins are hosted by hydrothermally altered late Miocene plagioclase porphyritic pyroxene andesite flows of the Waipupu formation which is part of the Waiwawa subgroup of the Coromandel group. Unaltered Waipupu formation andesite is composed of phenocrysts of plagioclase, augite, hypersthene, and minor amphibole in trachytic groundmass of plagioclase, Fe-Ti oxides, and interstitial glass. The lower part of the sequence contains minor quartz phenocrysts (Brathwaite & McKay, 1989). Dacitic lithic / crystal tuff beds and thin carbonaceous lake beds are found intercalated within the andesite flows at multiple depths within the sequence (Brathwaite & Faure, 2002). Most

veins are hosted by the lower quartz andesite except the Favona and Moonlight veins which are hosted in the upper, quartz-poor, andesite (Figure 4b). The district is extensively covered by post-mineralization dacites and ignimbrites. The eastern part of the system, including parts of Favona, is covered by unaltered late Miocene to early Pliocene hornblende dacite of the Uretara formation. These units are buried by late Pliocene to Quaternary ignimbrites of the Owharoa and Waikino formations (Brathwaite & Christie, 1996). The ignimbrites cover most of the Waihi area, though a small outcropping of the Martha vein was visible at Martha Hill prior to being excavated.

Figure 4. *A) Map of Waihi showing the locations of the Martha and Favona deposits with veins projected to the surface. Both deposits are hosted within the Waipupu andesite and occur within the same demagnetized zone of hydrothermal alteration. B) Cross section of Waihi with locations of the Martha and Favona veins. Favona is hosted in the upper andesite and overlain by a hydrothermal breccia and silica sinter. Martha is hosted in the lower quartz andesite. Modified from Simpson & Mauk, 2007 and Maton et al., 2020.*

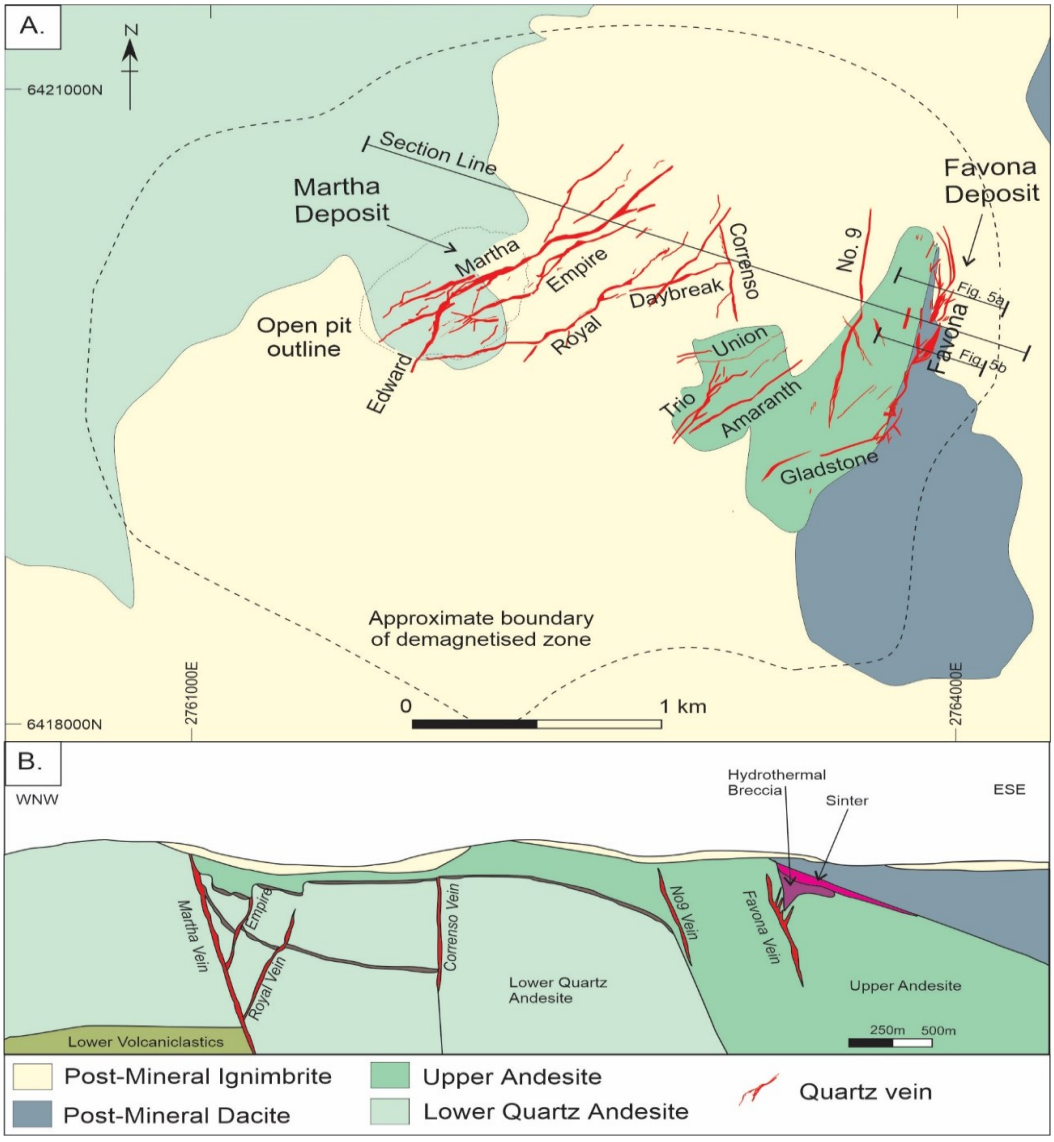

The Martha deposit consists of a complex braided network of large continuous auriferous quartz-adularia veins including the Martha, Welcome, Empire, Edward, and Royal veins which extend up to 1.6km along strike and are locally up to 50m wide and have been mined underground to a depth of 575m (Brathwaite & Faure, 2002). The western-most Martha vein dips southeast where it converges with the subparallel northwest striking Welcome, Empire, and Royal veins (Figure 4b). Vein textures consist of main stage microcrystalline quartz and adularia with late-stage amethyst. At shallow levels (above 1000m RL) colloform / crustiform microcrystalline quartz forms a major component of the veins. Adularia rich areas mainly occur in contact with the wallrock (Brathwaite & Faure, 2002). Very fine-grained electrum, acanthite, tetrahedrite, chalcopyrite, sphalerite, and pyrite occur associated with the colloform banding as well as bladed quartz after calcite (Figure 6b). Molybdenite occurs at deep portions of the northeastern periphery of the deposit. At increasing depths, mineralization becomes base metal rich and microcrystalline colloform quartz grades into crustiform comb quartz (Brathwaite & Faure, 2002). The vein adularia has been dated at 6.16 +/- 0.06Ma using $^{40}Ar/^{39}Ar$ dating (Mauk et al., 2011).

Hydrothermal wallrock alteration at Martha consists of a shallow smectite zone mainly above 1000m RL consisting of smectite with mixed layer smectite-chlorite completely replacing the groundmass (Brathwaite & Faure, 2002). Plagioclase phenocrysts are replaced by calcite and interlayered illite-smectite and the pyroxenes are partly altered to chlorite and calcite. At greater depth, the smectite zone grades into the mixed layer illite-smectite zone which contains higher amounts of illite to smectite interlayering around 80 - 90% (Brathwaite & Faure, 2002). The abundance of chlorite is higher in the groundmass and pyroxenes become completely altered to chlorite and calcite. Plagioclase phenocrysts are partly altered to an assemblage of adularia + illite +/- albite + calcite. The illite zone consists of intense alteration completely replacing all primary phases except quartz. Plagioclase phenocrysts are altered to adularia with minor albite which are variably overprinted by illite or calcite. Quartz and minor chlorite make up most of the groundmass. $^{40}Ar/^{39}Ar$ dates for adularia within the wallrock are 6.07 +/- 0.006 and 6.08 +/- 0.03 (Mauk et al., 2011).

The Favona deposit is located 2km east of Martha consisting of the eastern most set of veins including the Favona, Moonlight, Gladstone, Amaranth, and Western veins (Figure 4b). The Favona vein is the largest of the eastern set of veins with a strike length over 1km, 400m vertical extent, and is on average 1 - 3m wide. The vein primarily strikes northeast to north-northeast similar to the nearby veins with a subparallel shear zone in the footwall (Figures 7a & 7b) as well as in the hangingwall (Figure 7a). The Favona vein consists of the main east-dipping footwall vein with hangingwall vein splays. The vein

forms an upward widening horsetail structure (Rhys, 2008). Hangingwall splays are more abundant in the less steeply dipping sections (1200mN Figure 7b) than the less steeply dipping sections (100mN Figure 7a; Simpson & Mauk, 2007). At shallow levels the vein consists of colloform banded quartz with minor illite and adularia (Figure 6a). Very fine-grained metallic minerals compose <1% of the veins and consists of pyrite with minor galena, sphalerite, marcasite, electrum, naumannite, aguilarite, and tetrahedrite. Quartz after platy calcite occurs at intermediate levels. At deeper levels, the vein contains crystalline comb quartz with local chlorite bands and abundant base metal sulfide minerals (Simpson & Mauk, 2007). The Favona vein retains the entire vertical spectrum of one epithermal vein system which includes an overlying silica sinter and hydrothermal breccia. Vein adularia within the Favona vein has been dated at 6.05 +/- 0.04Ma using $^{40}Ar/^{39}Ar$ dating (Mauk et al., 2011).

The andesite which hosts the Favona deposit is intensely altered with 99-100% replacement of the primary minerals. All minerals except zircon and minor quartz have been replaced. Primary plagioclase phenocrysts have been completely replaced by adularia and white mica with rare calcite and/or albite. Chlorite and minor quartz typically replace the augite and hypersthene phenocrysts. Chlorite is restricted to the footwall of the Favona vein. Groundmass consists of a mixture of fine-grained quartz, white mica, and disseminated pyrite +/- chlorite. Adularia alteration is common in wallrock around the Favona vein and is variably overprinted by illite (Simpson & Mauk, 2007). Albite alteration is rare at Favona and only occurs within select samples primarily within the footwall. Calcite occurs at depth near the Cowshed and Amaranth veins but is nearly absent adjacent the Favona vein (Simpson & Mauk, 2007). Illite +/- mixed layer smectite occurs replacing 50 - 80% of the adularia altered plagioclase phenocrysts. Smectite grades into mixed layer illite-smectite to illite with depth and that mixed illite-smectite is generally restricted to the hanging wall of the Favona vein (Simpson & Mauk, 2007). $^{40}Ar/^{39}Ar$ age of wallrock containing adularia at Favona gives 6.07 +/- 0.02 and 6.01 +/- 0.07 (Mauk et al., 2011).

The age of the vein adularia at Martha (6.16 +/- 0.06 Ma; Mauk et al., 2011) based on $^{40}Ar/^{39}Ar$ dating overlaps within error of the age of the veining at the Favona deposit (6.05 +/- 0.08 Ma; Mauk et al., 2011). This indicates these two deposits formed around the same time about 6.1Ma (Mauk et al., 2011). Many believing the two deposits formed within the same hydrothermal system (Brathwaite & Faure, 2002; Simpson & Mauk, 2007) which resulted in the 10km^2 demagnetized zone of hydrothermal alteration observed surrounding the Waihi area (Figure 4a). Furthermore, there is a shallow southeast dip of the silica sinter at Favona which indicates that there is a post-mineralization tilting of the Waihi

area to the southeast (Figure 4b). The evidence suggests that the Martha deposit formed at deeper levels than the Favona deposit. This is consistent with the fluid inclusion data by Simpson and Mauk (2007) who suggested a difference of 220m in depth between the two deposits.

2.2.2 Wharekirauponga (WKP)

Wharekirauponga (WKP) is a prospect located approximately 10km north of the Waihi district (Figure 3) with a resource of 0.42Moz Au indicated and 0.72Moz Au inferred (Maton et al., 2020). The deposit includes three main N-NE trending quartz-adularia auriferous veins occurring within a 2km^2 intensely hydrothermally altered prospective area. This includes the East-Graben (EG), T-stream, and Western veins (Figure 5). The East-Graben vein is planned to be entering production.

Unlike most deposits in the Hauraki goldfields, quartz-adularia veins at WKP are hosted in flow banded rhyolite domes of the Maratoto formation (Figure 5b). Surrounding the rhyolite flow domes is a lithic lapilli tuff unit which is part of the Edmonds formation (Christie et al., 2006). This pyroclastic unit tends to be the host of the near surface discontinuous sheeted vein complexes (Figure 5b). Both units being exposed at the surface. The rhyolites overlie older dacitic and andesitic rocks of the Waipupu formation which is the host of the mineralization at Waihi. These units are tilted to the SE and overlain by post-mineralization Whakamoehau formation andesite flows (Rhys, 2019).

The flow banded rhyolites were originally interpreted to be part of a gently dipping flow and tuff sequence overlain by lapilli tuff of the Edmonds formation (Rabone et al., 1989). However, drilling suggests that the flow banded rhyolite is rather a series of rhyolite cryptodomes which intrude the Edmonds formation (Christie et al., 2006; Rhys, 2019). The lapilli tuff conforming to the shape of the domes and filling the intervening space between the domes (Rhys, 2019; Figure 5b).

The Maratoto rhyolite domes are flow banded near the edges becoming massive towards the center of the dome. The rhyolite tends to be cream to pale green with quartz phenocrysts and is commonly feldspar-phyric especially towards the center of the dome. Minor biotite and ilmenite are also found within the unaltered rhyolite domes. Brecciation of the rhyolite is common along flow dome margins. The Edmonds formation polylithic lapilli tuff unit is composed of 5 – 40% lapilli sized, subangular to round lithic fragments within a pale grey to green-grey ash matrix. The matrix contains biotite, quartz, and angular feldspar fragments (Ross, 2019). Lithic fragments consist of pale grey to cream rhyolite, quartz grains in an ash matrix, and a variety of andesite and mudstone fragments (Rhys,

2019). The matrix and many fragments tend to become green grey coloured near mineralized zones due to the adularia-illite-quartz +/- pyrite alteration (Ross, 2019).

***Figure 5**. A) Geology map of the WKP prospect with drill hole traces and veins projected to the surface. B) Cross-section of the south end of WKP intersecting the Western and EG veins. Modified from Rhys, 2019.*

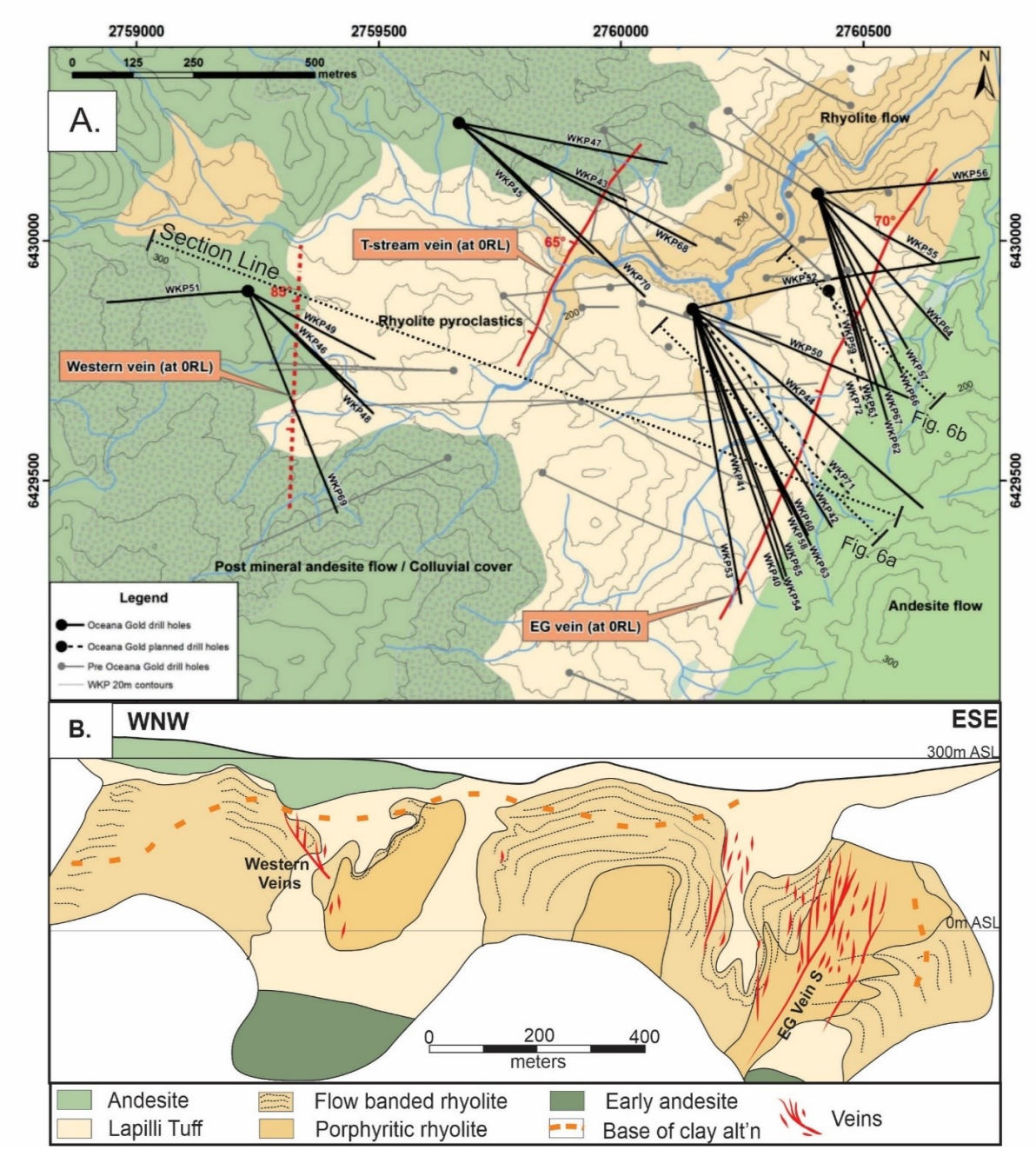

Hydrothermal alteration tends to form quartz and adularia with less common illite, mixed layer illite-smectite, chlorite, pyrite, halloysite, kaolinite, and albite. In the rhyolite flow domes, adularia alteration tends to be the most prominent especially near veins altering both the groundmass and the feldspar phenocrysts. The groundmass tends to also contain significant quartz and minor illite and/or chlorite. The quartz-adularia alteration tends to grade outwards into quartz-illite +/- smectite and halloysite alteration (Christie and Soong, 2001). This quartz-illite +/- smectite alteration being the most prominent in the shallow parts of the system away from the main mineralization. Illite is most prominent in these shallow zones though it locally forms as mixed layer illite-smectite. Albite is found in some drill holes and tends to occur solely in the southern part of the system. Alteration within the tuffs show similar styles and spatial variation as the rhyolite domes (Christie and Soong, 2001).

Mineralized quartz veins at WKP display characteristic low sulfidation epithermal characteristics such as quartz-adularia colloform/crustiform banding (Ross, 2019). The East-Graben vein is primarily composed of crustiform banded microcrystalline quartz intergrown with adularia. There is also significant development quartz replacing lattice bladed calcite (Figure 6c). The highest gold grades are within the areas of strong crustiform banding and abundant bladed calcite textures (Ross, 2019). Gold occurs as visible electrum with high silver content (40-60%) and is associated with Se and Sb bearing silver sulfosalts. The T-stream and Western veins are similar in character though are more faulted and more deeply eroded (Ross, 2019). Vein adularia at WKP has been dated using $^{40}Ar/^{39}Ar$ dating at ~6.3Ma (Mauk et al., 2011).

Figure 6. *Photographs of vein samples from Favona, Martha, & WKP. A) Favona vein sample showing colloform / crustiform quartz-adularia. B) Martha vein sample showing bladed calcite replaced by quartz. C) WKP vein sample showing crustiform quartz/adularia with possible bladed quartz / calcite.*

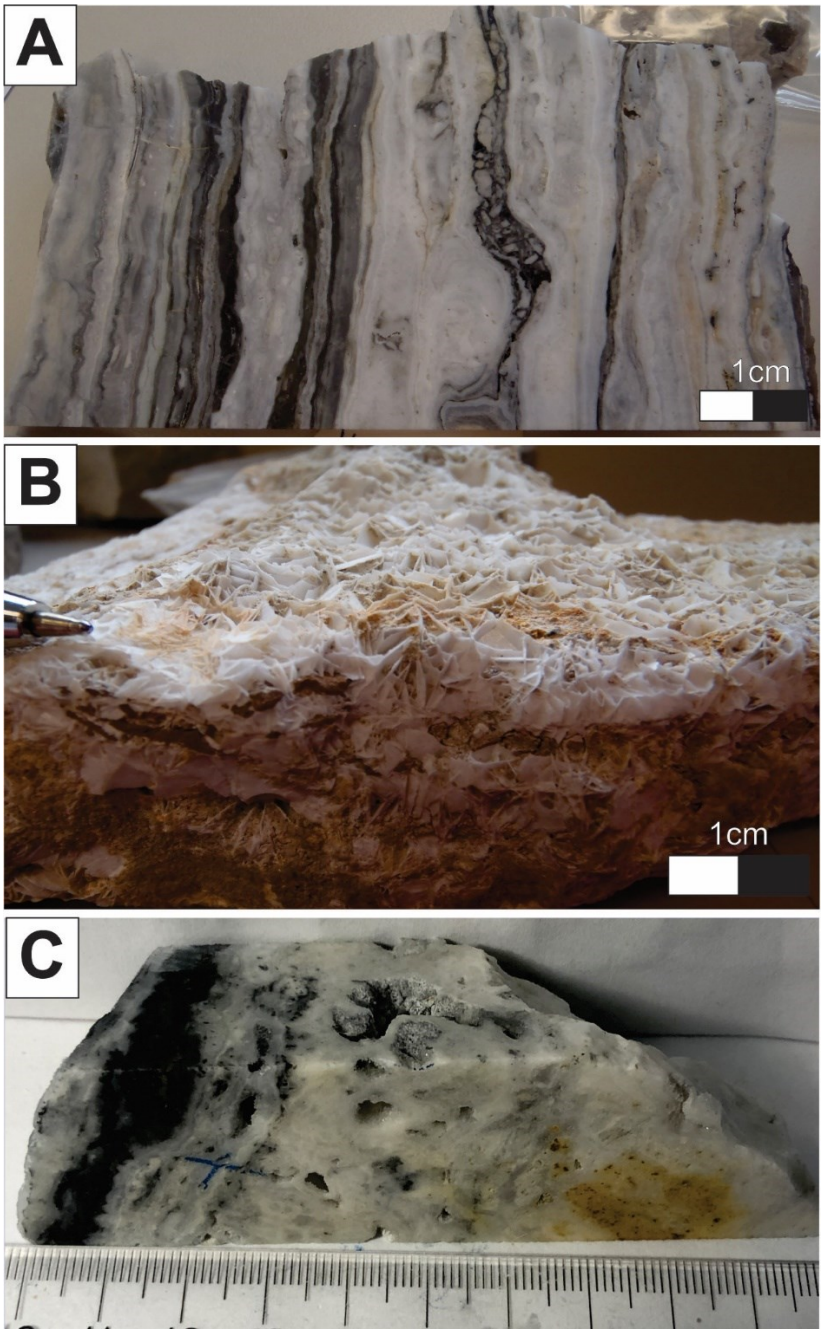

Chapter 3 | Sampling

3.1 Samples and Sample Locations

The Favona samples are part of the University of Auckland School of Environment collection. acquired for us by Mark Simpson in October 2019. Mark Simpson shipped 26 samples from diamond drill holes (DDH) 63, 87, and 104 analyzed and three underground vein samples to us in Ottawa (Figure 7). We collected the remaining samples at the GNS Science facility in Wairakei in February 2020 which consisted of 19 samples from DDH 69, 84, and 85. Most samples are ~3 cm long (half core of ~6cm diameter). These samples were analyzed using X-ray diffraction (XRD) in Simpson and Mauk (2007) and by short-wave infrared (SWIR) reflectance spectroscopy in Simpson (2015).

Martha samples include three samples collected by Devin N. Castendyke from the Martha open pit and ten drill core samples from the Martha Underground project. The open pit samples are from the specimen collection of the University of Auckland School of Environment initially studied by Castendyke et al. (2005). The samples were acquired from Mark Simpson along with the first batch of Favona samples in October 2019. The Martha Underground samples were collected by us at the OceanaGold core storage in Waihi in February 2020 from DDH 920SP4MR1460, 920SP8MR1496, and 800SP1MN1203. These samples are ~5 cm long quarter core offcuts (~6cm diameter core), six of which include veins and the remaining four being samples of wallrock.

Wharekirauponga (WKP) samples were collected at the OceanaGold core storage in Waihi, NZ and consist of 57 quarter core cuts (~6cm diameter core) and spectral chip samples from DDH 42, 44, 78, & 81 (Figure 8). Nineteen of which are core samples from DDH 42 & 81 with the remaining being chip samples. Chip samples are small ~3x3cm pieces originally chipped from core for SWIR analysis by OceanaGold. SWIR spectra for samples from DDH 42 were interpreted and are reported in Simpson (2018). All acquired samples are from diamond drill holes intersecting the East Graben (EG) vein and consist of wallrock and vein samples (Figure 8). In total 115 samples were collected from all three deposits for this study. A list of all samples is in Appendix A.

3.2 Strategy of Sampling

Samples were selected to provide a variety of rock types, mineralogy, alteration intensity, and textures at various depths and proximities to mineralization. A variety of representative samples were selected for laboratory analysis.

***Figure 7**. Cross sections of the Favona deposit at 1000mN and 1200mN showing the locations of samples used in this study. Modified from Simpson & Mauk, 2007.*

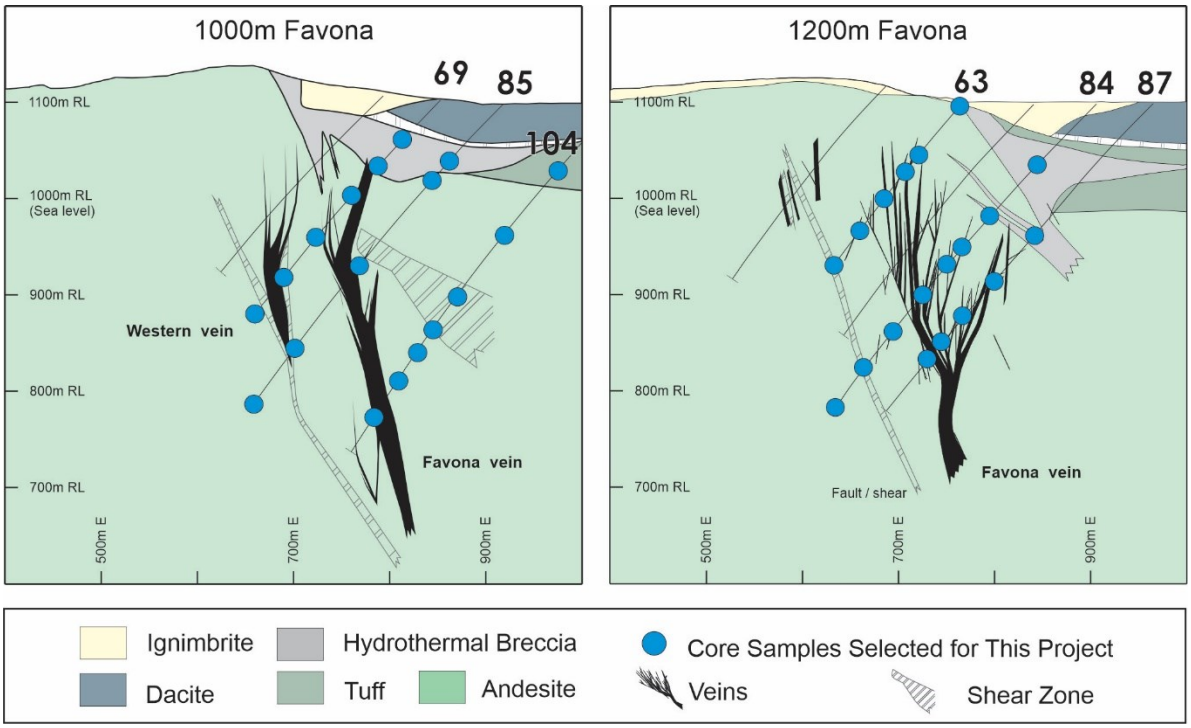

***Figure 8**. Cross-section of WKP EG vein south and north showing drill holes with sample locations. Modified from Rhys, 2019.*

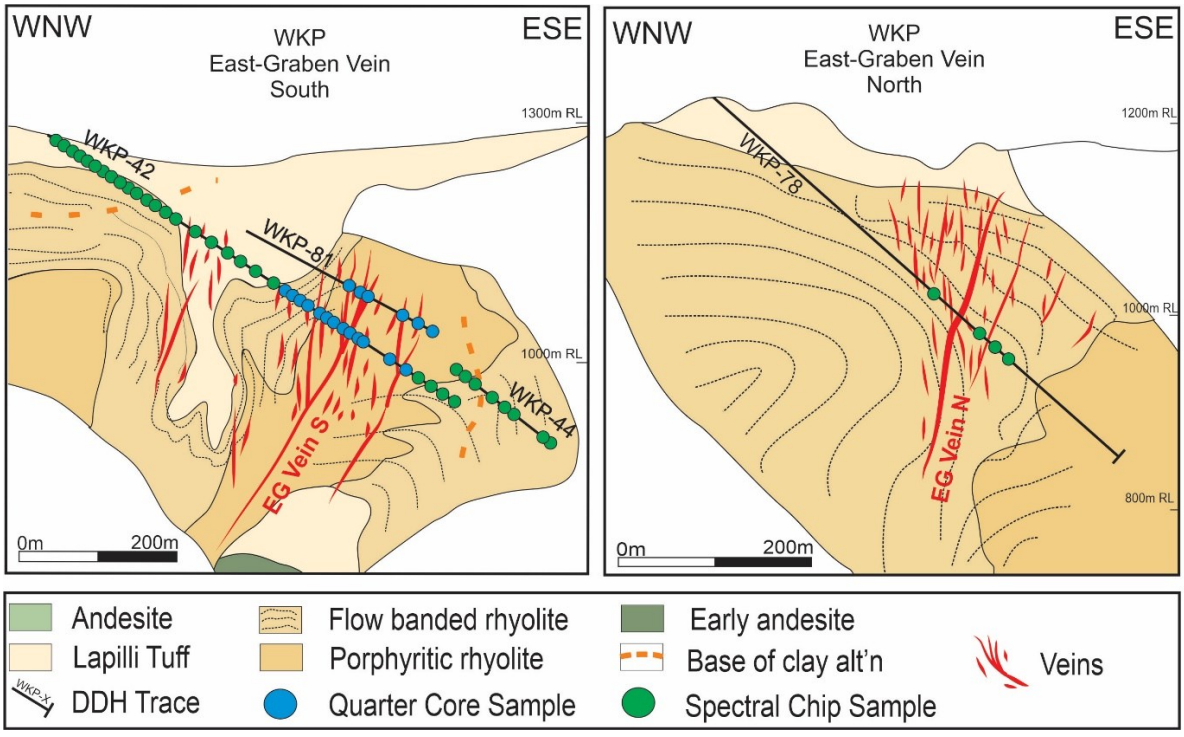

Chapter 4 | Analytical Methods

4.1 Cobaltinitrite Staining

Cobaltinitrite staining of thin section cut-offs was done to identify potassium-bearing minerals. Cut-offs were etched with concentrated hydrofluoric acid (HF) for three minutes followed by soaking in saturated cobaltinitrite solution for three minutes. After rinsing, the cut-off was photographed and compared with the photograph prior to staining to identify areas containing K-bearing minerals. Due to the fine-grained nature of illite it is lost during HF etching and does not stain. Stained cut-offs and the original cut-off are shown in Appendix B.

4.2 Thin Section Analysis

Samples were chosen for thin section petrographic examination based on their various rock types, locations, and mineralogies. Seventy polished thin sections were examined using polarizing transmitted and reflected light microscopy to examine textures and mineralogy. Thin section descriptions, thin section scans (PPL & XPL), and photomicrographs are in Appendix B.

4.3 SEM-EDS Mineral Chemistry

Selected thin sections were carbon coated and analyzed using scanning electron microscope (SEM) with an energy-dispersive spectrometer (EDS) to identify unknown minerals and determine mineral compositions. Analysis was done at the University of Ottawa Microprobe Laboratory. The backscattered electron (BSE) images as well as the EDS mineral composition data can be found in Appendix B.

4.4 Sample Preparation

Samples were pulverized to <2µm using a ceramic dish after crushing in a jaw crusher to <1mm.

4.5 Loss on Ignition (LOI)

Loss on ignition is measured by weighing one gram of the pulverized sample in a pre-weighed and pre-heated ceramic crucible. The crucible with sample was heated for an hour at 1050℃. Loss on ignition values are listed in Appendix A.

4.6 Ammonium Content Analysis

Bulk ammonium content is determined using the Elementar Vario EL cube elemental analyzer at the Ján Veizer Stable Isotope Laboratory at the University of Ottawa. 100mg of powdered sample (<2µ) is mixed with 100mg of WO_3 in an 8x10mm tin capsule and combusted at 1150^{o}C in CNS mode with atmospheric nitrogen removed by placing the auto-sampler balls under vacuum for 20 seconds before combustion. The nitrogen gas is separated from the other gases using chemical traps. Essentially following the same method described by Page et al (2018). The calibration curve is made by combusting 4, 10, 50, & 100mg of a reference (B2152 from Elemental Microanalysis) which contains 0.131% N. For samples with high N, a second calibration curve was made using 0.5, 1, 2, & 3mg of sulfanilamide (B2036 from Elemental Microanalysis) which contains 16.26% N. After approximately 40 samples are analyzed, the ash tube is cleared, and a new calibration curve is created. To ensure accuracy a blind standard (SO-3, MAG-1, SO-4, and/or SA) is run after every calibration. The ammonium content of these standards is reported in Appendix A Table 2. The results of the analysis of these blind standards show an accuracy of 0.46 – 1.01% (Appendix A Table 2). Furthermore, a duplicate sample is run every 10 samples to ensure precise values. The analyses suggest a precision of 0.03 – 0.55% for samples >400 ppm NH_4^+ and 0.04 - 12.45% for samples <400 ppm NH_4^+ (Appendix A Table 2). The detection limit of ammonium identified by this method is approximately 10 ppm. Most samples were analyzed twice during separate runs to ensure the reproducibility of the values. The bulk ammonium values in Appendix A Table 2 are reported as run 1 and run 2 as well as the average value.

4.7 Leaching of Adsorbed Ammonium

In order to determine the amount of adsorbed ammonium in samples, a leaching experiment was carried out following the procedure described by Mamo et al (1993). This involved stirring one gram of <2µm powdered sample into 50ml of a 2N KCl solution and stirring manually every 6-8 hours. After 24 hours, the sample was separated from the solution using a filter with a 0.45 µm pore size and rinsed with distilled water. The sample is dried on a 50℃ hot plate overnight. The leached sample was then run for bulk ammonium contents and compared to the non-leached sample. The results of ammonium leaching are in Appendix A.

4.8 Nitrogen Isotope Composition

Nitrogen isotope compositions are expressed by permil notation relative to the atmosphere where $\delta^{15}N = [(R_{sample})/(R_{air})-1] * 1000$ where R is $^{15}N/^{14}N$. For each sample up to 300 mg was weighed into a 10x10 tin capsule. The amount of sample weighed was relative to the ammonium contents of the sample to maintain a consistent amount of nitrogen released from each sample during combustion. Samples with low ammonium content (<100 ppm) could not be analyzed due to their low nitrogen content. One hundred mg of WO_3 was then added to a tin capsule and combusted at 1150°C after removal of atmospheric nitrogen under vacuum for 20 seconds using the Elementar Vario EL cube elemental analyzer attached with Delta Plus XP mass spectrometer at the Ján Veizer Stable Isotope Laboratory at the University of Ottawa. The analytical method is essentially like that described by Page et al. (2018). The calibration curve is made using three standards (C-51, C-52, C-54) with known $\delta^{15}N$ values and a new curve was calculated every 20 – 40 samples after the ash tube is cleared. Accuracy is determined using a blind standard (C-55) which showed an accuracy of 0.5 – 1.3%. Duplicate samples are run every ten samples to ensure precision. The duplicate analysis showed a precision of 2.5 – 15.1%. The $\delta^{15}N$ values are listed in Appendix A.

4.9 Size Separation for XRD

Samples were first crushed to <0.2mm using a disk mill then sieved to -200 mesh (<74µm). After sieving the samples were stirred into a glass beaker with a capacity of 400mL filled with 300mL of distilled water. The beaker was then placed in an ultrasonic bath for an hour to disaggregate the sample. Afterwards, the beaker was placed on a shaker and agitated overnight to suspend the particles. The <10µm fraction was obtained by decanting the top 10cm of the suspended solution in a 1L graduated cylinder after allowing the particles to settle undisturbed for 25 minutes (150 seconds per cm of depth). The <10µm fraction is then separated from the solution using a filter with a 0.45µm pore size. The sample is dried on a hot plate at 50°C overnight.

4.10 X-Ray Diffraction (XRD) Analysis

XRD analysis was completed at the University of Ottawa X-ray Core Facility utilizing the Rigaku Ultima IV Diffractometer using CuKa for WKP and Martha samples. Bulk rock powders were packed and flattened into low background powder sample holder. The powder was analyzed from 4^o to 46^o in 2θ values at one degree per minute. Fine-grain fractions, <10µm, were analyzed for samples containing small or insignificant peaks below 10^o in 2θ in bulk sample data. The <10µm powders were packed and

flattened into a glass autosampler powder sample holder and analyzed from 4^{o} to 46^{o} in 2θ at one degree per minute. The X-ray diffraction patterns for samples from WKP and Martha are in Appendix C. XRD data for the Favona wallrock samples are available in Simpson & Mauk, 2007 and in Table 9 Appendix D for the samples selected in this study. Appendix B also includes the XRD results and samples labelled (uO) were analyzed at the University of Ottawa.

4.11 Bulk Rock Composition Analysis

20 samples, including 18 from Favona and two from Martha, were analyzed for their bulk rock chemical compositions. 1mg of powdered sample was sent to ActLabs which was analyzed under the "1F2" package. This involves a 4-Acid (HCl, HNO_3, HF, $HClO_4$) "Near Total" digestion followed by analysis using ICP-OES. This method digests most silicate minerals but may only partially digest resistive minerals such as zircon, titanite, barite, cassiterite, etc. Quality assurance is guaranteed by ActLabs using a variety of standards and duplicates. Accuracy is guaranteed within 5%. Duplicate analysis gave a precision of <1% for all elements. Furthermore, a blind standard (JR-1) was run which gave an accuracy of <12% for all major elements and most trace elements. The results of this analysis can be found in Appendix A.

4.12 Mineral Abundance Estimation

Thin section observations were used in conjunction with bulk rock composition and XRD to evaluate the abundance of various minerals for 20 samples from Favona. The abundance of illite +/- mixed layer smectite as well as chlorite was estimated based on thin section observations. Mixed layer illite-smectite could not be distinguished from illite in thin section nor SEM-EDS. Illite and smectite abundances were then estimated using the illite/smectite ratios in mixed layer illite-smectite on XRD analysis carried out by Simpson & Mauk, 2007. Adularia abundance was calculated from bulk rock potassium content by subtracting potassium in illite based on the ideal composition of illite from Rieder et al. (1998). Adularia contents are also estimated visually in samples that had cobaltinitrite staining. Due to the lack of XRD and geochemical data for Martha and WKP samples, mineral abundance estimates for these samples were solely based on thin section observations and cobaltinitrite staining. Mineral abundance estimates are listed in Appendix A & B.

Chapter 5 | Results

5.1 Mineralogy / Petrography

5.1.1 Favona

Favona samples include plagioclase phyric andesite wallrock (Figure 9a), colloform / crustiform quartz-adularia veins, and hydrothermal breccia pipe samples (Figure 9b). The wallrock andesite contains phenocrysts of plagioclase (1-10 mm, 10-30 vol%), pyroxene, and amphibole which have all been intensely hydrothermally altered. Although the porphyritic texture is preserved in most samples, phenocrysts have been completely replaced by hydrothermal alteration (Figure 9a). All plagioclase phenocrysts appear to have been altered to adularia which has been overprinted by 20-80% illite +/- smectite and quartz (Figures 9a & 9c). Although not observed in thin section or SEM-EDS, XRD data from Simpson & Mauk (2007) shows that most of the wallrock samples in the hangingwall of the Favona vein contain mixed layer illite-smectite (Figure 2). The adularia shows yellow color after the cobaltinitrite staining (Appendix B). Many intensely illite altered samples do not stain because many fine-grained minerals are washed away during HF etching. Pyroxene and / or amphibole phenocrysts have been locally replaced by quartz and / or chlorite. The groundmass has been altered to form quartz, adularia, illite, pyrite +/- chlorite in all samples. Pyrite is finely disseminated throughout the groundmass. Calcite was only found in minor amounts (<2 vol%) in sample FVN85-404 which occurs in the deepest parts, >300m below the surface, of the Favona deposit.

Hydrothermal breccia pipe samples contain heterolithic angular clasts which range in size from 0.1 – 5cm (Figure 9b). Clasts consist of variably altered andesite flows / tuffs, quartz colloform / crustiform veins, and mudstone. The matrix is very fine-grained consisting of ash particles and dark coloured quartz / sediment grains with abundant disseminated sulfides. Some parts of the breccia have been hydrothermally altered forming a minor overprint of illite +/- mixed layer smectite.

Vein samples are primarily composed of quartz with minor adularia +/- illite. Cobaltinitrite staining only identified adularia in select samples. Crustiform veining with alternating 0.2 – 3cm bands of microcrystalline quartz with varying amounts of unidentified metallic minerals are common throughout all vein samples. Some bands contain finely (0.1mm) brecciated microcrystalline quartz incorporated into the bands. One sample contains a large clast of crustiform colloform quartz adularia which has been incorporated into the vein with a cockade texture. Metallic minerals are primarily concentrated into the dark-coloured bands.

5.1.2 Martha

Wallrock samples from Martha consist of quartz-plagioclase porphyritic andesites overprinted by varying degrees of hydrothermal alteration (Figures 9b & 9c). This quartz andesite contains phenocrysts of quartz (0.2-3 mm, 5-10 vol%), plagioclase (0.5-8 mm, 10-30 vol%), pyroxene (0.5-1mm, 2-5 vol%), and minor amphibole (0.5-4mm, <3 vol%). Many of which have been altered to adularia, illite, quartz, albite, calcite, or chlorite. Plagioclase phenocrysts have been completely overprinted by adularia in all samples as well as within the groundmass. The adularia altered plagioclase appears to have been variably overprinted by albite and / or illite in many samples. Albite overprinting up to about 40% of some phenocrysts. Illite only makes up a few percent of the phenocryst and occurs very minimally throughout the groundmass. Fine grained calcite also minimally overprints some plagioclase phenocrysts. Pyroxene and amphibole phenocrysts tend to be pseudomorphically replaced by chlorite and quartz. The groundmass is primarily composed of very fine-grained quartz, adularia, and pyrite with minor albite, chlorite, and calcite (up to 3 vol%). One wallrock sample is from a minimally altered plagioclase pyroxene phyric mafic dyke. The dyke occurs proximal to the mineralized zone within the intensely altered andesite. Plagioclase phenocrysts (0.2-2 mm, 10 vol%) show albite twinning as well as zoning. Clinopyroxene phenocrysts (~ 5 vol%) are overprinted by quartz and chlorite.

Vein samples from the Martha open pit show a variety of textures including colloform / crustiform, brecciation, comb quartz, and bladed quartz textures after bladed calcite (Figure 6b). Veins are mainly composed of fine-grained quartz and adularia. Aggregates of microcrystalline quartz appear to have formed from silica gel. Unlike Favona, the veins show yellow coloration after cobaltinitrite staining due to abundant adularia (Appendix B). The drill core samples from the Martha Underground project show different textures than the open pit samples. The latter samples tend to have no banding. Instead, quartz appears to be primarily microcrystalline quartz and minor adularia cementing 0.5-3cm sulfide rich patches. These patches contain a (unidentified) green coloured sheet silicate mineral (corrensite?). Some void filling comb quartz adularia textures are observed throughout these veins between the sulfide rich patches. Iron oxyhydroxide commonly coat quartz and adularia (Figure 9g).

5.1.3 Wharekirauponga (WKP)

Wallrock samples from WKP consist of rhyolite flow dome samples and rhyolitic lapilli tuffs. The rhyolite flow domes are green to cream-brown in colour, are flow banded to massive, and contain varying amounts of phenocrysts (Figure 9e). Euhedral quartz phenocrysts are common throughout all samples at about 10 – 20% and are 0.2 - 3mm in size. 0.1 – 2mm feldspar phenocrysts are found in most

of the rhyolite dome samples though the abundance ranges from about 5 – 20% between samples. Minor (<5%) chlorite is found throughout the groundmass as well as pseudomorphically replacing biotite. Feldspar phenocrysts tend to be overprinted by 10 – 60% albite which appears as a dusty brown mineral forming along fractures (Figure 10g). Illite is common in small amounts occurring as patches within the albite (Figure 10h). Some feldspar phenocrysts, within the same albite altered samples, are however rather overprinted by illite than albite (Sample WKP42-407 in Appendix B). The groundmass of the rhyolite dome samples is composed of primarily quartz and adularia (strong cobaltinitrite staining) with minor localized patches of illite and chlorite.

Tuff samples are beige to green coloured with 0.2 – 2mm sized fragments throughout. Fragments are altered to white-coloured fine-grained minerals and are difficult to differentiate the different fragment types in thin section. Based on XRD, illite appears to be the predominant alteration mineral in these samples though Simpson, 2018 reports that mixed layer illite-smectite occurs in the XRD profile of some shallow samples from DDH WKP42 (Appendix D). Kaolinite was also common in SWIR patterns reported by Simpson, 2018 but was not observed in the thin sections of these samples. The matrix is also intensely altered to fine-grained minerals in many samples though some tuff samples are slightly hard due silicification (Figure 9f).

DDH WKP42 contains a green lapilli tuff unit which extends to about 120m downhole depth with a gradational contact becoming flow banded rhyolite below 124m downhole. Between 225m to 313m downhole another intercalated pyroclastic unit is observed again grading to flow banded rhyolite. The EG vein occurring at ~423m downhole. Samples from WKP44 were taken from the EG vein footwall and consist of an intensely illite altered unit which could be either flow banded rhyolite or another rhyolitic lapilli tuff unit. It is quite difficult to differentiate the rock type due to the intense alteration. This is similar to WKP78 which drilled the northern part of the EG vein. Samples from WKP81 are mainly EG vein samples with one rhyolite flow banded sample from the footwall. The locations of the drill holes are shown in Figure 8.

Auriferous vein samples are all quartz-adularia colloform banded collected from the EG vein. Crustiform / colloform bands consist of 0.2 – 5mm alternating bands of gel to microcrystalline quartz with minor to significant amounts of fine-grained adularia. Vugs are common in many samples mainly concentrated along crustiform bands potentially due to dissolution of minerals such as calcite (Figure 12f). Some vuggy bands look as though they contain illite, but it was not observed in thin section. Dark sulfide rich bands are 1mm to 20mm in size. Brecciation with 1 - 3mm vein clasts are common in the

wide sulfide rich bands (Figure 9h). The sulfide rich bands appear to contain an unidentified greenish coloured sheet silicate mineral.

Figure 9. *Examples of rock samples from Favona, Martha, and WKP. A) FVN84-316. An illite-chlorite altered andesite wallrock from Favona. B) FVN69-62. A heterolithic hydrothermal breccia pipe sample from Favona. C) MTA1460-204. An adularia altered andesite wallrock sample from Martha. D). MTA1460-182. An unaltered mafic post-mineralization mafic dyke sample from Martha. E) WKP42-409. A flow banded adularia altered rhyolite dome sample from WKP. F) WKP42-59. An illite altered rhyolite pyroclastic sample from WKP. G) MTA1496-115. A brecciated vein sample with minor fine-grained alteration minerals from Martha. H) WKP42-435. A high grade mineralized brecciated vein sample from WKP. Ruler and scale card are in cm scale.*

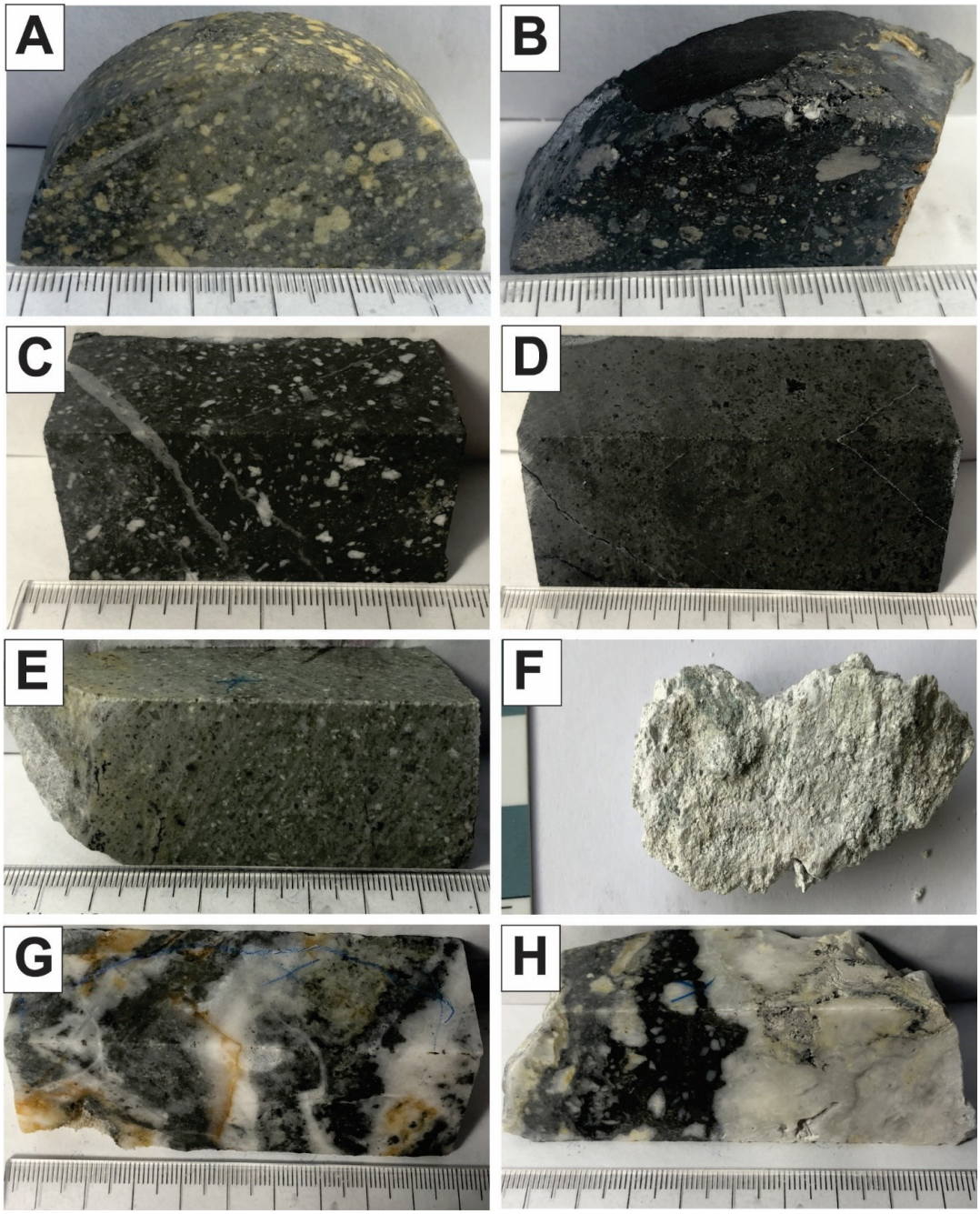

5.2 Hydrothermal Alteration Minerals

Apart from quartz, adularia is the most common alteration mineral at all three deposits. In all wallrock samples it forms as a fine-grained aggregate replacing feldspar in the groundmass and feldspar phenocrysts. At WKP, adularia makes up most of the rhyolite dome samples with all phenocrysts having been adularia altered and the groundmass being composed of adularia with minor quartz, illite, and chlorite (Figures 10g & 10h). Similarly, the Martha samples have been strongly adularia altered replacing both the phenocrysts and the groundmass (Figures 10e). At Favona, adularia is less abundant but still occurs in most samples (Figure 10a & 10b, Table 9 Appendix D). There is a later overprint of illite +/- smectite on the adularia which commonly destroys most adularia (Figures 10c & 10d).

Illite is found in most samples from all three deposits. It is, however, much more abundant at Favona than at Martha or WKP. Illite overprints the adularia at Favona usually ~20 - 60% although in some cases it replaces up to 100% of the adularia (Figures 10c & 10d). This occurs within phenocrysts as well as the groundmass and the adularia tends to make up ~10 – 60% of the overall sample. Based on XRD data from Simpson & Mauk (2007), illite within the hangingwall of the Favona vein occurs as mixed layer illite-smectite. They showed that the ratio of illite to smectite tends to be higher closer to the vein and decreases towards the surface away from the Favona vein. SEM-EDS did not detect any smectite in many of the mixed layer illite-smectite samples due to the low abundance of smectite to illite. In addition, the samples which contain pure smectite were not examined with EDS. The EDS data shows illite at Favona is composed of 30 – 33 wt% Al_2O_3, 57 – 59 wt% SiO_2, 5 – 7 wt% K_2O, 1 – 2 wt% MgO, & 0 – 1.5wt% Fe_2O_3(t) where the values are anhydrous based. The illite at Martha and WKP tends to be similar in composition to Favona but at Martha illite contains slightly higher MgO at 2 – 3 wt% and WKP has slightly higher Fe_2O_3 (t) at 1 – 2wt%. This composition fits within the ideal composition of illite described by Rieder et al. (1998).

Illite is much less abundant at WKP (5 – 20%) and Martha (<5%). Many phenocrysts, especially at Martha, appear to be overprinted by a dark dusty brown mineral which is a fine-grained aggregate of albite (Figures 10e & 10g). This albite forms along fractures overprinting the adularia altered phenocrysts. Within the albite, minor amounts of illite can be found occurring as small (20 – 100 μm) rounded clusters (Figure 10f). Within the rhyolite dome samples at WKP, illite is minor (<10%) and found to alter some feldspar phenocrysts as well as forming small (20 – 50μm) clusters along with chlorite in the matrix. The tuff samples at WKP tend to contain more abundant illite / smectite and are much more friable than the dome samples. The illite / smectite intensely altering both the clasts and the matrix.

Figure 10. *Photomicrographs (left) of variously altered feldspar phenocrysts from Favona, Martha, and WKP wallrock samples with corresponding BSE images (right). A & B) Favona | FVN63-180. An adularia altered plagioclase phenocryst overprinted by illite. C & D) Favona | FVN87-211. A presumably originally adularia altered plagioclase phenocryst completely overprinted by illite. Illite appears brown in C due to poor polishing. E & F) Martha | MTA1460-204. An adularia altered plagioclase phenocryst overprinted by albite and minor illite. G & H) WKP | WKP42-407. An adularia feldspar phenocryst overprinted by albite and minor illite. Adl = Adularia, Qz = Quartz, Ab = Albite, Ilt = illite, Chl = Chlorite, Py = Pyrite.*

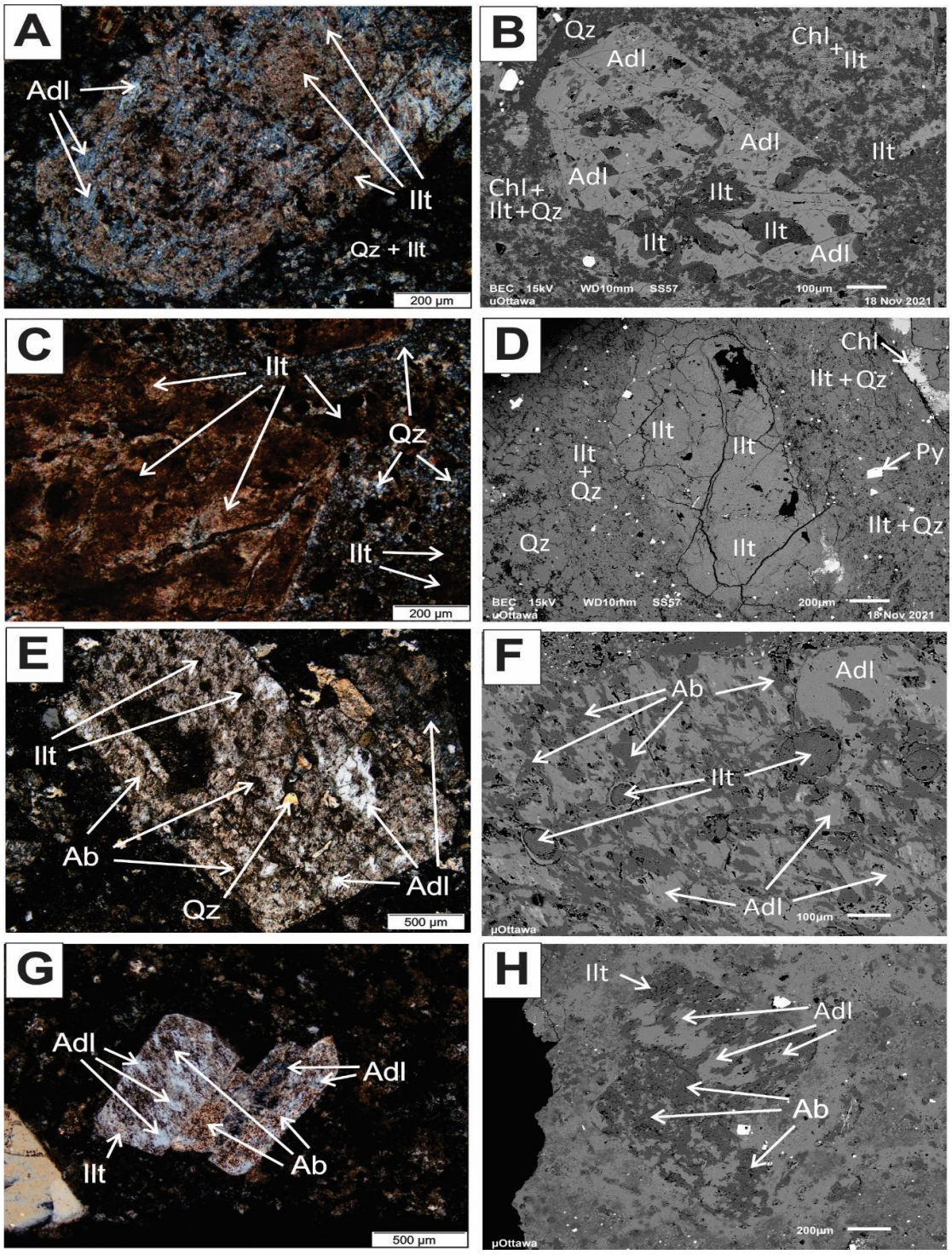

Chlorite is common at all three deposits. At Favona, chlorite seems to be restricted to the footwall of the Favona vein. At both Favona and Martha, it is typically found as patches throughout the groundmass and pseudomorphically replacing pyroxene and amphibole. At WKP it is primarily found occurring as patches within the groundmass along with illite (See Sample WKP42-407 in Appendix B). Chlorite tends to be more abundant at Favona (5 – 30 vol%) than at Martha and WKP (5 – 10 vol%).

The alteration at Favona and Martha is quite different as shown in the diagram of K/Al vs 2Ca + Na + K/Al (Figure 11). All wallrock samples have been enriched in potassium and lost calcium and sodium compared to the unaltered country rocks. However, Favona samples contain less K, Ca, and Na than those at Martha. Favona samples plot near the compositions of illite from EDS meaning illite is the dominant alteration mineral. The Martha samples, however, contain higher K, Ca, and Na and plot closer to the adularia field meaning adularia is much more abundant at Martha than Favona. The Martha samples have increased Ca, up to 0.42 %, and Na, up to 0.99 % (Table 6), due to calcite (up to 3 vol%) and albite. Neither of which are common at Favona.

Figure 11*. Plot of K/Al vs (2Ca + Na + K)/Al of bulk rock compositions. Shows the alteration differences between Favona and Martha in comparison to unaltered Waipupu andesite. Unaltered andesite compositions from Booden et al., 2012 and Adams et al., 1994. Illite and K-Feldspar fields are based on EDS compositions in samples (Appendix B). Kfs = K-Feldspar / Adularia, Ilt = Illite, Mnt = Montmorillonite.*

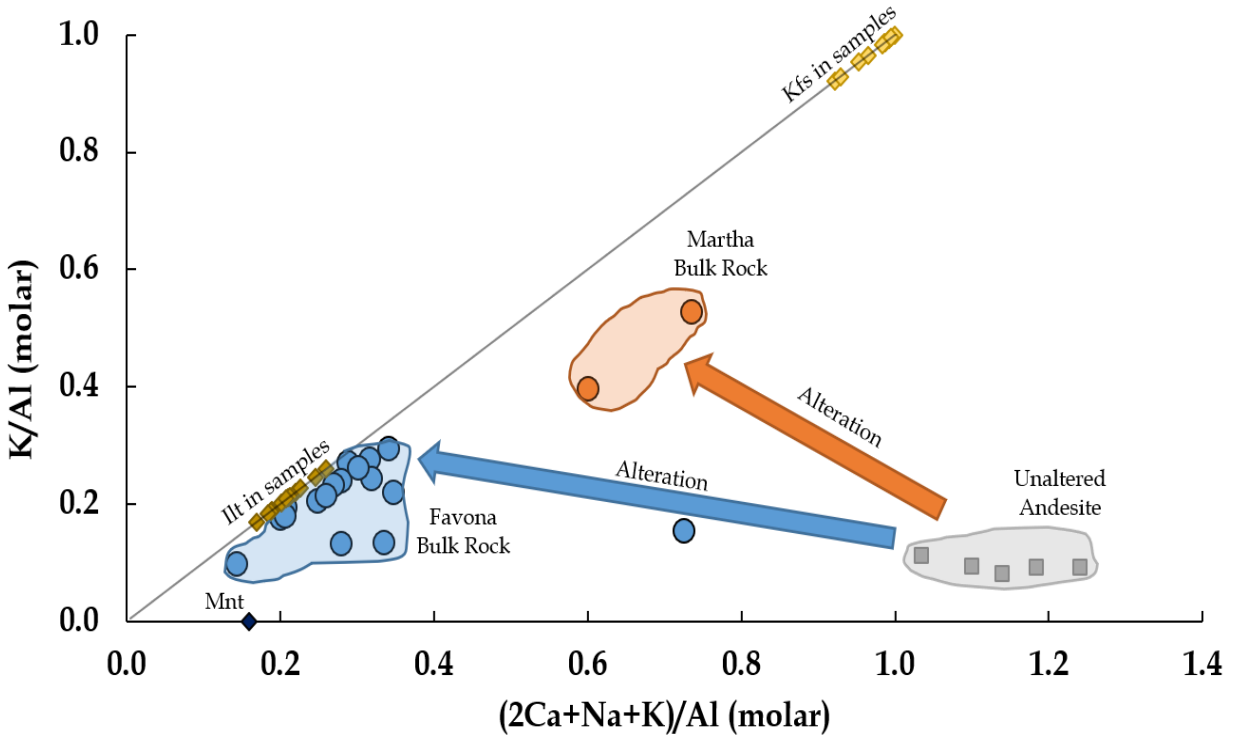

5.3 Loss on Ignition

Loss on ignition values range from 0.0 – 13.6 wt%. Vein samples tend to have low values, 0.0 – 3.2wt%, whereas high values are found in intensely illite and / or smectite altered wallrock. Favona wallrock samples have high LOI values (4.2 – 13.6wt%) compared to WKP (0.9– 5.8wt%) and Martha (2.0 – 3.8wt%). The Favona samples are much more intensely illite +/- mixed layer smectite altered than the other two deposits. The sample with the highest LOI, FVN104-270, is part of an intensely illite-smectite altered unit along a shear zone (Figure 12Aa & 12Ab). At WKP, LOI values are higher in the illite and / or smectite altered pyroclastic rocks (1.8 – 7.8wt%) and lower in the intensely adularia altered rhyolite flow samples (0.1 – 3.7wt%; Figure 12B & 12Bb). The sample with the highest LOI is from the northern part of the EG vein (Figure 12Bb) and is very intensely illite altered. Martha samples have low LOI values (2 – 4wt%) except for two vein samples (MTA1203-300 and MTA1460-177) which have an LOI of ~11wt%. These are two vein samples with high calcite content. Generally, vein samples from all three deposits have a low LOI (0.0 – 3.2wt%) except for those that contain significant amounts of calcite. Calcite is insignificant in most wallrock samples and therefore LOI should be a proxy for hydrous mineral alteration.

***Figure 12**. A) Cross-section of Favona showing the distribution of loss on ignition (LOI) values around the Favona vein. B). Cross-section of WKP showing the distribution of loss on ignition (LOI) values around the EG vein. All values are in wt% LOI. Vertical sections modified from Simpson & Mauk, 2007, Maton et al., 2020, and Rhys, 2019.*

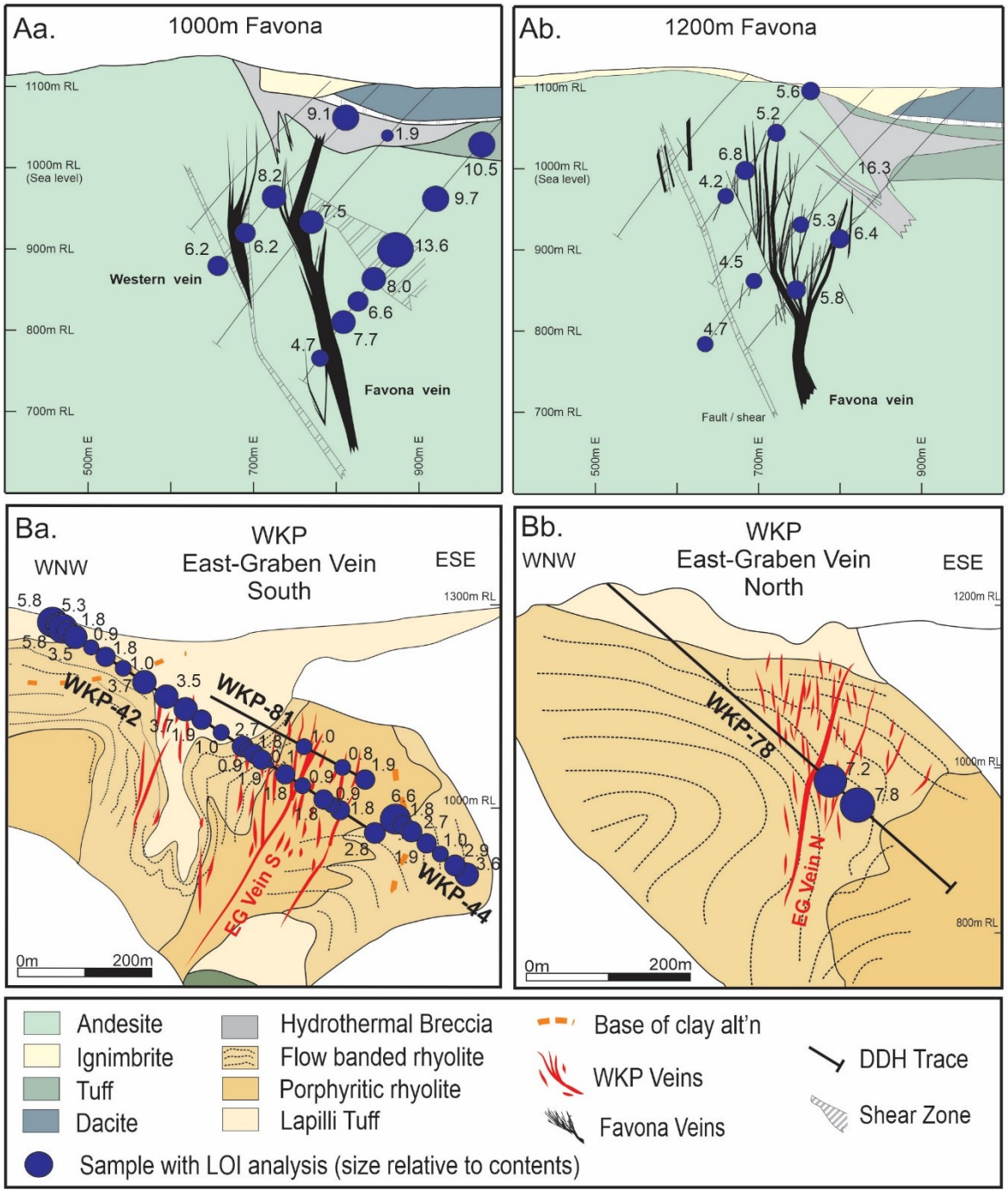

5.4 Ammonium Abundance

Ammonium contents range from 10 – 10,675 ppm. Vein samples tend to be low in ammonium (10 – 94 ppm). Wallrock samples typically contain high ammonium (137 – 10,675 ppm) especially in samples which are intensely illite and / or smectite altered such as the wallrock andesite at Favona or the pyroclastic units at WKP. Overall, ammonium values at Favona (107 – 10,675 ppm) tend to be higher than those at both WKP (67 – 2,645 ppm) and Martha (75 – 192 ppm).

At Favona, there is a 100m halo of high values (990 – 10,675 ppm NH_4^+) surrounding the Favona vein within the plagioclase phyric andesite unit (Figure 13Aa & 13Ab). This ammonium halo lies within the illite and mixed layer illite-smectite alteration zones identified in Simpson & Mauk, 2007. High values (1,827 – 10,675 ppm NH_4^+) occur in the hanging wall within 100m of the vein primarily within the mixed layer illite-smectite zone. The highest value (10,675 ppm NH_4^+) is from an intensely mixed layer illite-smectite altered sample (FVN104-207). Outside of this halo, values are much lower (77 – 301 ppm NH_4^+) occurring in the hanging wall within 150m of the surface. This includes the overlying smectite altered tuff samples (FVN63-12 [204 ppm NH_4^+] & FVN104-103 [107 ppm NH_4^+]) and the hydrothermal breccia samples (FVN69-62 [120 ppm NH_4^+] & FVN85-85 [284 ppm NH_4^+]) as well as some illite-smectite altered plagioclase phyric andesite wallrock.

Martha wallrock samples contain low concentrations of ammonium (<200 ppm). The highest value is 172 ppm NH_4^+ in a quartz-plagioclase phyric andesite (MTA1460-204.8). This sample is very similar compositionally to MTA1460-165.3 which shows similar ammonium values (129 ppm NH_4^+). These samples are adularia, albite, and illite altered similarly to Favona but have abundant adularia and albite with minor illite (Figure 10f). Occurring between these two wallrock samples is an unaltered mafic melanocratic intrusion which contains ammonium below the detection limit (<10 ppm).

At WKP, ammonium contents vary between lithological units and alteration zones from high values (298 – 2,783 ppm NH_4^+) in the intensely illite +/- smectite altered tuff units to low values (142 – 421 ppm NH_4^+) within the adularia altered rhyolite flow domes that host the auriferous veins. Rhyolite flow domes are primarily adularia altered with little to no illite or smectite. Although there is no obvious halo of ammonium minerals surrounding the EG vein, like what is seen at Favona, the highest ammonium value (2,783 ppm NH_4^+) is from an intensely illite altered sample occurring proximal to the EG vein in the north (WKP78-394). The lowest wallrock value (142 ppm NH_4^+) is from an intensely adularia altered rhyolite dome sample from the south also near the EG vein (Figure 13Ba).

Vein samples from all three deposits tend to be very low in ammonium (10 – 94 ppm NH_4^+). At Favona, values range from 10 – 46 ppm NH_4^+. Martha vein samples from the open pit tend to have

slightly higher values at 25 – 94 ppm NH_4^+ though vein samples from deep drilling at Martha contain ~10 ppm NH_4^+. At WKP, samples from the East-Graben vein contain 37 – 67 ppm NH_4^+.

5.5 Leaching of Adsorbed Ammonium

The amount of adsorbed ammonium ranges from 1.2 – 27.3% of total ammonium in all samples. Favona wallrock samples tend to have the lowest amount of adsorbed ammonium (1.2 – 12.72%, 5.3% average n = 15) compared to Martha wallrock (15.7 –18.2%, 16.9% average n = 2) and WKP wallrock (2.5 – 27.3%, 12.3% average n = 17). At Favona, there seems to be no obvious correlation of the amount of adsorbed ammonium with the ratio of illite to smectite (obtained from Simpson and Mauk, 2007 XRD data). However, this does not necessarily reflect the amount of illite or smectite within the sample due to varying abundances of these minerals. The sample containing pure smectite had 6.1% adsorbed ammonium. Mixed layer illite-smectite samples had values ranging from 2.4 – 12.7% with an average of 5.4% (n=7). Samples containing illite with no smectite yielded 1.2 – 9.0% with an average of 5.0% (n=7) adsorbed ammonium. Most of these samples containing chlorite instead of smectite. Two samples that yielded 3.4% and 4.5% adsorbed ammonium (of a total of 980 ppm and 4,402 ppm NH_4^+, respectively) did not show any XRD peaks (from Simpson & Mauk, 2007 XRD data) of chlorite or smectite. Low abundance of these minerals may explain the lack of XRD peaks.

Adsorbed ammonium values at WKP and Martha tend to be significantly higher than at Favona. At Martha, values range from 15 – 18% and at WKP values range from 2 – 27%. Chlorite is abundant at Martha. The data suggests that significant fractions of ammonium are adsorbed in chlorite in chlorite-bearing samples and not fixed in the crystal lattice. At WKP, samples likely contain mixed layer illite-smectite and many samples, especially at depth, contain chlorite based on thin section examination. Overall, low bulk ammonium contents in these samples, <200 ppm), make for a large uncertainty and may explain the large variation in the values.

Figure 13. *A) Cross-section of Favona showing distribution of bulk rock ammonium concentrations around the Favona vein. Ammonium concentrations are elevated in the hangingwall occurring as a ~100m halo surrounding the Favona vein. The dashed blue line shows the area in which ammonium was identified by SWIR in Simpson & Mauk, 2007. B) Cross-section of WKP showing ammonium values. All values are in ppm NH_4^+. Vertical sections modified from Simpson & Mauk, 2007, Maton et al., 2020, and Rhys, 2019.*

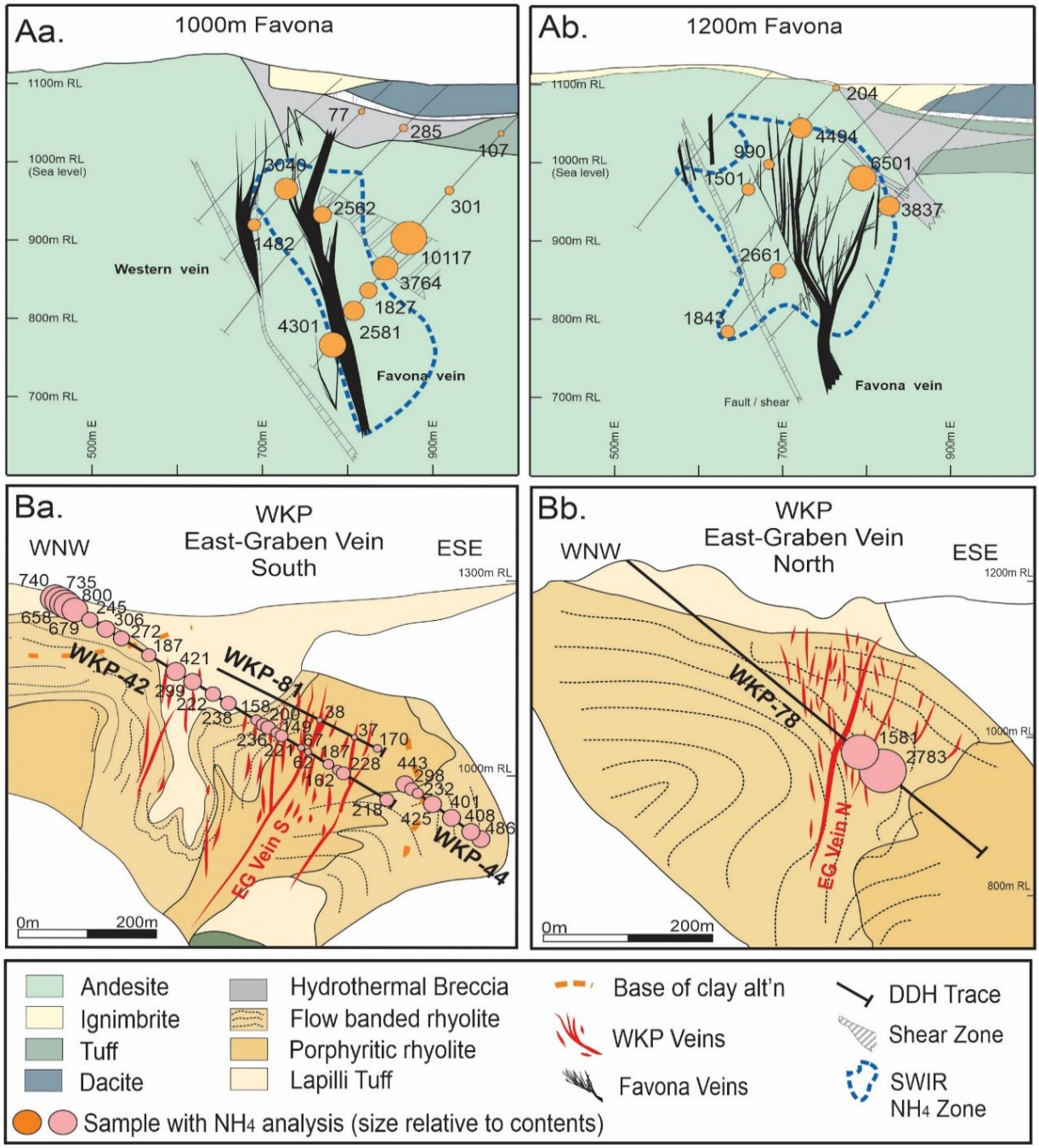

5.6 Nitrogen Isotope Composition

$\delta^{15}N$ values from all three deposits range from +0.5 – +8.1‰ with an average value (n = 56) of +5.3‰. At Favona, values range from +1.2 – +7.1‰ with an average value (n = 19) of +4.7‰. The highest value, +7.1‰, is from the bulk rock of a heterolithic hydrothermal breccia sample (FVN85-85). Siltstone clasts of a hydrothermal breccia sample (FVN69-62C) shows the lowest value of +1.2‰. Considering that unaltered siltstones would be enriched in ^{15}N, low $\delta^{15}N$ values of altered siltstone clasts suggest that the hydrothermal fluids contained NH_4^+ with low ^{15}N. The vein sample FVN63-88V also had a similarly low value at +1.6‰. The remaining 19 samples from Favona are all andesite wallrock samples ranging from +2.2 – +6.8‰. All the samples, except FVN69-249, which have values >6‰ occur in the hanging wall of the Favona vein (FVN104-270, FVN63-12, and FVN63-80; Figure 14Aa & 14Ab). Sample FVN69-249 is within the footwall of the Favona vein but in the hanging wall of Western vein. Samples with the high ammonium values, such as FVN104-270 (10,675 ppm NH_4^+) and FVN63-80 (4,494 ppm NH_4^+), tend to have high $\delta^{15}N$ values (+6.4‰ and +6.8‰ respectively). Both are plagioclase phyric andesites in which the plagioclase phenocrysts have been completely altered to illite +/- mixed layer smectite. However, one mixed layer illite-smectite altered sample (FVN63-12) contains low ammonium (204ppm) but a high $\delta^{15}N$ (+6.3‰). This sample occurs close to the surface (Figure 14Ab). The near surface smectite altered sample (FVN104-103) contains low ammonium (107 ppm NH_4^+) and a $\delta^{15}N$ of +4.9‰. Furthermore, $\delta^{15}N$ values are generally low (<4.3‰) within 50m of the Favona vein, however, samples FVN104-374 and FVN63-135, which are located adjacent to the Favona vein, have values of +5.1‰ and +5.4‰ respectively. The Martha wallrock samples show similar values to Favona. The two samples analyzed (MTA1460-165 and MTA1460-204) containing +3.6‰ and +6.4‰ respectively.

At WKP, values range from +0.5 to +8.2‰ with an average value (n=32) of +5.9‰. Samples from DDH WKP42 tend to be slightly higher (+6.5‰, n=21) than WKP44 (+5‰, n=7) and WKP78 (+1.1‰, n=2; Figure 14Ba & 14Bb). The two samples from WKP78 are intensely illite altered possibly pyroclastic samples with high LOI (7.2 and 7.8%) and ammonium (1,581 ppm and 2,783 ppm). They occur near the East-Graben vein (Figure 14Bb). These are the only samples with <+2‰ $\delta^{15}N$ and are also the only samples containing >1,000 ppm NH_4^+. The remaining pyroclastic samples show very similar values (+5.9‰, n=11) to the flow dome samples (+6.3‰, n =7). Furthermore, similarly to Favona, hanging wall samples from WKP42 and WKP44 tend to be slightly higher (+6.6‰, n=17) than the footwall samples (+5.4‰, n=11).

Figure 14. *A) Cross-section of Favona showing the distribution of $\delta^{15}N$ isotope values around the Favona vein. B) Cross-section of WKP showing the distribution of $\delta^{15}N$ isotope values around the EG vein. All values are in ‰. Vertical sections modified from Simpson & Mauk, 2007, Maton et al., 2020, and Rhys, 2019.*

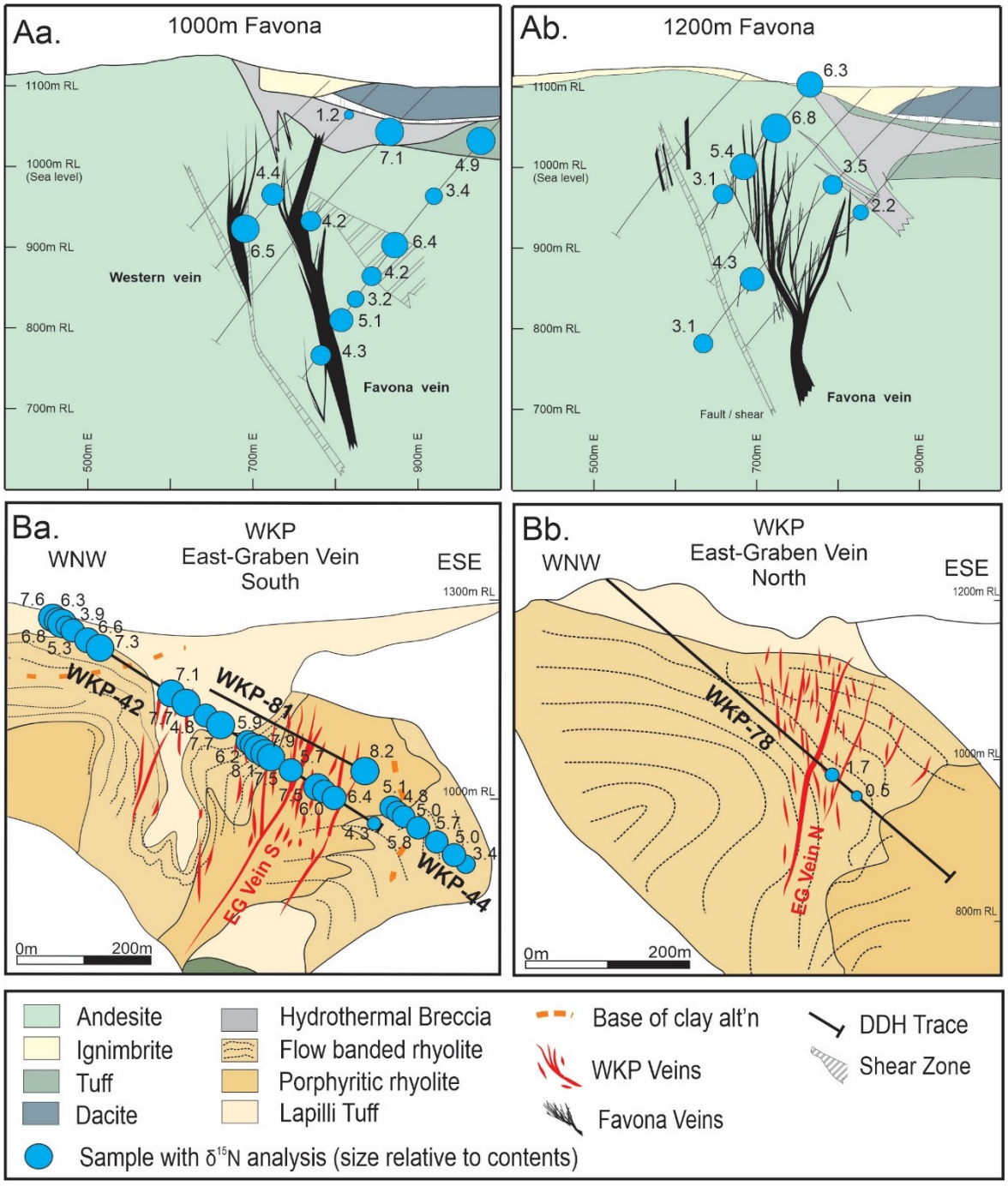

5.7 Major and Trace Element Abundances of Bulk Rock Samples

There is a broad weak correlation of ammonium contents to potassium (Figure 15a) due to a substitution of NH_4^+ for K^+ in most samples. One sample (FVN63-12), however, contains high K_2O (3.57 wt.%) and low ammonium (164 ppm) which is a shallow (<12m downhole depth) illite-smectite adularia altered sample. The other outlier is a low potassium and high ammonium sample (FVN104-270) which contains the highest ammonium (10,675 ppm) yet has low K_2O (1.72 wt.%). This sample occurs within a shear zone in the hanging wall of the Favona vein. Both of which are samples with $\delta^{15}N$ values >+6‰. Furthermore, aluminum also shows a positive correlation with ammonium (Figure 15b) which is consistent with ammonium being hosted in Al-bearing minerals. The main outliers are those which contain low ammonium and high aluminum which are the near surface samples FVN63-12 and FVN104-103. FVN104-103 being a shallow smectite kaolinite altered sample. In the Favona samples, Na_2O is quite low (<0.5 wt.%) across all samples except for FVN104-340 and FVN84-421 which have 0.84wt.% and 0.80 wt.% Na_2O respectively. The sodium is presumably hosted in smectite, relict plagioclase, and/or hydrothermal albite. In the Martha samples the plagioclase phyric andesites (MTA1460-165 & MTA1460-204) contain 1.15 & 1.33wt.% Na_2O respectively. Sodium does not show a correlation with ammonium which is to be expected as ammonium is not expected to be hosted in Na minerals. There is also a broad correlation of ammonium with sulfur (Figure 15c). Sulfur forming primarily as pyrite and is most abundant within the most intensely altered rocks nearest the mineralization. This may indicate that the introduction of ammonium is coeval with that of sulfur. There is a broad correlation of ammonium with arsenic (Figure 15d) which is presumably also associated with the pyrite.

Figure 15. *Plots of Bulk Rock Geochemistry vs Ammonium A) NH_4^+ vs K_2O. Shows a broad positive correlation with most outliers having high potassium (3-3.6%) and low ammonium. B) NH_4^+ vs Al_2O_3. Broad correlation of ammonium with aluminum. Smectite rich samples are outliers. C) NH_4^+ vs S. Shows a broad correlation with sulfur content. D) NH_4^+ vs As. Shows a broad positive correlation with arsenic content.*

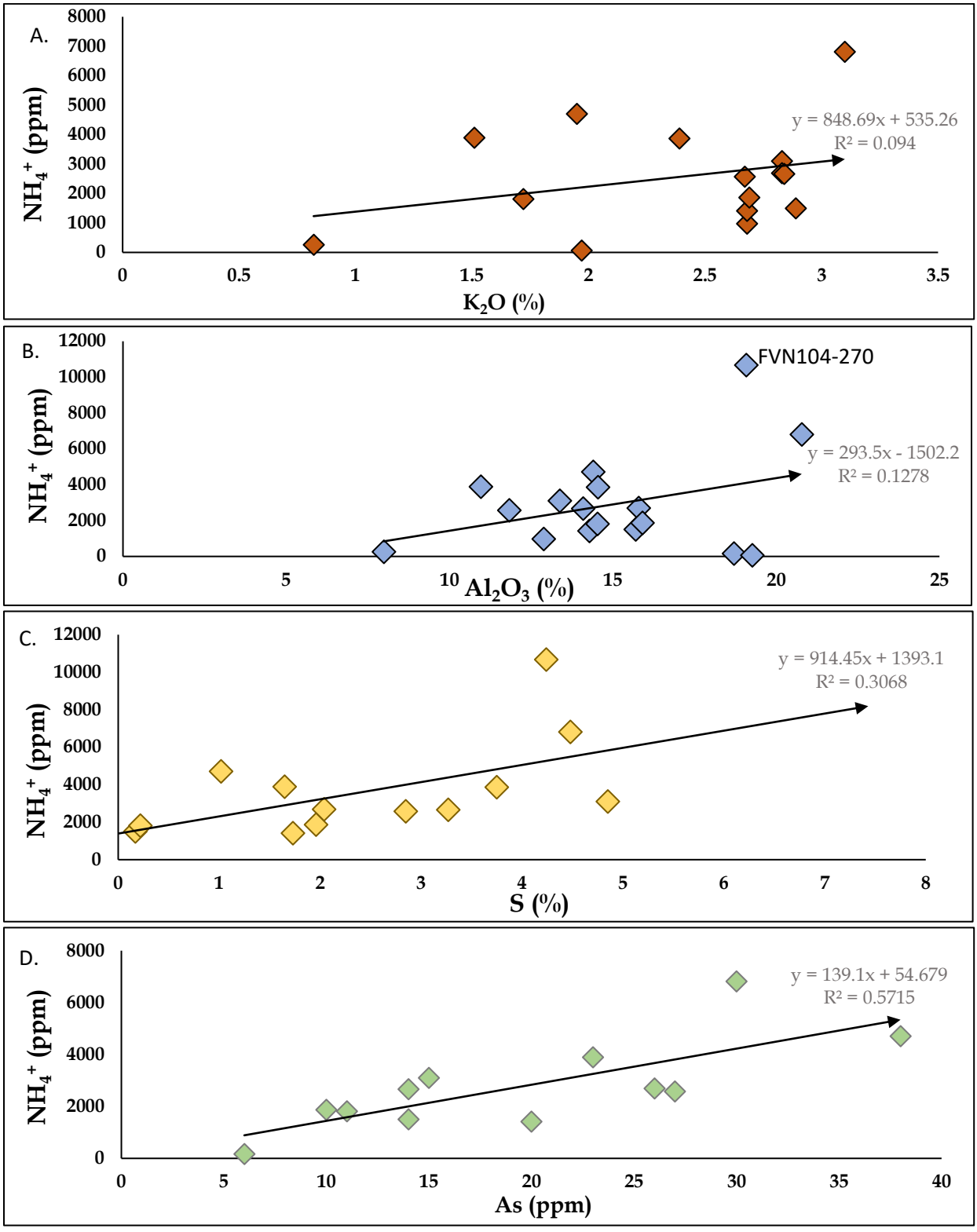

Chapter 6 | Discussion

6.1 Host of the Ammonium

Due to the similar ionic radius and charge of the ammonium molecule to potassium, ammonium is known to be able to be incorporated into the potassium site of various minerals (Harlov et al., 2002) and therefore fixed within the crystal structure. However, ammonium could also be adsorbed onto the surface or into the interlayer of expandable sheet silicate minerals such as smectite or some types of chlorite (Mamo et al., 1993).

6.1.1 Adsorbed Ammonium

Analysis of bulk ammonium contents before and after potassium chloride leaching showed that most ammonium occurs as ammonium fixed within the crystal structure. At Favona only about 5 – 10% of the ammonium occurs as adsorbed ammonium, whereas this value is up to 18% at Martha and 27% at WKP (Appendix A). Adsorbed ammonium values at Favona were plotted against the estimated mineral abundances for illite, smectite, adularia, and chlorite. The data showed that there is no correlation of ammonium with adularia and illite and a weak positive correlation with smectite and chlorite (Figure 16). This indicates that the leachable ammonium is likely adsorbed by smectite and/or chlorite or on the surface of various minerals. The remaining 90 – 95% of ammonium occurs as fixed ammonium.

***Figure 16**. Leachable ammonium vs chlorite and smectite mineral abundances. Smectite occurs mixed layer with illite. Smectite abundance was calculated based on the illite to smectite ratio from Simpson & Mauk, 2007 XRD data as well as the estimated abundance of mixed layer illite-smectite from thin section observations. Chlorite abundance was estimated from thin section observations.*

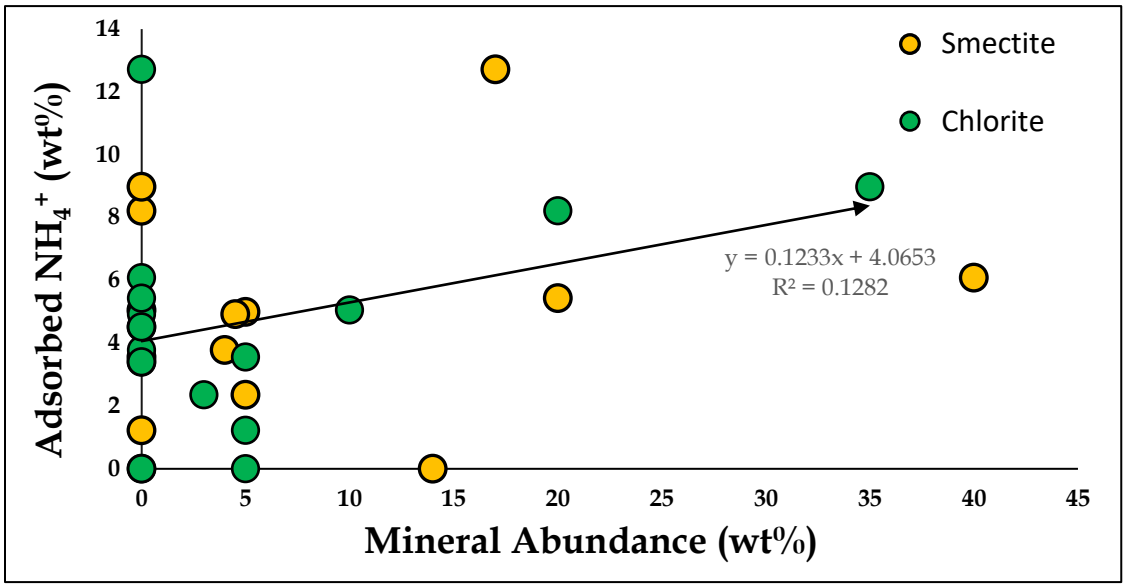

6.1.2 Fixed Ammonium

There is a positive correlation of ammonium fixed in crystals with bulk rock Al_2O_3 (Figure 15b) indicating ammonium is incorporated by an Al-bearing mineral. Based on the mineralogy of these samples, this could be either illite, adularia, smectite, chlorite, or kaolinite. As ammonium is known to substitute for potassium in various minerals (Harlov et al., 2002) it is expected there would be a positive correlation of ammonium with K_2O. There is, however, only a weak positive correlation of fixed ammonium with potassium contents (Figure 15a). Outliers, which have high potassium and low ammonium, are samples containing abundant adularia. There is also an observed positive correlation of ammonium contents to loss on ignition (Figure 17). As there is an essential lack of calcite in most samples, there is a relationship between fixed ammonium and a hydrous mineral. The sole hydrous potassium mineral in these samples is illite. Other hydrous minerals, such as smectite, chlorite, and kaolinite, do not have a potassium site and are unable to fix ammonium within their crystal structures (Figure 18).

Figure 17*. Ammonium contents vs loss on ignition (LOI) for Martha-Favona (plot A) and WKP (plot B). LOI is thought to be a proxy for hydrous mineral abundances due to the lack of calcite in most samples.*

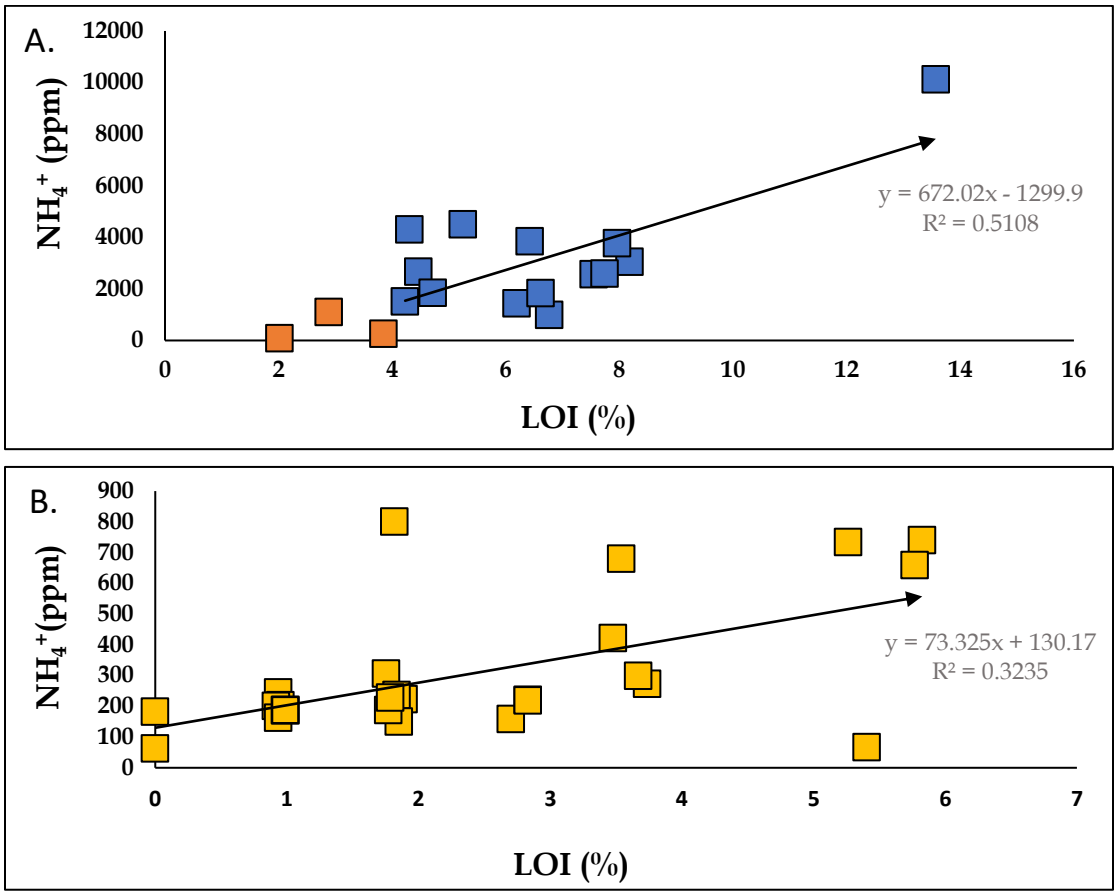

Figure 18. *Crystal structure of chlorite, kaolinite, and mixed layer illite-smectite. The mixed layer illite-smectite can be seen broken down into its smectite and illite units.* NH_4^+ *can be fixed in the* K^+ *site of illite. Chlorite and smectite can adsorb* NH_4^+ *into the exchangeable cation site.*

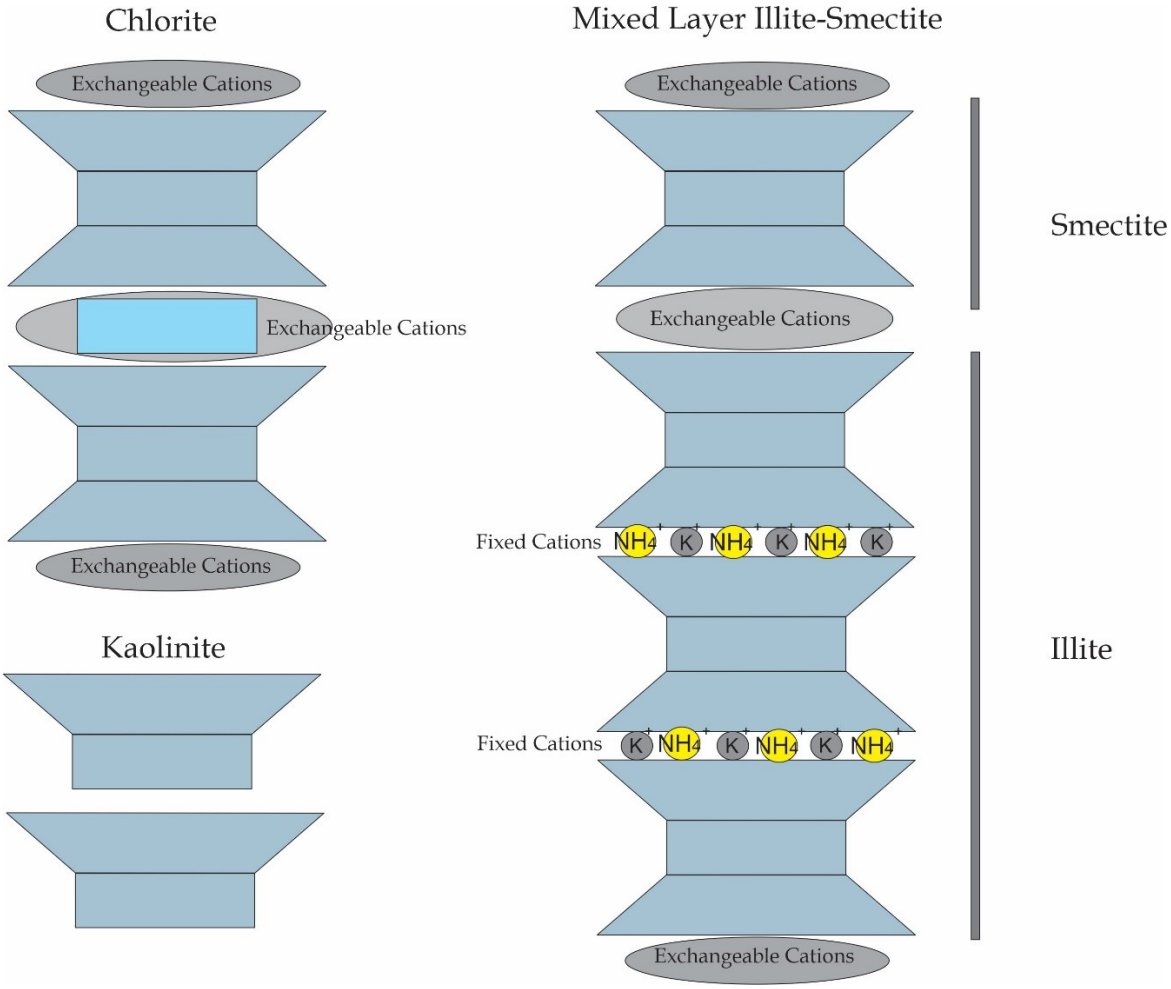

Ammonium contents were plotted against estimated mineral abundances from Favona and Martha (Figure 19). There is a strong positive correlation of fixed ammonium with illite (Figure 19a). There was no observed correlation of fixed ammonium with chlorite or smectite (Figures 19c & 19d) and an inverse correlation with adularia (Figure 19b). This, along with the correlation with loss on ignition, indicates that illite is the host of the fixed ammonium. The inverse correlation with adularia potentially is a result of illite occurring as a secondary replacement of the adularia alteration. This comparison of ammonium to mineral abundances was only completed for Favona and Martha. For WKP there were insufficient bulk rock data, and many samples were too small to be made into thin sections. However, at WKP there is a positive correlation of ammonium with loss on ignition (Figure 17b) similarly to Favona and Martha. Again, an indication of a hydrous mineral, such as illite, being the host of the fixed ammonium.

Figure 19. *Plot of ammonium contents in bulk rocks vs mineral abundance. There is a correlation of ammonium to illite (A) but not with smectite (B) or chlorite (C). Adularia (D) shows a weak inverse correlation. Smectite occurs mixed layer with illite. Smectite abundance was calculated based on the illite to smectite ratio from Simpson & Mauk, 2007 XRD data as well as the estimated abundance of mixed layer illite-smectite from thin section observations. Chlorite abundance was estimated from thin section observations. Adularia was calculated based on the illite abundance and potassium contents.*

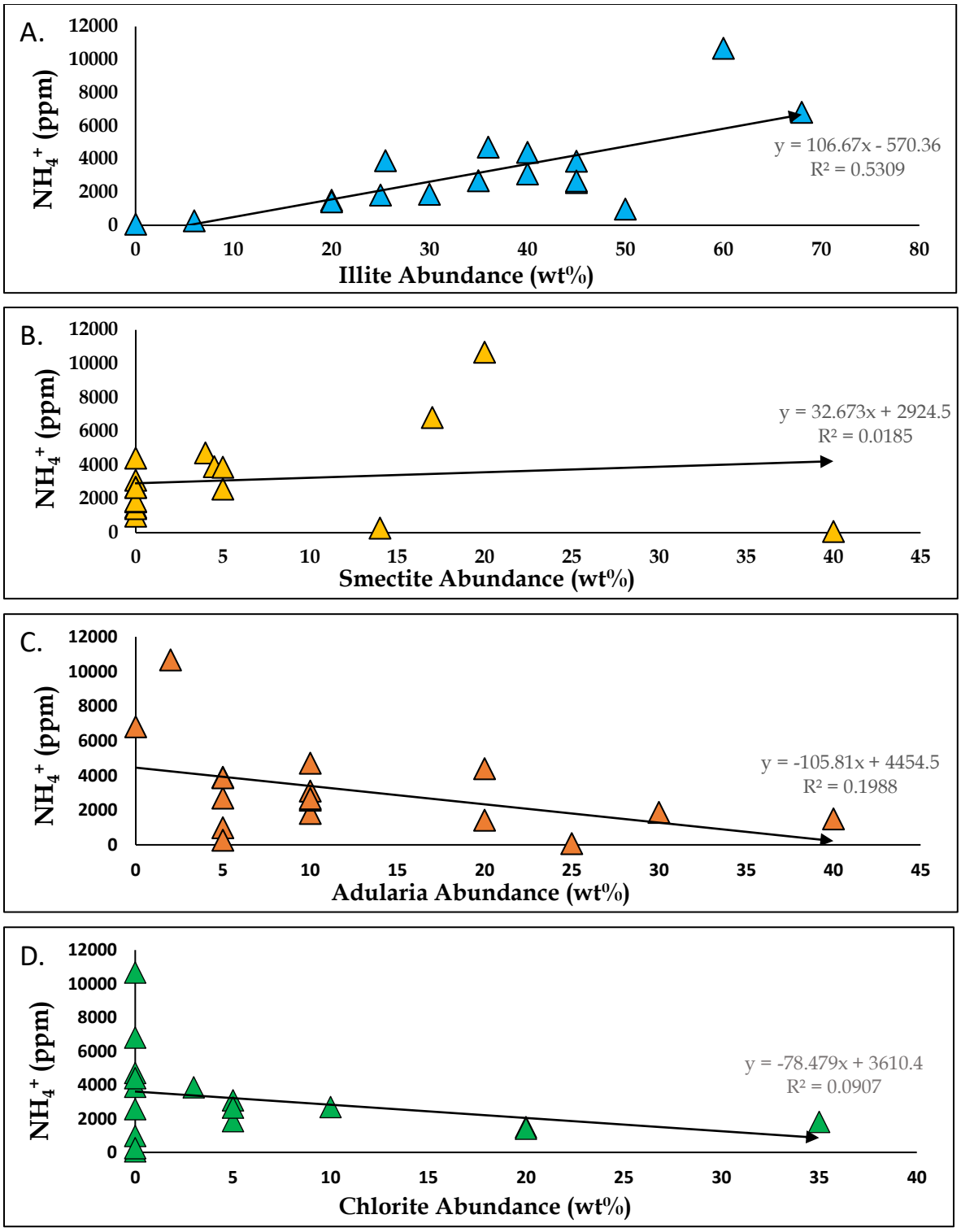

Furthermore, when examining K/Al atomic ratios of adularia obtained with SEM-EDS, values are near 1 in samples from all three deposits (Figure 20). This indicates little to no substitution of ammonium for potassium in the adularia. There may be small amounts (1 – 3%) of ammonium substituting for potassium, however, this cannot account for the ammonium contents in many of these samples.

At all three deposits samples with the intense illite alteration have high ammonium contents and those with intense adularia alteration have low ammonium contents. At Favona, illite contents range from about 20 – 50vol.% whereas at Martha illite contents are ~1 – 3vol.% and contain much more abundant adularia. At WKP, where mineral abundances were based solely on hand sample and some thin section observations, illite tends to be low (~1 – 5vol.%) in the intensely adularia altered rhyolite dome samples and high (>10%) in the intensely illite altered tuff samples. These adularia rich samples from Martha and WKP tend to be very low in ammonium (~200 ppm) and the more illite rich samples from Favona and WKP tend to be much higher in ammonium (~400 – 10,000 ppm). For example, sample FVN84-161 from Favona contains 6,811 ppm ammonium and has the highest estimated illite abundance (~50%). In comparison, at WKP where the rhyolite flow dome samples tend to be strongly altered to form aggregates of fine-grained adularia, but contain minimal illite, ammonium contents are only around 200 ppm. Furthermore, the intensely illite altered rocks at WKP contain ~400 – 2,800 ppm ammonium. At Martha, the plagioclase phyric quartz andesite wallrock tends to contain very little illite (~1 - 5%) but abundant adularia and contains only up to 192 ppm ammonium. Illite seemingly has a much more significant effect on fixing ammonium in the wallrock than the adularia in samples from all three deposits.

6.1.3 Incorporation of Ammonium by K-Minerals

Since the ammonium molecule has a slightly larger ionic radius (1.69Å) than potassium (1.52 Å) ammonium may preferentially substitute for potassium in illite rather than adularia because the crystal lattice of feldspar is tighter than that of micas. This relationship is also observed in rubidium (1.61Å) which is also slightly larger than potassium. Muscovite (K/Rb: 67) preferentially incorporates Rb over microcline (K/Rb: 97) in pegmatites (Riber, 1966). This effect would most likely be enhanced in epithermal systems due to lower temperatures and the lower crystallinity of illite. Furthermore, Hallam & Eugster, 1976 showed that muscovite was able to incorporate ammonium at very low fNH_3 levels at temperatures <600°C in comparison to adularia which required high fNH_3 levels.

***Figure 20**. K/Al molar ratios of adularia altered feldspar phenocrysts from various samples. Red dot denotes spot analyzed by EDS. A) Favona | FVN63-180. K/Al values range from 0.94-1.00. BSE image shows adularia (light grey) and illite (dark grey). Sample contains 980 ppm NH_4^+. B) WKP42-407. Values range from 0.93-1.00. BSE image shows adularia and illite. Sample contains 158 ppm NH_4^+. C) WKP42-124. Values range from 0.97-1.00. BSE image shows adularia and illite. SWIR of this sample is interpreted to contain buddingtonite by Simpson, 2018. D) WKP42-174. Values range from 0.99-1.00. BSE image shows adularia and illite. SWIR of this sample is interpreted to contain buddingtonite by Simpson, 2018. E) MTA1460-204. Values range from 0.93-0.99. BSE image shows adularia and albite (dark grey). F) MTA1460-165. Values range from 0.95-1.00. BSE image shows adularia (light grey) +/- quartz (dark grey).*

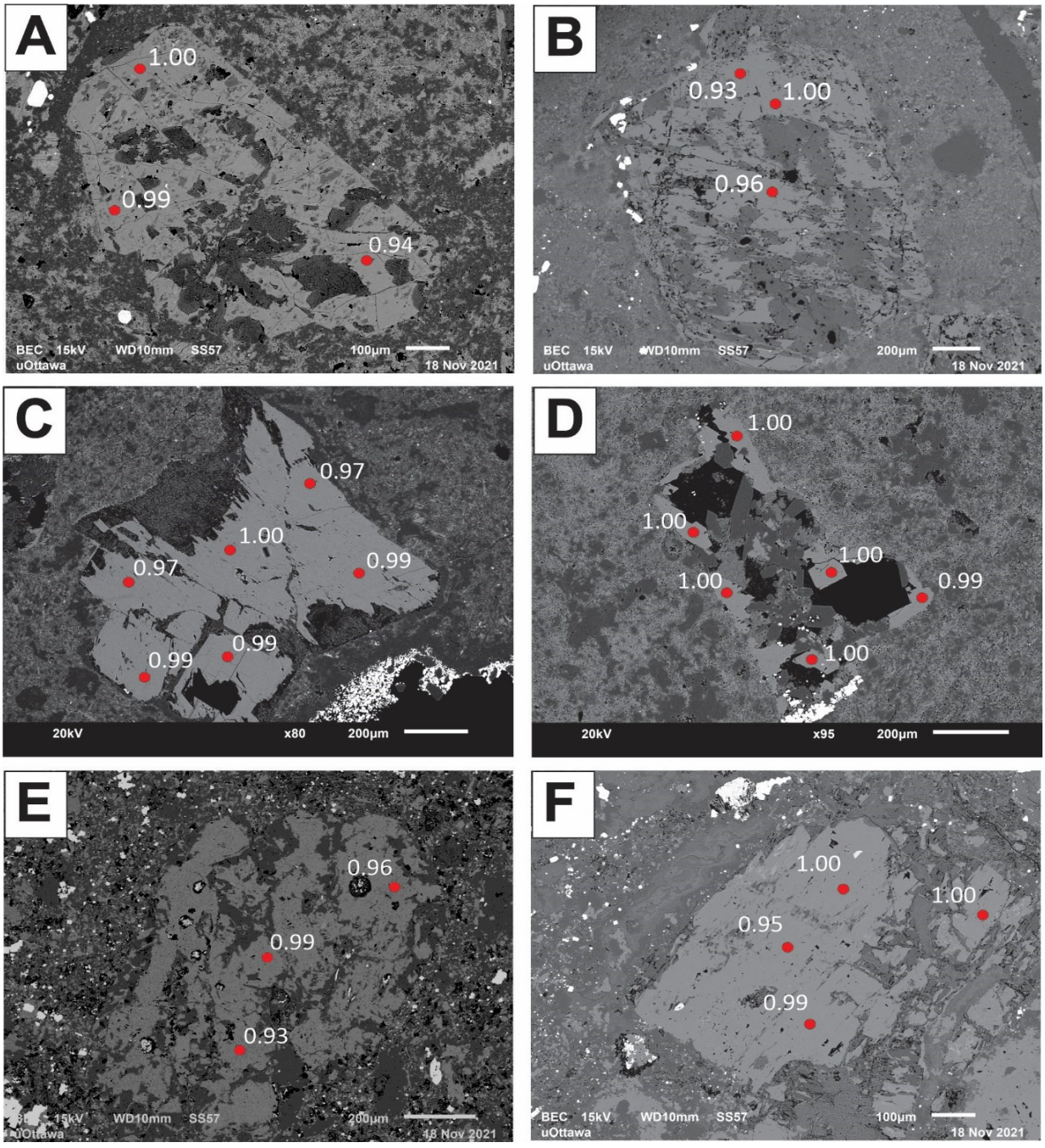

6.2 Distribution of Ammonium

All hydrothermally altered wallrock samples are enriched in ammonium (>137 ppm) compared to unaltered volcanic rocks which should contain <20 ppm NH_4^+ (e.g., Hall et al., 1994; Marty & Zimmermann, 1999). Vein samples tend to be quite low in ammonium (10 – 92 ppm) likely due to boiling where ammonium would be volatilized as NH_3 along with CO_2 and H_2 (Giggenbach, 1980). Boiling is evidenced by lattice bladed calcite / platy textures within the veins from all three deposits (Figure 6; Favona - Simpson & Mauk, 2007; Martha - Brathwaite & Faure, 2002; WKP - Ross, 2019). It is also possible that veins are low in ammonium due to low illite contents as they are made up of mainly quartz +/- adularia, and as per the previous section, adularia has been shown to have little capability of fixing ammonium. Wallrock ammonium concentrations vary widely between the deposits with many Favona samples containing much more ammonium than Martha and most of WKP.

6.2.1 Martha-Favona

At Favona, ammonium was found to occur in high concentrations (>1,000 ppm) within 100m of the Favona vein within the illite and mixed layer illite-smectite zones defined by Simpson & Mauk, 2007. This corresponds to the ammonium zone identified by SWIR spectroscopy in Simpson, 2015 (Figure 13A). Within this ammonium zone, ammonium contents in the hanging wall in the mixed layer illite-smectite zone tend to be higher (4,460 ppm NH_4^+ n = 8) than those in the footwall (2,116 ppm NH_4^+ n = 7). The highest ammonium value (10,675 ppm) occurs within the shear zone in the hanging wall (Figure 13Ab) which likely also contains the second highest sample FVN84-161 (6,501 ppm, Figure 13Aa). These samples are intensely illite-smectite altered where mixed layer illite-smectite completely overprints the adularia alteration destroying or nearly destroying the original porphyritic texture of the rock. Other than these two, the porphyritic textures have been preserved in most ammonium-rich (>1,000 ppm) samples although plagioclase phenocrysts have been completely replaced by adularia & illite +/- smectite. Samples outside of this ammonium zone are much lower in ammonium (77 – 300 ppm), although still enriched in ammonium compared to unaltered volcanic rocks (<20 ppm NH_4^+; Hall et al., 1994, 1991). These samples tend to contain smectite or have a high proportion of smectite to illite (~4:1) in the mixed layer illite-smectite based on XRD data from Simpson & Mauk, 2007 which are listed in Table 9 in Appendix D. The lack of significant illite in these samples result in low ammonium contents. Adularia appears to have little effect on fixing ammonium in these samples.

Martha and Favona are two related hydrothermal systems based on their ages, proximity, and alteration (Brathwaite & Faure, 2002; Simpson & Mauk, 2007). Favona is hosted within Upper Andesite

unit and Martha in Lower Quartz Andesite unit and therefore the host rock composition differences might influence the alteration minerals produced. The differences in alteration could also be due to temperature differences between the two deposits. Favona represents a fully vertically intact low sulfidation vein system including the overlying silica sinter on the paleosurface and hydrothermal breccia. There is a gradual tilt of the andesite units across the Waihi area where the Martha deposit would represent a deeper part of the hydrothermal system. The upper part of the Martha deposit has also presumably been eroded. The intense adularia alteration at Martha potentially reflects this deeper alteration. Favona is nearer to the paleosurface and may be lower temperature thus forming more intense illite alteration within the wallrock. Illite and smectite are temperature sensitive and are usually zoned symmetrically outwards from upflow zones (Simmons & Browne, 2000). The zonation of illite and smectite subparallel to the Favona vein may mean that the Favona vein is formed along the margin of an upflow zone occurring to the west (Simpson & Mauk, 2007). The Martha deposit presumably being more centralized in an upflow zone.

Furthermore, the Martha samples analyzed in this study came from the Martha Underground drilling project and therefore the samples were from deep (>400m below the surface) within the Martha deposit. As alteration at Martha is zoned (Brathwaite & Faure., 2002; Figure 21) these samples would be from within the deep adularia +/- minimal illite altered zone whereas the more intensely illite altered rocks would occur farther away from the mineralization. This illite rich zone would likely contain higher ammonium.

6.2.2 Wharekirauponga (WKP)

In the southern part of WKP (Figure 13Ba), we see essentially the opposite relationship as to what was seen at Favona. Ammonium values tend to be low (<200 ppm) <100m from the EG vein and high (400 – 2,800 ppm) >100-200m away from the EG vein. The samples proximal (~100m) to the vein are the intensely adularia altered rhyolite flow dome samples (e.g., Figure 9e) which contain very little illite. The low ammonium in this intense adularia alteration zone surrounding the EG vein could be either due to the fact adularia does not as easily incorporate ammonium or that ammonium is rather lost during boiling. Boiling is common within these upwelling zones along the mineralized fluid conduit. Adularia as well as calcite is produced along these conduits where permeability is high and fluid flow in unimpeded (Simmons & Browne, 2000). As there is a loss of ammonium during boiling and the formation of adularia, ammonium would not be able to be incorporated into the adularia. Illite on the

other hand is produced away from the upflow zone where ammonium would not be volatilized and thus it would be able to be incorporated into the illite.

Away from the vein, samples tend to become much more illite +/- mixed layer smectite rich and contain much higher ammonium. Many of these intensely illite altered rocks are mainly lapilli tuff samples occurring above the rhyolite domes (e.g., Figure 9f), although, some may be rhyolite flow dome samples where the intense illite alteration has destroyed any identifiable features; especially within the footwall of the EG vein. Out of the samples from the southern part of the EG vein, the near surface (<100m downhole depth) lapilli tuff samples from DDH WKP42 contain the highest ammonium (<800 ppm). However, in the north (Figure 13Bb), the two samples from DDH WKP78 occur proximal (<100m) to the EG vein (358m and 394m downhole depth) and are the highest and second highest in ammonium (1,581 ppm and 2,783 ppm). These are two of the most intensely illite altered samples. They may be either from a rhyolite flow dome or the lapilli tuff unit but any identifiable features in the original rock have been destroyed by the intense illite alteration. Therefore, the distribution of the ammonium seems to not depend on proximity to the mineralization but rather more corresponds to the distribution of illite and illite alteration intensity.

6.2.3 Fluid-Wallrock Interaction

Generally, in low sulfidation epithermal gold systems, there tends to be a zonation of alteration based on the ratio of water to rock during the alteration, temperature, and permeability (Simmons & Browne, 2000). A central upflow zone >250°C has high water to rock ratios. This zone produces a quartz, adularia, albite, chlorite, pyrite, calcite, and minor illite assemblage. Fluid-dominated conditions extend upwards along the permeable fluid conduits where there is cooling due to boiling. This produces silica, adularia, and calcite alteration along these upwelling zones. At shallow depths and along the periphery water/rock ratios decrease and hydrothermal fluids mix with groundwaters to produce illite, smectite, kaolinite, and calcite due to cooling (Simmons & Browne, 2000). In this area illite is produced rather than adularia due to lower temperatures and / or lower K/H of the fluids. The distribution of adularia and illite are especially sensitive to pH-controlled CO_2 gradients around these hydrothermal systems (Browne & Ellis, 1970). Smectite would form at lower temperatures farthest from the upwelling zone.

This distribution of alteration minerals, adularia occurring in the central upflow zone with illite and / or smectite towards the margins, occurs at WKP but not necessarily at Favona. At Favona, wallrock is intensely illite and / or smectite altered proximal to the Favona vein and contains very little adularia due to the overprinting of adularia by illite. Here, the illite alteration likely occurred at lower K/H ratios

in the fluid than WKP due to being hosted in andesite rather than rhyolite. Simpson & Mauk (2007) theorize that the upwelling zone may occur associated with veins and/or a shear zone to the west and the Favona vein occurs along the margin of this upwelling zone. If this is the case, then the adularia rich upwelling zone surrounding the Favona vein would have likely been overprinted by illite +/- mixed layer smectite. It is likely during this illite overprinting event that ammonium was introduced.

6.2.4 Timing of the Ammonium Alteration

The measured contents of ammonium in all hydrothermally altered wallrock samples are high (>137 ppm) compared to unaltered volcanic rocks. The unaltered, post-mineralization, mafic dyke observed at Martha is not enriched in ammonium (<10 ppm NH_4^+). Therefore, ammonium was introduced by hydrothermal fluids at all three deposits.

The timing of the illite alteration is important to understand as ammonium is mostly hosted by illite. Illite commonly overprints the adularia, especially at Favona, and therefore occurs later then adularia. The illite likely formed either by cooling of the hydrothermal fluids over time or rather during a secondary hydrothermal event. It is unsure whether the ammonium was only introduced during this later event or if ammonium was always within the system and just preferentially incorporated into the illite rather than the adularia. Since ammonium seems to be preferentially incorporated into illite rather than adularia it seems most likely ammonium was always present in the fluids and just incorporated into illite rather than the adularia.

There is also a positive correlation of ammonium with sulfur (Figure 15c) and arsenic (Figure 15d) which indicates that ammonium was introduced coeval to arsenic-bearing pyrite since pyrite is the sole sulfide in the wallrock. Simpson & Mauk, 2007 show that pyrite was introduced during the early adularia alteration as well as overlapping into the same timing as the illite overprint. This could indicate that ammonium was in the fluids during the early alteration phases as well as during the illite overprint. This correlation with pyrite also indicates ammonium was likely transported by the sulfur-rich auriferous fluids as pyrite crystallization is related to the introduction of Au. Although, ammonium likely had little to no role in transporting the Au as Mei et al., 2020 has shown that Au is only carried by ammonium in small amounts in near-neutral to alkaline reduced sulfur-bearing fluids. Therefore, naturally in these systems, Au would not be carried by an ammonium ligand but rather by sulfur.

Figure 21. *Cross-section schematic from Brathwaite & Faure, 2002 showing distribution of alteration minerals at the Martha deposit. I/S= mixed layer illite-smectite.*

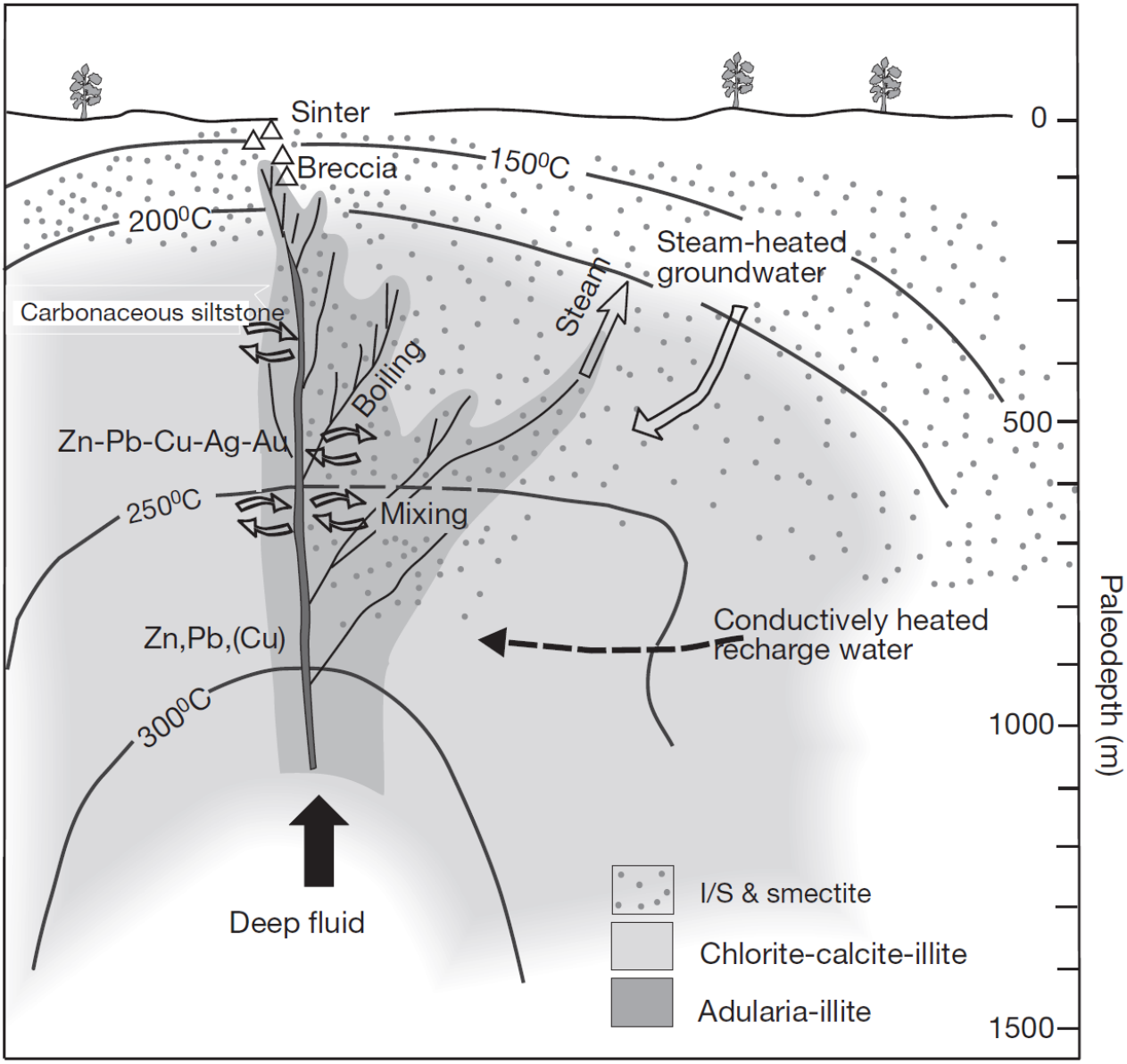

6.3 Source of the ammonium

Nitrogen isotope values range between +0.5‰ and +8.1‰ which falls within the range for sediments and low-grade metasedimentary rocks (Pitcairn et al., 2005). Most samples fall within the range for sediments or within low end of the low-grade metasedimentary rock field (Figure 22). The Jurassic greywacke basement is most likely the low-grade metasedimentary source as it has been metamorphosed to the prehnite-pumpellyite facies (Woldemichael & Black, 2002). It is thought to underlie the entirety of the Coromandel peninsula and presumably underlies all three deposits though this unit has never been drilled at Waihi or WKP. Furthermore, at Waihi, intercalated within the andesitic rocks there are widespread thin carbonaceous sedimentary lake beds which are commonly found at multiple levels (Brathwaite & Faure, 2002). Hydrothermal fluids may have interacted with either or both units which would have provided ammonium to the fluids. This interaction of the fluids with sedimentary rocks likely creates a reducing environment which promotes the leaching of ammonium from the sediments and retention of ammonium within the fluids.

Favona samples tend to plot primarily within the sedimentary source in Figure 22 whereas WKP and Martha samples plot more towards a metasedimentary source. It is possible that at Favona there is more of an influence of a nearby intercalated sedimentary source than at Martha or WKP. This could be why ammonium contents tend to be higher at Favona than the other two deposits. However, there are also known intercalated carbonaceous sediments at Martha and ammonium contents are still quite low in those samples. Furthermore, the average value for each of the three deposits is very similar (Favona +4.7‰, WKP +5.3‰, Martha, +5.0‰). This may indicate that all three deposits have a similar source.

Many low sulfidation epithermal deposits elsewhere in the world which contain ammonium are also underlain by a metasedimentary basement or are hosted in metasedimentary rocks. For example, El Zapote, Mexico (Hattori et al., 2019) and Esquel, Argentina (Soechting et al., 2008) both form within volcanic rocks which overlie a metasedimentary basement which are often organic rich such as the Piltriquitron black shale at Esquel. Some may also be fully or partially hosted in metasedimentary rocks such as Hishikari, Japan (Izawa et al., 1990) which is hosted in the Cretaceous Shimanto Shale. Where analyzed, these deposits also show similar $\delta^{15}N$ values to the Martha, Favona and WKP deposits (+1 – +9 at El Zapote from Hattori et al., 2019; -4.9 – +11.2 at Hishikari, Japan from Kristoffersen, 2019). Heated ascending / circulating hydrothermal fluids likely interacted with the metasedimentary basement complexes which provided the ammonium. Nitrogen having been sourced from organic matter which has been fixed in the rocks as ammonium (Stevenson, 1962). As there is a correlation of the ammonium

contents with sulfur and arsenic it is possible that sulfur, arsenic, and ammonium were all derived from the same sedimentary or low-grade metasedimentary source. Sedimentary rocks contain elevated As and S compared to igneous rocks. The presence of mercury could also indicate a sedimentary source though this was not analyzed for.

Many active geothermal systems in New Zealand contain ammonia within the fluids and steam discharged from the wells. These systems are all either hosted in volcanic rocks which overlie the greywacke basement (e.g., Wairakei, Broadlands) or hosted by the greywacke basement (e.g., Kawerau, Ngawha). Giggenbach, 1980 analyzed the compositions of steam discharged from various geothermal systems within the TPZ (Wairakei, Broadlands, and Kawerau). It was found that ammonia within the produced steam was higher at Wairakei (7.2 – 35.7 mmol/mol) than at Kawerau (3.4 – 9.1 mmol/mol) and Broadlands (1.3 – 4.5 mmol/mol). Kawerau is hosted solely within the greywacke basement which means that all ammonium in this system was sourced from the metasedimentary host rocks. The Ngawha geothermal system in Northland, New Zealand which is also hosted solely within the greywacke basement was shown in Sheppard, 1987 to contain similar concentrations of ammonia (3.3 – 12.0 mmol/mol) within the steam to Kawerau 100 – 293 ppm ammonium within the fluids. Overall, this data shows that the metasedimentary basement is able to provide significant amounts of ammonium and is therefore likely the source of ammonium at Favona, Martha, and WKP, although it is probable that there is also some contribution of ammonium by intercalated sediments within the volcanic rocks.

Figure 22. Plot of nitrogen isotopes ($\delta^{15}N$) vs ammonium (NH_4^+) contents. Shows the fields for sediments and low-grade metasedimentary rocks. Fields are from Pitcairn et al., 2005.

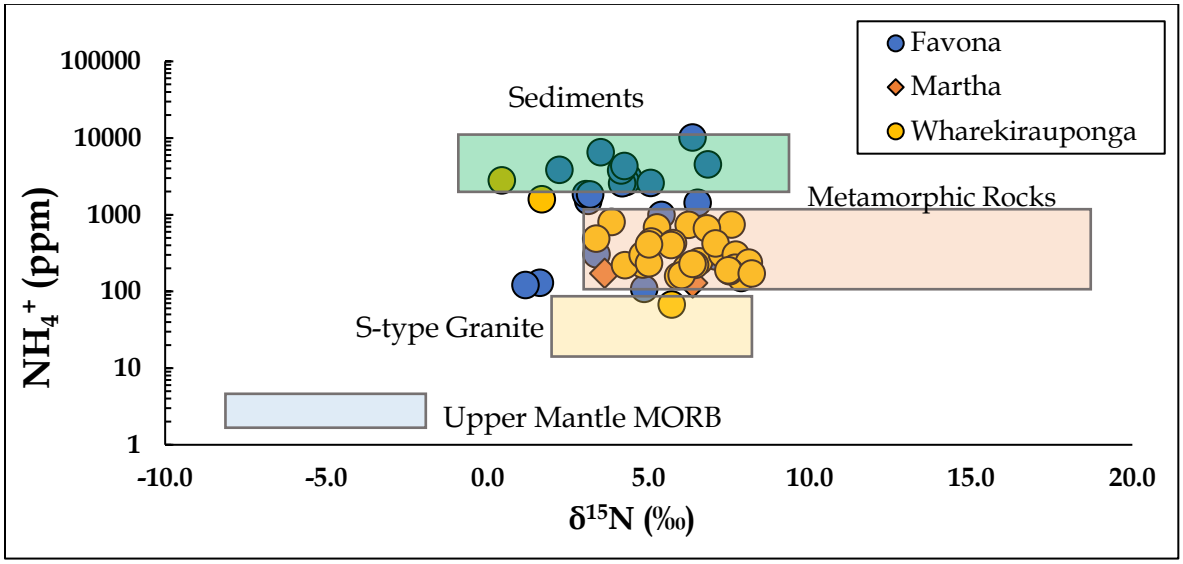

6.4 Reflectance Spectroscopy of Ammonium

6.4.1 Background on VNIR / SWIR Reflectance Spectroscopy

Reflectance spectroscopy is a non-destructive method which can be used to identify various common hydrothermal alteration minerals (Clark et al., 1990). Portable reflectance spectrometers use short-wave infrared (SWIR) and the visible/near-infrared (VNIR) light for the mapping of the alteration halos of epithermal deposits (e.g., Soechting et al., 2008; Mugas Lobos et al., 2018; Carrino et al., 2015) due to their portability, minimal sample preparation, and ability to quickly identify alteration minerals (Simpson & Rae, 2018).

Samples used for this study were analyzed using a handheld ASD TerraSpec 4 Hi-ReS Mineral Spectrometer on drill core by Mark Simpson for the Favona samples and by OceanaGold for the WKP samples. The spectra were then interpreted by Mark Simpson. The Favona data are published in Simpson, 2015. Selected spectra from Favona are available in Appendix C. WKP spectral data are published in Simpson, 2018. Selected spectra for WKP are available in Appendix C as well as a spectra interpretation results table by Mark Simpson for the WKP42 spectral chip samples.

6.4.2 Ammonium in SWIR

Ammonium produces absorption features at ~1560nm, ~2020nm, and ~2120nm (Krohn and Altaner, 1987) which are commonly used to identify the presence of ammonium (Soechting et al., 2008). Buddingtonite was shown by Erd et al. (1964) to produce absorption features at ~2120nm, ~2020nm, 1914nm, and ~1560nm. Figure 23 shows a reference reflectance pattern for buddingtonite from Simpson, 2015. Ammonium-bearing illite has a similar absorption pattern as buddingtonite with an additional absorption feature at the ~2200nm Al-OH band (Figure 23). A pattern produced for a sample containing both buddingtonite and illite is similar to that for ammonium illite (Simpson, 2015). Therefore, identification of buddingtonite based on SWIR spectra for such rocks is difficult.

Figure 23. *Representative reflectance profiles / patterns for samples from Favona acquired and interpreted by Mark Simpson. Shows location of ammonium features at ~2000nm and ~2120nm in ammonium illite. Includes a buddingtonite reference profile. The buddingtonite pattern may show a slight Al-OH feature due to the presence of illite and / or smectite within samples used to identify buddingtonite. From Simpson, 2015.*

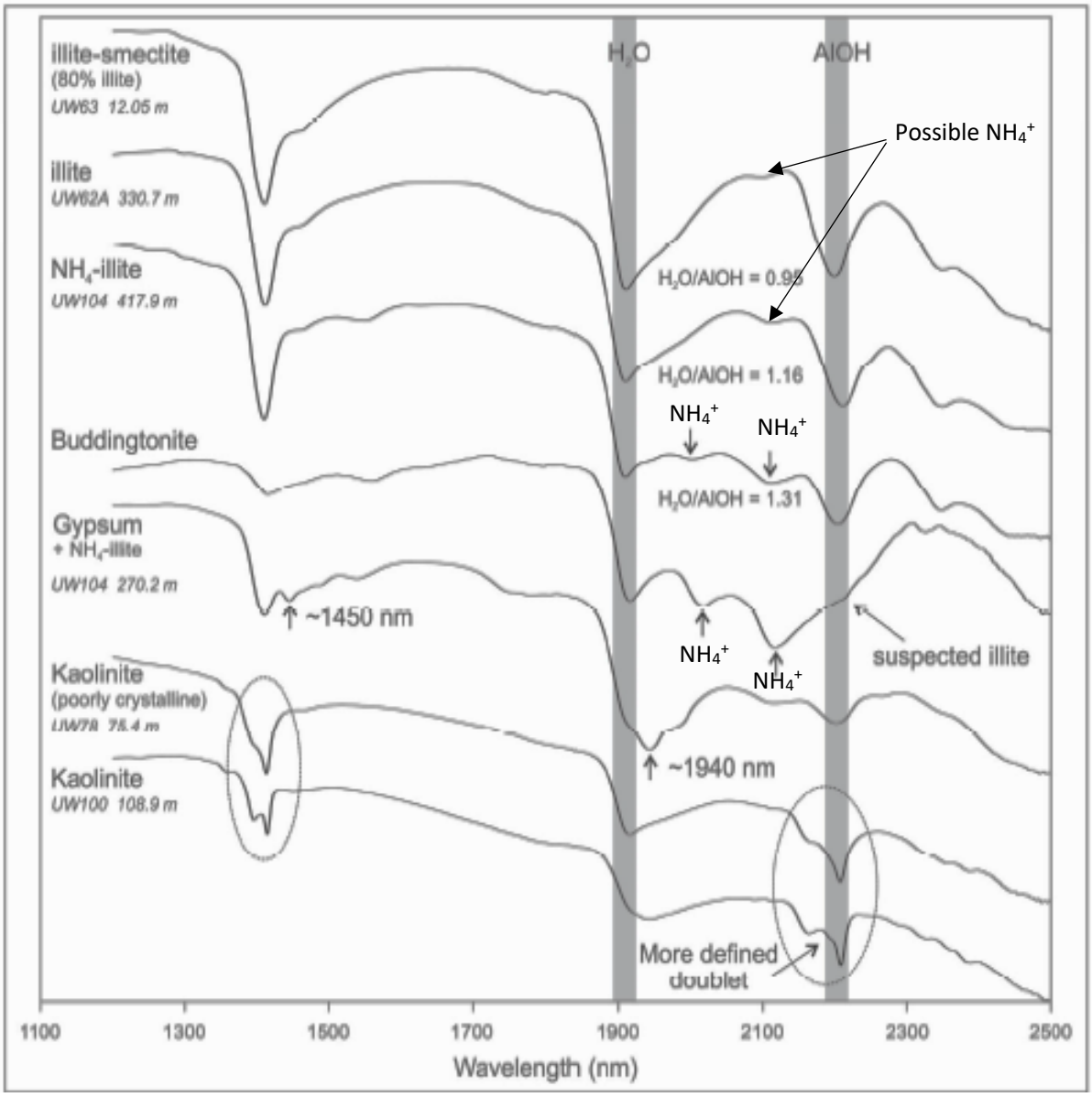

6.4.3 Quantifying Ammonium

Felzer et al (1994) showed that the amount of ammonium in a sample is positively correlated with the degree of the ~2120nm absorption feature in samples containing buddingtonite. This is consistent with the illite-bearing samples from Favona but only amongst samples which have the same mineralogy, colour, textures, and grain size (Figure 24). These samples all have similar SWIR patterns and thus the degree of the absorption is related to the concentration of ammonium. Samples which do not have the same mineralogy will have a different absorption pattern and have a different degree of absorption at ~2120nm. For example, the SWIR pattern of a sample containing a chlorite-illite-adularia (Figure 24d) assemblage will not be comparable to that of a sample with an illite-adularia assemblage (Figure 24a, b, c). This also holds true when comparing samples with different grain size or texture. Grain size affects the amount of light scattered and absorbed (Clark, 1999). Different textures or varying grain sizes will also cause colour differences which results in varied SWIR patterns. Furthermore, only samples of the same lithology should be compared. For example, an andesite flow sample containing ammonium illite should only be compared to another andesite flow sample also containing ammonium illite. Quantitatively comparing the spectra between the rhyolites at WKP and andesites at Favona is difficult and may result in varying detection limits of ammonium between the deposits. Some minerals such as kaolinite, smectite, and jarosite have been shown by Felzer et al. (1994) to affect the quantification of ammonium by suppressing the 2120nm ammonium band. This suppression effect is thought to also occur in samples with a strong absorption at the 2200 Al-OH band (Felzer et al., 1994). Alternatively, minerals such as chlorite will affect the colour of the sample and thus affect the SWIR pattern.

6.4.4 Favona

Simpson, 2015 identified an ammonium rich zone in SWIR surrounding the Favona vein (Figure 2). Mark Simpson interpreted ammonium illite patterns and / or overlapping patterns of buddingtonite and illite occurring together within this zone. We have shown ammonium is hosted by the illite. Furthermore, all samples within this ammonium rich zone contain high (>1,000 ppm) ammonium (Figure 13). This sets a broad detection limit of ammonium at Favona of ~1,000 ppm where all samples above 1,000 ppm NH_4^+ had ammonium detected and all samples below 1,000 ppm NH_4^+ did not have ammonium detected. This detection limit would likely vary between localities as varying lithologies and alteration types affect the colour and grain size of the sample which could suppress or intensify the ammonium absorption features. At Favona, the andesite can be quite dark coloured which would reduce reflectance and not allow for proper light absorption thus suppressing the ammonium features.

This may mean this detection limit of 1,000 ppm is high compared to other localities. However, a ~1,000 ppm detection limit was also shown at El Zapote, Mexico (Hattori et al., 2020).

***Figure 24**. Comparison of reflectance spectroscopic patterns to bulk rock ammonium contents for illite bearing samples from Favona. The 2120nm absorption feature is the most prominent of the ammonium absorption bands and therefore used for this comparison. All samples show patterns for illite. Patterns were acquired and interpreted by Simpson, 2015. All samples contain illite and adularia identified by XRD (from Simpson & Mauk, 2007). Sample D contains chlorite.*

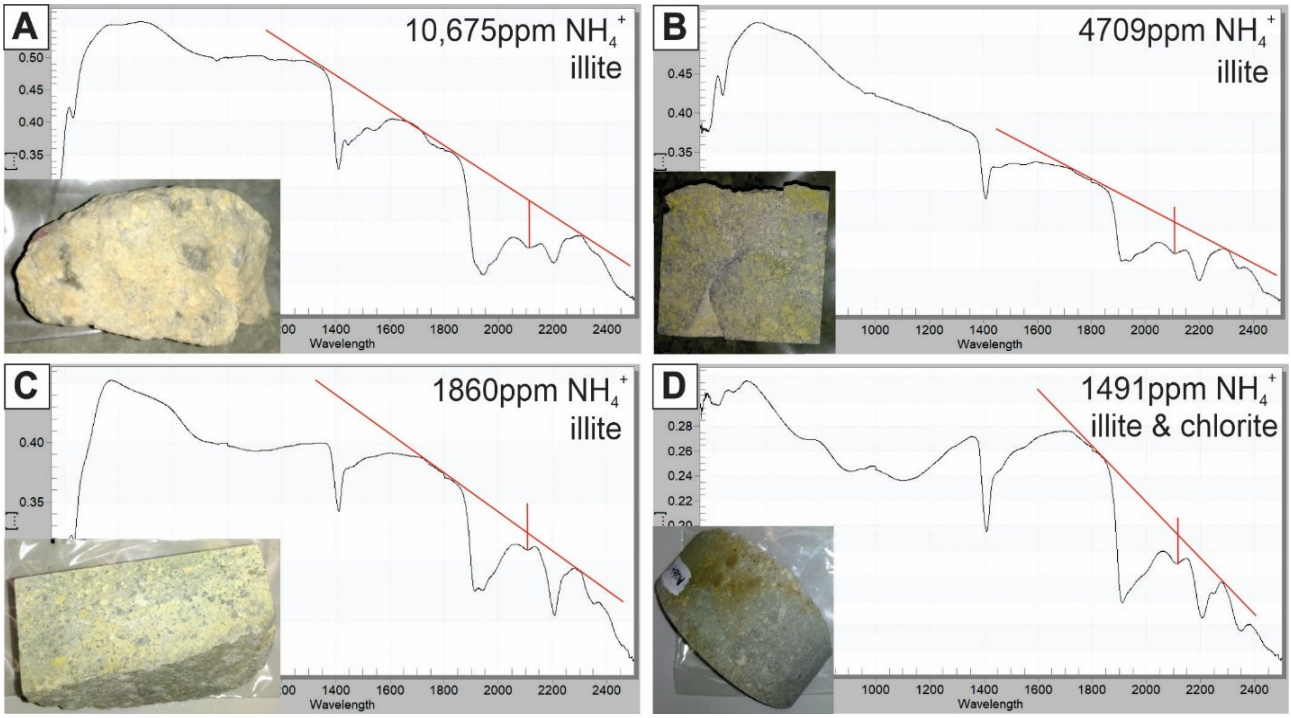

6.4.5 WKP

In the case of WKP, ammonium was commonly detected in SWIR by Simpson, 2018, but neither the SWIR data nor the bulk ammonium contents seem to show an ammonium zone surrounding the vein. There also seems to be no consistency of where ammonium was detected in SWIR (by Simpson, 2018) with the ammonium of contents of the rocks. Looking at DDH WKP42, ammonium was more often detected in SWIR at the shallow parts of the deposit which does generally correspond to the areas with higher ammonium values (400 – 800 ppm) and less often in the deeper parts which corresponds to lower ammonium values (<300 ppm). However, on a sample-by-sample basis many samples which had no ammonium (e.g., WKP42-46 & WKP42-74) had moderate ammonium values (740 ppm & 800 ppm respectively). On the other hand, some samples where ammonium was detected (e.g., WKP42-56 & WKP42-59) did have moderate ammonium contents (736 ppm & 658 ppm respectively) but others (e.g., WKP42-80 & WKP42-103) had quite low ammonium (245 ppm & 306 ppm respectively). There appears

to be no real consistency with the detection limit. This could be because the varying lithology, mineralogy, colour, and grain size between samples alters the overall absorption suppressing the ammonium features which changes the ammonium detection limit.

Unlike Favona, reflectance patterns at WKP commonly appear for either buddingtonite or ammonium illite (Simpson, 2018). For example, sample WKP42-124 was interpreted by Mark Simpson to contain buddingtonite based on the SWIR pattern (Appendix D). This sample contains abundant adularia with less abundant illite and jarosite based on SEM-EDS (Appendix B). Adularia is common in both the groundmass and altered feldspar phenocrysts. In most phenocrysts adularia has been overprinted by illite and jarosite although some adularia altered feldspar phenocrysts remain unaltered by illite. The adularia altered phenocrysts show K/Al ratios of ~0.97 – 1.0 (Figure 20c) meaning only up to 3% of the potassium within the adularia could be replaced by ammonium. The minimal amount of ammonium within the adularia could account for some of the ammonium but it is likely the illite hosts most of ammonium within this sample. The lack of jarosite identified by Simpson, 2018 in the SWIR pattern for WKP42-124 could be due to the fact the jarosite is quite localized and was likely not present on the surface which was analyzed. This shows us that localized ammonium minerals might not always be detected as they are not near the surface that was analyzed. Overall, all K/Al ratios in adularia from samples from all three deposits (Figure 20) are near 1. This indicates that there is little to no substitution of ammonium in adularia in any of the samples. Even for those that had buddingtonite detected by reflectance spectroscopy.

6.4.6 Martha

Significant ammonium has never been identified at Martha in a variety of SWIR spectroscopy studies (e.g., Bodger, 2015). Due to this, it was expected that there would not be any ammonium in the wallrock. This study found that there was ammonium in the hydrothermally altered wallrock, though values are low (<200ppm NH_4^+) compared to Favona or WKP. These values appear to be below the detection limit of SWIR spectroscopy which is likely why ammonium had never been detected. The samples at Martha contain very little illite which may explain why values are low. As illite appears to be the host of most of the ammonium, minimal illite means that the wallrock is unable to fix significant amounts of ammonium. Other deposits elsewhere in the world which have not had ammonium detected may also contain ammonium in the hydrothermal alteration but in concentrations below the detection limit of SWIR spectroscopy.

Chapter 7 | Summary and Conclusions

7.1 Summary

It was found that all hydrothermally altered wallrock samples were enriched in ammonium (137 – 10,675 ppm) in comparison to unaltered volcanic rocks. Most (>73%) of the ammonium occurs within the crystal structure of illite at all three deposits. This interpretation is supported by positive correlations of ammonium contents with potassium, loss on ignition, and illite abundances. Some (<5% for most samples) of the ammonium occurs as adsorbed ammonium likely within smectite and/or chlorite. Wallrock samples at Favona are intensely illite altered and contain high ammonium values (<10,675 ppm). Ammonium is high (>1000 ppm) within 100m of the Favona vein within the ammonium zone identified by Simpson, 2015. Samples outside of this zone had less than 300 ppm NH_4^+. The data suggests a detection limit of ammonium in SWIR at Favona of about 1000 ppm. At WKP, ammonium values are higher (400 – 800 ppm) >100m from the EG vein and low (<200 ppm) <100m from the EG vein. The distribution of ammonium coincides with that of illite and the intensity of the illite alteration rather than the proximity to mineralization. In general, samples with abundant illite contain high ammonium and those with abundant adularia are low in ammonium. The Martha samples are rich in adularia with minor illite and contain low ammonium (<200 ppm). The low values at Martha explain why there has been no detection of ammonium using SWIR spectroscopy.

Based on $\delta^{15}N$ values ranging from about +1 – +8‰ the source of the ammonium is likely the metasedimentary greywacke basement and / or intercalated carbonaceous sediments within the host volcanic rocks. Many deposits elsewhere in the world which contain ammonium in their alteration halos also are hosted in or above a metasedimentary basement complex, such as Esquel, Argentina, Hishikari, Japan, or El Zapote, Mexico, or have intercalated sediments within the host volcanic rocks.

Since colour, texture, mineralogy, and grain size tend to affect the SWIR pattern, the quantity of ammonium is only correlated with absorption depths of 2120nm feature in similar samples. These factors likely also affect the detection limit of ammonium between samples.

Buddingtonite is often reported based on SWIR spectroscopy in many deposits including the studied deposits. The K/Al ratios of adularia in our samples show that ammonium in adularia is negligible in the overall budget of ammonium in the rocks.

7.2 Ammonium in SWIR as a Mineralization Pathfinder

Ammonium has been suggested to be useful to identify mineralized hydrothermal systems (e.g., Simpson, 2015, Hattori et al., 2019). This study showed that the distribution of ammonium around auriferous veins corresponds to the distribution of illite and illite alteration intensity. Therefore, the presence of ammonium does not necessarily depend on the proximity to the mineralization but rather the presence of illite alteration, which can vary in proximity to mineralization depending on factors such as temperature or fluid composition. Therefore, ammonium in SWIR likely corresponds to the presence of illite alteration rather than proximity to mineralization. However, this may depend on whether a buddingtonite or ammonium illite is identified. Although, this is complicated by the fact that these patterns likely overlap.

Furthermore, the detection limit of ammonium in SWIR spectroscopy varies depending on a variety of factors, therefore, it is important when using ammonium in SWIR as vector to only compare similar samples. Finally, ammonium alteration was shown to extend beyond the zones where it was identified by SWIR thus identifying this ammonium enriched zone may be useful to extend the footprint of the auriferous hydrothermal system. Since SWIR is unable to identify ammonium at these low concentrations, samples could be analyzed for ammonium contents in a laboratory for a relatively low cost.

7.3 Future Work

Future work should be focused on comparing ammonium contents and host minerals to SWIR spectral patterns with a focus on differentiating ammonium-illite and buddingtonite patterns. One should also build a better understanding of the factors which affect the ammonium absorption features, and thus the detection limit, to better use ammonium as mineralization pathfinder.

It would also be interesting look at wallrock ammonium contents in deposits elsewhere in the world which have not had ammonium detected with SWIR. It is possible, similarly to Martha, that ammonium is below the detection limit of SWIR spectroscopy. If the greywacke basement underlies all three deposits in the Hauraki goldfield, then all deposits in this area likely have a source of ammonium and thus likely have ammonium that just has not been detected by SWIR. Likewise, if ammonium is low in deposits where ammonium was not detected, do they still have a possible source?

References

Adams, C.J., Graham, I.J., Seward, D., Skinner, D.N.B., Moore, P.R. (1994). *Geochronological and geochemical evolution of late Cenozoic volcanism in the Coromandel Peninsula, New Zealand*. New Zealand Journal of Geology and Geophysics, v37:3, p359-379.

Alshameri, A., He, H., Zhu, J., Xi, Y., Zhu, R., Ma, L., Tao, Q. (2018). *Adsorption of ammonium by different clay minerals: Characterization, kinetics, and adsorption isotherms*. Applied Clay Science v158, p83-93.

Baranova, N.N., Zotov, A.V. (1998). *The stability of gold sulfide species, Au(HS)(aq) and $Au(HS)^{2-}$, at 300 and 350°C and 500 bar: Experimental study*. Mineralogical Magazine, v62A, p116-117.

Bentabol, M., Ruiz Cruz, M.D. (2016). *NH_4^+ for K^+ substitution in dioctahedral mica synthesis at 200C*. Applied Clay Science v126, p268-277.

Bodger, B. (2015). *Andesite volcanic facies and hydrothermal alteration in the subsurface peripheral to existing Waihi mine workings.* University of Waikato MSc Thesis. 249 pages.

Booden, M.A., Smith, I.E.M., Mauk, J.L., Black, P.M. (2012). *Geochemical and isotopic development of the Coromandel Volcanic Zone, northern New Zealand, since 18 Ma*. Journal of Volcanology and Geothermal Research, v219-220, p15-32.

Brathwaite, R.L., Faure, K. (2002). *The Waihi Epithermal Gold-Silver-Base Metal Sulfide-Quartz Vein System, New Zealand: Temperature and Salinity Controls on Electrum and Sulfide Deposition.* Economic Geology, v97, p269-290.

Browne, P.R.L., Ellis, A.J. (1970). *The Ohaki-Broadlands geothermal area, New Zea7land*. Mineralogy and related geochemistry: American Journal of Science, v269, p97–131.

Canet, C, Hernandez-Cruz, B., Jimenez-Franco, A. Pi. T., Pelaez, B., Villanueva-Estrada, R.E., Alfonso, P., Gonzalez-Partida, E., Salinas, S. (2015). *Combining ammonium mapping and short-wave infrared (SWIR) reflectance spectroscopy to constrain a model of hydrothermal alteration for the Acoculco geothermal zone, Eastern Mexico*. Geothermics, v53, p154-165.

Carrino, T.A., Crosta, A.P., Toledo, C.L.B., Silva, A.m. (2015). *Unveiling the hydrothermal mineralogy of the Chapi Chiara gold prospect, Peru, through reflectance spectroscopy, geochemical and petrographic data*. Ore Geology Reviews, v64, p299-315.

Castendyk, D.N., Mauk, J.L., Webster, J.G. (2004). *A mineral quantification method for wall rocks at open pit mines, and application to the Martha Au-Ag mine, Waihi, New Zealand*. Applied Geochemistry, v20, p135-156

Christie, A.B., Simpson, M.P., Brathwaite, R.L., Mauk, J.L., Simmons, S.F. (2007). *Epithermal Au-Ag and Related Deposits of the Hauraki Goldfield, Coromandel Volcanic Zone, New Zealand*. Economic Geology v102, p785-816.

Christie, A.B., Simpson, M.P., Barker, R.G., Brathwaite, R.L. (2019). *Exploration for epithermal Au-Ag deposits in New Zealand: history and strategy*. New Zealand Journal of Geology and Geophysics v62, No 4, p414-441.

Christie, A.B., Soong, R. (2001). *Down-hole XRD analyses as a guide to hydrothermal alteration in the Wharekirauponga epithermal gold-silver prospect, Hauraki Goldfield, New Zealand*. Proceedings of the 34th annual conference, New Zealand Branch of the Australasian Institute of Mining and Metallurgy, p227-234.

Erd, R.C., White, D.E., Fahey, J.J., Lee. D.E. (1964). *Buddingtonite, an ammonium feldspar with zeolitic water*. American Mineralogist, v49, p831-850.

Felzer, B., Hauff, P., Goetz, A.F.H. (1994). *Quantitative reflectance spectroscopy of buddingtonite from the Cuprite mining district, Nevada*. Journal of Geophysical Research, v99, p2887-289.

Gadsby, M.R., Spörli, K.B., and Clarke, D.S. (1990). *Structural elements in epithermal gold deposits of the Coromandel peninsula, New Zealand*. Australasian Institute of Mining and Metallurgy Annual Conference, Rotorua, Proceedings, p145–151.

Giggenbach, W.F. (1980). Geothermal gas equilibria: Geochimica et Cosmochimica Acta, v.44, p. 2021–2032.

Giggenbach, W.F. (1984). *Mass transfer in hydrothermal alteration systems—A conceptual approach*. Geochimica et Cosmochimica Acta, v48, p2693–2711.

Hall, A., Stamatakis, M.G., Walsh, J.N. (1994). *Ammonium enrichment associated with diagenetic alteration in Tertiary pyroclastic rocks from Greece.* Chemical Geology, v118, p173–183.

Hall, A. Bencini, A., Poli, G. (1991). *Magmatic and hydrothermal ammonium in granites of the Tuscan magmatic province, Italy*. Geochmica et Cosmochimica Acta, v55, p3657–3664.

Hallam, M., Eugster, H.P. (1976). *Ammonium silicate ability relations*. Contributions to Mineralogy and Petrology, v57, p227-244.

Harlov, D.E., Andrut, M., Poter, B. (2001). *Characterization of tobelite and ND4-tobelite using IR spectroscopy and Rietveld refinement of XRD spectra*. Phys Chem Minerals, v28, p268-276.

Harlap, A. (2008). *Alteration and ammonium enrichment vectors to low-sulfidation epithermal mineralization: insights from the Banderas gold-silver prospect*. Unpublished Master's thesis, McGill University. 144 pages.

Hattori, K., Fonseca, A., Sheppard, T. (2020). *Ammonium abundance and short-wave infrared absorption spectra of altered rocks*. Geochemistry: Exploration, Environment, Analysis, v20(4), p451-460.

Izawa, E. Urashima, Y., Ibaraki, K., Suzuki, R., Yokoyama, T., Kawasaki, K., Koga, A., Sachichiro, T. (1990). *The Hishikari gold deposit: high-grade epithermal veins in Quaternary volcanics of southern Kyushu, Japan*. Journal of Geochemical Exploration, v36, p1-56.

Krohn, M.D., Altaner, S.P. (1987). *Near-infrared detection of ammonium minerals*. Geophysics, v52, p924-930.

Marty, B., Zimmermann, L. (1999). *Volatiles (He, C, N, Ar) in mid-ocean ridge basalts: Assessment of shallow-level fractionation and characterization of source composition*. Geochimica et Cosmochimica Acta, v63, p3619–3633.

Mateers, M.A. (2010). *Ammonium illite at the Jerritt Canyon district and Goldstrike property, Nevada: Its spatial distribution and significance in the exploration of Carlin-type deposits*. University of Wyoming Ph.D. Thesis. 228 pages.

Mauk, J.L., Hall, C.M., Chesley, J.T., Barra, F. (2011). *Punctuated Evolution of a Large Epithermal Province: The Hauraki Goldfield, New Zealand.* Economic Geology, v106, p921-943.

Mauk, J.L., Simpson, M.P., Hollinger, H., Morrell, A.E., Smith, N., Locke, C.A. and Cassidy, J. (2006b). *The Favona epithermal Au-Ag deposit, Hauraki goldfield—mineralogy, geochemistry and geophysics*. Australasian Institute of Mining and Metallurgy Monograph v25, p185–190

Maton, T., Carr, D., Townsend, D., Church, P. (March 2019). *NI43-101 Technical Report for the OceanaGold, Waihi Mine*. Technical Report published by OceanaGold. 166 pages.

Maton, T., Carr, D., Townsend, D., Church, P. (August 2020). *Waihi District Study Preliminary Economic Assessment*. Technical Report published by OceanaGold. 241 pages.

Mamo, M., Taylor, R.W., Shuford, J.W. (1993). *Ammonium fixation by soil and pure clay minerals*. Communications in Soil Science and Plant Analysis, v24, p1115-1126.

Mei, Y., Liu, W., Brugger, J., Guan, Q. (2020). *Gold solubility in alkaline and ammonia-rich hydrothermal fluids: Insights from ab initio molecular dynamics simulation*. Geochimica et Cosmochimica, v291, p62-78.

Mugas Lobos, A.C., Marquez-Zavalia, M.F., Galliski, M.A., Walle, M. (2018). The Permian-Triassic low sulfidation epithermal Au deposit of Don Sixto, Mendoza. Revista de la Asociacion Geologica Argentina, v75, p441-456.

Page, L., Hattori, K., Guillot, S. (2018). Mantle wedge serpentinites: A transient reservoir of halogens, boron, and nitrogen for the deeper mantle. Geology, v46, p883–886.

Rhys, D., Keall, P. (2008). *Structural style and controls on the Favona epithermal gold deposit, Waihi Mining District, New Zealand*. AusIMM NZ Branch Conference 2008 Paper.

Riber, J.I. (1966). *The Behavior of Thalium with Respect to Potassium and Rubidium in Coexisting Micas and Feldspars*. Unpublished Master's thesis, Rice University, Texas.

Ridgway, J., Martiny, B., Gomez-Caballero, A., Marcias-Romo, C., Villasenor-Cabral, M.G. (1991). *Ammonium geochemistry of some Mexican silver deposits*. Journal of Geochemical Exploration, v40 p311-327.

Rieder, M., Cavazzini, G., D'Yankonov, Y.S., Frank-Kamenetskii, V.A., Gottardi, G., Guggenheim, S., Koval, P.V., Muller, G., Neiva A.M.R., Radoslovich, E.W., Robert, J.L., Sassi, F.P., Takeda, H., Weiss, Z., Wones, D.R. (1998). *Nomenclature of Micas*. Clays and Clay Minerals, v46, p586-595.

Rhys, D., Keall, P. (2008). *Structural style and controls on the Favona epithermal gold deposit, Waihi Mining District, New Zealand*. AusIMM NZ Branch Conference 2008 Paper.

Rhys, D.A. (2019). *Review of the Geological Setting, Style, and Structural Controls on Mineralization at the WKP Project*. Unpublished Report Prepared for OceanaGold by Panterra Geoservices Inc. 54 pages.

Rhys, D.A., Lewis, P.D., Rowland, J.V. (2020). *Structural Controls on Ore Localization in Epithermal Gold-Silver Deposits: A Mineral Systems Approach*. Economic Geology, v21, p83-145.

Rowan, L.C., Hook, S.J., Abrams, M.J., Mars, J.C. (2003). *Mapping hydrothermally altered rocks at Cuprite, Nevada, using the advanced spaceborne thermal emission and reflection radiometer (ASTER), a new satellite imaging system*. Economic Geology, v98, p1019-1027

Rowland, J.V., Wilson, C.J.N., Gravley, D.M. (2010). *Spatial and Temporal Variations in Magmas-Assisted Rifting, Taupo Volcanic Zone, New Zealand*. Journal of Volcanology and Geothermal Research, v190, p89-108.

Seward, T.M. (1973). *Thiocomplexes of gold and the transport of gold in hydrothermal ore solutions*. Geochimica et Cosmochimica Acta, v37, p45-54.

Skinner, D.N.B. (1986). *Neogene volcanism of the Hauraki volcanic region*. Royal Society of New Zealand Bulletin 23, p21–47

Skinner, D.N.B. (1967). *Geology of the Coromandel region with emphasis on some economic aspects*. Unpublished Ph.D. thesis, Auckland, University of Auckland, 330 pages.

Smith, J.M. (2014). Controls of High Grades within the Clementine Vein System in the Hollister Low-Sulfidation Epithermal Au-Ag Deposit, NV. University of Nevada, Reno. M.Sc. Thesis. 169 pages.

Simpson, M.P., Mauk, J.L. (2007). *The Favona Epithermal Gold-Silver Deposit, Waihi, New Zealand*. Economic Geology, v102, p817-839.

Simpson, M.P. (2015). *Reflectance spectrometry (SWIR) of alteration minerals surrounding the Favona epithermal vein, Waihi vein system, Hauraki Goldfield*. Proceedings of the 48th annual conference, New Zealand Branch of the Australasian Institute of Mining and Metallurgy, p409-418.

Simpson, M.P. (2018). *Hyperspectral (SWIR) characterization of alteration at the Wharekirauponga epithermal Au-Ag prospect, Hauraki Goldfield, New Zealand*. Proceedings of the 49th annual conference, New Zealand Branch of the Australasian Institute of Mining and Metallurgy, p287-293.

Simpson, M.P., Rae, A.J. (2017). *Short-wave infrared (SWIR) reflectance spectrometric characterisation of clays from geothermal systems of the Taupō Volcanic Zone, New Zealand*. Geothermics, v73, p74-90.

Simpson, M.P., Christie, A.B. (2019). *Hydrothermal alteration mineralogical footprints for New Zealand epithermal Au-Ag deposits*. New Zealand Journal of Geology and Geophysics v62, No4, p483-512.

Simpson, M.P., Gazley, M.F., Stuart, A.G.J., Pearce, M.A., Birchall, R., Chappell, D., Christie, A.B., Steven, M.R. (2019). *Hydrothermal Alteration at the Karangahake Epithermal Au-Ag Deposit, Hauraki Goldfield, New Zealand*. Economic Geology, v114 no. 2, p243-273.

Simmon, S.F., Browne, P.R.L. (2000). *Hydrothermal Minerals and Precious Metals in the Broadlands-Ohaaki Geothermal System: Implications for Understanding Low-Sulfidation Epithermal Environments*. Economic Geology, v95, p971-999.

Simmons, S.F., White, N.C., John, D.A. (2005). *Geological Characteristics of Epithermal Precious and Base Metal Deposits*. Economic Geology, 100th Anniversary Volume, p485-522.

Soechting, W., Rubenstein, N., Godeas, M. (2008). *Identification of Ammonium-Bearing Minerals by Short-Wave Infrared Spectroscopy at the Esquel Gold Deposit, Argentina*. Economic Geology, v103, p865-869.

Spectral Evolution. (2020). *Buddingtonite as a Pathfinder Mineral for Gold and Silver.* Identifying Buddingtonite. Retrieved May 26, 2022, from https://spectralevolution.com/applications/mining/identifying-buddingtonite/.

Stevenson, F.J. (1962). *Chemical state of nitrogen in rocks*. Geochimica et Cosmochimica Acta, v26, p797-809.

Travers, S.J., Wilson, C.J.L. (2015). *Reflectance spectroscopy and alteration assemblages at the Leven Star gold deposit, Victoria, Australia*. Australian Journal of Earth Sciences, v62, p873-882.

Voncken, J.H.L, Van Roermund, H.L.M., Van Der Eerden, A.M.J., Jansen, J.B.H., Erd, R.C. (1993). *Holotype buddingtonite: An ammonium feldspar without zeolitic H_2O*. American Mineralogist, v78, p204-209.

Warren, I., Simmons, S.F., Mauk, J.L. (2007). *Whole-Rock Geochemical Techniques for Evaluating Hydrothermal Alteration, Mass Changes, and Compositional Gradients Associated with Epithermal Au-Ag Mineralization*. Economic Geology v102, p923-948.

Appendix A | Data Tables

Table 1. List of Samples. Sample IDs are FVN, MTA, or WKP followed by DDH number and DDH Depth. A "V" at the end of the label denotes a vein sample.

Our ID	Deposit	Drill Hole	Depth (m)	Sample Type	Rock Type		Our ID	Deposit	Drill Hole	Depth (m)	Sample Type	Rock Type
Martha - Favona							WKP					
FVN063-12	Favona	UW63	12.0	Core Cut	Wallrock		WKP42-26	WKP EG Vein	42	26.0	Core Chip	Wallrock
FVN063-80	Favona	UW63	80.7	Core Cut	Wallrock		WKP42-46	WKP EG Vein	42	46.0	Core Chip	Wallrock
FVN063-88V	Favona	UW63	88.5	Core Cut	Vein		WKP42-51.7	WKP EG Vein	42	51.7	Core Chip	Wallrock
FVN063-117V	Favona	UW63	117.3	Core Cut	Vein		WKP42-56.3	WKP EG Vein	42	56.3	Core Chip	Wallrock
FVN063-135	Favona	UW63	135.6	Core Cut	Wallrock		WKP42-59	WKP EG Vein	42	59.0	Core Chip	Wallrock
FVN063-180	Favona	UW63	180.9	Core Cut	Wallrock		WKP42-68	WKP EG Vein	42	68.0	Core Chip	Wallrock
FVN063-185V	Favona	UW63	185.8	Core Cut	Vein		WKP42-74.2	WKP EG Vein	42	74.2	Core Chip	Wallrock
FVN63-226.8	Favona	UW63	226.8	Core Cut	Wallrock		WKP42-75.5	WKP EG Vein	42	75.5	Core Chip	Wallrock
FVN69-62.1	Favona	UW69	62.1	Core Cut	Breccia		WKP42-80.3	WKP EG Vein	42	80.3	Core Chip	Wallrock
FVN69-101.2	Favona	UW69	101.2	Core Cut	Breccia		WKP42-103.9	WKP EG Vein	42	103.9	Core Chip	Wallrock
FVN69-135.1	Favona	UW69	135.1	Core Cut	Wallrock		WKP42-118.2	WKP EG Vein	42	118.2	Core Chip	Wallrock
FVN69-194.0	Favona	UW69	194.0	Core Cut	Wallrock		WKP42-119.8	WKP EG Vein	42	119.8	Core Chip	Vein
FVN69-249.0	Favona	UW69	249.0	Core Cut	Wallrock		WKP42-124	WKP EG Vein	42	124.0	Core Chip	Wallrock
FVN69-292.5	Favona	UW69	292.5	Core Cut	Wallrock		WKP42-142.1	WKP EG Vein	42	142.1	Core Chip	Wallrock
FVN84-91.0	Favona	UW84	91.0	Core Cut	Wallrock		WKP42-162	WKP EG Vein	42	162.0	Core Chip	Wallrock
FVN84-161.7	Favona	UW84	161.7	Core Cut	Wallrock		WKP42-174	WKP EG Vein	42	174.0	Core Chip	Wallrock
FVN84-202.9	Favona	UW84	202.9	Core Cut	Wallrock		WKP42-196	WKP EG Vein	42	196.0	Core Chip	Wallrock
FVN84-228.4	Favona	UW84	228.4	Core Cut	Wallrock		WKP42-225.7	WKP EG Vein	42	225.7	Core Chip	Wallrock
FVN84-285.5V	Favona	UW84	285.5	Core Cut	Vein		WKP42-245.1	WKP EG Vein	42	245.1	Core Chip	Wallrock
FVN84-316.4	Favona	UW84	316.4	Core Cut	Wallrock		WKP42-277.4	WKP EG Vein	42	277.4	Core Chip	Wallrock
FVN84-365.9	Favona	UW84	365.9	Core Cut	Wallrock		WKP42-313.5	WKP EG Vein	42	313.5	Core Chip	Wallrock
FVN84-421.7	Favona	UW84	421.7	Core Cut	Wallrock		WKP42-397	WKP EG Vein	42	397.0	Core Chip	Wallrock
FVN85-85.7	Favona	UW85	85.7	Core Cut	Breccia		WKP42-522.5	WKP EG Vein	42	522.5	Core Chip	Wallrock
FVN85-114.3	Favona	UW85	114.3	Core Cut	Wallrock		WKP42-553.2	WKP EG Vein	42	553.2	Core Chip	Wallrock
FVN85-226.6	Favona	UW85	226.6	Core Cut	Wallrock		WKP42-573.6	WKP EG Vein	42	573.6	Core Chip	Wallrock
FVN85-338.5	Favona	UW85	338.5	Core Cut	Wallrock		WKP42-604.8	WKP EG Vein	42	604.8	Core Chip	Wallrock
FVN85-404.3	Favona	UW85	404.3	Core Cut	Wallrock		WKP44-540.0	WKP EG Vein	44	540.0	Core Chip	Wallrock
FVN87-211.0	Favona	UW87	211.0	Core Cut	Wallrock		WKP44-554.0	WKP EG Vein	44	554.0	Core Chip	Wallrock
FVN87-251.8	Favona	UW87	251.8	Core Cut	Wallrock		WKP44-564.0	WKP EG Vein	44	564.0	Core Chip	Wallrock
FVN87-299.6	Favona	UW87	299.6	Core Cut	Wallrock		WKP44-607.0	WKP EG Vein	44	607.0	Core Chip	Wallrock
FVN87-337.6	Favona	UW87	337.6	Core Cut	Wallrock		WKP44-628.0	WKP EG Vein	44	628.0	Core Chip	Wallrock
FVN87-346.7V	Favona	UW87	346.7	Core Cut	Vein		WKP44-641.0	WKP EG Vein	44	641.0	Core Chip	Wallrock
FVN104-103	Favona	UW104	103.4	Core Cut	Wallrock		WKP44-695.0	WKP EG Vein	44	695.0	Core Chip	Wallrock
FVN104-188	Favona	UW104	188.2	Core Cut	Wallrock		WKP44-711.0	WKP EG Vein	44	711.0	Core Chip	Wallrock
FVN104-270	Favona	UW104	270.2	Core Cut	Wallrock		WKP78-332.0	WKP EG Vein	78	332.0	Core Chip	Wallrock
FVN104-312	Favona	UW104	312.3	Core Cut	Wallrock		WKP78-358.0	WKP EG Vein	78	358.0	Core Chip	Wallrock
FVN104-340	Favona	UW104	340.2	Core Cut	Wallrock		WKP78-372.0	WKP EG Vein	78	372.0	Core Chip	Wallrock
FVN104-374	Favona	UW104	374.2	Core Cut	Wallrock		WKP78-394.0	WKP EG Vein	78	394.0	Core Chip	Wallrock
FVN104-417	Favona	UW104	417.9	Core Cut	Wallrock		WKP42-407.9	WKP EG Vein	42	407.9	Quarter Core	Wallrock
FVN60281V	Favona	Underground	x	Underground	Vein		WKP42-409.3	WKP EG Vein	42	409.3	Quarter Core	Wallrock
FVN60290V	Favona	Underground	x	Underground	Vein		WKP42-412	WKP EG Vein	42	412.0	Quarter Core	Wallrock
FVN60292V	Favona	Underground	x	Underground	Vein		WKP42-416.2	WKP EG Vein	42	416.2	Quarter Core	Wallrock
FVN58180V	Favona	Underground	x	Underground	Vein		WKP42-421.2	WKP EG Vein	42	421.2	Quarter Core	Wallrock
FVN60248V	Favona	Underground	x	Underground	Vein		WKP42-422.3	WKP EG Vein	42	422.3	Quarter Core	Wallrock
MTA1460-165.3	Martha Underground	920SP4MR1460	165.3	Quarter Core	Wallrock		WKP42-423.2V	WKP EG Vein	42	423.2	Quarter Core	Vein
MTA1460-166.9	Martha Underground	920SP4MR1460	166.9	Quarter Core	Vein		WKP42-430.7V	WKP EG Vein	42	430.7	Quarter Core	Vein
MTA1460-177.8	Martha Underground	920SP4MR1460	177.8	Quarter Core	Vein		WKP42-435.8V	WKP EG Vein	42	435.8	Quarter Core	Vein
MTA1460-182.1	Martha Underground	920SP4MR1460	182.1	Quarter Core	Wallrock		WKP42-438.7V	WKP EG Vein	42	438.7	Quarter Core	Vein
MTA1460-204.8	Martha Underground	920SP4MR1460	204.8	Quarter Core	Wallrock		WKP42-438.9V	WKP EG Vein	42	438.9	Quarter Core	Vein
MTA1496-113	Martha Underground	920SP8MR1496	113.0	Quarter Core	Wallrock		WKP42-489.2	WKP EG Vein	42	489.2	Quarter Core	Wallrock
MTA1496-115.1	Martha Underground	920SP8MR1496	115.1	Quarter Core	Vein		WKP42-509.0	WKP EG Vein	42	509.0	Quarter Core	Wallrock
MTA1496-115.7	Martha Underground	920SP8MR1496	115.7	Quarter Core	Vein		WKP81-437.5V	WKP EG Vein	81	437.5	Quarter Core	Vein
MTA1496-117.4	Martha Underground	920SP8MR1497	117.4	Quarter Core	Vein		WKP81-448.6V	WKP EG Vein	81	448.6	Quarter Core	Vein
MTA1203-300	Old Martha	800SP1MN1203	300.0	Quarter Core	Vein		WKP81-455.3V	WKP EG Vein	81	455.3	Quarter Core	Vein
MTA46853V	Martha Open Pit	Open Pit	x	Open Pit	Vein		WKP81-456.5V	WKP EG Vein	81	456.5	Quarter Core	Vein
MTA57459V	Martha Open Pit	Open Pit	x	Open Pit	Vein		WKP81-459.6V	WKP EG Vein	81	459.6	Quarter Core	Vein
MTA57466V	Martha Open Pit	Open Pit	x	Open Pit	Vein		WKP81-475.1	WKP EG Vein	81	475.1	Quarter Core	Vein

Table 2. Bulk Rock Ammonium Contents. x = not analyzed.

	Run 1	Run 2	Average			Run 1	Run 2	Average			Run 1	Run 2	Average
Sample ID	NH4 (ppm)	NH4 (ppm)	NH4 (ppm)			NH4 (ppm)	NH4 (ppm)	NH4 (ppm)			NH4 (ppm)	NH4 (ppm)	NH4 (ppm)
Favona					MTA1460-182	<10	x	<10		WKP42-522.5	228	x	228
FVN063-12	144	164	154		MTA1460-204	129	137	133		WKP42-604.8	218	142	180
FVN063-80	4709	x	4709		MTA1496-113	75	x	75		WKP44-540.0	443	x	443
FVN063-88V	128	x	128		MTA1496-117V	8	x	8		WKP44-554.0	298	x	298
FVN063-117V	46	x	46		MTA46853V	65	x	65		WKP44-564.0	232	170	201
FVN063-135	970	980	975		MTA57459V	25	x	25		WKP44-607.0	425	340	382
FVN063-180	1491	x	1491							WKP44-641.0	401	x	401
FVN063-185V	10	x	10		**WKP**					WKP44-695.0	408	x	408
FVN69-62 C	120	x	120		WKP42-46.0	740	982	861		WKP44-711.0	486	394	440
FVN69-62 M	77	x	77		WKP42-56.3	734	656	695		WKP78-358.0	1581	1461	1521
FVN069-194	3040	3099	3069		WKP42-59.0	658	598	628		WKP78-394.0	2783	2645	2714
FVN69-249	1428	1416	1422		WKP42-74.2	800	731	766		WKP81-437.5	38	x	38
FVN084-161	6501	6811	6656		WKP42-75.5	679	x	679		WKP81-455.3	37	x	37
FVN084-316	2661	2691	2676		WKP42-80.3	245	195	220		WKP81-475.1	170	x	170
FVN84-421	1843	1815	1829		WKP42-103.9	306	236	271		**Blind Standards**			
FVN85-85	284	x	284		WKP42-124.0	272	x	272		SO-3		155	
FVN085-226	2562	2575	2568		WKP42-162.1	187	x	187		MAG-1	3644	3712	
FVN087-211	3837	3896	3867		WKP42-196.0	421	463	442		SA		104747	
FVN104-103	49	68	58		WKP42-225.7	299	194	247		**Reported Value**			
FVN104-188	270	261	266		WKP42-277.4	222	190	206		SO-3	154	Reported by Page, 2018	
FVN104-270	10675	x	10675		WKP42-313.5	203	166	184		MAG-1	3681	Reported by Page, 2018	
FVN104-312	3830	3867	3849		WKP42-407.9	158	x	158		Sulphanilic Acid	104014	Elemental Microanalysis	
FVN104-340	1855	1865	1860		WKP42-409.3	200	128	164		**Accuracy (%)**			
FVN104-374	2609	2663	2636		WKP42-412.0	236	x	236		SO-3	x	0.46	
FVN104-417	4486	4402	4444		WKP42-416.2	149	97	123		MAG-1	1.01	0.84	
FVN58180V	26	x	26		WKP42-421.2	182	x	182		Sulphanilic Acid	x	0.70	
FVN60248V	29	x	29		WKP42-422.3	221	137	179		**Duplicates**			
Martha					WKP42-430.7	67	x	67		FVN84-316	2683	0.33%	
MTA1203-300V	12	x	12		WKP42-435.8	62	0	31		FVN104-270	10120	0.23%	
MTA1460-165	172	192	182		WKP42-489.2	187	x	187		WKP42-313	156	5.97%	
MTA1460-177V	12	x	12		WKP42-509.0	162	x	162		WKP42-489	210	11.40%	

Table 3. Loss on Ignition

Sample ID	% LOI		Sample ID	% LOI		Sample ID	% LOI		Sample ID	% LOI
Favona			FVN87-337.6	5.8		WKP			WKP42-422.3	2.8
			FVN104-103	10.5					WKP42-423.2	1.8
			FVN104-188	9.7					WKP42-430.7	5.4
FVN063-12	5.6		FVN104-270	13.6		WKP42-46.0	5.8		WKP42-435.8	0.0
FVN063-80	5.2		FVN104-312	8.0		WKP42-56.3	5.3		WKP42-438.7	0.9
FVN063-88V	0.8		FVN104-340	6.6		WKP42-59.0	5.8		WKP42-438.9	0.0
FVN063-117V	1.5		FVN104-374	7.7		WKP42-74.2	1.8		WKP42-489.2	1.8
FVN063-135	6.8		FVN104-417	4.3		WKP42-75.5	3.5		WKP42-509.0	0.9
FVN063-180	4.2		FVN58180V	1.0		WKP42-80.3	0.9		WKP42-522.5	1.8
FVN063-185V	0.9		FVN60248V	3.2		WKP42-108.9	1.8		WKP42-604.8	2.8
FVN69-62.1C	5.3		Martha			WKP42-119.8	1.0		WKP44-540.0	6.6
FVN69-62.1M	9.1					WKP42-162.0	3.7		WKP44-554.0	1.8
FVN69-194.0	8.2					WKP42-196.0	3.5		WKP44-564.0	2.7
FVN69-249.0	6.2		MTA1460-165.3	3.8		WKP42-225.7	3.7		WKP44-607.0	1.9
FVN69-292.5	6.2		MTA1460-177.8	11.3		WKP42-277.4	1.9		WKP44-641.0	1.0
FVN84-161.7	16.3		MTA1460-204.8	2.9		WKP42-313.5	1.0		WKP44-695.0	2.9
FVN84-228.4	5.3		MTA1496-113.0	2.0		WKP42-397.0	0.8		WKP44-711.0	3.6
FVN84-316.4	4.5		MTA1496-115.7	6.1		WKP42-407.9	2.7		WKP78-358.0	7.2
FVN84-421.7	4.7		MTA1203-300.0	11.2		WKP42-409.3	0.9		WKP78-394.0	7.8
FVN85-85.7	1.9		MTA46853V	1.0		WKP42-412.0	1.8		WKP81-437.5	1.0
FVN85-226.6	7.5		MTA57459V	0.6		WKP42-416.2	1.9		WKP81-455.3	0.8
FVN87-211.0	6.4		MTA57466V	0.8		WKP42-421.1	0.0		WKP81-475.1	1.9

Table 4. Ammonium Leaching Results

	Original	Leached	Amount Adsorbed	% Adsorbed			Original	Leached	Amount Adsorbed	% Adsorbed
Sample ID	NH_4^+ (ppm)	NH_4^+ (ppm)	NH_4^+ (ppm)	%		Sample ID	NH_4^+ (ppm)	NH_4^+ (ppm)	NH_4^+ (ppm)	%
Favona						**WKP**				
FVN63-12	164	158	6	3.78		WKP42-46	982	904	78	7.99
FVN063-80	4709	4531	178	3.78		WKP42-56	656	598	58	8.88
FVN63-135	980	946	33	3.40		WKP42-59	636	598	38	5.94
FVN69-194	3099	2989	110	3.56		WKP42-74	731	733	-1	-0.20
FVN69-249	1416	1300	116	8.22		WKP42-80	195	175	20	10.10
FVN84-161	6811	5944	867	12.73		WKP42-103	236	172	65	27.30
FVN84-316	2691	2555	136	5.06		WKP42-196	463	346	117	25.19
FVN84-421	1815	1652	163	8.99		WKP42-225	194	178	16	8.46
FVN85-226	2575	2446	129	5.00		WKP42-277	190	148	42	22.10
FVN87-211	3896	3704	192	4.93		WKP42-313	166	147	19	11.29
FVN104-103	68	64	4	6.09		WKP42-409	128	137	-10	-7.69
FVN104-188	261	278	-16	-6.20		WKP42-416	97	78	19	20.00
FVN104-270	10675	10095	580	5.43		WKP42-422	137	130	7	5.36
FVN104-312	3867	3776	91	2.35		WKP42-435V	0	0	0	0.00
FVN104-340	1865	1842	23	1.22		WKP42-604	136	119	17	12.49
FVN104-374	2663	2671	-8	-0.30		WKP44-564	170	156	14	8.51
FVN104-417	4402	4203	199	4.51		WKP44-607	340	311	29	8.65
						WKP44-711	394	384	10	2.55
Martha						WKP78-358	1461	1292	169	11.56
MTA1460-165	192	157	35	18.17		WKP78-394	2645	2411	233	8.82
MTA1460-182	0	0	0	0.00						
MTA1460-204	137	116	22	15.72						
MTA1496-117V	8	0	8	100.00						

Table 5. Nitrogen Isotopes.

Sample ID	δ15N (‰)		Sample ID	δ15N (‰)		Sample ID	δ15N (‰)
Favona			FVN104-374	5.1		WKP42-412.0	8.1
FVN63-12	6.3		FVN104-417	4.3		WKP42-416.2	7.9
FVN63-80	6.8		**Martha**			WKP42-421.2	7.5
FVN63-88V	1.6		MTA1460-165	3.6		WKP42-422.3	6.5
FVN63-135	5.4		MTA1460-204	6.4		WKP42-430.7V	5.7
FVN63-180	3.1					WKP42-489.2	7.5
FVN69-62 C	1.2		**WKP**			WKP42-509.0	6.0
FVN69-194	4.4		WKP42-46.0	7.6		WKP42-522.5	6.4
FVN69-249	6.5		WKP42-56.3	6.3		WKP42-604.8	4.3
FVN84-161	3.5		WKP42-59.0	6.8		WKP44-540.0	5.1
FVN84-316	4.3		WKP42-74.2	3.9		WKP44-554.0	4.8
FVN84-421	3.1		WKP42-75.5	5.3		WKP44-564.0	5.0
FVN85-85	7.1		WKP42-80.3	6.6		WKP44-607.0	5.8
FVN85-226	4.2		WKP42-103.9	7.3		WKP44-641.0	5.7
FVN87-211	2.2		WKP42-196.0	7.1		WKP44-695.0	5.0
FVN104-103	4.9		WKP42-225.7	7.7		WKP44-711.0	3.4
FVN104-188	3.4		WKP42-277.4	4.8		WKP78-358.0	1.7
FVN104-270	6.4		WKP42-313.5	7.7		WKP78-394.0	0.5
FVN104-312	4.2		WKP42-407.9	5.9		WKP81-475.1	8.2
FVN104-340	3.2		WKP42-409.3	6.2			

Table 6. Major Element Bulk Rock Data. Analyzed by ActLabs "1F2" package which involves a 4-Acid (HCl, HNO_3, HF, $HClO_4$) near total digestion followed by analysis using ICP-OES.

Analyte Symbol	Al (%)	Ca (%)	Fe (%)	K (%)	Mg (%)	Na (%)	P (%)	S (%)	Ti (%)
Detection Limit	0.01	0.01	0.01	0.01	0.01	0.01	0.001	0.01	0.01
FVN63-12	9.9	0.29	0.17	2.96	0.39	0.02	0.002	0.01	0.21
FVN63-80	7.62	0.12	0.85	1.95	0.38	0.02	0.003	1.02	0.16
FVN63-135	6.82	0.07	3.46	2.68	0.34	0.02	0.005	4.39	0.33
FVN63-180	8.31	0.2	2.78	2.89	2.17	0.05	0.051	0.17	0.35
FVN69-194	7.08	0.18	3.97	2.83	1.36	0.04	0.042	4.85	0.33
FVN69-249	7.56	0.19	3.41	2.68	2.49	0.26	0.041	1.73	0.32
FVN84-161	11	0.09	3.72	3.1	0.82	0.02	0.003	4.48	0.44
FVN84-316	8.36	0.2	2.42	2.83	1.56	0.03	0.046	2.04	0.36
FVN84-421	7.69	2.75	4.04	1.72	2.79	0.59	0.041	0.22	0.28
FVN85-226	6.26	0.19	2.28	2.67	0.59	0.03	0.038	2.85	0.3
FVN87-211	5.8	0.1	1.38	1.51	0.44	0.02	0.004	1.65	0.25
FVN104-103	10.2	0.79	2.05	1.97	0.58	0.36	0.013	1.43	0.45
FVN104-188	4.23	0.58	5.64	0.82	0.6	0.06	0.09	7.43	0.19
FVN104-270	10.1	0.32	3.53	1.43	0.69	0.03	0.047	4.24	0.41
FVN104-312	7.7	0.24	3.01	2.39	0.64	0.02	0.045	3.75	0.33
FVN104-340	8.42	0.25	2.51	2.69	1.51	0.62	0.048	1.96	0.36
FVN104-374	7.46	0.19	3.53	2.84	2.31	0.03	0.04	3.27	0.33
MTA1460-165	7.64	0.42	2.9	4.39	2.44	0.85	0.042	2.07	0.32
MTA1460-204	6.92	0.2	3.25	5.3	1.24	0.99	0.039	3.54	0.34
JR-1 (Reported)	6.77	0.5	0.56	3.19	0.07	2.79	0.006	< 0.01	0.07
JR-1 (Actual)	6.79	0.48	0.62	3.66	0.07	2.98	0.009		0.066
% Error	0.29	4.17	9.68	12.84	0.00	6.38	33.33		6.06

Table 7. Trace Element Bulk Rock Data Analyzed by ActLabs "1F2" package which involves a 4-Acid (HCl, HNO_3, HF, $HClO_4$) near total digestion followed by analysis using ICP-OES.

Analyte Symbol	Ag (ppm)	As (ppm)	Ba (ppm)	Be (ppm)	Bi (ppm)	Cd (ppm)	Co (ppm)	Cr (ppm)	Cu (ppm)	Ga (ppm)	Li (ppm)	Mn (ppm)	Ni (ppm)
Detection Limit	0.3	3	7	1	2	0.3	1	1	1	1	1	1	1
FVN63-12	< 0.3	6	107	< 1	< 2	< 0.3	2	37	2	27	78	63	3
FVN63-80	0.3	38	108	< 1	< 2	< 0.3	5	32	14	12	73	54	9
FVN63-135	0.6	45	43	< 1	< 2	< 0.3	16	50	13	14	59	42	21
FVN63-180	0.4	14	758	1	< 2	< 0.3	13	57	18	16	66	431	21
FVN69-194	1	15	30	1	< 2	< 0.3	17	68	11	15	59	344	23
FVN69-249	0.4	20	104	1	< 2	< 0.3	15	56	14	16	75	1010	20
FVN84-161	0.4	30	73	< 1	< 2	< 0.3	21	105	16	19	24	114	25
FVN84-316	0.6	26	106	1	< 2	< 0.3	18	78	21	17	56	218	22
FVN84-421	< 0.3	11	368	1	< 2	0.5	7	57	11	18	100	1110	15
FVN85-226	1.6	27	44	1	< 2	< 0.3	14	46	11	14	56	90	18
FVN87-211	1.1	23	90	< 1	< 2	< 0.3	10	49	5	11	66	80	15
FVN104-103	< 0.3	89	163	1	< 2	< 0.3	10	45	17	21	22	103	13
FVN104-188	< 0.3	140	34	< 1	< 2	< 0.3	13	39	12	8	100	104	14
FVN104-270	0.4	22	56	< 1	< 2	< 0.3	21	50	13	21	30	138	21
FVN104-312	< 0.3	11	33	1	< 2	< 0.3	17	47	13	15	49	161	22
FVN104-340	0.4	10	111	1	< 2	< 0.3	16	58	18	17	55	446	20
FVN104-374	0.4	14	55	1	< 2	< 0.3	17	58	10	15	68	551	22
MTA1460-165	2.9	16	91	1	< 2	0.6	16	60	16	15	80	2660	34
MTA1460-204	1.4	34	59	< 1	< 2	< 0.3	16	73	13	12	48	805	42
JR-1 (Reported)	< 0.3	18	49	3	< 2	< 0.3	< 1	4	2	18	60	716	1
JR-1 (Actual)	0.031	16.3	50.3	3.34			0.83	2.83	2.68	16.1	61.4	770	1.67
% Error		10.43	2.58	10.18				41.34	25.37	11.80	2.28	7.01	40.12

Analyte Symbol	Pb (ppm)	Sb (ppm)	Sc (ppm)	Sr (ppm)	Te (ppm)	Tl (ppm)	U (ppm)	V (ppm)	W (ppm)	Y (ppm)	Zn (ppm)	Zr (ppm)
Detection Limit	3	5	5	1	2	5	10	2	5	1	1	5
FVN63-12	< 3	< 5	11	27	< 2	< 5	< 10	97	< 5	13	7	59
FVN63-80	< 3	12	8	14	< 2	< 5	< 10	70	5	5	8	53
FVN63-135	6	7	17	11	< 2	< 5	< 10	115	5	21	29	70
FVN63-180	< 3	< 5	17	43	< 2	< 5	< 10	126	< 5	16	92	95
FVN69-194	8	< 5	16	24	5	< 5	< 10	119	9	16	57	83
FVN69-249	6	< 5	16	32	5	< 5	< 10	116	6	17	61	51
FVN84-161	7	< 5	23	13	3	< 5	< 10	158	8	22	111	122
FVN84-316	3	< 5	20	15	6	< 5	< 10	133	5	18	33	106
FVN84-421	17	< 5	16	79	2	< 5	< 10	111	< 5	14	120	5
FVN85-226	< 3	< 5	15	16	2	< 5	< 10	110	< 5	18	43	76
FVN87-211	4	< 5	15	14	3	< 5	< 10	91	7	33	9	53
FVN104-103	6	6	27	81	12	< 5	< 10	172	< 5	91	62	56
FVN104-188	8	8	11	48	4	< 5	< 10	75	< 5	15	33	49
FVN104-270	10	< 5	22	36	10	< 5	< 10	129	< 5	17	74	121
FVN104-312	7	< 5	16	20	2	< 5	< 10	116	< 5	14	48	72
FVN104-340	5	< 5	19	61	< 2	< 5	< 10	136	< 5	16	85	92
FVN104-374	10	< 5	17	29	7	< 5	< 10	120	6	16	56	77
MTA1460-165	15	< 5	15	93	< 2	< 5	< 10	100	6	18	345	70
MTA1460-204	22	< 5	16	133	5	< 5	< 10	98	7	13	60	71
JR-1 (Reported)	16	< 5	< 5	29	< 2	< 5	< 10	6	< 5	41	31	91
JR-1 (Actual)	19.3			29.1						45.1	30.6	99.9
% Error	17.10			0.34						9.09	1.31	8.91

***Table 8**. Mineral Abundance Estimates. %Ilt+Sme and %Chl were estimated based on modal abundances from thin section. %Sme and %Ilt were calculated from Ilt/Sme ratio from Simpson & Mauk, 2007 XRD data. %Adl was calculated from the %K2O and illite abundance.*

ID	K_2O (%)	Ilt/Sme Ratio	% Ilt+Sme (from TS)	% Sme (calculated)	% Ilt (calculated)	% Chl (from TS)	wt% Adl (calculated)
FVN63-80	2.3	0.9	25	2.5	22.5	0	4.2
FVN63-135	3.2	1	30	0	30	0	6.2
FVN63-180	3.5	1	10	0	10	20	16.2
FVN69-194	3.4	1	25	0	25	5	9.4
FVN69-249	3.2	1	10	0	10	20	14.7
FVN84-161	3.7	0.8	65	13	52	0	0.0
FVN84-316	3.4	1	30	0	30	10	7.2
FVN84-421	2.1	1	10	0	10	35	7.9
FVN85-226	3.2	0.9	35	3.5	31.5	0	5.5
FVN87-211	1.8	0.85	15	2.25	12.75	0	5.3
FVN104-103	2.4	1	25	25	0	0	14.0
FVN104-188	1.0	0.3	5	3.5	1.5	0	5.2
FVN104-270	1.7	0.75	30	7.5	22.5	0	0.5
FVN104-312	2.9	0.9	35	3.5	31.5	3	3.5
FVN104-340	3.2	1	15	0	15	5	12.7
FVN104-374	3.4	1	30	0	30	5	7.3
FVN104-417	No Data	1	25	0	25	0	?

Appendix B | Samples and Petrography

*Appendix B images show a hand sample photo with a description as well as the samples corresponding XRD, SWIR, LOI, bulk NH_4^+ content, and $\delta^{15}N$ values if available. Images from left to right for each sample which has had a thin section made show the (1) thin section cut off followed by (2) thin section cut off with cobaltinitrite staining and the (3) scanned thin section in PPL and (4) XPL. SEM-EDS analysis data and BSE images as well as photomicrographs are available for some samples. All EDS values are in oxide wt%. XRD analysis for most wallrock samples are from data acquired for Simpson & Mauk, 2007 and provided by Mark Simpson. The fraction of illite in illite-smectite mixed layer clay was also analyzed in Simpson & Mauk, 2007 and is shown as $illite_{x,x}$smectite. For example, a mixed clay with 90% illite is shown as $illite_{0.9}$smectite. XRD results labelled (uO) were analyzed at the University of Ottawa. SWIR data for Favona and WKP was provided by Mark Simpson and published in Simpson, 2015 & Simpson, 2018 respectively.

Favona

DDH63

FVN63-12

DDH Depth: 12.05m

Sample Desc: Strongly illite-smectite altered pyroclastic. Pervasive clay alteration throughout.

XRD Minerals: Quartz, $Illite_{0.8}Smectite$ (Simpson & Mauk, 2007)

SWIR Minerals: Illite-Smectite (Simpson, 2015)

LOI: 5.6%

NH4+: 204ppm

δ15N: +6.3‰

No Petrographic Data

FVN63-80

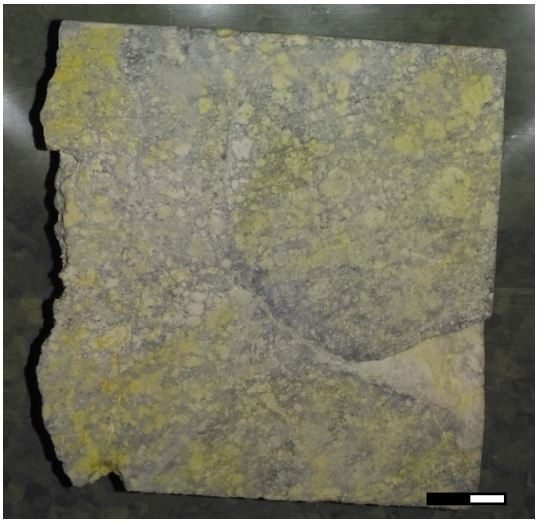

DDH Depth: 80.7m

Hand Sample Desc: Altered plagioclase phyric andesite. Large, rounded plagioclase phenocrysts (2-9mm) have pervasively altered to illite-smectite. Groundmass appears to be primarily quartz.

XRD Minerals: Quartz, $Illite_{0.9}Smectite$, Adularia, Pyrite (Simpson & Mauk, 2007)

SWIR Minerals: Ammonium Mineral, Minor Gypsum (Simpson, 2015)

(Gypsum due to alteration of sulphides while in storage)

LOI: 5.2%

NH_4^+: 4494ppm

$\delta^{15}N$: +6.8‰

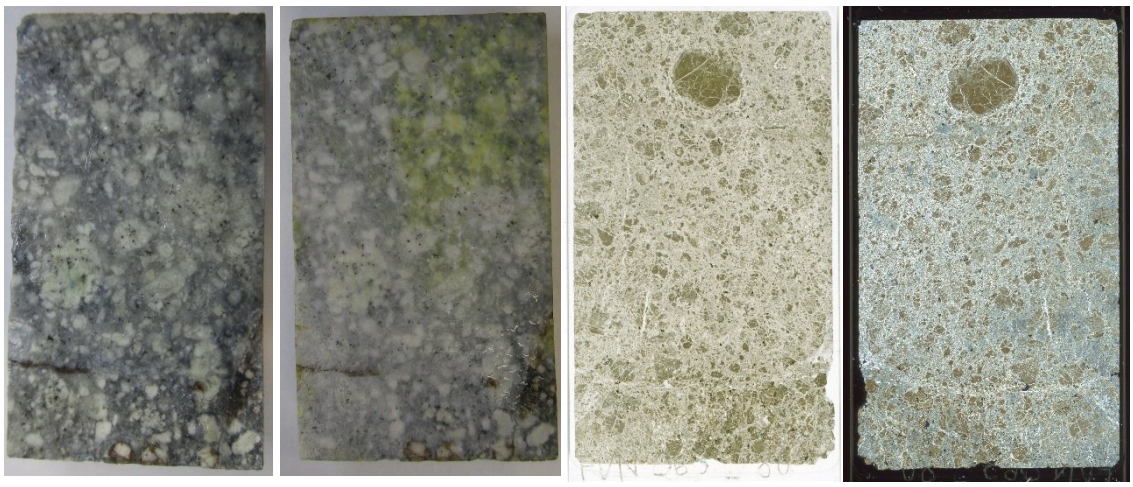

Thin Section Description:

Intensely clay altered plagioclase phyric andesite. 30% plagioclase phenocrysts ranging from 2-9mm the largest of which are rounded. All plagioclase phenocrysts are completely white mica altered (Photomicrograph A) with microcrystalline quartz filling fractures within the phenocrysts. The groundmass is primarily microcrystalline quartz with minor (~15%) white mica. Disseminated euhedral pyrite throughout.

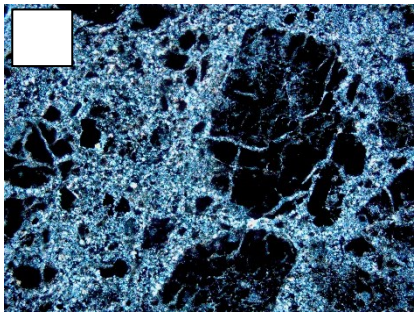

A

FVN63-88V

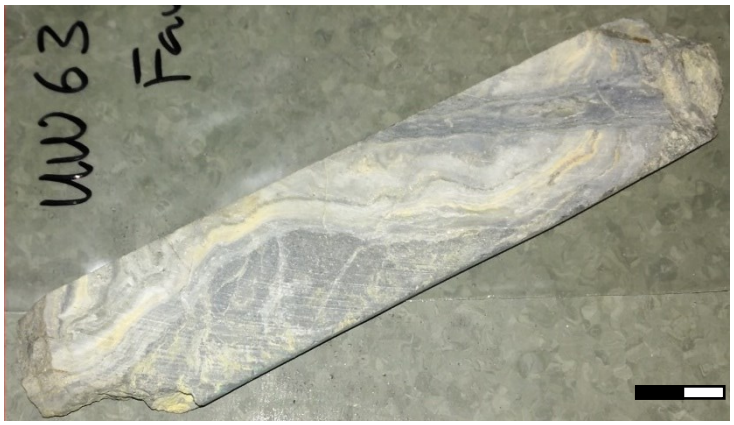

Depth: 88.5m
Sample Desc: Vein sample. Appears to contain significant portions of silicified dark coloured wallrock. Contains significant clay minerals.
XRD Minerals: Qz (uO)
SWIR Minerals: No data
LOI: 0.8%
NH_4^+: 128ppm
δ15N: Too low

No Petrographic Data

FVN63-117V

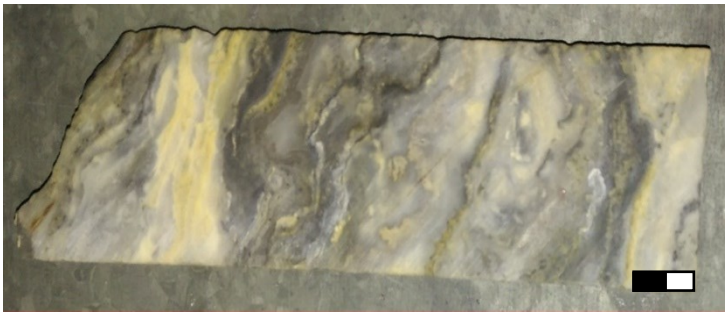

Depth: 117.3m
Sample Desc: Vein sample. Shows crustiform banding. Primarily microcrystalline quartz. Minor clays / adularia + ore minerals.
XRD Minerals: Qz (uO)
SWIR Minerals: No data
LOI: 1.5%

NH_4^+: 46ppm
δ15N: Too low

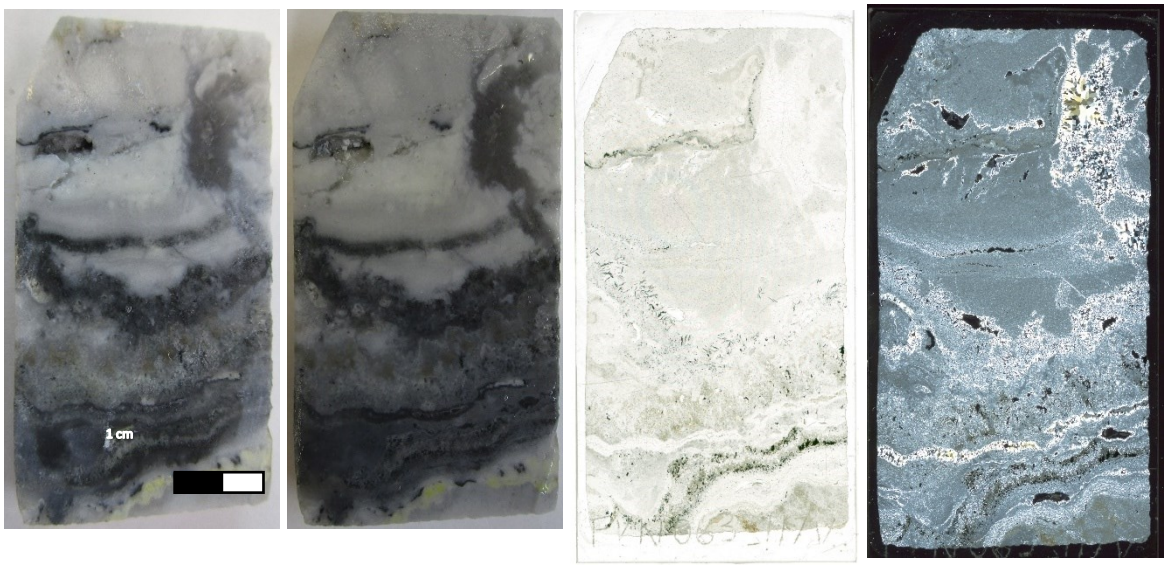

Thin Section Description:

Colloform quartz vein sample. Primarily composed of microcrystalline gel quartz with bands of crystalline quartz +/- adularia. Dark bands contain abundant sulphides. The larger crystalline sulphides showing an elongate shape (Photomicrograph A and B).

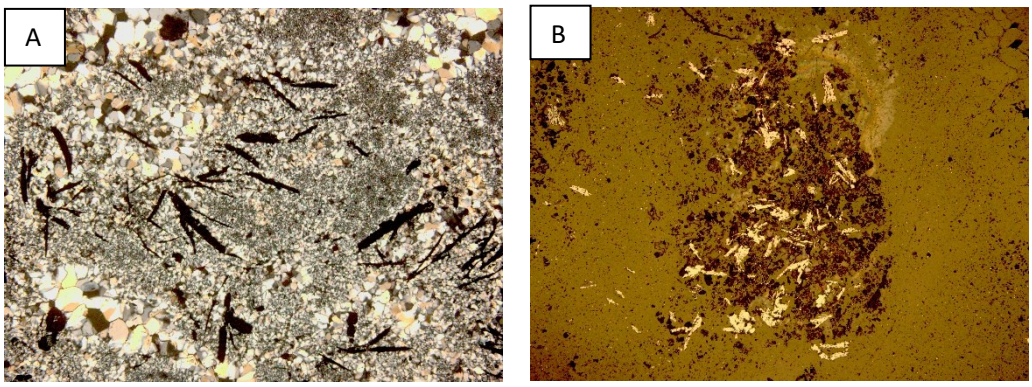

FVN63-135

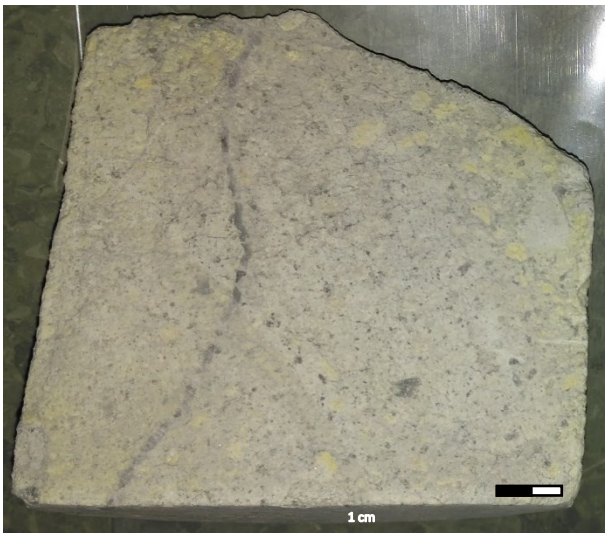

DDH Depth: 135.6m
Sample Desc: Pervasively illite + adularia altered andesite. Plagioclase phenocrysts are not as large as 063-80, but the groundmass appears to be more altered. Small 2mm wide quartz veinlet.
XRD Minerals: Quartz, Adularia, Illite, Pyrite (Simpson & Mauk, 2007)
SWIR Minerals: Illite, Gypsum (Simpson, 2015)
LOI: 6.8%
NH_4^+: 990ppm
δ15N: +5.4‰

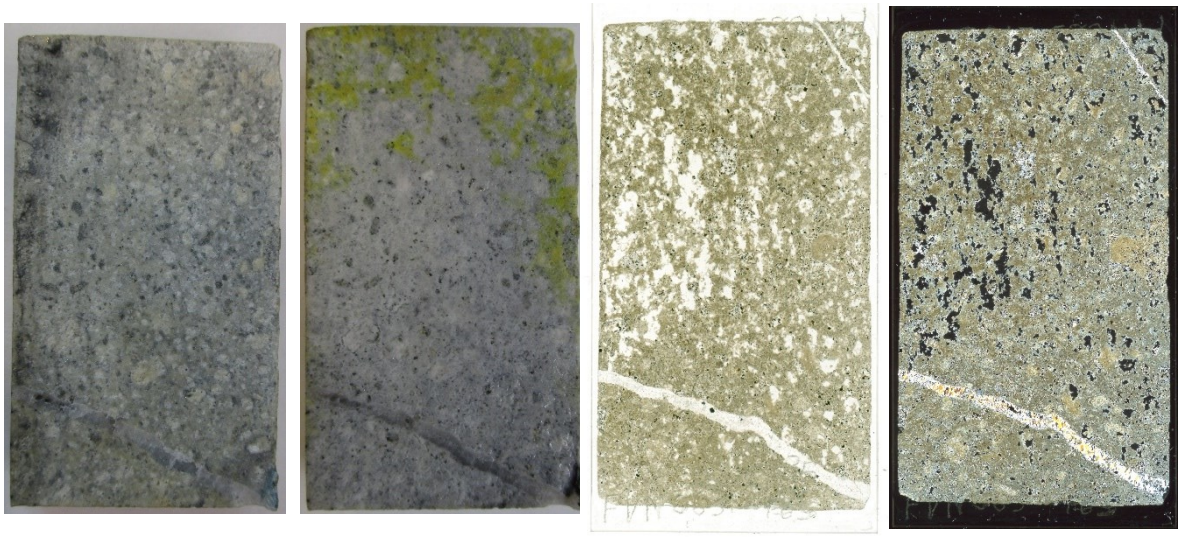

Thin Section Description:

Very intensely altered andesite. Most plagioclase phenocrysts appear to have been completely obliterated and polished out leaving pits. Those that remain are completely replaced by white mica. White mica abundant throughout groundmass as well. Some areas have been completely replaced by fine grained microcrystalline quartz or adularia. Groundmass is primarily white mica with <30% quartz / adularia throughout. Very abundant (>15%) disseminated euhedral pyrite.

FVN63-180

DDH Depth: 180.9m
Hand Sample Desc: Illite, adularia, and chlorite altered andesite. Plagioclase phenocrysts are adularia altered. Chlorite altered mafic phenocrysts. Chlorite and adularia rich groundmass.
XRD Minerals: Quartz, Adularia, Chlorite, Illite, Pyrite (Simpson & Mauk, 2007)
SWIR Minerals: Illite, Chlorite, Minor Gypsum, Suspected NH4 mineral (Simpson, 2015)
LOI: 4.2%
NH_4^+: 1501ppm
δ15N: +3.1‰

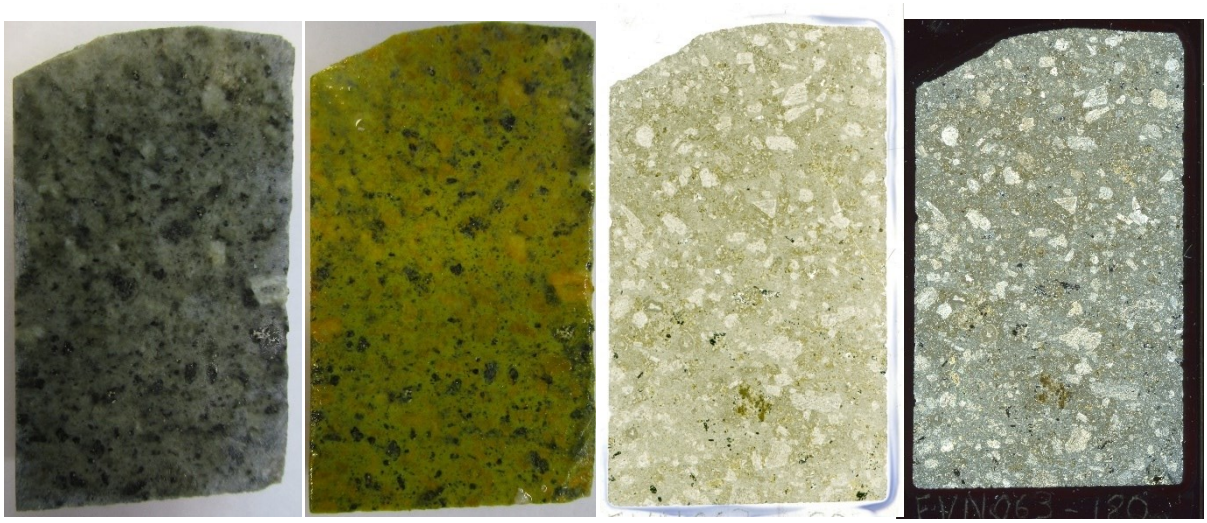

Thin Section Description:

Clay and chlorite altered plagioclase phyric andesite. 20% 0.3-2mm plagioclase phenocrysts which have been completely adularia altered and overprinted by white mica. White mica alteration is intense replacing 70-100% of the adularia in the phenocryst (Photomicrograph A). Pyroxene / amphibole phenocrysts have been altered to chlorite + quartz with minor white mica. The groundmass is primarily microcrystalline quartz and adularia (strong K staining) with minor disseminated white mica. Chlorite also appears in small patches throughout the groundmass.

A

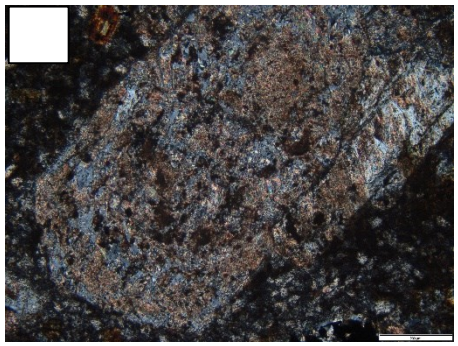

FVN63-180 SEM-EDS

SEM-EDS (1)

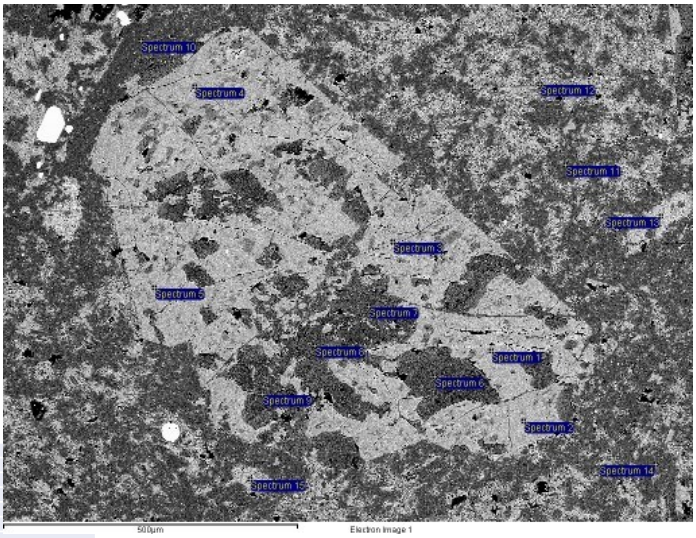

Spectrum	Mg	Al	Si	K	Ca	Fe	Mineral
Spectrum 1	0	18.02	66.29	15.7	0	0	Adularia
Spectrum 2	0	17.57	65.79	16.64	0	0	Adularia
Spectrum 3	1.46	18.7	63.71	14.8	0	1.32	Adularia + chlorite?
Spectrum 4	0	17.55	66.05	16.41	0	0	Adularia
Spectrum 5	0	18.08	65.4	16.53	0	0	Adularia
Spectrum 6	2	33.14	55.86	7.98	0	1.02	Illite
Spectrum 7	1.55	34.19	57.53	6.73	0	0	Illite
Spectrum 8	1.93	34.81	56.81	5.63	0	0.82	Illite
Spectrum 9	2.08	33.46	56.49	6.69	0	1.28	Illite
Spectrum 10	0	1.56	97.88	0.55	0	0	Quartz + Adularia (Groundmass)
Spectrum 11	1.2	16.87	76.36	4.66	0	0.9	Illite (Groundmass)
Spectrum 12	7.73	22.53	51.59	8.03	0	10.11	Illite + Chlorite (Groundmass)
Spectrum 13	18.53	20.19	36.93	0.6	0	23.77	Illite + Chlorite (Groundmass)
Spectrum 14	0	12.77	75.75	11.48	0	0	Quartz + Adularia (Groundmass)
Spectrum 15	19.92	19.19	34.33	0	0	26.57	Illite+ Chlorite (Groundmass)

High Resolution BSE image

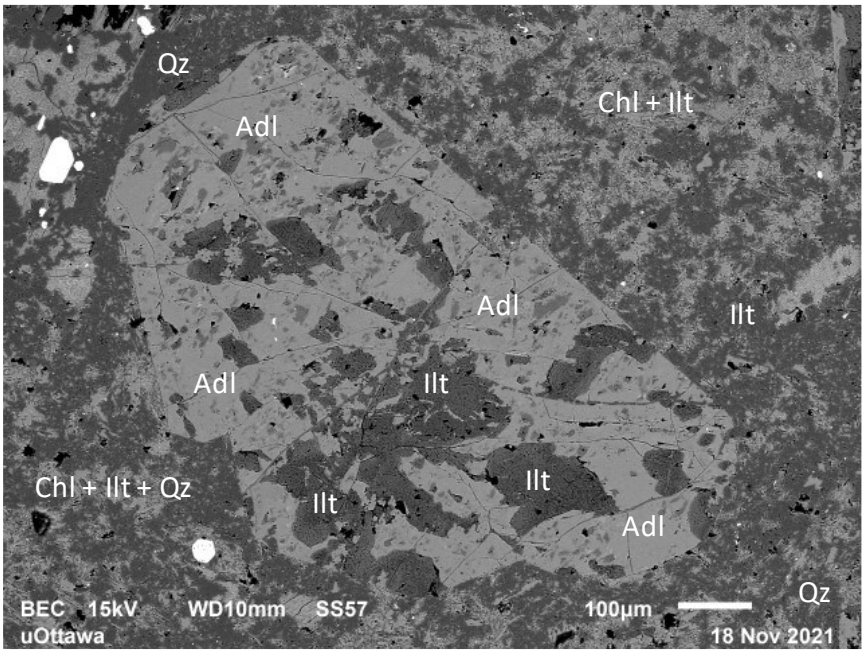

SEM-EDS (2)

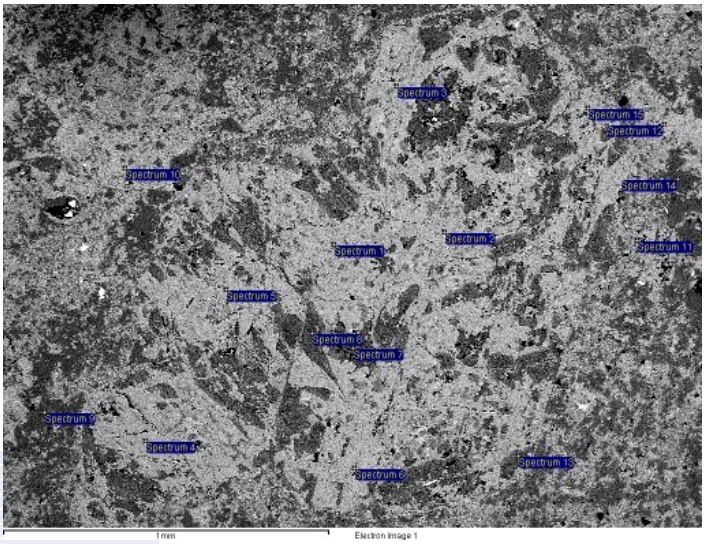

Spectrum	Mg	Al	Si	K	Ca	Fe	Mineral
Spectrum 1	0	20.46	64.09	15.46	0	0	Adularia
Spectrum 2	0	17.92	66.06	16.02	0	0	Adularia
Spectrum 3	0	17.55	65.97	16.47	0	0	Adularia
Spectrum 4	0	18.05	65.37	16.58	0	0	Adularia
Spectrum 5	0.44	19.66	64.41	15.49	0	0	Adularia
Spectrum 6	7.18	20.22	50.99	9.14	0	12.47	Adularia + Chlorite
Spectrum 7	3.01	29.6	57.79	8.73	0	0.88	Illite
Spectrum 8	2.19	33.01	57.28	6.37	0	1.15	Illite
Spectrum 9	0	0	100	0	0	0	Quartz
Spectrum 10	20.41	18.4	33.97	0	0	27.22	Chlorite (Groundmass)
Spectrum 11	16.33	21	38.89	1.93	0.43	21.43	Chlorite + minor illite (Groundmass)
Spectrum 12	19.32	18.36	40.18	0.25	0	21.89	Chlorite + minor illite (Groundmass)
Spectrum 13	2.27	31.71	57.2	7.48	0	1.34	Illite (Groundmass)
Spectrum 14	1.82	34.15	57.13	5.94	0.33	0.63	Illite + minor smectite (Groundmass)
Spectrum 15	0	18.96	65.53	15.51	0	0	Adularia

High Resolution BSE image

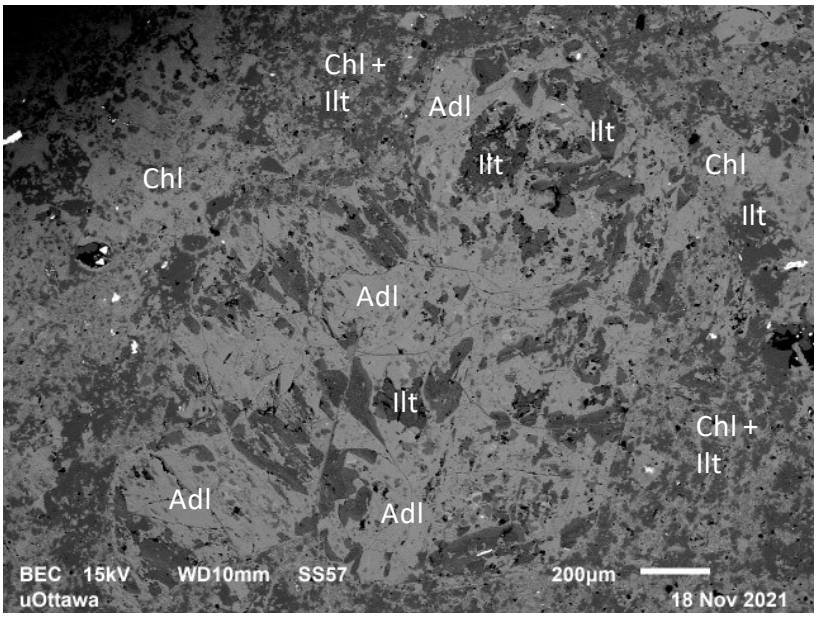

FVN63-185V

DDH Depth: 185.8m
Sample Desc: Vein sample. Almost entirely composed on quartz. Dark area is finely brecciated + sulfide minerals.
XRD Minerals: Qz (uO)
SWIR Minerals: Not Analyzed
LOI: 0.9%
NH_4^+: 10ppm
δ15N: Too low

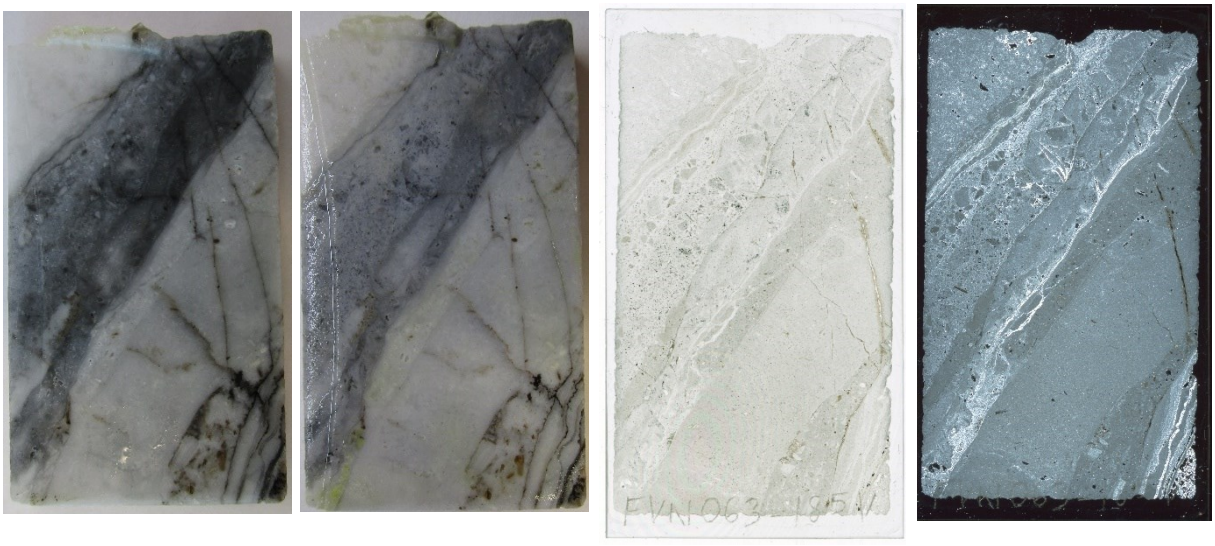

No Thin Section Description

FVN63-226

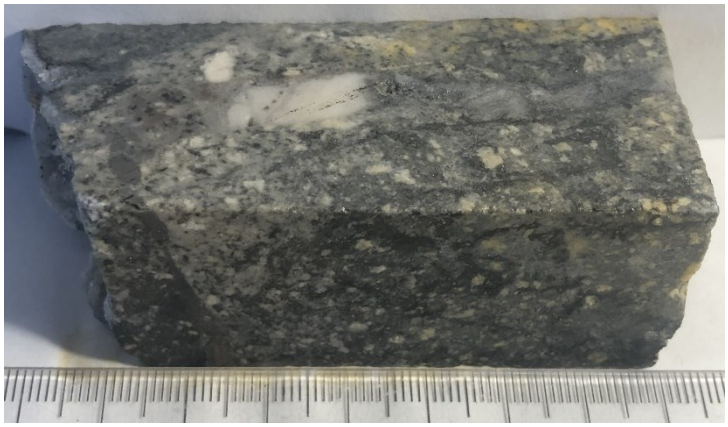

DDH Depth: 226.8m
Sample Desc: Strongly silica + clay altered plagioclase phyric (1-2mm) andesite. Plagioclase crysts have been strongly clay altered. 2cm vuggy quartz vein on backside.
XRD Minerals: Quartz, $Illite_{0.9}$Smecite, Chlorite, Pyrite (Simpson & Mauk, 2007)
SWIR Minerals: Suspected NH4-mineral, Gypsum (Simpson, 2015)
LOI: Not Analyzed
NH_4^+: Not Analyzed
δ15N: Not Analyzed

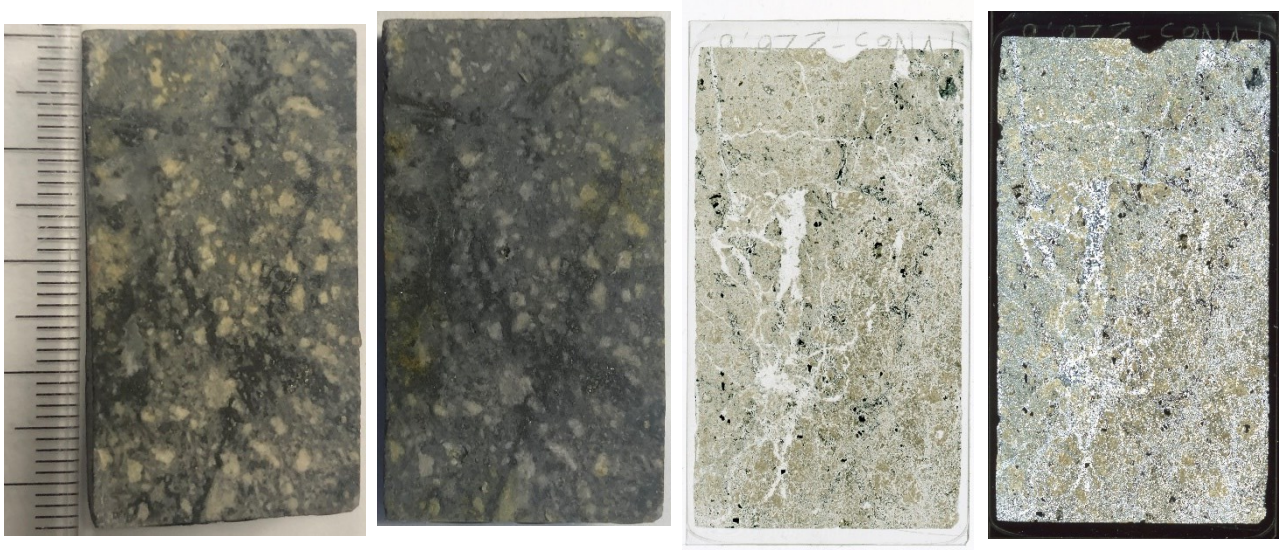

Thin Section Description:

Intensely clay altered plagioclase phyric andesite. 30% 0.2-3mm plagioclase phenocrysts have been entirely replaced by white mica. White mica on phenocrysts is fine grained but more coarse than previous samples. Groundmass is composed of primarily microcrystalline quartz +/- adularia with disseminated white mica throughout. White mica in groundmass varies in abundance throughout sample from 10-30%. Pyrite is finely disseminated throughout the groundmass and fills void space within quartz veinlets (10% of the sample).

DDH69

FVN69-62

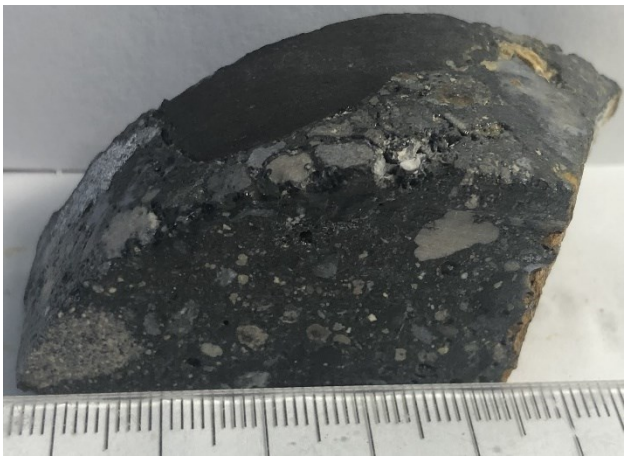

DDH Depth: 62.1m
Sample Desc: Polymictic (hydrothermal) breccia. Clasts are 0.1cm to 1cm in size and are varying compositions. Large dark aphanitic / very fine-grained clast (appears to be mudstone). Quartz vein and altered andesite clasts (1-10mm). Matrix is dark gray aphanitic / glassy.
XRD Minerals: $Illite_{0.9}$Smectite, Adularia (Simpson & Mauk, 2007)
SWIR Minerals: Not acquired
LOI: Matrix: 9.1% "Mudstone" Clast: 5.3%
$NH4^+$: Matrix: 77ppm, Clast: 120ppm
δ15N: Clast: +1.2‰

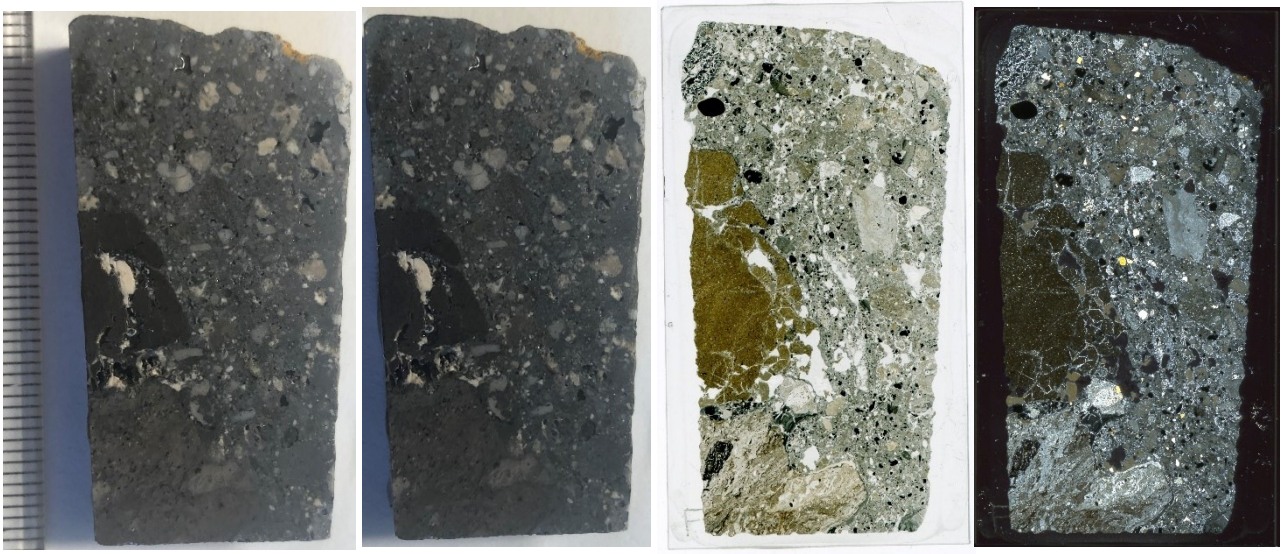

Thin Section Description:
Hydrothermal breccia. Heterolithic angular clasts which range in size from 0.1 – 50mm. Composed of vein and wallrock breccia. Wallrock appears to be variably altered andesite flows / tuffs though one large clast of what appears to be a mudstone. Mudstone clast is very fine grained dark brown colour with rounded quartz and pyrite grains. Other clasts consist of colloform / gel microcrystalline quartz, altered andesites, and pyrite fragments. Matrix is very fine-grained dark coloured quartz / sediment with pyrite. Pyrite grains are highly rounded, disseminated, or colloform.

FVN69-101

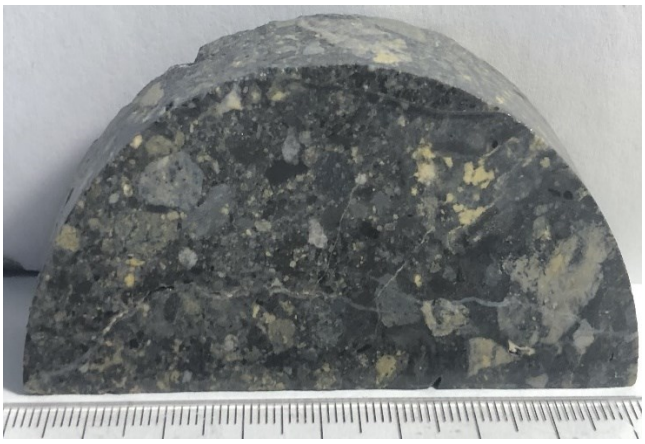

DDH Depth: 101.2m
Sample Desc: Polymictic (hydrothermal) breccia. Clasts are 0.1cm to 3cm in size and are varying compositions. Primarily wallrock fragments. Quartz vein clasts. Matrix is dark gray aphanitic / glassy.
XRD Minerals: $Illite_{0.9}$Smectite, Adularia (Simpson & Mauk, 2007)
SWIR Minerals: Not acquired
LOI: Not Analyzed
$NH4^+$: Not Analyzed
δ15N: Not Analyzed

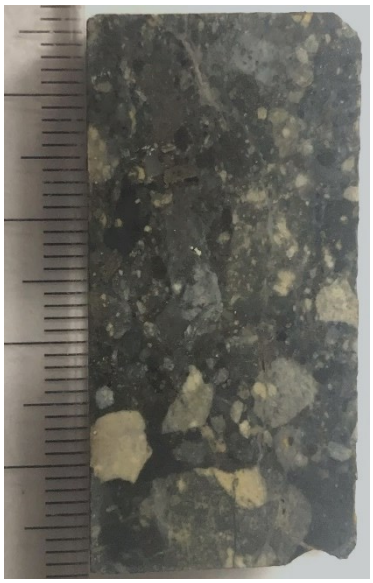

Thin Section Description:

Hydrothermally altered hydrothermal breccia. Matrix is entirely microcrystalline gel quartz with small (<0.1mm) patches of clay minerals. There are 0.5-2mm heterolithic clasts throughout which have been strongly clay and/or silica altered. Vein breccia and wallrock clasts throughout. Wallrock is variably altered andesites. Similar to previous sample but overprinted by slight clay mineral alteration. Abundant pyrite throughout.

FVN69-135

DDH Depth: 135.1m
Sample Desc: Intensely clay altered plagioclase phyric andesite. Groundmass and phenocrysts (1-6mm) both intensely clay altered.
XRD Minerals: $Illite_{0.85}Smectite$ (Simpson & Mauk, 2007)
SWIR Minerals: Not acquired
LOI: Not Analyzed
$NH4^+$: Not Analyzed
δ15N: Not Analyzed

Thin Section Description:

Intensely clay altered plagioclase phyric andesite. Sample is nearly entirely composed of white mica which is completely replacing the plagioclase phenocrysts and makes up 50-70% of the groundmass. Relict plagioclase phenocrysts make up ~20% of the sample and range in size from 0.5-1mm. Groundmass contains abundant white mica and microcrystalline quartz +/- adularia. Quartz veinlets and quartz rich patches / vugs are common. One single euhedral 1mm quartz phenocryst.

FVN69-194

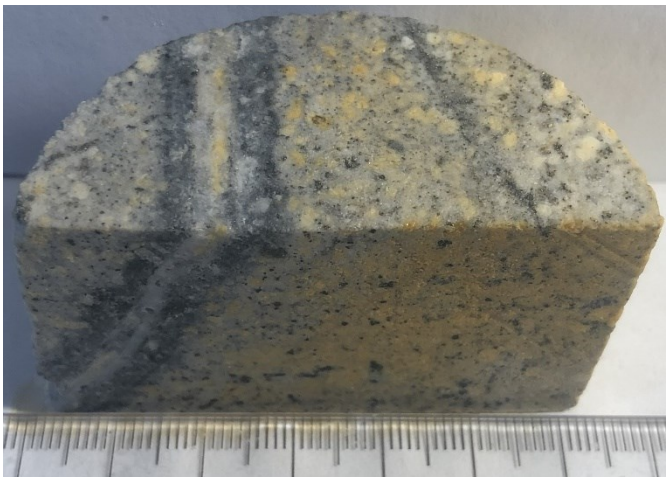

DDH Depth: 194.0m
Sample Desc: Strongly altered plagioclase phyric (~2mm) andesite. Plagioclase phenocrysts have been clay +/- adularia altered. Disseminated pyrite (5%) throughout. Small 1-2mm quartz vein with contact halo around it possibly chlorite rich halo.
XRD Minerals: Illite, Adularia, Chlorite (Simpson & Mauk, 2007)
SWIR Minerals: Not acquired
LOI: 8.2%
NH_4^+: 3040ppm
δ15N: +4.4‰

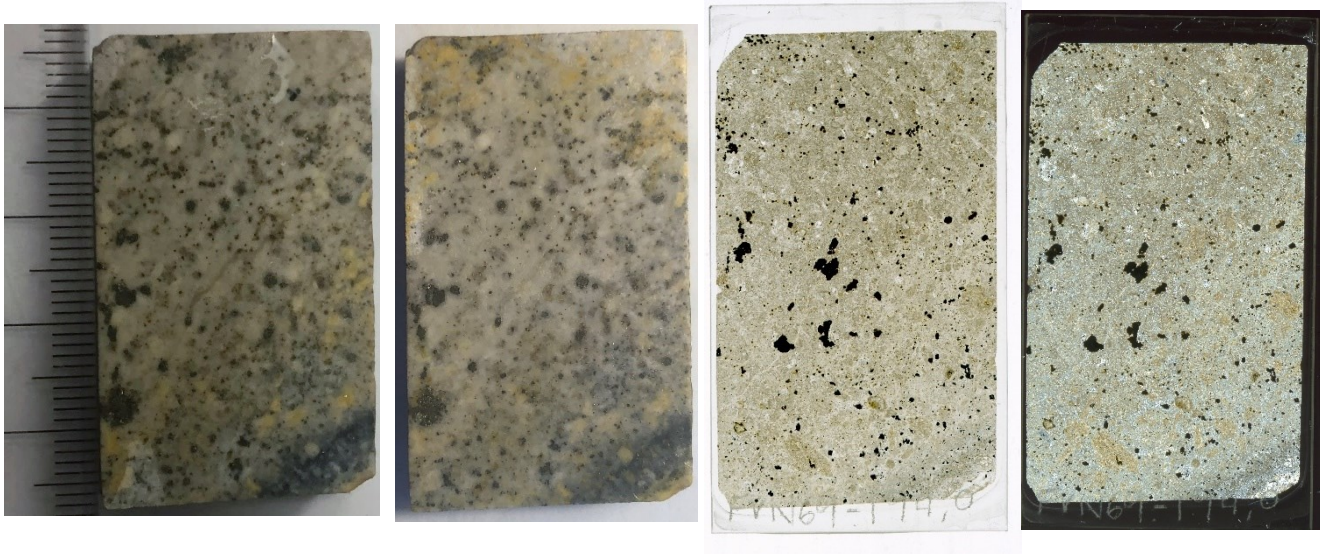

Thin Section Description:

Intensely clay altered plagioclase phyric andesite. 30% adularia plagioclase phenocrysts which have been replaced by 70-90% fine-grained white mica. Groundmass is primarily fine / microcrystalline quartz and adularia (10%). Approximately 30% of the groundmass is white mica. Minor chlorite (<5%) occurs finely within the groundmass. 20% of the sample is euhedral >0.1mm pyrite occurring disseminated throughout. Pyrite is oxidizing leaving rusted areas.

FVN69-249

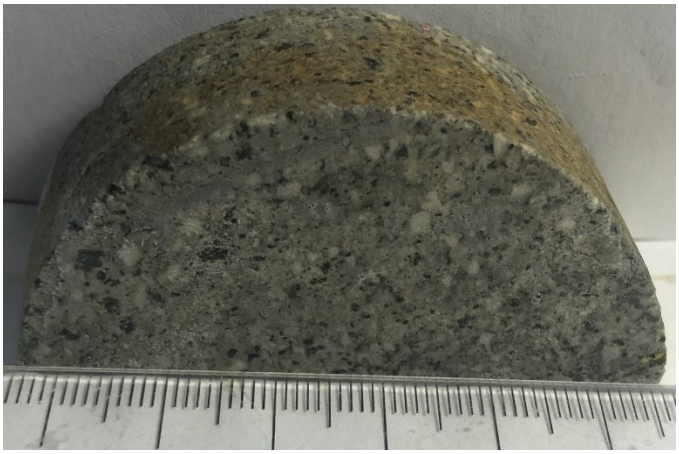

DDH Depth: 249.0m
Sample Desc: Clay altered plagioclase phyric (1-2mm, 15%) andesite. Dark patches / phenocrysts (1-2mm, 10%). May be mafic minerals or chlorite. Groundmass appears bleached / clay altered (+silicified).
XRD Minerals: Illite, Adularia, Albite, Chlorite (Simpson & Mauk, 2007)
SWIR Minerals: Not acquired
LOI: 6.2%
NH_4^+: 1428ppm
δ15N: +6.5‰

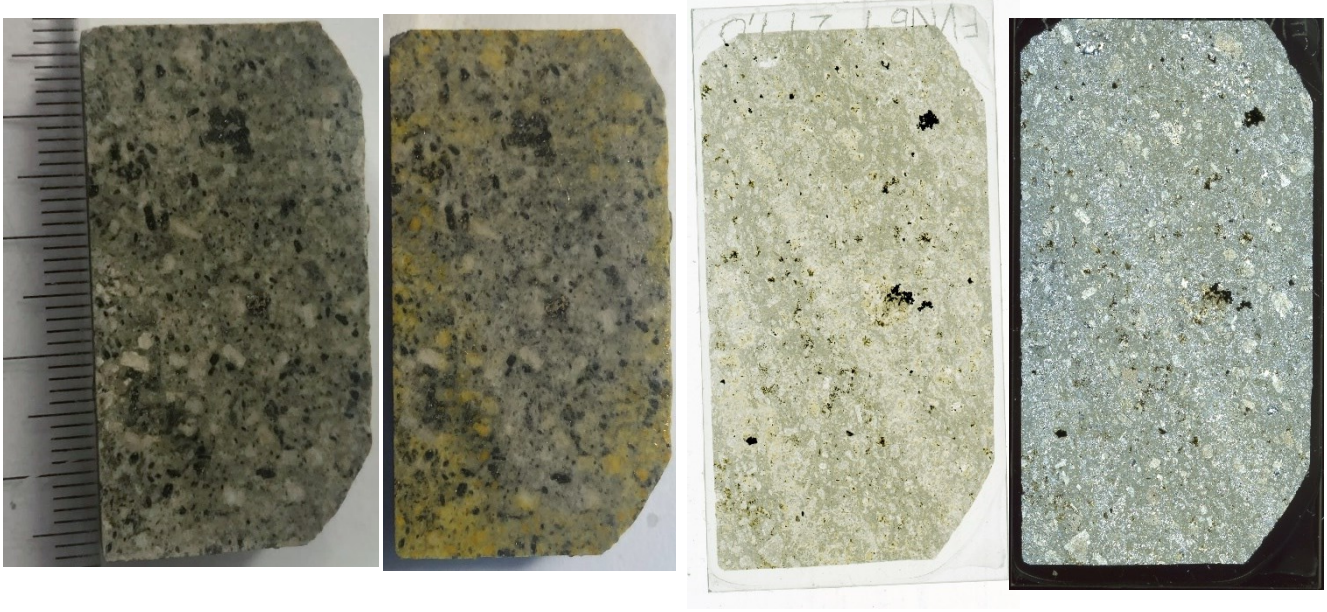

Thin Section Description:

Clay altered andesite. 30% adularia altered plagioclase phenocrysts which have been moderately (40-70%) replaced white mica. 10% pyroxene phenocrysts have been completely altered to chlorite (80%) and quartz (20%). Chlorite also occurs as radiating patches in the groundmass composing 20% of the groundmass. The groundmass is primarily quartz +/- adularia with minor white mica.

FVN69-292

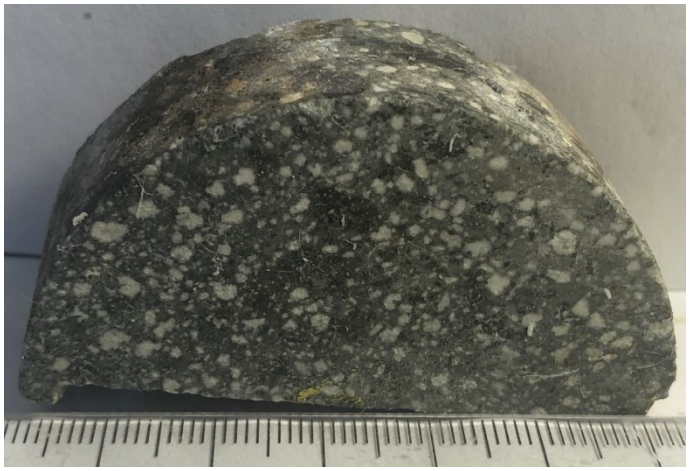

DDH Depth: 292.5m

Sample Desc: Chlorite altered plagioclase phyric andesite. Plagioclase phenocrysts (1-3mm) appear clay altered. Groundmass is greenish gray with 1-5mm chlorite patches.

XRD Minerals: $Illite_{0.9}$Smectite, Adularia, Chlorite (Simpson & Mauk, 2007)

SWIR Minerals: Not Acquired

LOI: 6.2%

NH_4^+: Not Analyzed

δ15N: Not Analyzed

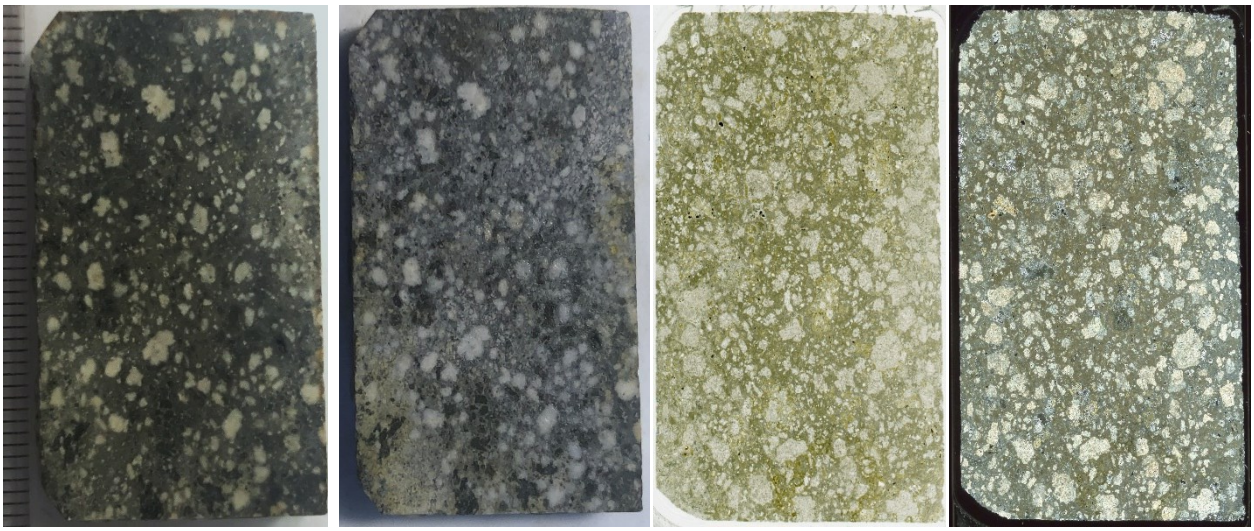

Thin Section Description:

Clay altered andesite. 30% adularia altered plagioclase phenocrysts which have been moderately (40-70%) replaced white mica (Photomicrograph A and B). 10% pyroxene phenocrysts have been completely altered to chlorite (80%) and quartz (20%). Chlorite also occurs as radiating patches in the groundmass composing 20% of the groundmass. The groundmass is primarily quartz +/- adularia with minor white mica.

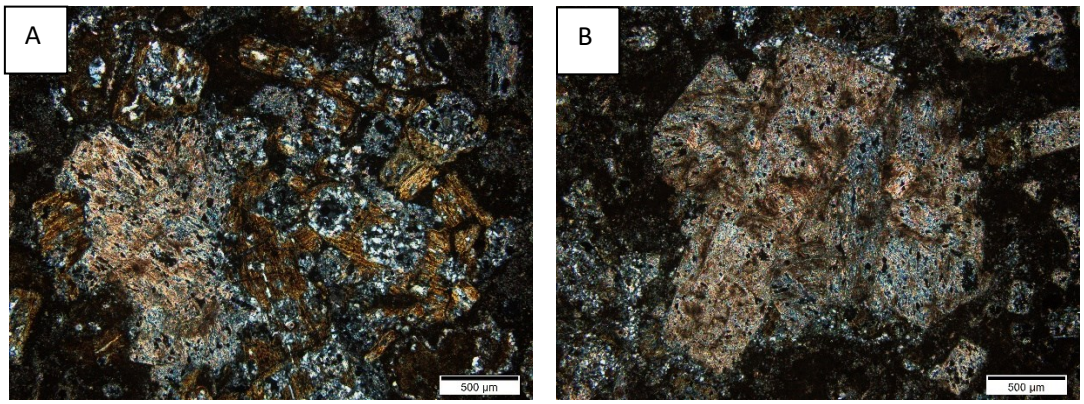

FVN69-292 SEM-EDS

SEM-EDS (1)

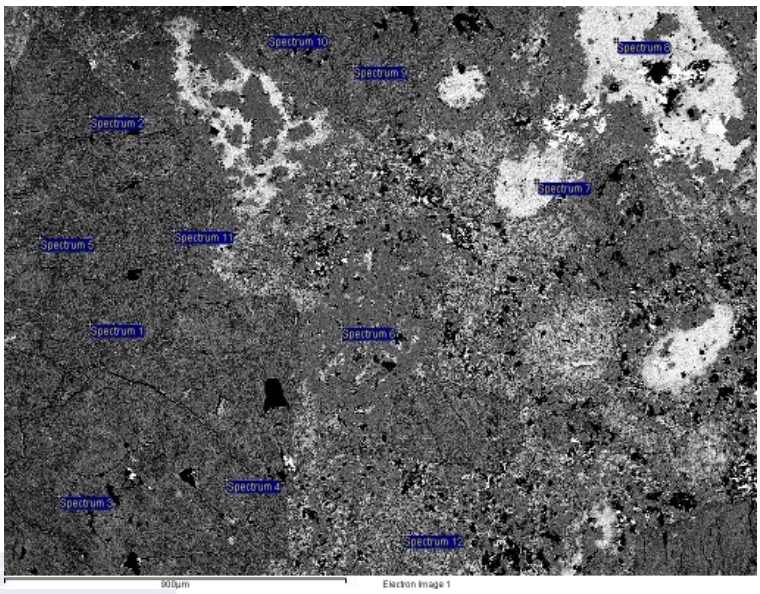

Spectrum	Na	Mg	Al	Si	K	Ca	Ti	Fe	Mineral
Spectrum 1	0	1.39	34.63	56.29	7.69	0	0	0	Illite
Spectrum 2	0.47	5	30.84	47.13	5.33	0	0	11.23	Illite + Smectite + Chlorite?
Spectrum 3	0	1.17	35.16	56.89	6.77	0	0	0	Illite
Spectrum 4	0	1.31	34.23	56.56	7.9	0	0	0	Illite
Spectrum 5	0	1.55	34.57	55.78	8.1	0	0	0	Illite
Spectrum 6	0	0	0.85	96.59	0	0	2.55	0	Quartz + Rutile? (Groundmass)
Spectrum 7	0.49	11.62	26.42	36.46	1.8	0.35	0	22.86	Chlorite + Illite + Smectite (Groundmass)
Spectrum 8	0	15.06	23.88	33.29	0.49	0	0	27.27	Chlorite + Illite (Groundmass)
Spectrum 9	0.73	1.22	33.83	54.14	8.6	0.53	0	0.96	Illite + Smectite
Spectrum 10	0	1.6	33.44	55.71	8.25	0	0	1.01	Illite
Spectrum 11	1.05	1.52	34.96	54.96	6.77	0	0	0.73	Illite + Smectite
Spectrum 12	0	11.51	25.31	35.69	1.82	0	0	25.67	Chlorite +Illite(Groundmass)

High Resolution BSE Image

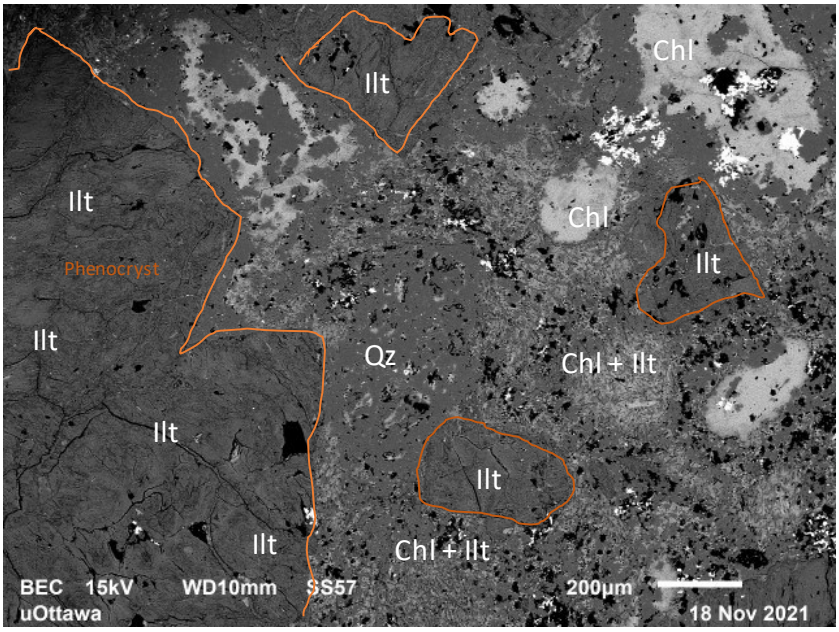

SEM-EDS (2)

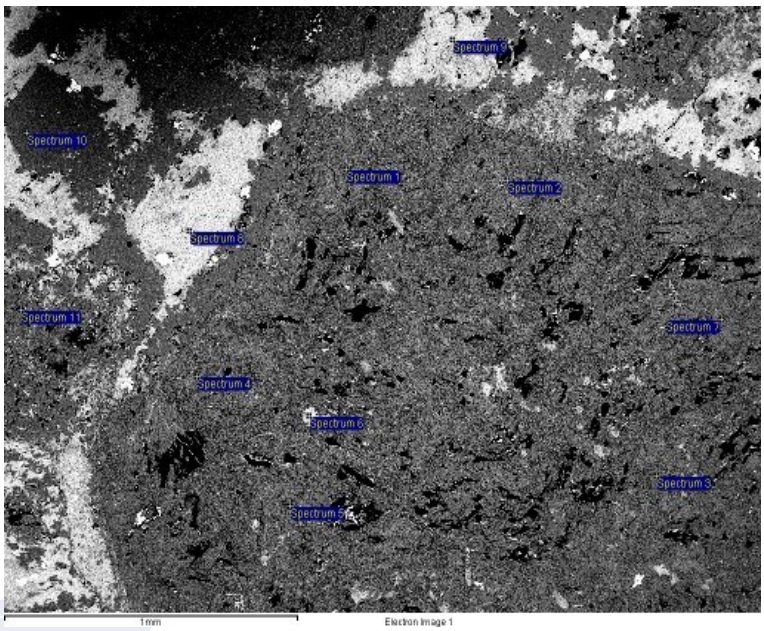

Spectrum	Na	Mg	Al	Si	K	Ca	Mn	Fe	Mineral
Spectrum 1	0.75	1.74	34.39	54.52	7.62	0	0	0.97	Illite + Smectite
Spectrum 2	0	0	2.98	96.59	0.43	0	0	0	Quartz + Minor Illite
Spectrum 3	0	1.36	34.17	55.13	7.66	0	0	1.67	Illite
Spectrum 4	0.64	1.33	33.92	54.64	8.37	0	0	1.11	Illite + Smectite
Spectrum 5	0.68	1.53	33.38	55	8.8	0.63	0	0	Illite + Smectite
Spectrum 6	0	15.04	23.32	30.67	0.52	0.58	0	29.87	Chlorite + minor illite + smectite
Spectrum 7	0.84	1.7	34.29	53.74	8.17	0.42	0	0.83	Illite + Smectite
Spectrum 8	0	14.02	23.94	33.4	0.72	0	0	27.92	Chlorite + minor illite (Groundmass)
Spectrum 9	0	14.52	23.63	32.94	0.67	0	0.85	27.39	Chlorite + minor illite (Groundmass)
Spectrum 10	0	0	0.77	99.23	0	0	0	0	Quartz (Groundmass)
Spectrum 11	0	0	1.57	96.72	0	1.71	0	0	Quartz + minor smectite (Groundmass)

High Resolution BSE Image

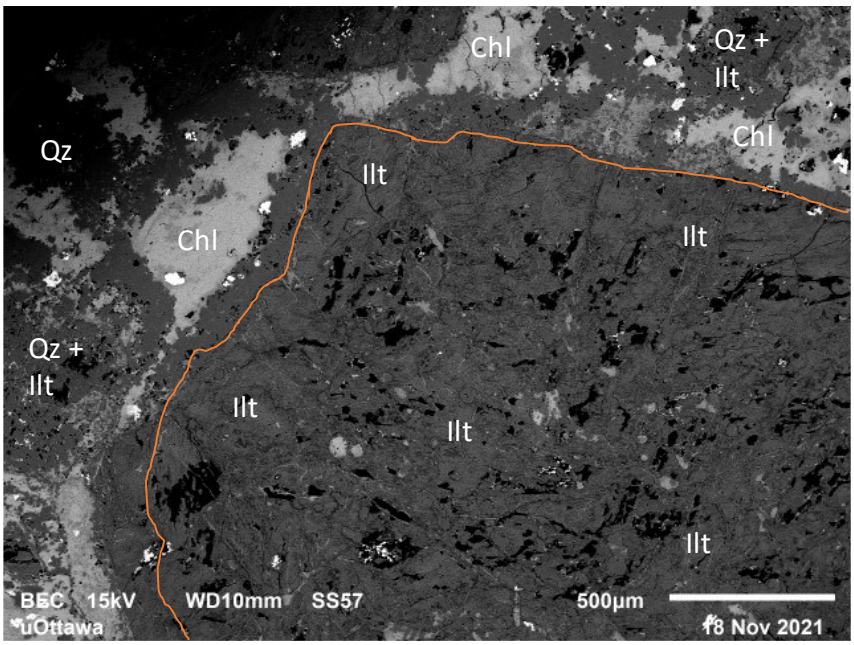

DDH84

FVN84-91

DDH Depth: 91.0m
Sample Desc: Very friable and incoherent. Likely as the result of intense alteration of a less coherent rock type (pyroclastic). Almost entirely composed of gray colour clay minerals with very small (~1mm) white less altered clasts throughout.
XRD Minerals: $Illite_{0.6}$Smectite, Adularia (Simpson & Mauk, 2007)
SWIR Minerals: Not acquired
LOI: Not Analyzed
NH_4^+: Not Analyzed
δ15N: Not Analyzed

No Petrographic Data

FVN84-161

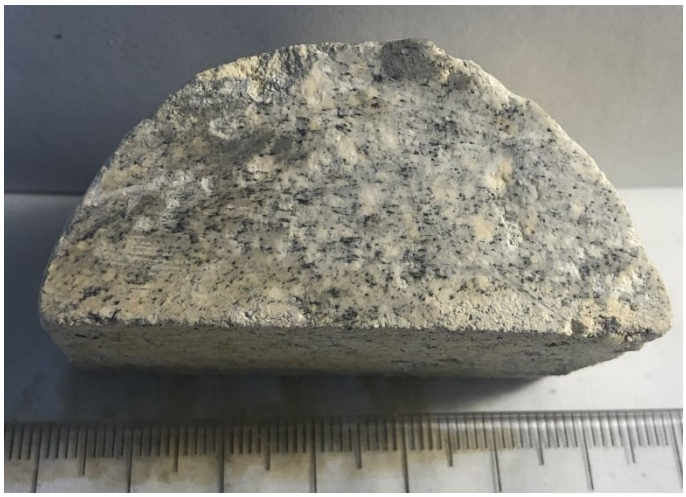

DDH Depth: 161.7m
Sample Desc: Very strongly clay altered andesite. Potential relict clay altered plagioclase although groundmass has also been intensely altered. Abundant disseminated pyrite.
XRD Minerals: $Illite_{0.8}Smectite$ (Simpson & Mauk, 2007)
SWIR Minerals: Not acquired
LOI: 16.3%
NH_4^+: 6501ppm
δ15N: +3.5‰

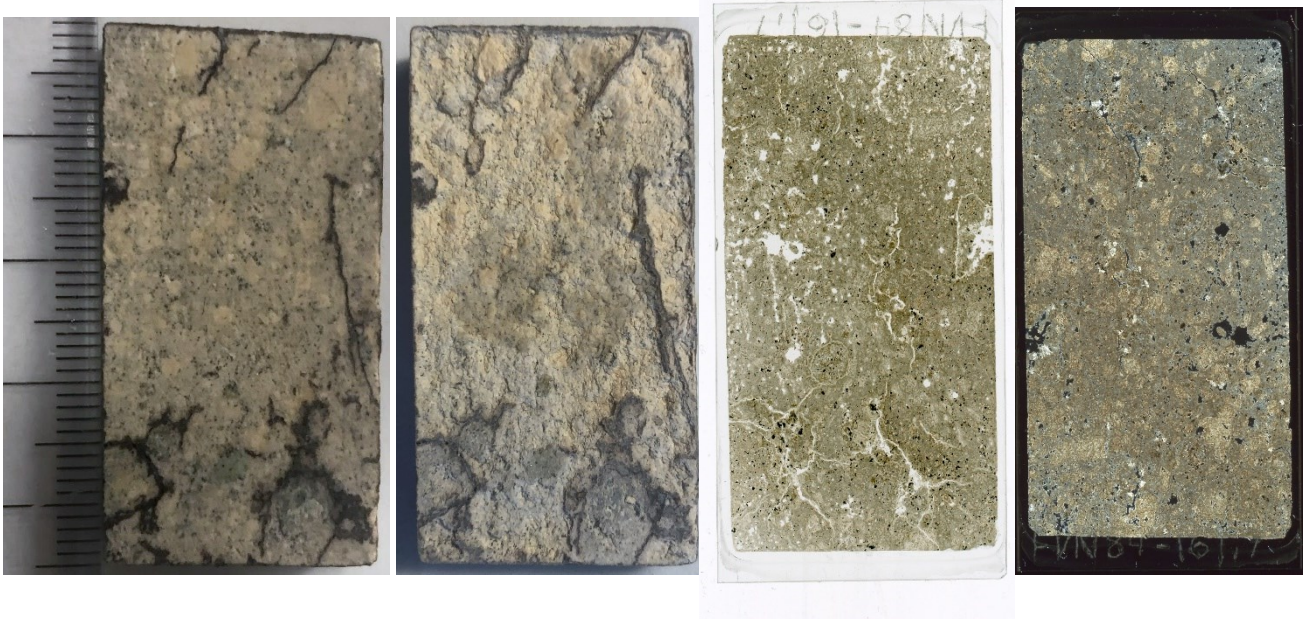

Thin Section Description:

Intensely clay altered andesite. Plagioclase phenocrysts have been completely clay altered. Groundmass contains abundant clay minerals also. Unidentified radiating bladed mineral occurring in patches throughout. Appears to be a phyllosilicate. Abundant disseminated pyrite.

FVN84-202

DDH Depth: 202.9m
Sample Desc: Very strongly clay altered andesite. Potential relict clay altered plagioclase although groundmass has also been intensely altered. Some silicification. Small 2mm gray coloured quartz vein.
XRD Minerals: $Illite_{0.85}$Smectite, Adularia (Simpson & Mauk, 2007)
SWIR Minerals: Not acquired
LOI: Not Analyzed
NH_4^+: Not Analyzed
δ15N: Not Analyzed

Thin Section Description:

Clay altered andesite. Groundmass is intensely altered with abundant brown coloured clay minerals. Some plagioclase phenocrysts are intensely altered whereas other show small amounts of white mica alteration. Minimally altered phenocrysts appear to be adularia altered. Disseminated pyrite throughout.

FVN84-228

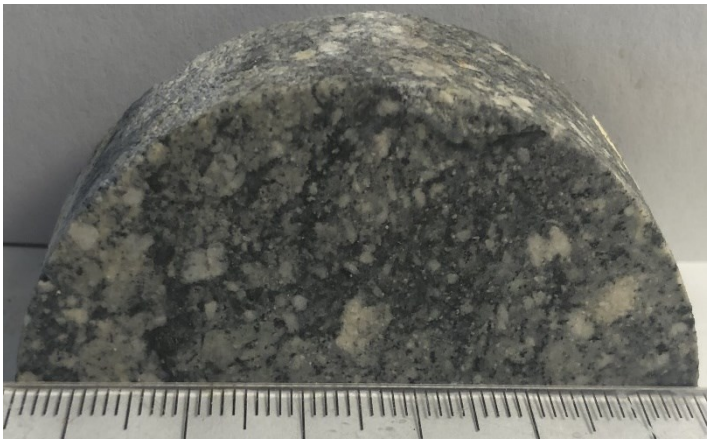

DDH Depth: 228.4m
Sample Desc: Very strongly clay altered andesite. Strongly clay altered plagioclase phenocrysts (1-5mm). Groundmass is gray coloured and has also been intensely altered with minor bleaching.
XRD Minerals: $Illite_{0.85}Smectite$, Adularia (Simpson & Mauk, 2007)
SWIR Minerals: Not acquired
LOI: 5.3%
NH_4^+: Not Analyzed
δ15N: Not Analyzed

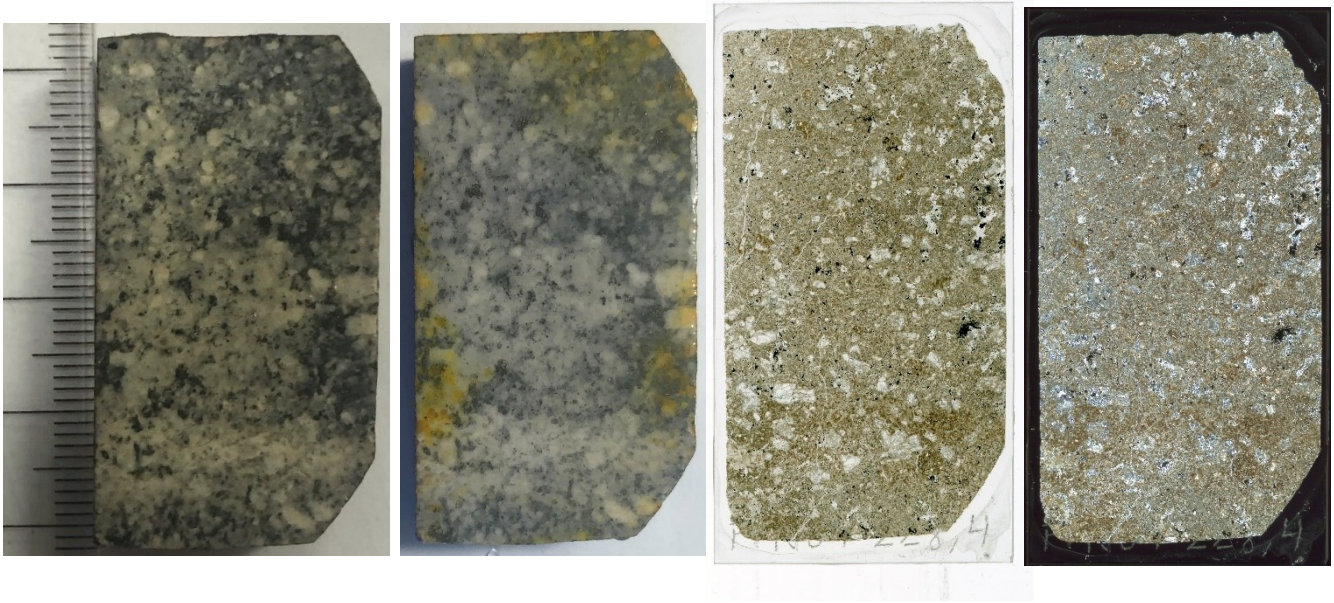

Thin Section Description:

Clay altered andesite. Groundmass is intensely altered with abundant brown coloured clay minerals. Some plagioclase phenocrysts are intensely altered whereas other show small amounts of white mica alteration. Minimally altered phenocrysts appear to be adularia altered. Disseminated pyrite throughout.

FVN84-285V

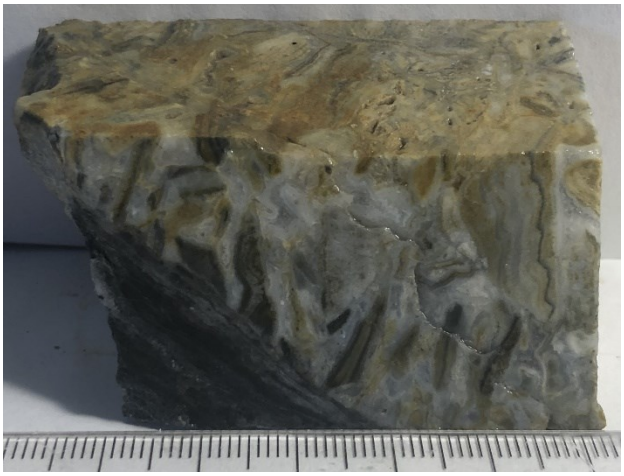

DDH Depth: 285.5m
Sample Desc: Collected at OceanaGold. Vein sample. "Oatmeal" breccia. Small, brecciated fragments of veins and wallrock cemented by silica. Large dark wallrock fragment at bottom left. Some clasts contain abundant clay minerals.
XRD Minerals: Not acquired
SWIR Minerals: Not acquired
LOI: Not Analyzed
NH_4^+: Not Analyzed
δ15N: Not Analyzed

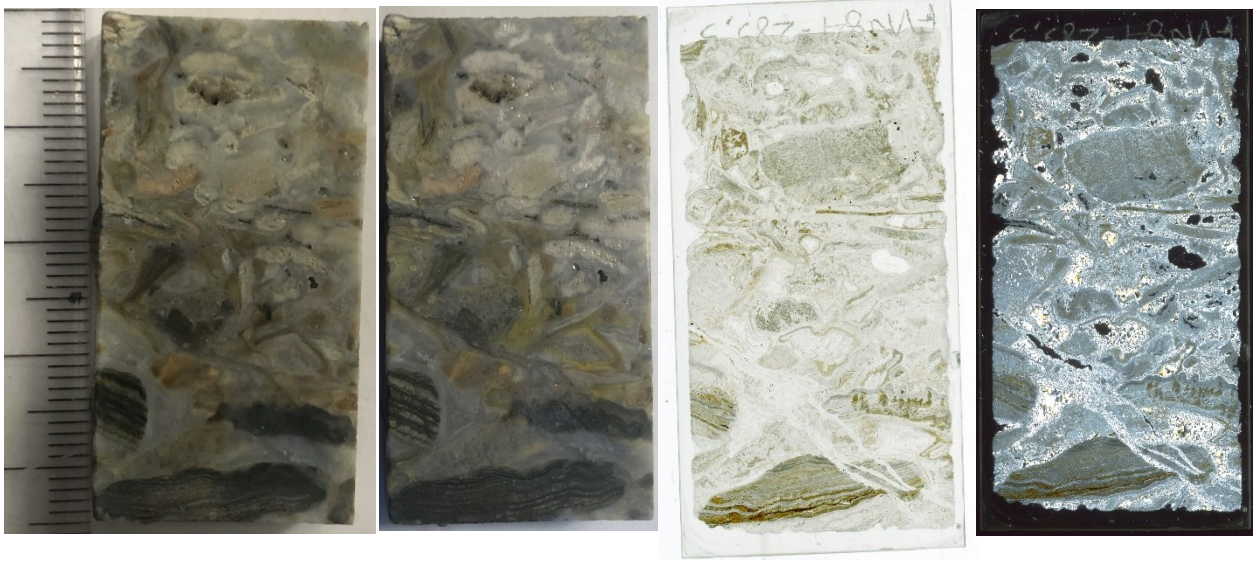

No Thin Section Description

FVN84-316

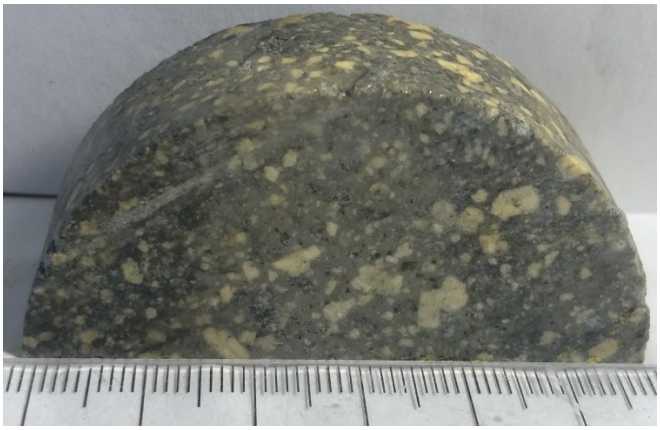

DDH Depth: 316.4m
Sample Desc: Clay (+chlorite) altered plagioclase phyric andesite. Plagioclase phenocrysts (1-5mm) are intensely clay (+/- adularia) altered. Groundmass is a greenish brown colour (chlorite). Disseminated pyrite throughout.
XRD Minerals: Illite, Adularia, Chlorite (Simpson & Mauk, 2007)
SWIR Minerals: Not acquired
LOI: 4.5%
NH_4^+ : 2661ppm

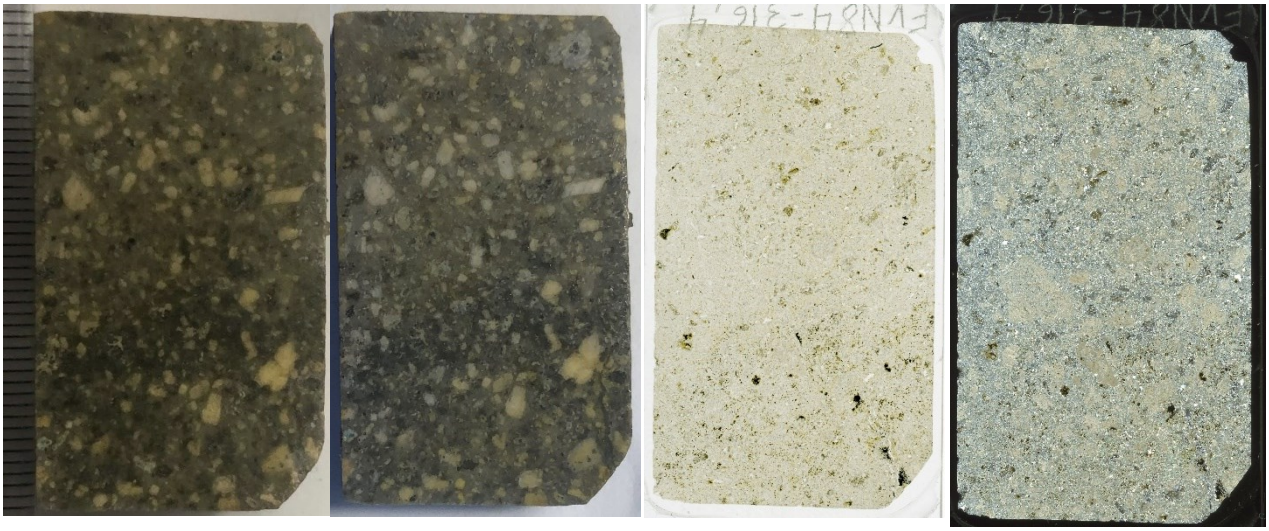

Thin Section Description:
Plagioclase phyric andesite. 40% plagioclase phenocrysts which have been adularia altered and strongly (90-100%) altered to white mica. The white mica appears to be quite coarsely crystalline in some phenocrysts (Photomicrograph A). 10% pyroxene phenocrysts which have been completely replaced by chlorite (70%) and quartz. Groundmass appears to be composed of quartz +/- adularia and white mica. There appears to be a primary plagioclase lath texture in the groundmass which has been overprinted and completely replaced by white mica and quartz. White mica makes up 30% of the groundmass. Quartz is quite coarse within the groundmass. 15% euhedral pyrite disseminated throughout.

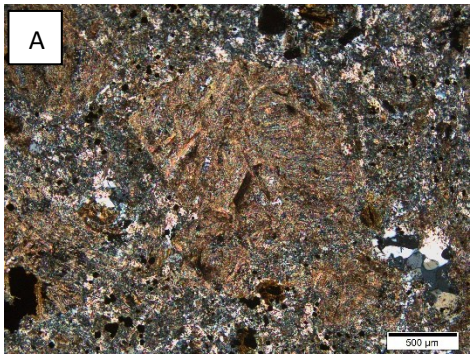

FVN84-365

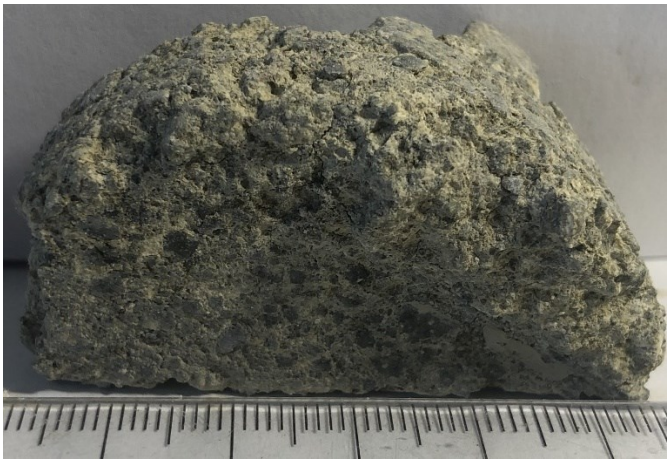

DDH Depth: 365.9m
Sample Desc: Very intensely clay altered. Difficult to discern primary textures though appears as if there are ~15% dark-coloured clasts ranging from 1-10mm. Matrix is yellowish brown and receded compared to clasts.
XRD Minerals: Illite, Chlorite (Simpson & Mauk, 2007)
SWIR Minerals: Not acquired
LOI: Not Analyzed
NH_4^+: Not Analyzed
δ15N: Not Analyzed

No Petrographic Data

FVN84-421

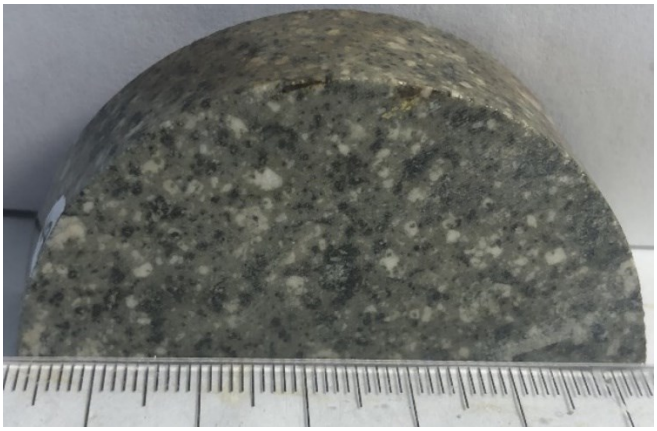

DDH Depth: 421.7m
Sample Desc: Plagioclase phyric (1-4mm) altered andesite. Intense chlorite alteration of groundmass. Chlorite patches throughout. Plagioclase phenocrysts appear to be clay altered.
XRD Minerals: Illite, Adularia, Chlorite (Simpson & Mauk, 2007)
SWIR Minerals: Not acquired
LOI: 4.7%
NH_4^+: 1843ppm
δ15N: +3.1‰

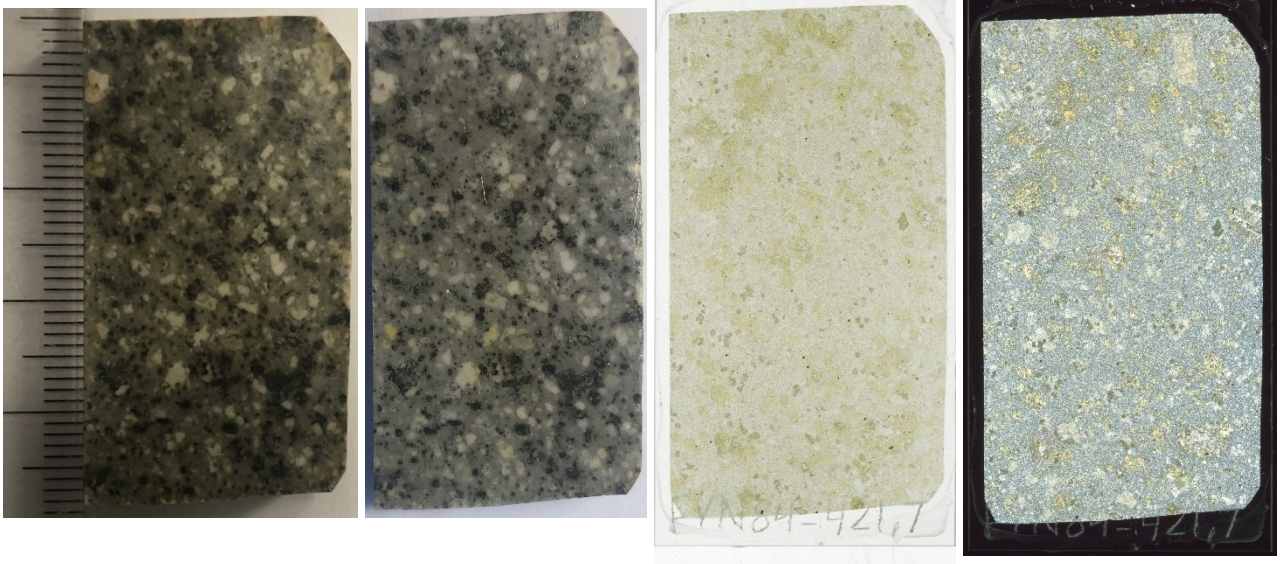

Thin Section Description:

Plagioclase phyric andesite. 20% plagioclase phenocrysts have been completely replaced by white mica +/- calcite (could be adularia or primary plagioclase (high Na so probably plag); check SEM). 20% pyroxene phenocrysts which have been completely replaced by chlorite. Groundmass contains abundant microcrystalline quartz +/- adularia though there is (10%) white mica and 10% fine grained chlorite distributed throughout the groundmass.

FVN85-85

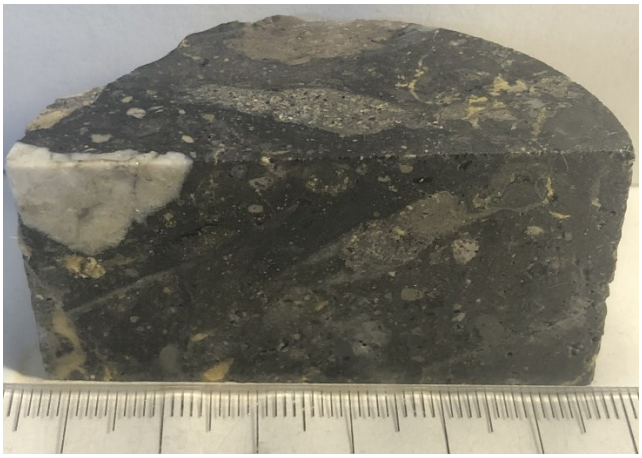

DDH Depth: 85.7m
Sample Desc: Polymictic (hydrothermal) breccia. Clasts are 0.1cm to 2cm in size and are varying compositions. The most abundant clasts are altered andesites. Large quartz vein clast. Minor clay rich clasts. Matrix is dark black aphanitic / glassy.
XRD Minerals: Illite0.8Smectite, Adularia (Simpson & Mauk, 2007)
SWIR Minerals: Not acquired
LOI: 1.9%
NH_4^+: 284ppm
δ15N: 7.1‰

Thin Section Description:

Hydrothermal breccia. Matrix is composed of gel microcrystalline quartz with small patches of clay minerals throughout. Clasts vary in size and composition. Most appear to be clasts of strongly clay altered wallrock. There are also (colloform) vein and sulfide clasts throughout.

FVN85-114

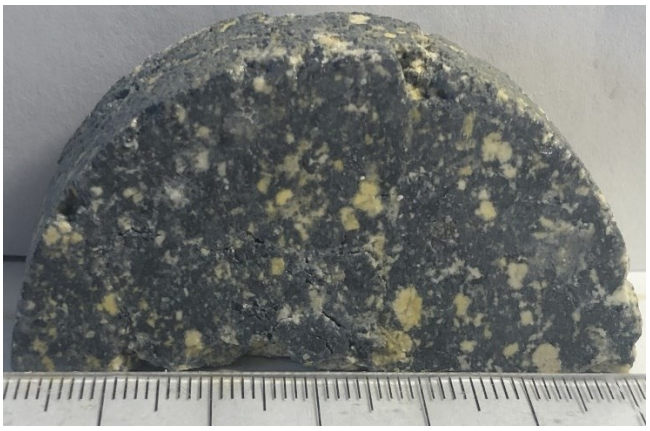

DDH Depth: 114.3m
Sample Desc: Moderately altered plagioclase phyric andesite or pyroclastic. Both phenocrysts and groundmass appear to be altered. Phenocrysts are 1-5mm altered to clays. Groundmass is light gray and is softer than similar samples.
XRD Minerals: Illite0.8Smectite, Adularia (Simpson & Mauk, 2007)
SWIR Minerals: Not acquired
LOI: Not Analyzed
NH_4^+: Not Analyzed
δ15N: Not Analyzed

Thin Section Description:

Intensely altered plagioclase phyric andesite. Plagioclase phenocrysts are intensely altered with fine grained white micas. The groundmass appears to be primarily quartz (and white mica) with fine opaque mineral throughout. Appears as though very fine pyrite is disseminated through the groundmass which is possibly causing the gray colour in the quartz.

FVN85-226

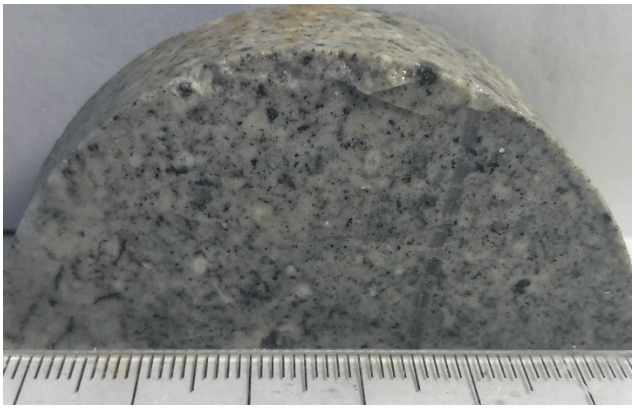

DDH Depth: 226.6m
Sample Desc: Plagioclase phyric andesite. Minor plagioclase phenocrysts (~1mm). Minor small dark phenocrysts (0.5-1mm). Disseminated pyrite throughout. Groundmass appears bleached / clay (+silica) altered. Small 1mm quartz vein.
XRD Minerals: Illite0.9Smectite, Adularia (Simpson & Mauk, 2007)
SWIR Minerals: Not acquired
LOI: 7.5%
NH_4^+: 2562ppm

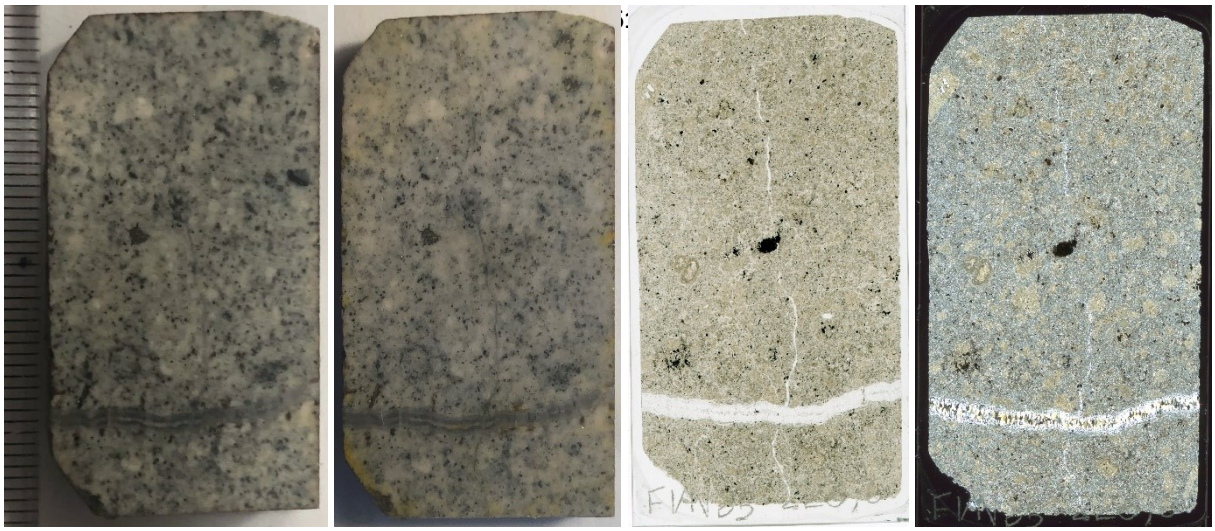

Thin Section Description:
Intensely white mica altered plagioclase phyric andesite. Contains 30% 0.1-2mm plagioclase phenocrysts which have been completely replaced by very fine-grained white mica +/- quartz. Quartz forms in fractures within the phenocrysts and as veinlets throughout the groundmass. Groundmass is primarily cryptocrystalline quartz (70%) with patchy white mica (30%) throughout. 10% pyrite disseminated throughout groundmass. Zoning of phenocrysts is visible in thin section (Photomicrograph A) but appears compositionally identical in SEM-EDS.

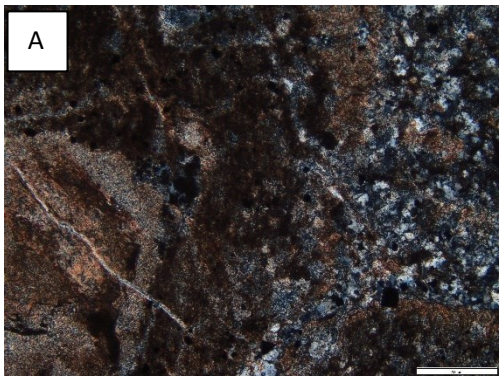

FVN85-226 SEM-EDS

SEM-EDS (1)

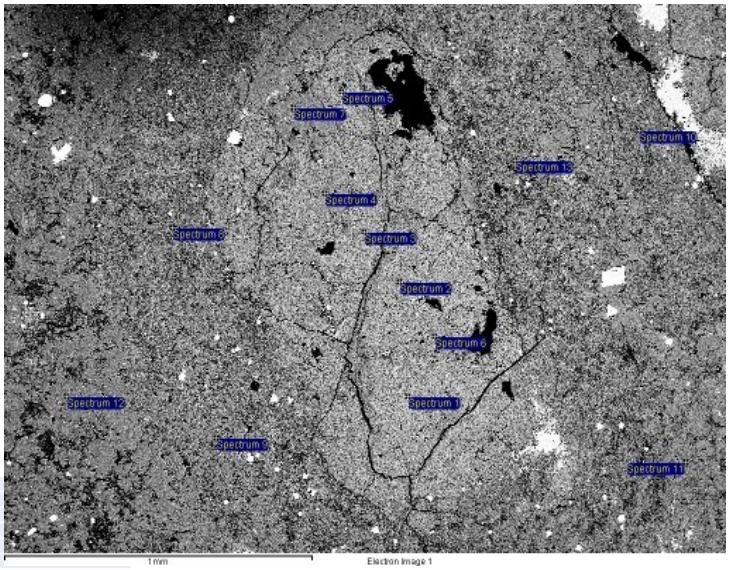

Spectrum	Mg	Al	Si	K	Fe	Mineral
Spectrum 1	1.66	33.77	57.98	6.59	0	Illite
Spectrum 2	2.51	32.74	56.61	6.95	1.19	Illite
Spectrum 3	2.56	33.15	58.48	5.81	0	Illite
Spectrum 4	2.48	32.37	58.54	6.61	0	Illite
Spectrum 5	2.52	32.17	57.43	6.9	0.98	Illite
Spectrum 6	2.16	31.9	57.11	7.86	0.98	Illite
Spectrum 7	0	0.91	99.09	0	0	Quartz
Spectrum 8	3.8	29.44	57.78	8.98	0	Illite (Groundmass)
Spectrum 9	0	1.93	98.07	0	0	Quartz (Groundmass)
Spectrum 10	3.25	30.56	58.87	7.32	0	Illite (Groundmass)
Spectrum 11	0.91	8.48	88.65	1.96	0	Quartz + Illite (Groundmass)
Spectrum 12	0	0	100	0	0	Quartz (Groundmass)
Spectrum 13	2.27	33.09	57.83	6.81	0	Illite (Groundmass)

High Resolution BSE Image

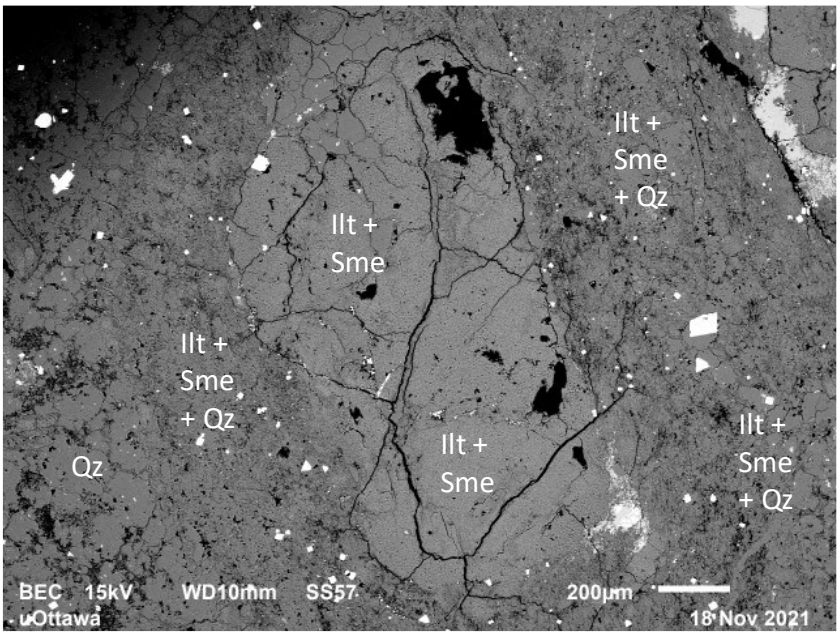

SEM-EDS (2)

600x zoom of (1) phenocryst

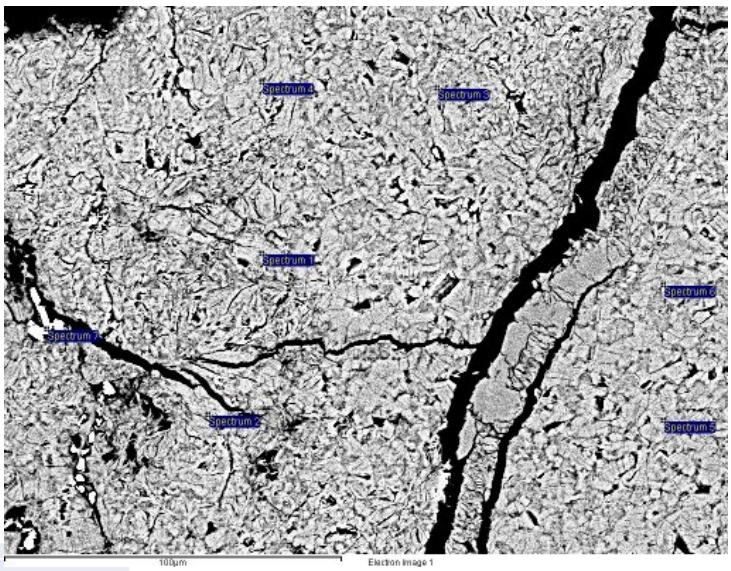

Spectrum	Mg	Al	Si	K	Ti	Mineral
Spectrum 1	2.65	31.61	57.44	8.3	0	Illite
Spectrum 2	2	32.86	57.64	7.49	0	Illite
Spectrum 3	2.33	33.37	56.94	7.35	0	Illite
Spectrum 4	2.24	33.01	56.84	7.91	0	Illite
Spectrum 5	2.35	32.55	58.57	6.53	0	Illite
Spectrum 6	2.35	33.05	57.66	6.94	0	Illite
Spectrum 7	0	2.36	5.28	0.85	91.51	Rutile + Illite

High Resolution BSE Image

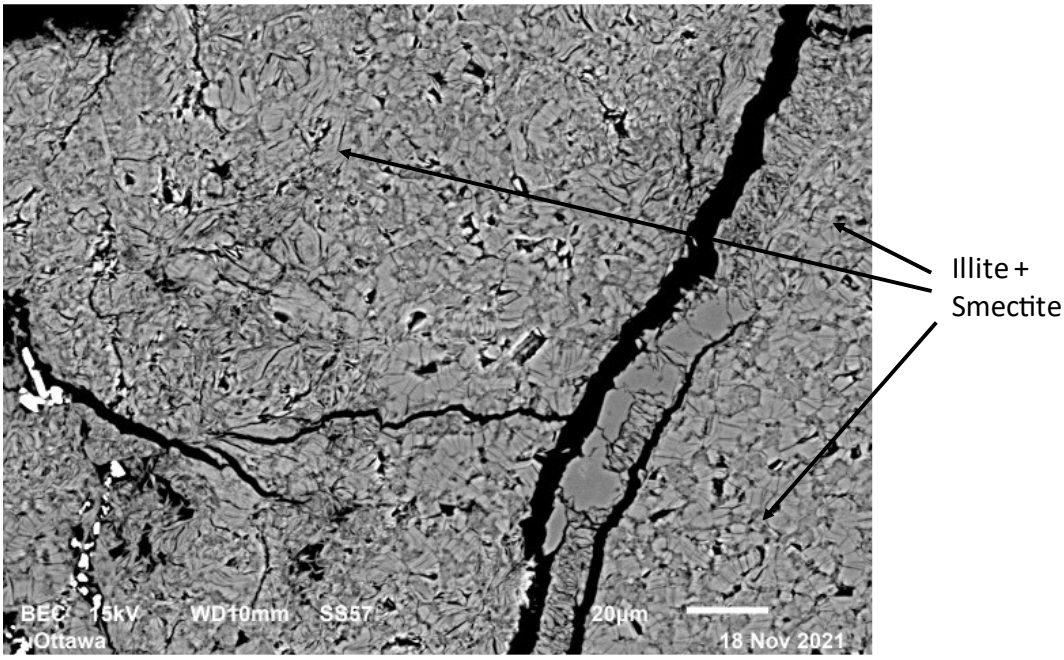

FVN85-338

DDH Depth: 338.5m
Sample Desc: Very intensely clay altered. Difficult to discern primary textures though appears as if there are ~5% slightly less altered clasts ranging from 1-10mm.
XRD Minerals: Illite, Chlorite (Simpson & Mauk, 2007)
SWIR Minerals: Not acquired
LOI: Not Analyzed
NH_4^+: Not Analyzed
δ15N: Not Analyzed

Thin Section Description:

Intensely clay altered volcaniclastic. Clasts range from 0.2-1cm and are very intensely clay altered along with the matrix. Textures difficult to discern due to high alteration intensity. Matrix is composed of fine clays. Fine quartz clasts distributed throughout. A few clasts are composed of jigsaw textured quartz (+/- adularia). Pyrite disseminated throughout.

FVN85-404

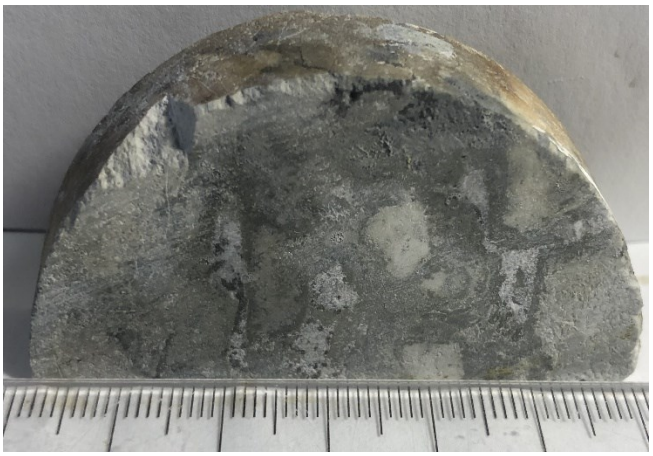

DDH Depth: 404.3m
Sample Desc: Intensely clay altered. Difficult to discern primary textures though appears as if there are ~5% slightly less altered clasts (lighter spots) ranging from 1-10mm.
XRD Minerals: Illite, Adularia, Chlorite (Simpson & Mauk, 2007)
SWIR Minerals: Not acquired
LOI: Not Analyzed
NH_4^+: Not Analyzed
δ15N: Not Analyzed

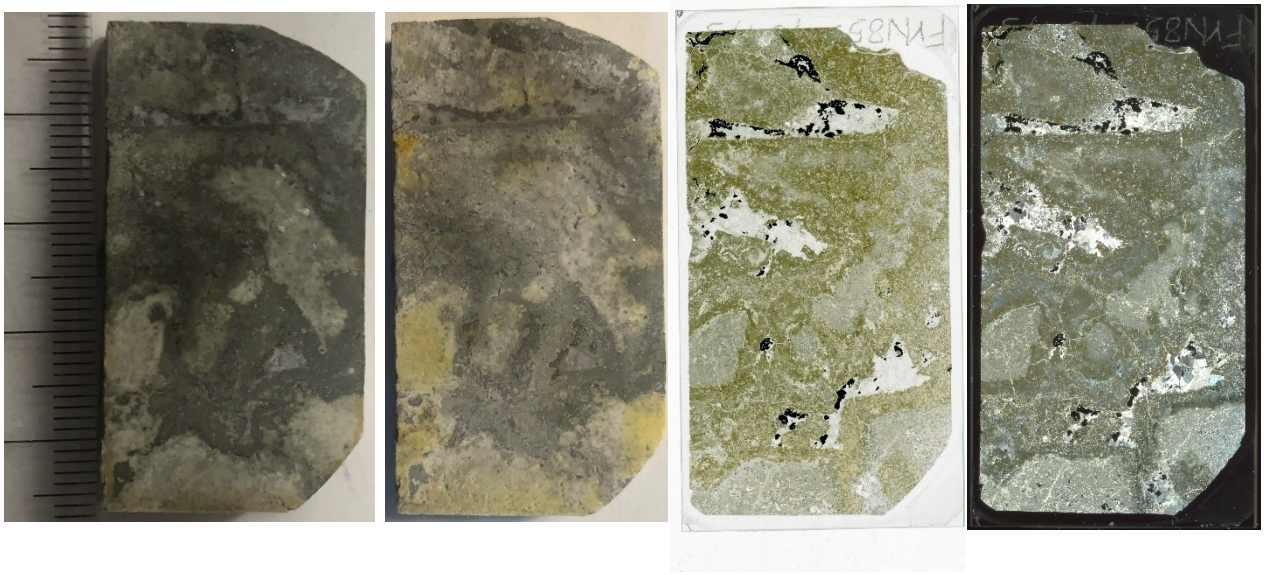

Thin Section Description:

Intensely clay altered volcaniclastic rock. White coloured clasts are composed fine grained white micas. Darker matrix is difficult to distinguish due to poor polishing though it appears to be mainly clay minerals (+possibly chlorite due to green tinge). Patches of vug filling calcite throughout. Calcite is associated with large euhedral pyrite grains. Finely disseminated pyrite elsewhere.

DDH 87

FVN87-211

DDH Depth: 211.0m

Sample Desc: Plagioclase phyric (0.1-0.4cm) altered andesite. Phenocrysts are clay +/- adularia altered. Groundmass is silicified. Disseminated pyrite.

XRD Minerals: Quartz, Adularia, $Illite_{0.85}$Smectite, Pyrite (Simpson & Mauk, 2007)

SWIR Minerals: NH4-mineral +/- Gypsum (Simpson, 2015)

LOI: 6.4%

NH_4^+: 3837ppm

δ15N: +2.2‰

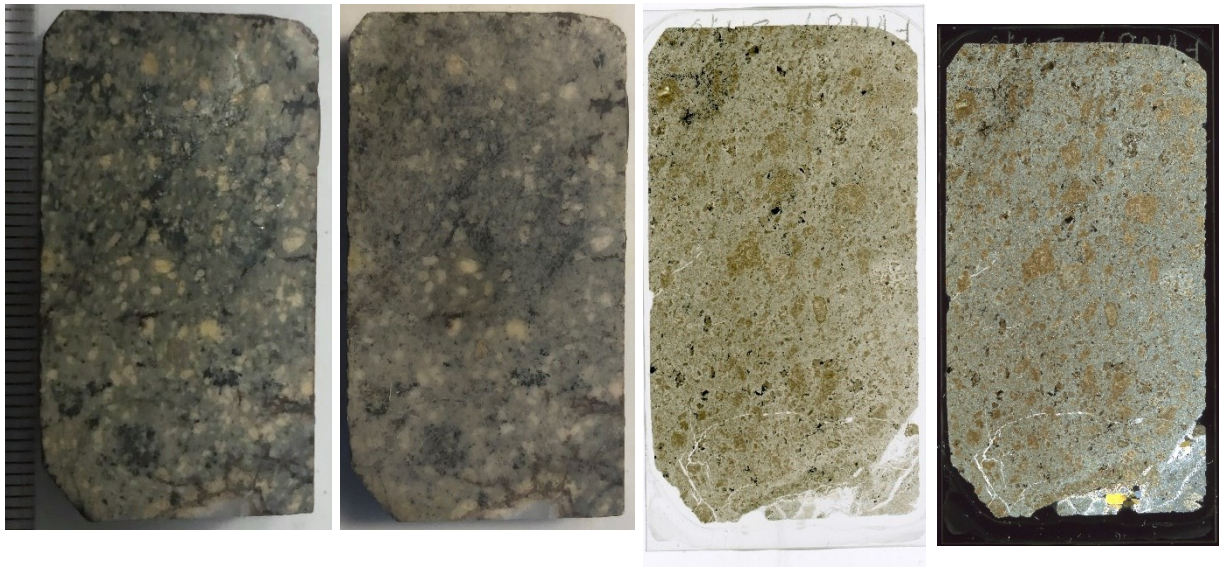

Thin Section Description:

Intensely white mica altered andesite. 30% 0.2-1.5mm plagioclase phenocrysts which have been completely replaced by fine-grained white mica. Groundmass is primarily cryptocrystalline quartz contains patchy fine white mica throughout. May contain very fine to microcrystalline adularia in the groundmass as it was identified by XRD though it was not discernable in SEM-EDS. Fine grained pyrite disseminated throughout.

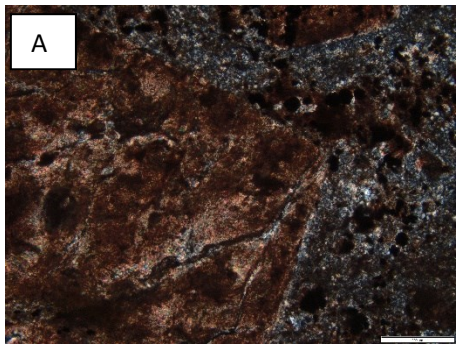

FVN87-211 SEM-EDS

SEM-EDS (1)

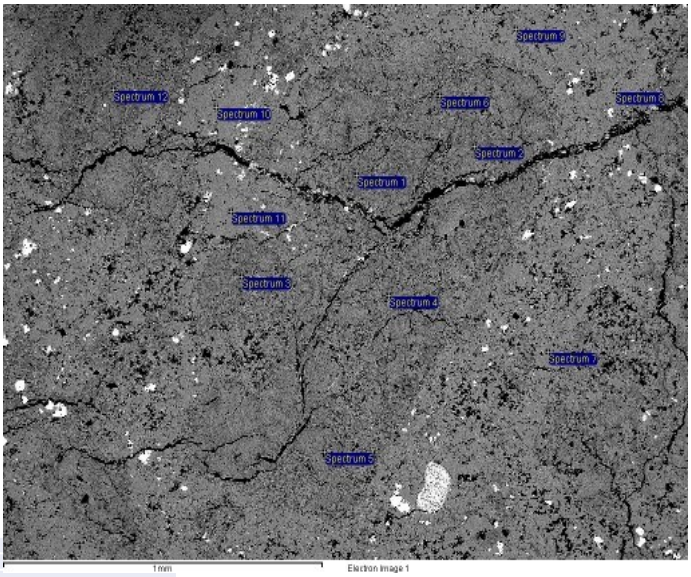

Spectrum	Mg	Al	Si	K	Ca	Fe	Mineral
Spectrum 1	2.38	32.86	58.28	5.72	0	0.76	Illite + Smectite
Spectrum 2	3.06	30.29	59.12	6.45	0	1.08	Illite + Smectite
Spectrum 3	2.09	32.95	57.88	6.19	0.9	0	Illite + Smectite
Spectrum 4	2.12	32.45	58.64	6.06	0	0.73	Illite + Smectite
Spectrum 5	0	5.52	93.62	0.86	0	0	Quartz + Illite
Spectrum 6	2.16	33.55	58.15	5.25	0	0.9	Illite + Smectite
Spectrum 7	0	2.22	97.78	0	0	0	Quartz + Illite (Groundmass)
Spectrum 8	0	2.85	96.85	0.3	0	0	Quartz + Illite (Groundmass)
Spectrum 9	0.66	12.13	85.49	1.71	0	0	Quartz + Illite + Smectite (Groundmass)
Spectrum 10	0	1.25	98.75	0	0	0	Quartz + Illite (Groundmass)
Spectrum 11	0	0.64	99.36	0	0	0	Quartz +Illite(Groundmass)
Spectrum 12	1.69	34.88	58.35	5.08	0	0	Illite+ Smectite

High Resolution BSE Image

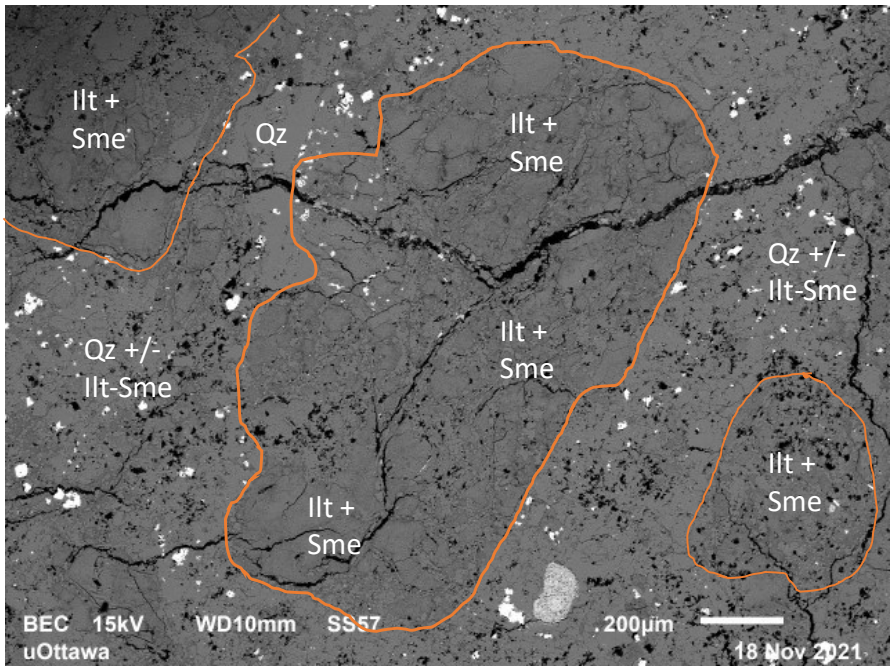

SEM-EDS (2)

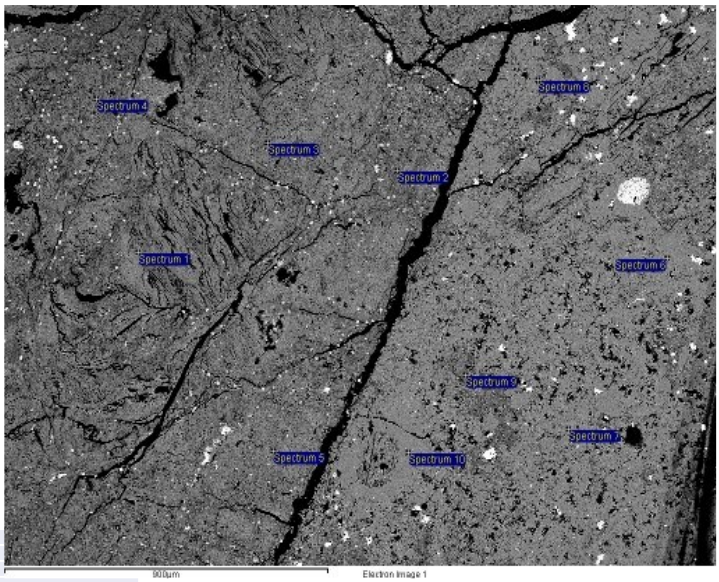

Spectrum	Mg	Al	Si	K	Ca	Mineral
Spectrum 1	1.67	33.86	59.15	5.32	0	Illite + Smectite
Spectrum 2	1.81	33.55	59.12	5.53	0	Illite + Smectite
Spectrum 3	2.26	32.73	59.48	5.54	0	Illite + Smectite
Spectrum 4	1.88	33.16	59.3	5.66	0	Illite + Smectite
Spectrum 5	2.1	32.82	59.32	5.76	0	Illite + Smectite
Spectrum 6	0	1.34	98.66	0	0	Quartz + minor illite (Groundmass)
Spectrum 7	0	0.95	99.05	0	0	Quartz + minor illite (Groundmass)
Spectrum 8	1.25	12.7	83.52	2.53	0	Quartz + illite + smectite (Groundmass)
Spectrum 9	1.35	17.58	76.82	4.25	0	Quartz + illite + smectite (Groundmass)
Spectrum 10	0	0.87	99.13	0	0	Quartz + minorillite(Groundmass)

High Resolution BSE Image

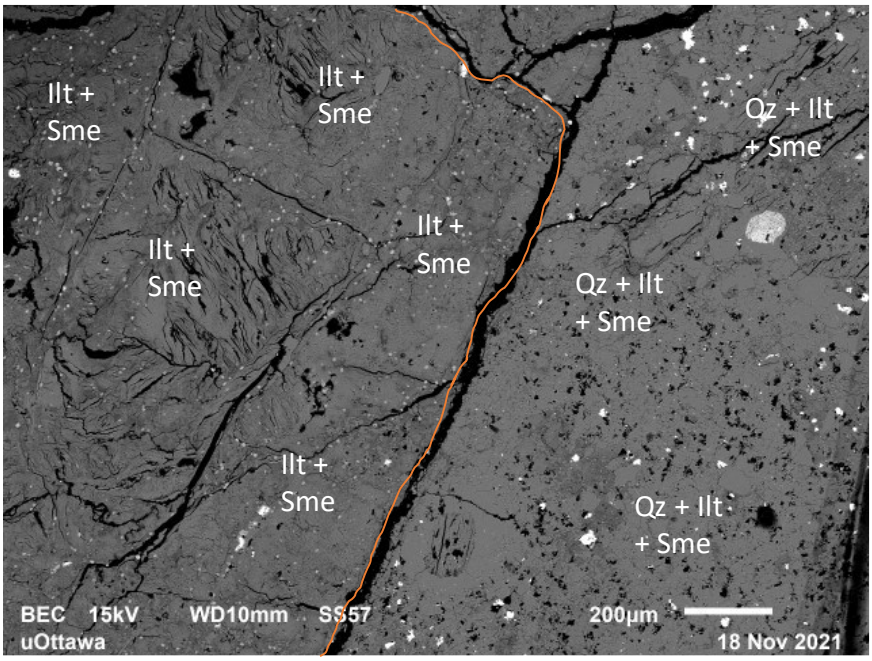

FVN87-251

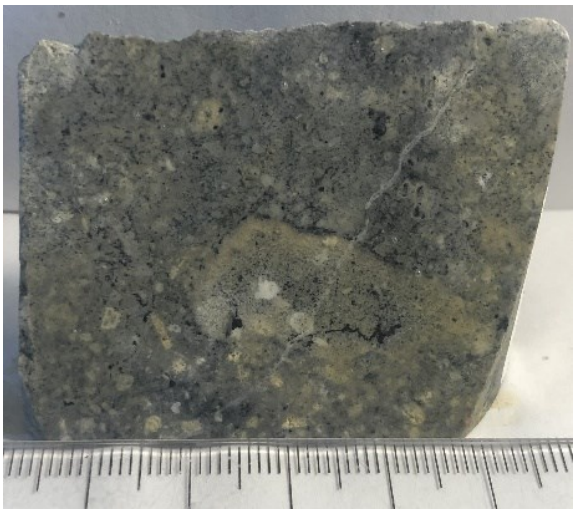

DDH Depth: 251.8m
Sample Desc: Altered plagioclase phyric (0.1-0.3cm) andesite. Phenocrysts have been clay altered. Groundmass appears silicified.
XRD Minerals: Quartz, Adularia, Illite, Pyrite (Simpson & Mauk, 2007)
SWIR Minerals: NH4-mineral +/- Gypsum (Simpson, 2015)
LOI: 5.8%
NH_4^+: Not Analyzed
δ15N: Not Analyzed

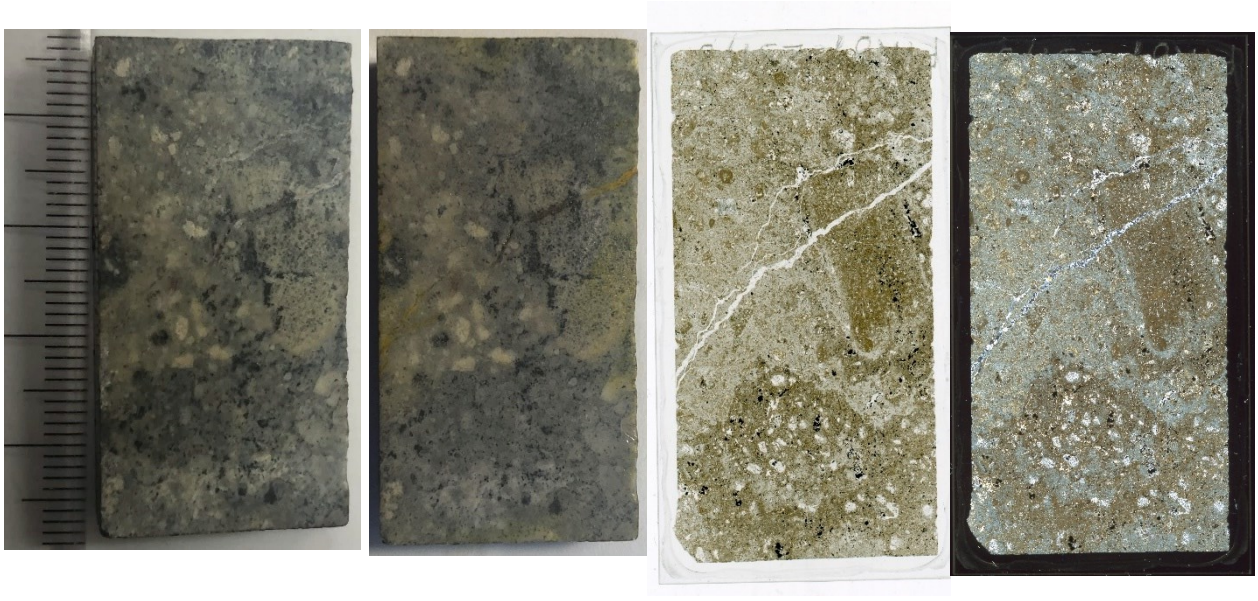

Thin Section Description:

Highly altered plagioclase phyric andesite or volcaniclastic rock. Appears to contain clasts of andesite within a plagioclase phyric andesite. Top right shows 1-2cm possible clasts of andesite. Is intensely clay altered with a brown-coloured clay rich groundmass and small to no phenocrysts. The bottom of the sample appears to contain a different rock with brown clay altered groundmass and euhedral microcrystalline quartz (probably silica filling weathered out plagioclase?). The rest of the sample (top-middle left) appears like the typical plagioclase phyric andesite. Intensely clay altered plagioclase phenocrysts with a quartz rich groundmass. Veinlet containing quartz and adularia.

FVN87-299

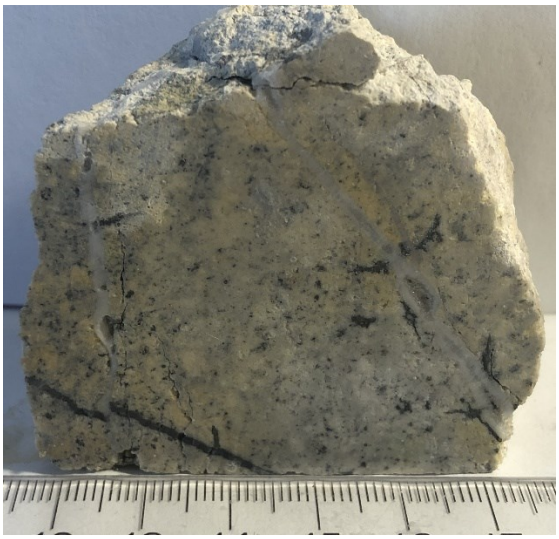

DDH Depth: 299.6m
Sample Desc: Intensely clay altered plag phyric andesite. Groundmass and phenocrysts have both been clay altered. Phenocrysts are small (~1mm). Pyrite blebs associated with minor 1mm quartz veins.
XRD Minerals: Quartz, Illite, Pyrite (Simpson & Mauk, 2007)
SWIR Minerals: Illite +/- Gypsum (Simpson, 2015)
LOI: Not Analyzed
NH_4^+: Not Analyzed
δ15N: Not Analyzed

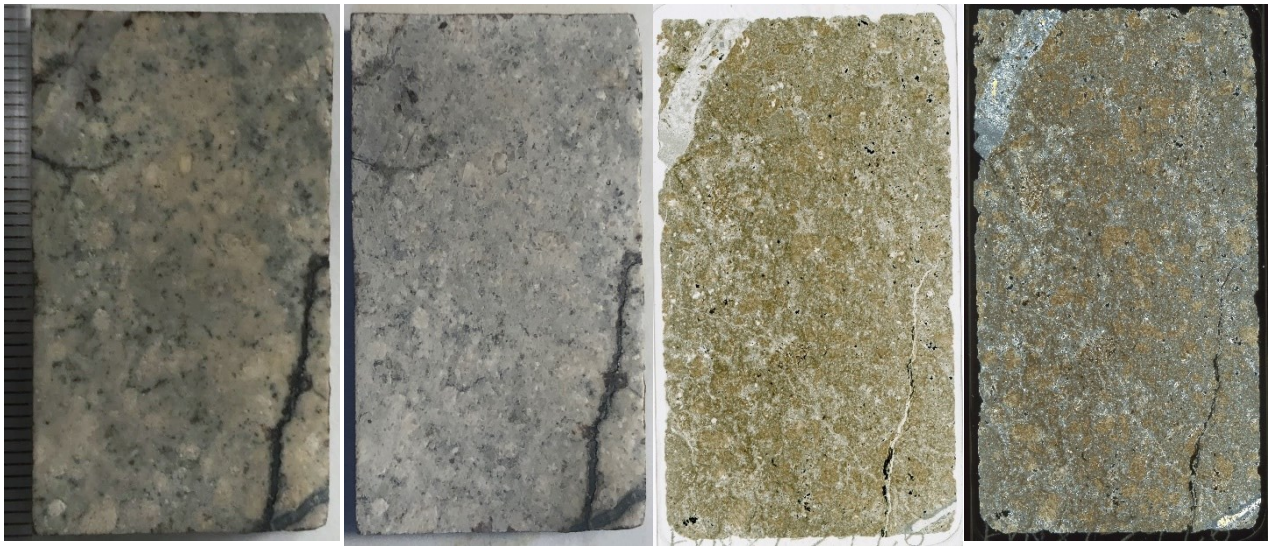

Thin Section Description:

Intensely clay altered plagioclase phyric andesite. Plagioclase phenocrysts have been completely white mica altered. Groundmass is composed of fine quartz and abundant dark brown coloured clay minerals.

FVN87-337

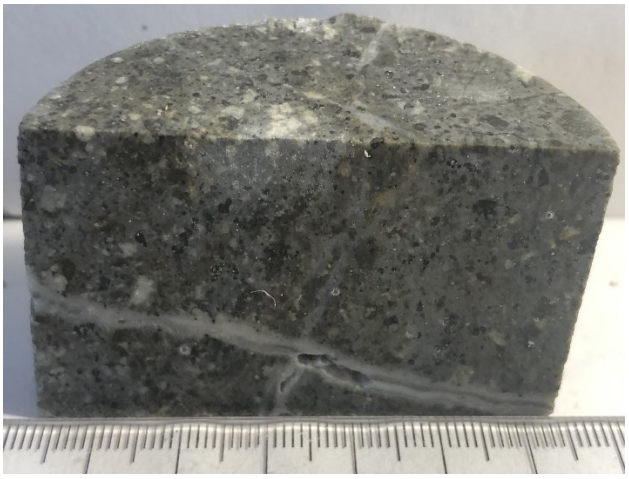

DDH Depth: 337.6m

Sample Desc: Plagioclase phyric andesite. Minimal alteration although plagioclase phenocrysts (0.1-0.5cm) appear to be clay altered. Adularia altered. Small 2mm quartz vein. Chlorite in groundmass.

XRD Minerals: Quartz, Adularia, Chlorite, $Illite_{0.95}$Smectite, Pyrite (Simpson & Mauk, 2007)

SWIR Minerals: NH4-mineral +/- Chlorite (Simpson, 2015)

LOI: 5.8%

$NH4^+$: Not Analyzed

δ15N: Not Analyzed

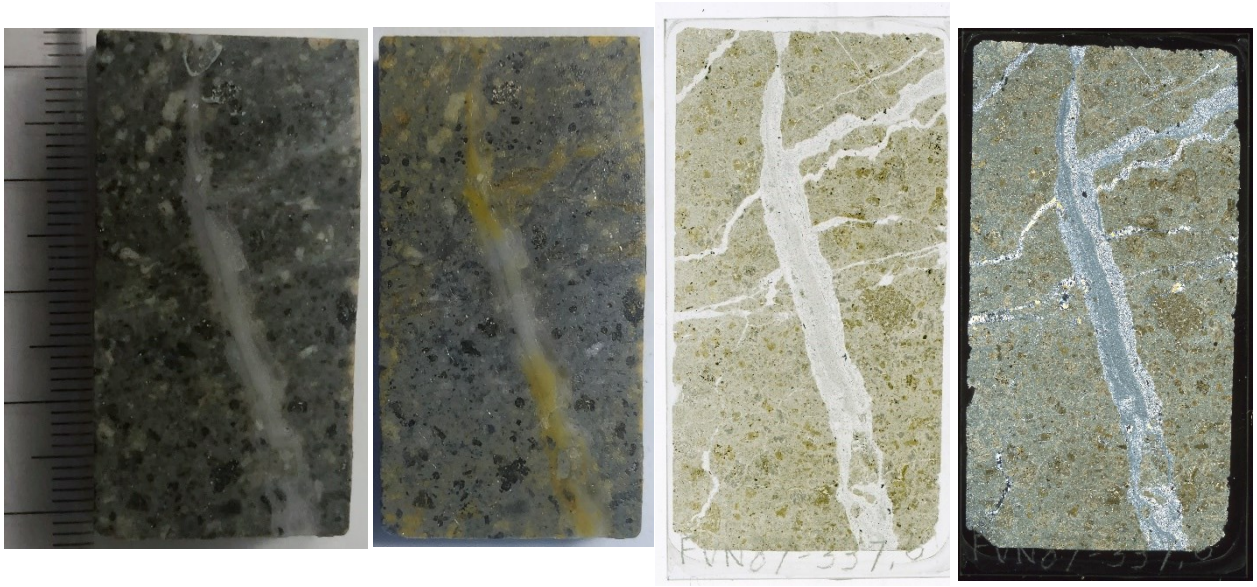

Thin Section Description:

Altered plagioclase phyric (+ hornblende) andesite. Plagioclase phenocrysts have been completely sericitized. Dark patches seen in hand sample appear to be completely chloritized amphibole / pyroxene. The groundmass contains abundant clay minerals. Adularia is primarily found in the quartz adularia veinlets cross cutting the samples.

FVN87-346

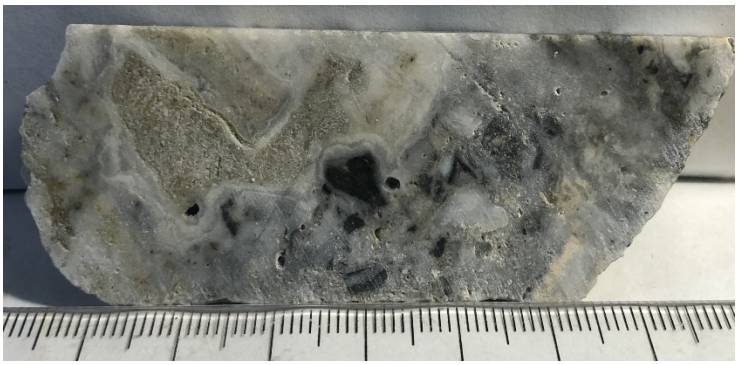

DDH Depth: 346.7m
Sample Desc: Vein or hydrothermal breccia. Highly silicified wallrock + vein breccia. Colloform bands surrounding brecciated area. Potential clay rich patch in top left.
XRD Minerals: Not Acquired
SWIR Minerals: Not Acquired
LOI: Not Analyzed
NH_4^+: Not Analyzed
δ15N: Not Analyzed

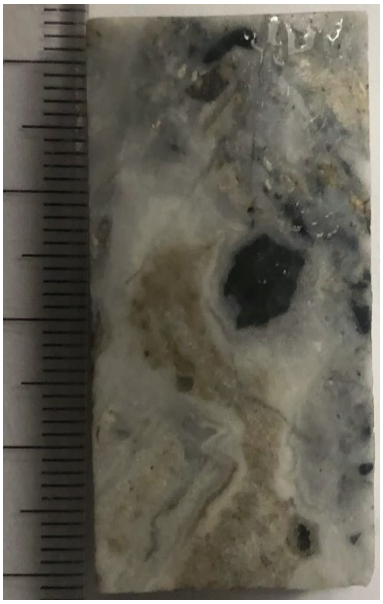

No Thin Section Description

FVN104-103

DDH Depth: 103.4m
Sample Desc: Strongly clay (kaolinite & smectite) altered andesite / tuff. Appears similar to shallowest sample in UW63. No discernable primary textures.
XRD Minerals: Quartz (Cristobalite), Adularia, Smectite, Kaolinite, Pyrite (Simpson & Mauk, 2007)
SWIR Minerals: Kaolinite (Simpson, 2015)
LOI: 10.5%
NH4+: 107ppm
δ15N: Too low

No Petrographic Data

FVN104-188

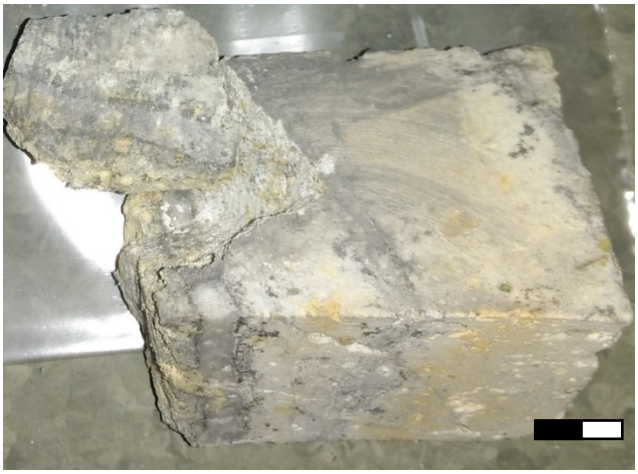

DDH Depth: 188.2m
Sample Desc: Strongly clay (Illite-smectite + kaolinite) altered tuff / andesite. Possible relict plagioclase phenocrysts.
XRD Minerals: Quartz, Adularia, $Illite_{0.3}Smectite$, Kaolinite (Simpson & Mauk, 2007)
SWIR Minerals: Illite-Smectite (Simpson, 2015)
LOI: 9.7%
NH4+: 301ppm
δ15N: +3.4‰

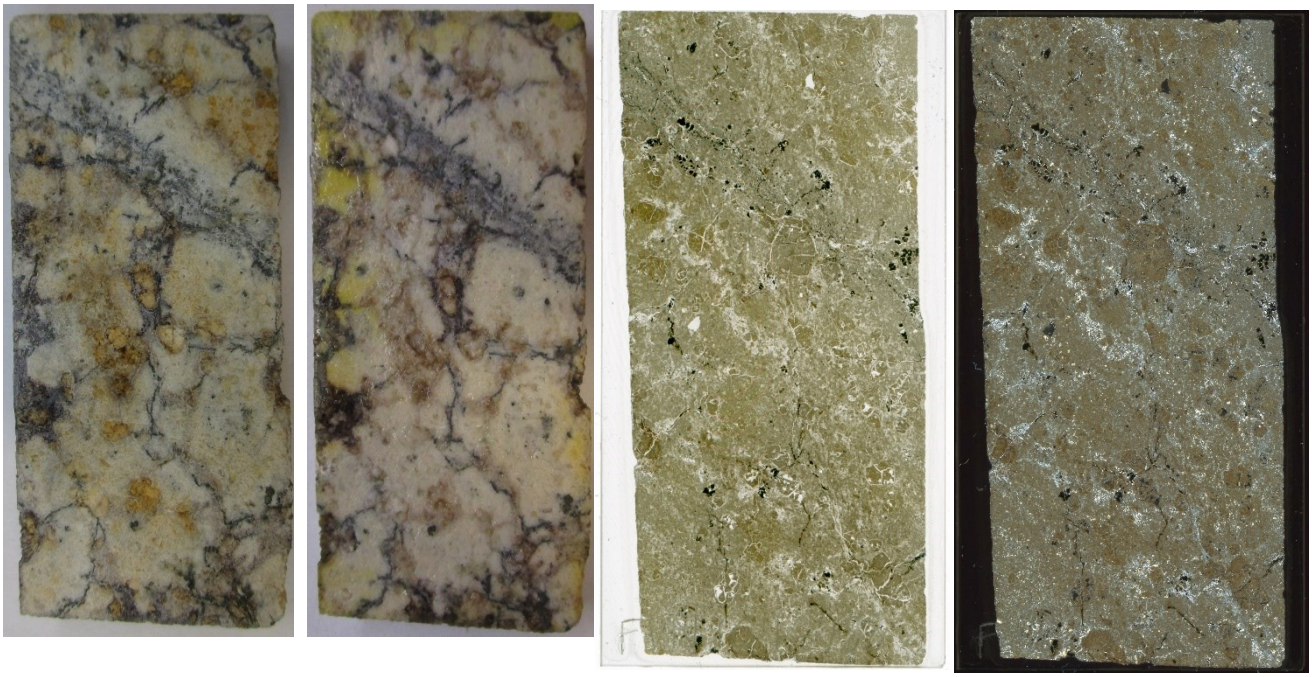

Thin Section Description:

Intensely clay altered volcaniclastic or andesite. Thin section is thick making it difficult to discern clasts vs phenocrysts. Intense alteration of both groundmass and clasts plus angular clasts suggest volcaniclastic. Quartz and clay rich groundmass / matrix.

FVN104-270

DDH Depth: 270.2m
Sample Desc: Strongly clay (illite0.75smectite) altered tuff / andesite. Very high in ammonium. No discernable primary textures.
XRD Minerals: Quartz, $Illite_{0.75}$Smectite, +/- Adularia (Simpson & Mauk, 2007)
SWIR Minerals: Ammonium Mineral, Gypsum (Simpson, 2015)
LOI: 13.6%
NH4+: 10120ppm
δ15N: +6.4‰

No Petrographic Data

FVN104-312

DDH Depth: 312.3m
Sample Desc: Illite-smectite altered plagioclase phyric (1-9mm) andesite. Plagioclase phenocrysts have pervasively altered to clays +/- adularia. Chlorite altered groundmass. High in ammonium.
XRD Minerals: Quartz, $Illite_{0.9}Smectite$, Pyrite, +/- Adularia, Chlorite (Simpson & Mauk, 2007)
SWIR Minerals: Ammonium Mineral, Gypsum (Simpson, 2015)
LOI: 8.0%
NH4+: 3764ppm
δ15N: +4.2‰

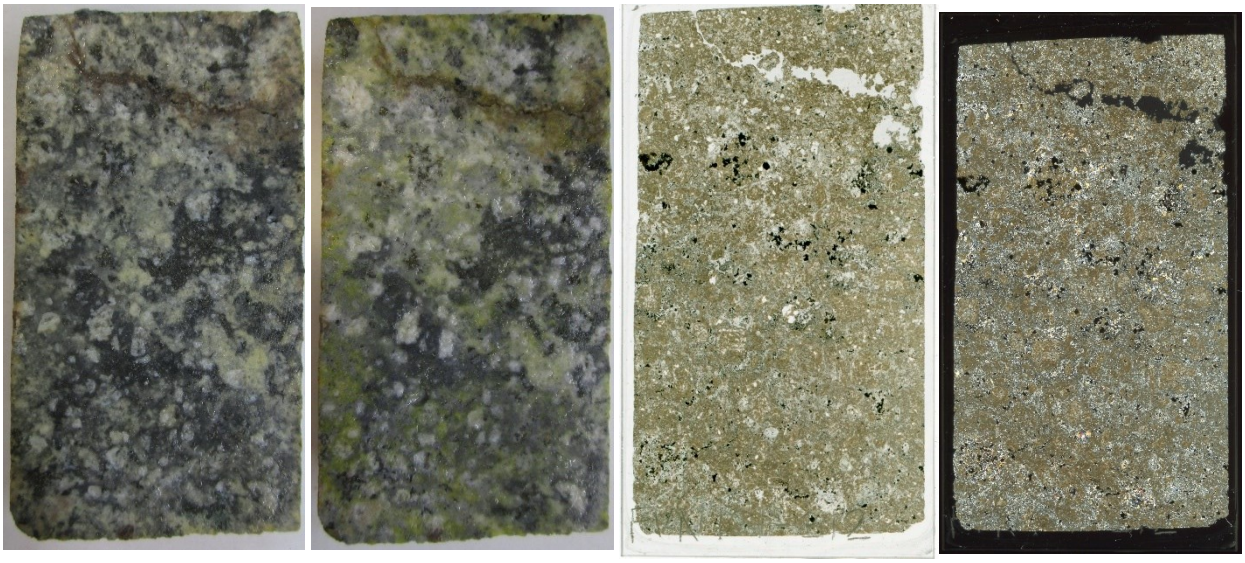

Thin Section Description:
Clay altered plagioclase phyric andesite. 20% plagioclase 0.5-2mm phenocrysts have been completely altered to white mica with minor quartz (Photomicrograph A). Groundmass is composed of interlocking fine grained quartz with minor (<5%) adularia and 20% clay minerals disseminated throughout. Dark colour may be caused by the high sulfide content and / or fine chlorite throughout the groundmass. Though, no chlorite is visible in TS. Could be due to poor polishing.

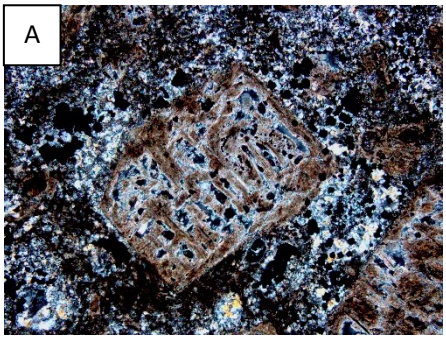

FVN104-340

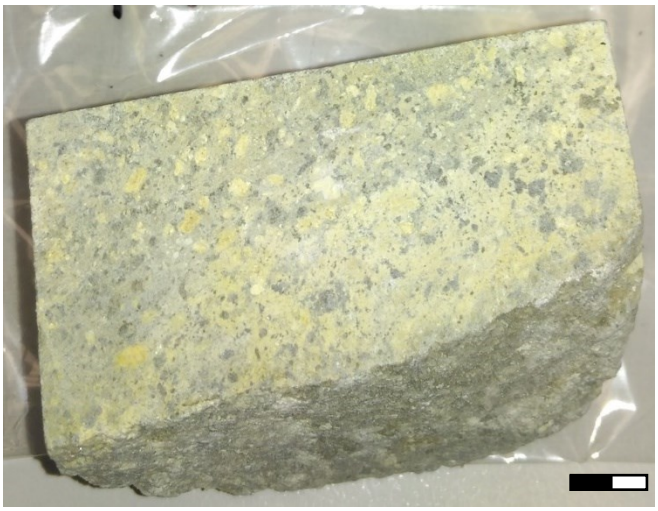

DDH Depth: 340.2m
Sample Desc: Illite-smectite altered plagioclase phyric (1-9mm) andesite. Plagioclase phenocrysts have pervasively altered to clays +/- adularia. Chlorite altered groundmass. High in ammonium.
XRD Minerals: Quartz, Adularia, Albite, Chlorite, Illite, Pyrite (Simpson & Mauk, 2007)
SWIR Minerals: Illite, minor Gypsum (Simpson, 2015)
LOI: 6.6%
NH4+: 1827ppm
δ15N: +3.2‰

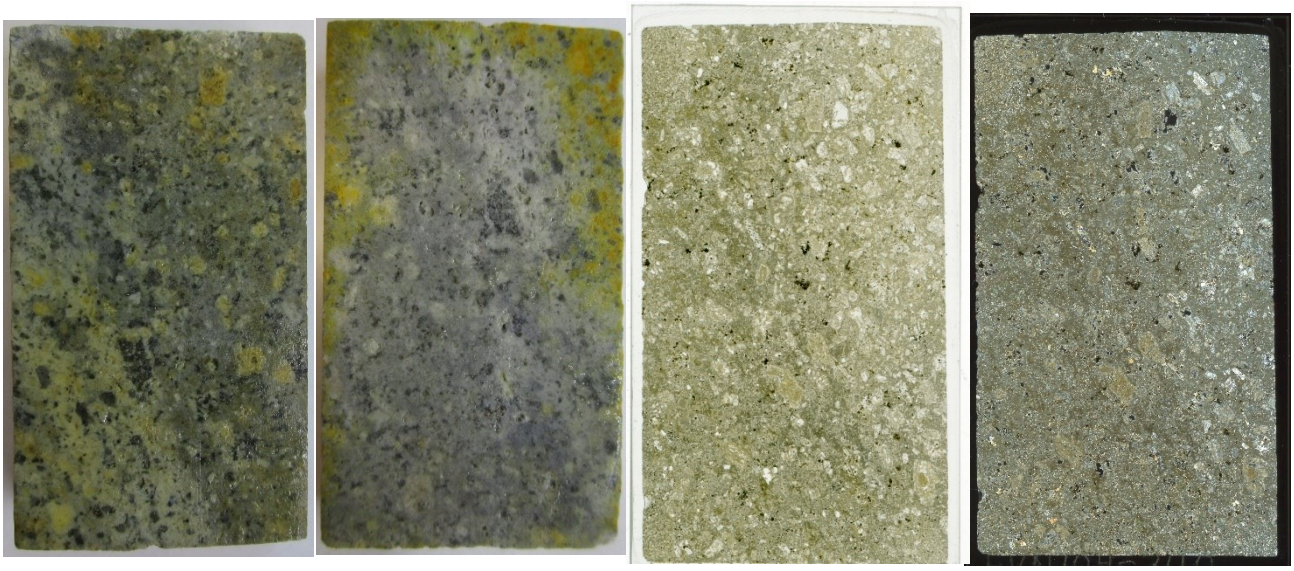

Thin Section Description:

Clay altered plagioclase phyric andesite. 30% 0.2-1.5mm plagioclase phenocrysts have been intensely altered to adularia and moderately replaced (30-70%) by white mica. Groundmass is very fine grained and poorly polished. Primarily fine-grained quartz and adularia crystals throughout though appears to contain significant (30%) clay minerals (white mica and chlorite though poorly polished and difficult to discern).

FVN104-374

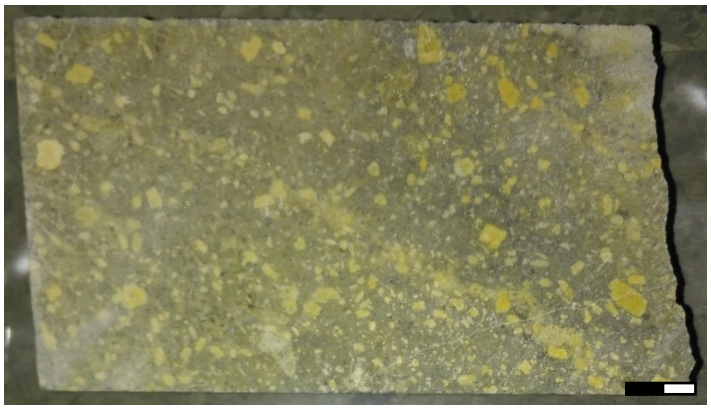

DDH Depth: 374.2m
Sample Desc: Illite, adularia, and chlorite altered andesite. Plagioclase phenocrysts (1-5mm) may be adularia altered. Mafic mineral phenocrysts(1-2mm). Chlorite (+illite?) rich groundmass.
XRD Minerals: Quartz, Adularia, Chlorite, Illite, Pyrite (Simpson & Mauk, 2007)
SWIR Minerals: Minor ammonium mineral, chlorite, gypsum (Simpson, 2015)
LOI: 7.7%
NH4+: 2581ppm
δ15N: +5.1‰

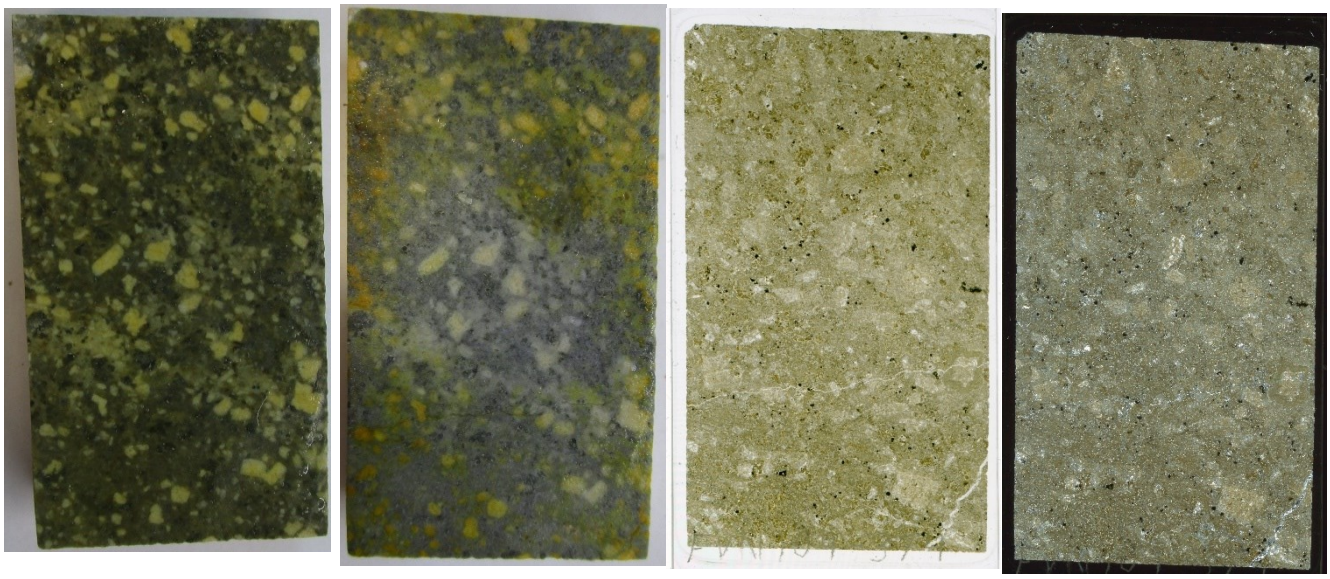

Thin Section Description:

Clay altered plagioclase phyric andesite. 20% 0.5-3mm plagioclase phenocrysts which have been adularia altered and 80-100% replaced by white mica. 10% 0.2-1mm pyroxene phenocrysts have been replaced by chlorite and quartz. Groundmass is composed of fine quartz +/- adularia (60%) and fine-grained brown-coloured clays minerals (poorly polished). Probably white mica with significant chlorite component. 25-25%. Disseminated pyrite throughout.

FVN104-417

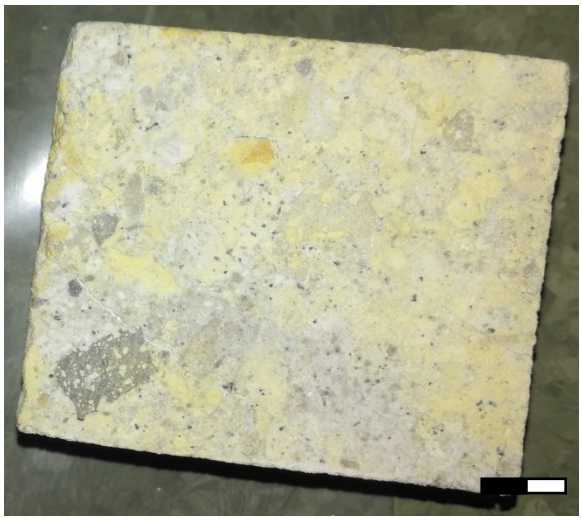

DDH Depth: 417.9m
Sample Desc: Strongly adularia and illite altered. Quartz rich. Groundmass stains indicating adularia content. Clay altered relict plagioclase phenocrysts. Sieve texture / brecciated fragment.
XRD Minerals: Quartz, Adularia, Illite, Pyrite (Simpson & Mauk, 2007)
SWIR Minerals: Ammonium mineral, minor gypsum (Simpson, 2015)
LOI: 4.3%
NH4+: 4301ppm
δ15N: +4.3‰

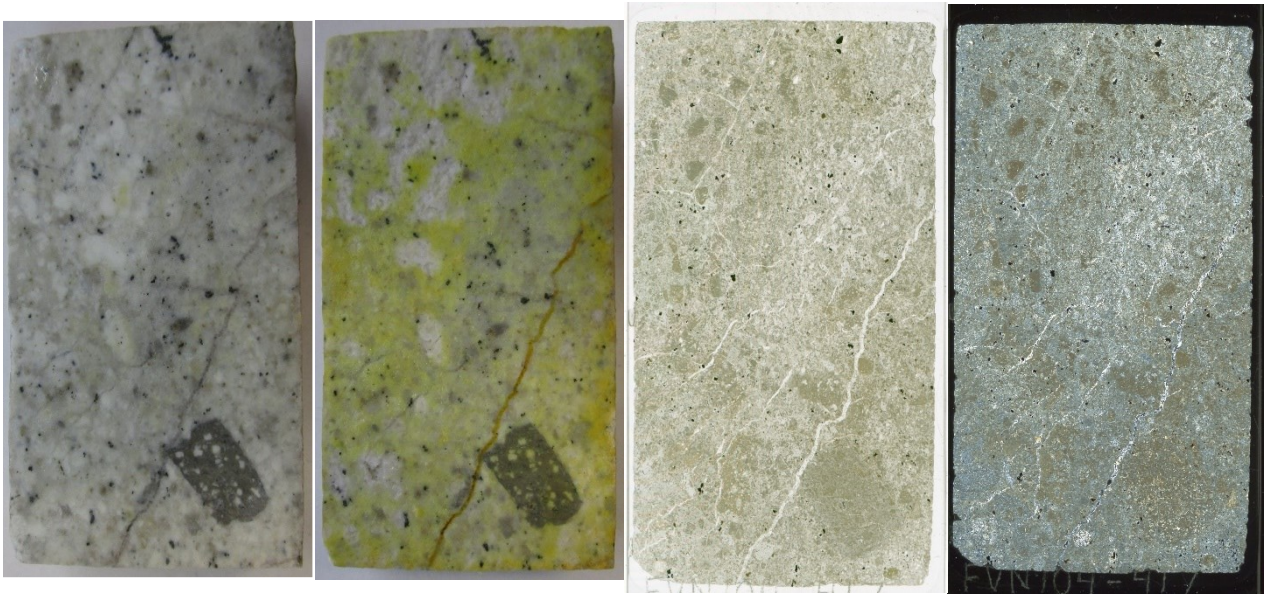

Thin Section Description:
Clay altered plagioclase phyric andesite. 15% 0.5-3mm plagioclase phenocrysts have been completely replaced by white mica (Photomicrograph A) mainly appearing brown in thin section (due to poor polishing). No visible chlorite. Groundmass is rich (70%) in microcrystalline quartz (and/or adularia) containing ~30% white mica distributed throughout. <5% pyrite disseminated throughout.

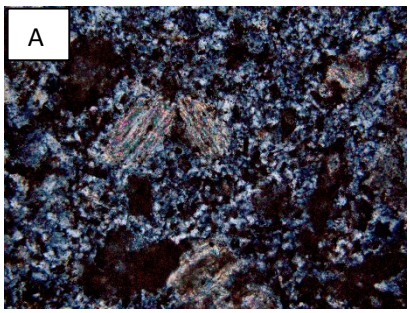

Favona Underground

FVN58180V

DDH Depth: N/A
Sample Desc: Vein sample. Intense potassium staining indicating high adularia content. Some silica replaced bladed calcite textures in bottom sample. Indicates boiling. Low in ammonium.
XRD Minerals: Qz (uO)
SWIR Minerals: Not Analyzed
LOI: 1.0%
NH4+: 26ppm
δ15N: Too low

No Petrographic Data

FVN60248V

Depth: N/A
Sample Desc: Vein sample. Large crustiform colloform vein clast contained within second generation vein. Primarily quartz minor clay minerals and adularia.
XRD Minerals: Qz (uO)
SWIR Minerals: Not Analyzed
LOI: 3.2%
NH4+: 29ppm
δ15N: Too low

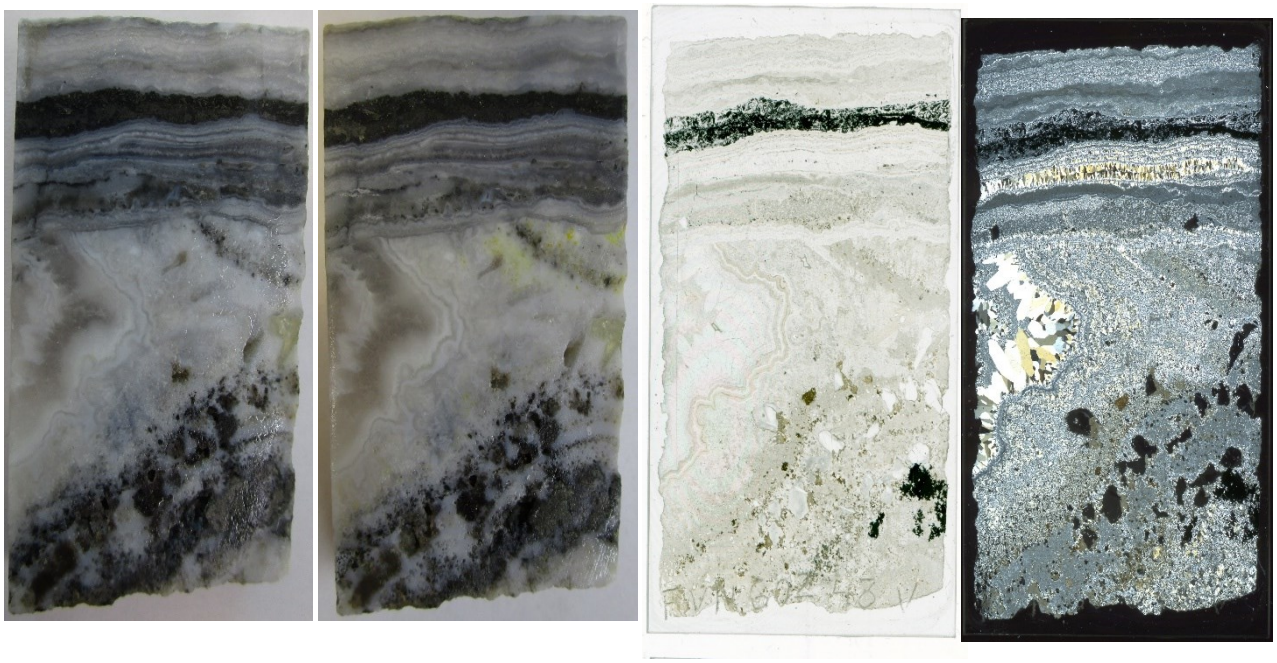

No Thin Section Description

FVN60281V

DDH Depth: N/A
Sample Desc: Crustiform banded (~1cm bands). Alternating crystalline, microcrystalline quartz and a large 1cm dark coloured sulfide rich band.
XRD Minerals: Not Analyzed
SWIR Minerals: Not Analyzed
LOI: Not Analyzed
NH_4^+: Not Analyzed
δ15N: Not Analyzed

No Thin Section Description

FVN60290V

DDH Depth: N/A
Sample Desc: Crustiform / colloform banded (1cm bands). Alternating white crystalline quartz (1cm bands) and microcrystalline quartz +/- adularia & clays (1-2mm bands). Comb textured quartz. Small 2mm veinlet cross-cutting banding.
XRD Minerals: Not Analyzed
SWIR Minerals: Not Analyzed
LOI: Not Analyzed
NH_4^+ : Not Analyzed
δ15N: Not Analyzed

No Petrographic Data

Martha

DDH 920SP4MR1460

MTA1460-165

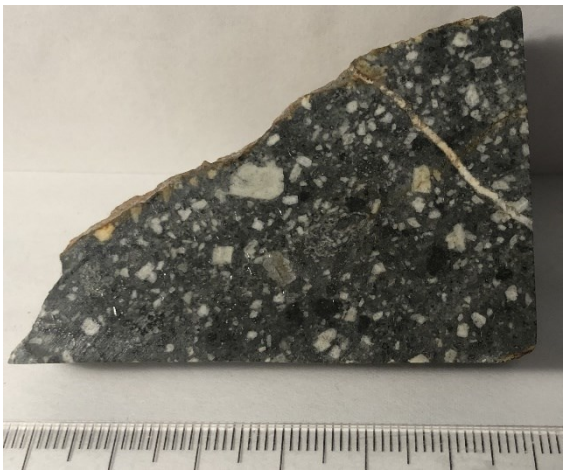

Depth: 165.3m
Sample Desc: Plagioclase phyric andesite. Plagioclase phenocrysts are 1-5mm. Appear slightly clay altered. Groundmass is dark gray with 1-3mm dark patches of sulfides + chlorite. Minor quartz phenocrysts in some sections. Small 1mm quartz veinlet.
XRD Minerals: Not Analyzed
SWIR Minerals: Not Analyzed
LOI: 3.8%
NH4+: 182ppm
δ15N: +3.6‰

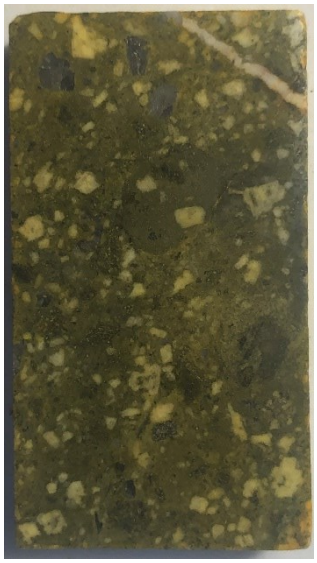

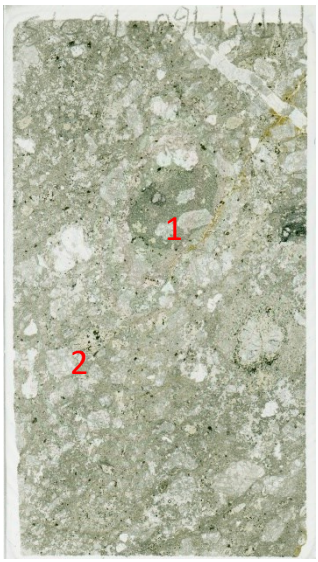

Thin Section Description:
Altered quartz and plagioclase phyric andesite. 1-2mm plagioclase phenocrysts which have been adularia altered overprinted by white mica alteration. 50% of each plagioclase phenocryst has been overprinted by the white mica alteration. Quartz phenocrysts are anhedral and very irregular. 1-5mm euhedral relict amphibole phenocrysts throughout which appear to be completely replaced by chlorite and quartz. Patchy chlorite throughout. Groundmass appears originally trachytic with plagioclase lathes but has been completely replaced by quartz and clay minerals. Small 1mm veinlets of quartz, calcite, and adularia. Disseminated pyrite.

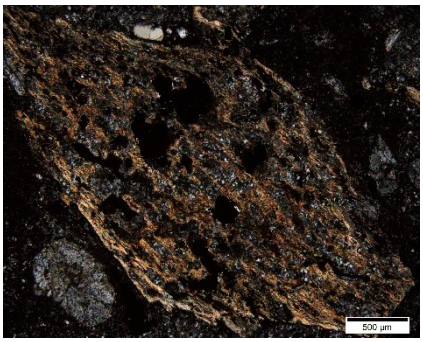

MTA1460-165 SEM-EDS

SEM-EDS

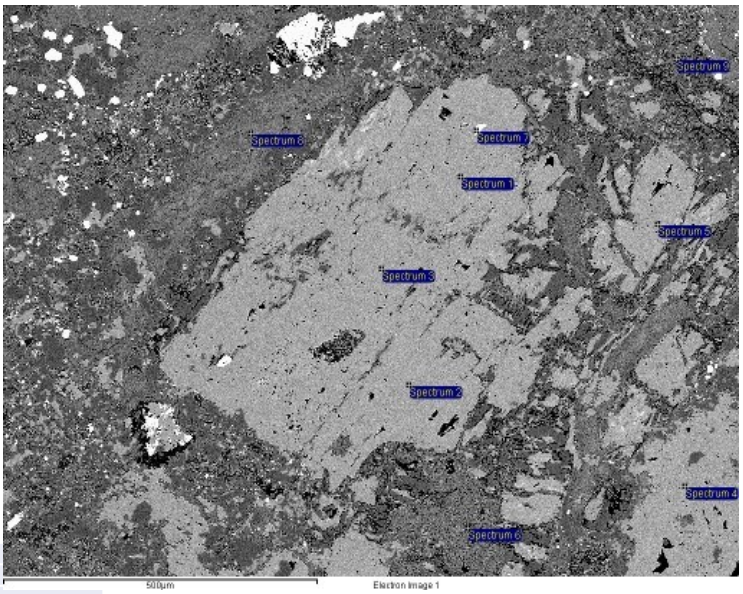

Spectrum	Na	Mg	Al	Si	K	Ca	Ti	Mn	Fe	Mineral
Spectrum 1	0	0	17.96	64.93	16.64	0	0.47	0	0	Adularia
Spectrum 2	0	0	17.6	66.38	16.03	0	0	0	0	Adularia
Spectrum 3	0.4	0	17.95	65.93	15.72	0	0	0	0	Adularia
Spectrum 4	0.36	1.16	18.02	65.32	15.15	0	0	0	0	Adularia + Smectite?
Spectrum 5	0	0	17.58	66.22	16.2	0	0	0	0	Adularia
Spectrum 6	0	3.44	30.47	56.99	9.1	0	0	0	0	Adularia (+ bright spot)
Spectrum 7	0	0	15.99	63.48	15.24	2.47	2.82	0	0	Adularia
Spectrum 8	0.53	24.06	22.41	38.71	0.93	0	0	1.93	11.42	Adularia + Chlorite? (Groundmass
Spectrum 9	10.17	0.64	19.07	68.03	2.1	0	0	0	0	Albite? (Groundmass)

High Resolution BSE Image

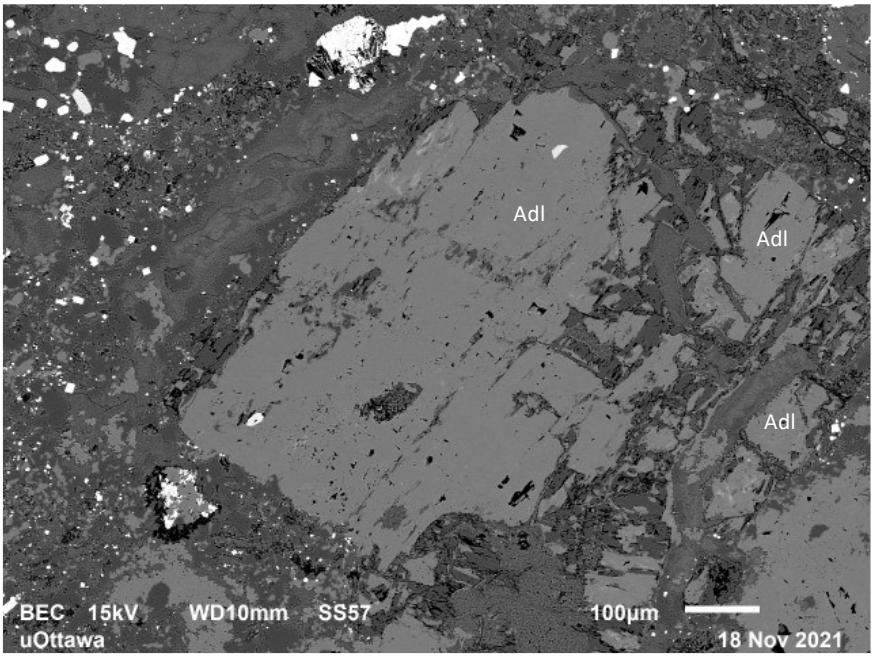

MTA1460-166V

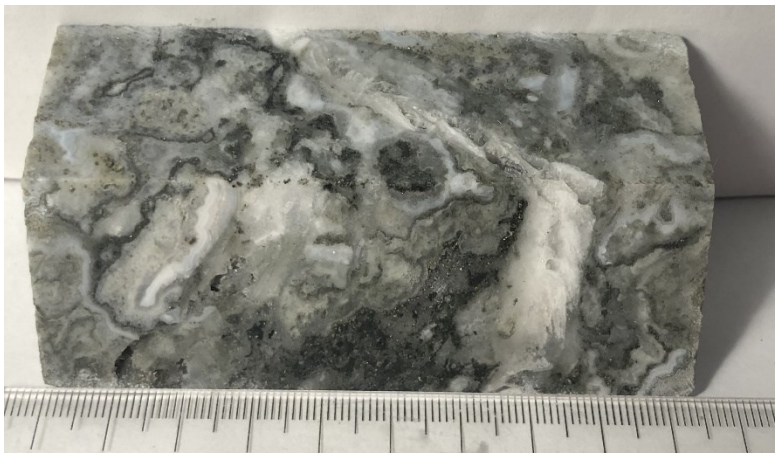

Depth: 166.9m
Sample Desc: Brecciated / colloform vein sample. Vein is very irregular with small bands of sulfides coating part of fragmented colloform veins. Multiple generations of mineralization and veining / brecciation. Latest is vuggy quartz veinlet transecting sample.
XRD Minerals: Not Analyzed
SWIR Minerals: Not Analyzed
LOI: Not Analyzed
NH4+: Not Analyzed
δ15N: Not Analyzed

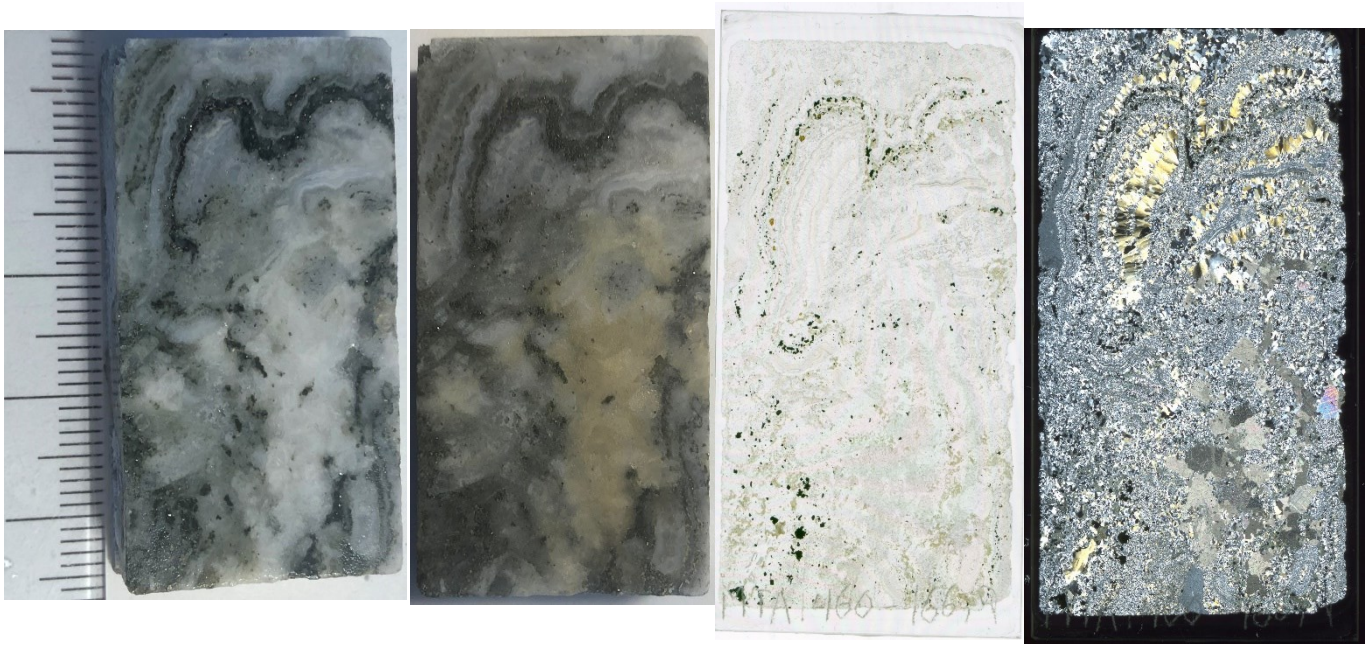

No Thin Section Description

MTA1460-177V

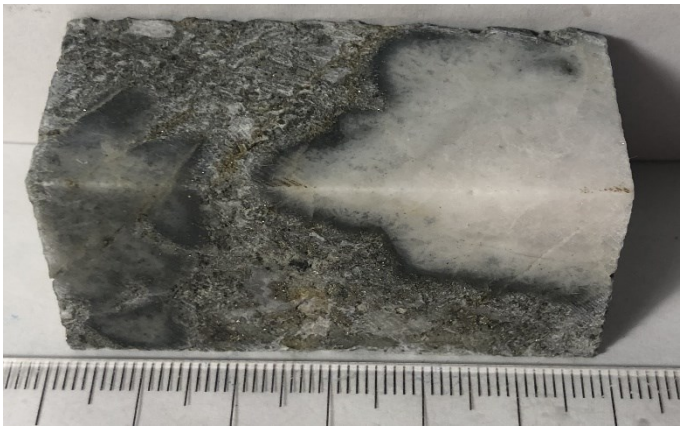

Depth: 177.8m
Sample Desc: Vein / massive ore sample. Irregular microcrystalline quartz patch near edges. The bulk of the sample is composed of clay minerals with abundant sulfide minerals. Sulfides appear blebby or disseminated throughout the clay rich areas.
XRD Minerals: Not Analyzed
SWIR Minerals: Not Analyzed
LOI: 11.3%
NH4+: 12ppm
δ15N: Too low

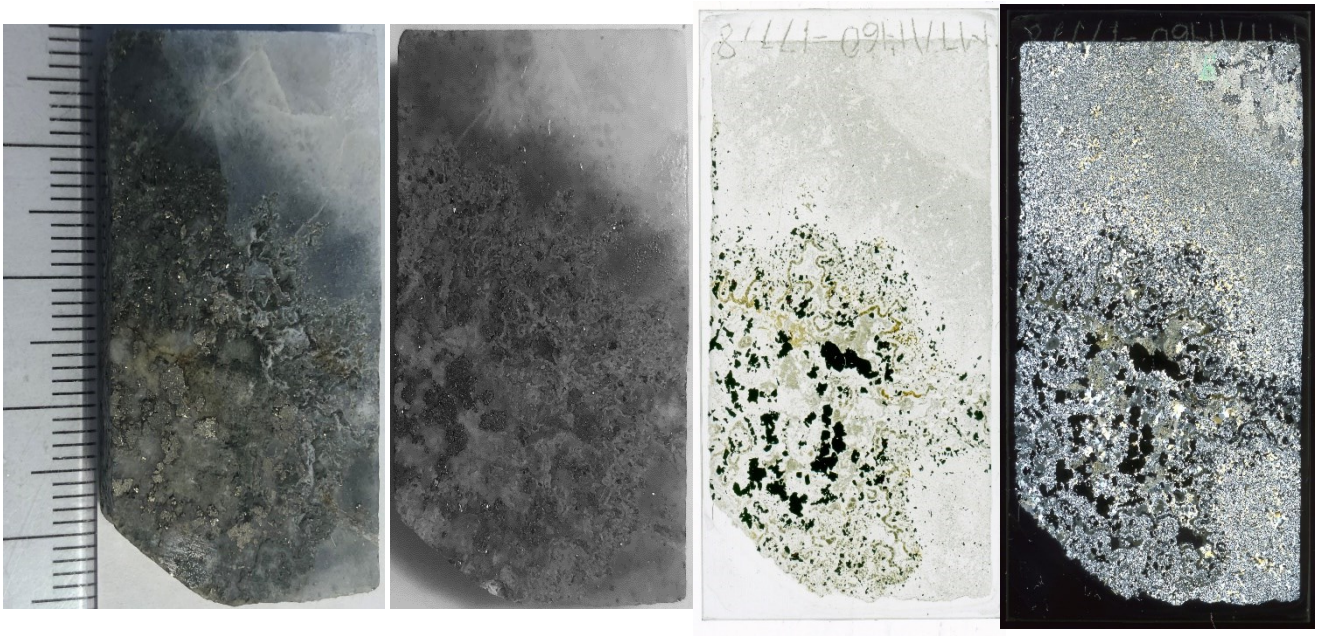

No Thin Section Description

MTA1460-182

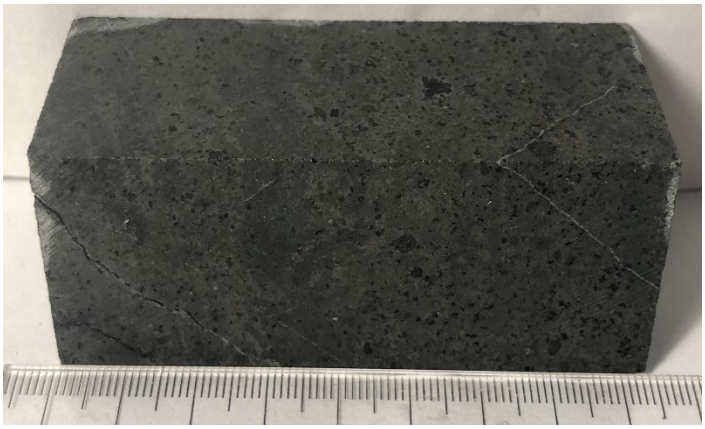

Depth: 182.1m
Sample Desc: Minimally altered mafic melanocratic intrusion. "Hard bar?". Phenocrysts of mafic minerals (amphibole / chlorite or pyroxene? Multiple dark minerals). Disseminated reddish brown mineral throughout (rusted pyrite?)
XRD Minerals: Not Analyzed
SWIR Minerals: Not Analyzed
LOI: Not Analyzed
NH4+: <10ppm
δ15N: Too Low

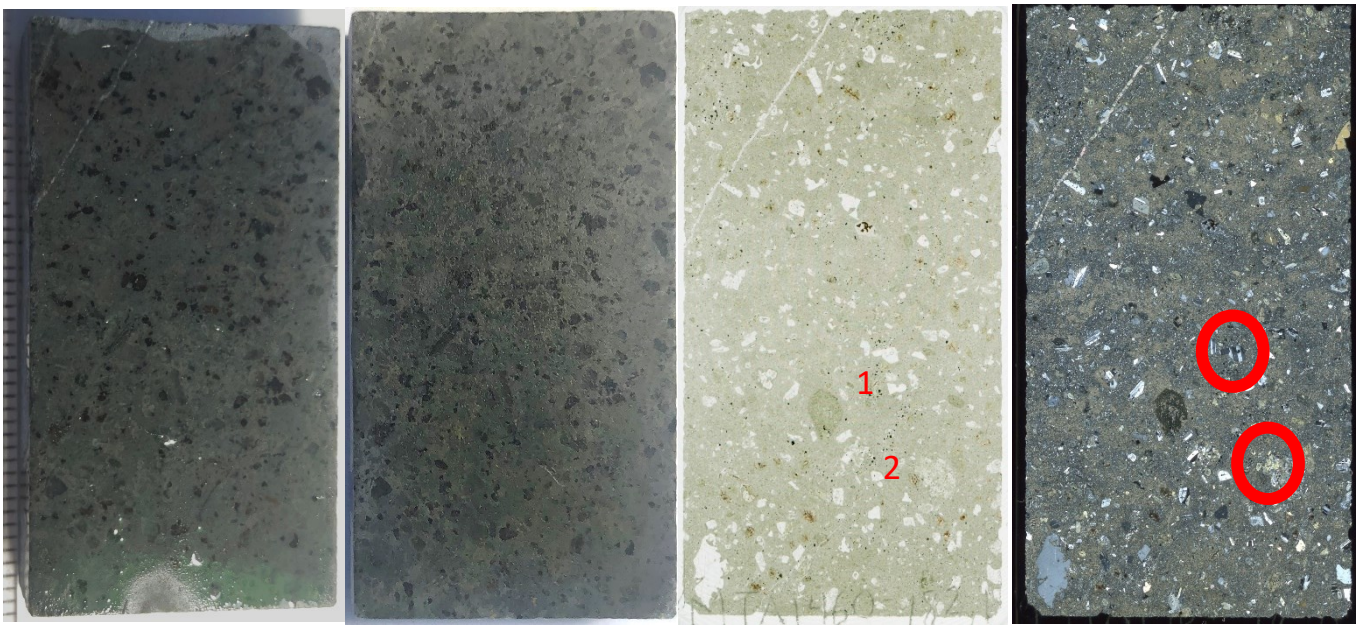

Thin Section Description:
Minimally altered mafic intrusion. Plagioclase phenocrysts with albite twinning (image 1). No alteration adulariatization or illitization of the plagioclase. Chlorite altered pyroxene phenocrysts (image 2).

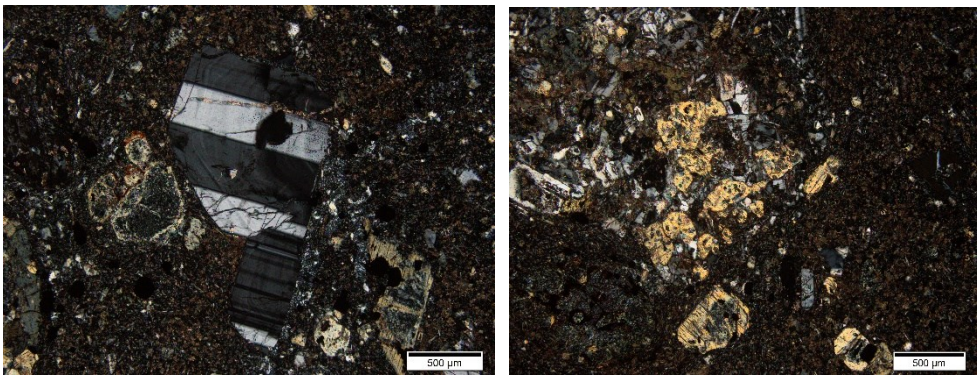

MTA1460-204

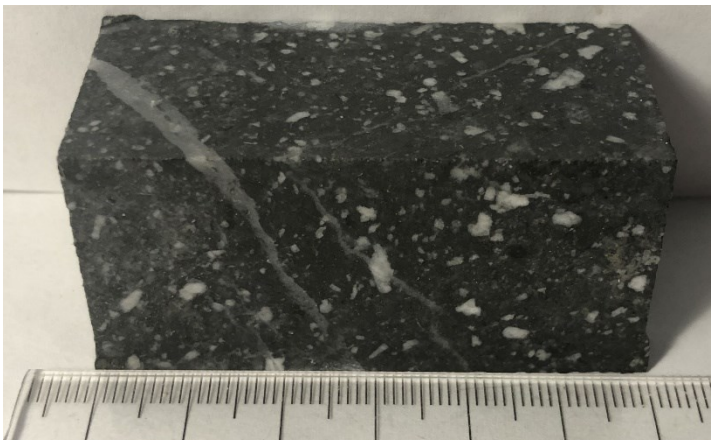

Depth: 204.8m
Sample Desc: Altered plagioclase phyric andesite. Plagioclase phenocrysts are rounded or lathe shape and range from 0.5mm - 3mm. Groundmass is dark gray with greenish patches (chlorite). Minor quartz eyes. 3mm quartz veinlet and possible silica alteration**.**
XRD Minerals: Qz, Ad, Ilt, Sm, Chl (uO)
SWIR Minerals: Not Analyzed
LOI: 2.9%
NH4+: 129ppm
δ15N: +6.4‰

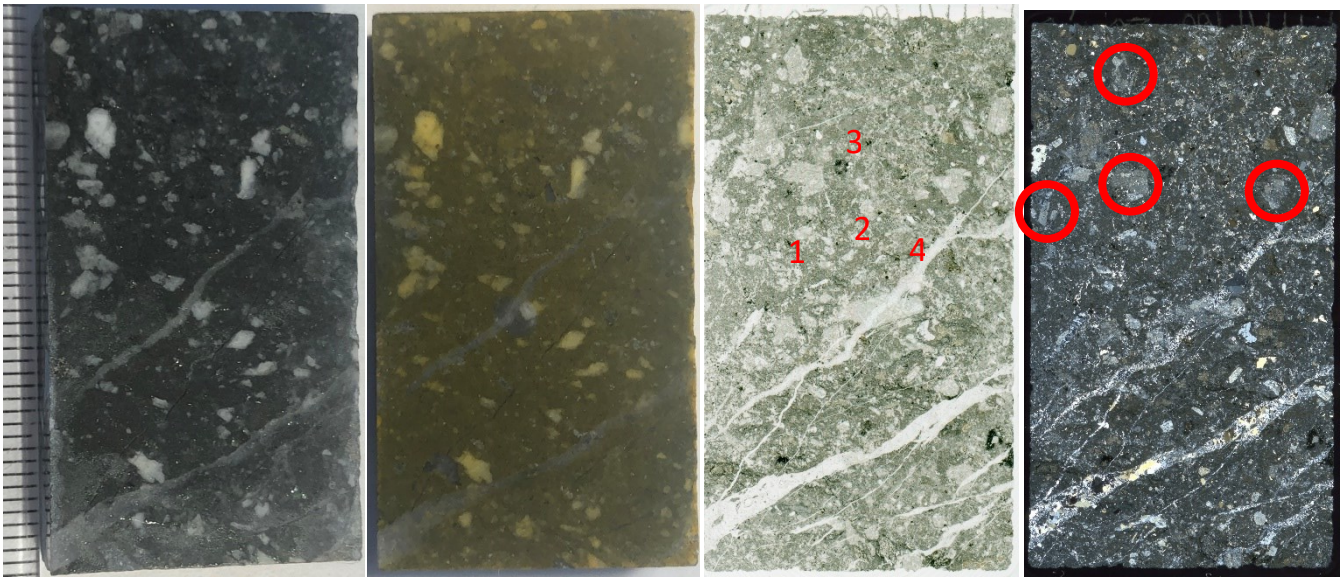

Thin Section Description:
Altered quartz and plagioclase phyric andesite. Plagioclase phenocrysts range 1-4mm having been strongly adularia and clay altered. Overprinting Albite alteration appears to have replaced a majority (60-70%) of the feldspar. Some plagioclase phenocrysts have been also replaced by calcite and/or quartz. 0.2-1mm quartz phenocrysts throughout though they are smaller and more rounded than the above sample. Patchy chlorite occurs through the groundmass and do not appear to be associated with amphibole minerals. The rest of the groundmass has been intensely silicified and clay altered with irregular patches of quartz throughout. Numerous small 0.1mm in width quartz-adularia veinlets throughout. Disseminated pyrite.

MTA1460-204 Photomicrographs

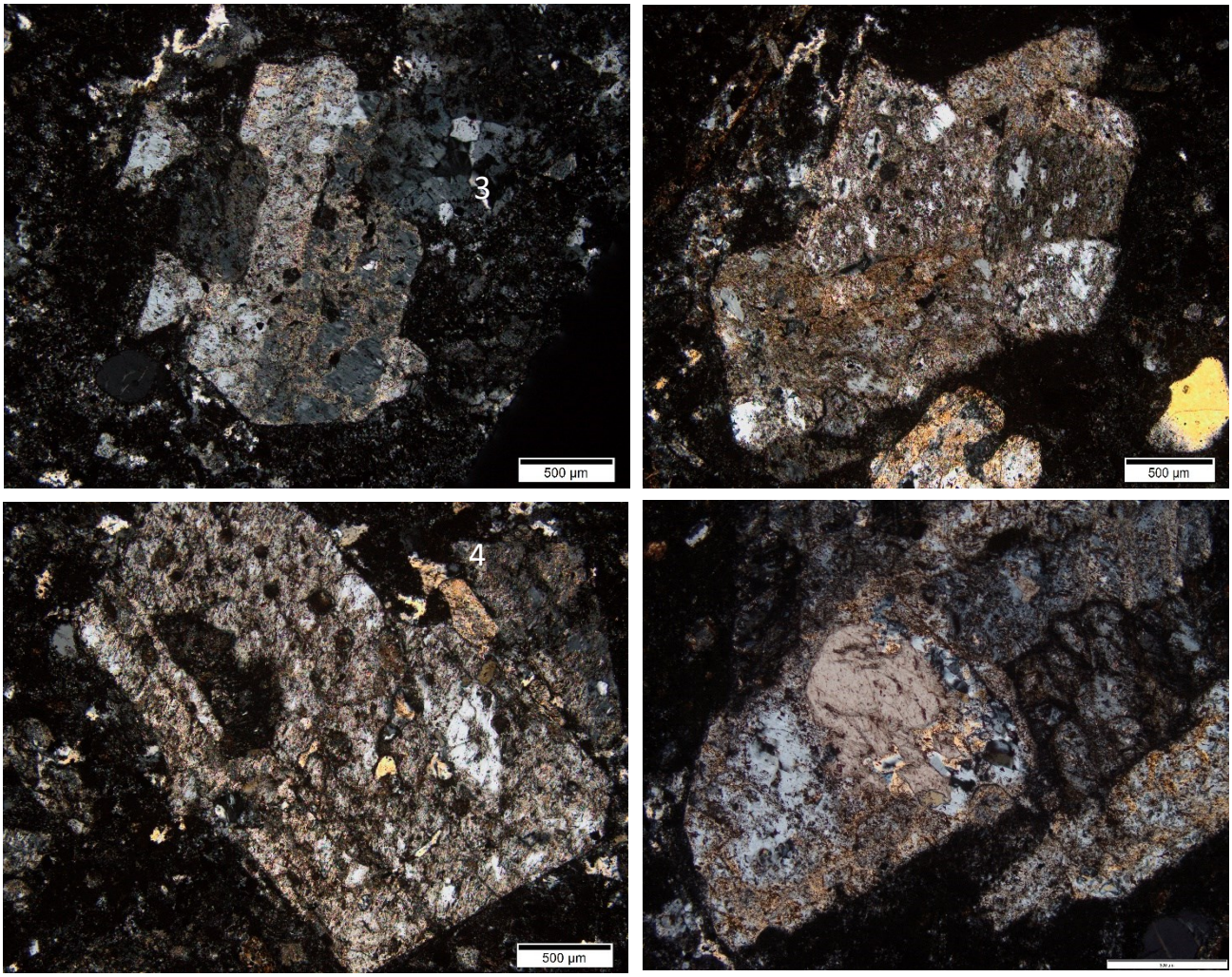

MTA1460-204 SEM-EDS

SEM-EDS (1)

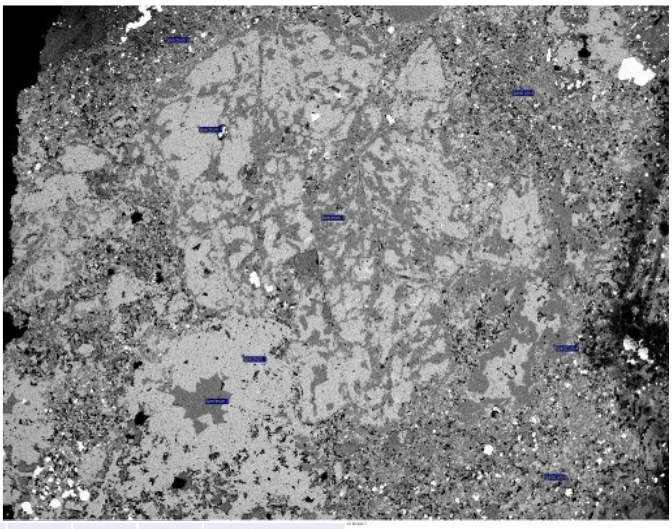

Spectrum	In stats.	Na	Mg	Al	Si	K	Ca	Mn	Fe	Total	Mineral
Spectrum 1	Yes	0	0	17.93	65.97	16.1	0	0	0	100	Adularia
Spectrum 2	Yes	0	0	0	100	0	0	0	0	100	Quartz
Spectrum 3	Yes	10.52	0	19.7	69.11	0	0.67	0	0	100	Albite
Spectrum 4	Yes	0	0	0.95	99.05	0	0	0	0	100	Quartz
Spectrum 5	Yes	1.22	21.18	22.13	44.49	1.5	0.51	1.46	7.51	100	Groundmass
Spectrum 6	Yes	2.82	2.9	19.12	63.36	10.01	0	0	1.79	100	Groundmass
Spectrum 7	Yes	0	0	17.69	66	16.31	0	0	0	100	Adularia
Spectrum 8	Yes	5.2	5.63	15.51	68.28	2.9	0.45	0	2.02	100	Groundmass

High Resolution EDS Image

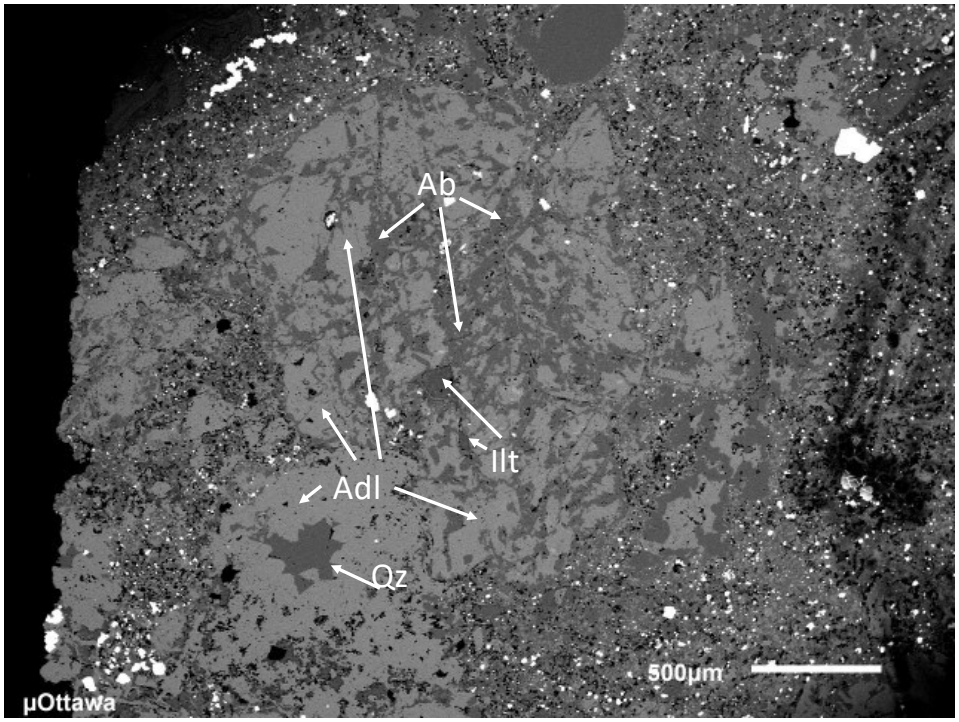

SEM-EDS (2)

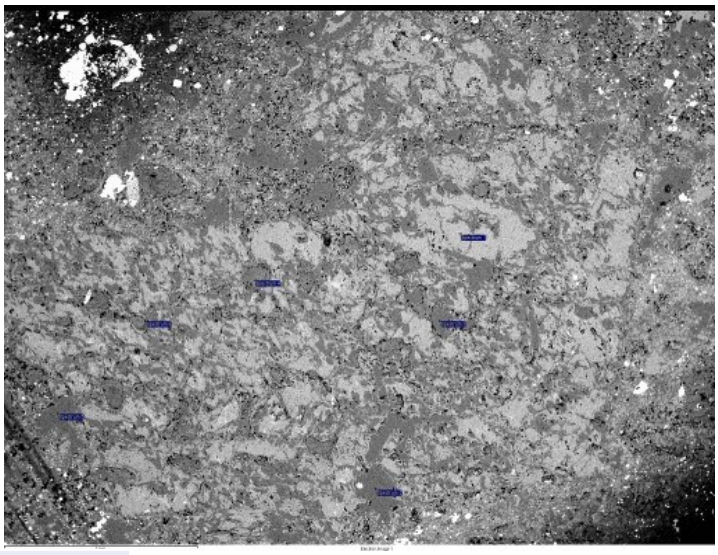

Spectrum	In stats.	Mg	Al	Si	K	Total	Mineral
Spectrum 1	Yes	0	17.91	65.52	16.57	100	Adularia
Spectrum 2	Yes	0	0	100	0	100	Quartz
Spectrum 3	Yes	0	0.86	99.14	0	100	Quartz
Spectrum 4	Yes	2.74	30.07	58.42	8.77	100	?
Spectrum 5	Yes	0	0	100	0	100	Quartz
Spectrum 6	Yes	0.8	3.85	93.36	1.99	100	Quartz + Adularia

High Resolution EDS Image (Zoom)

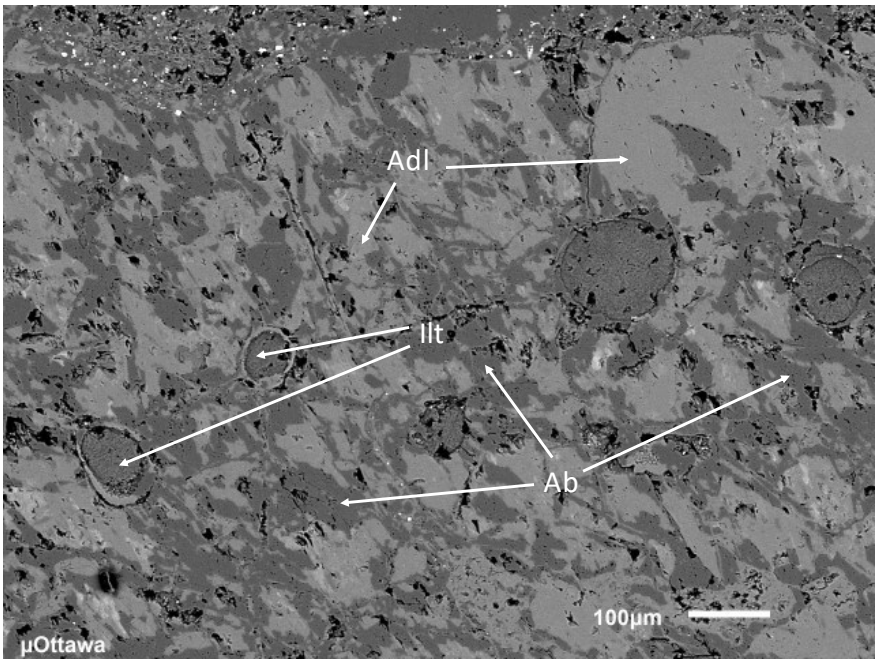

SEM-EDS (4)

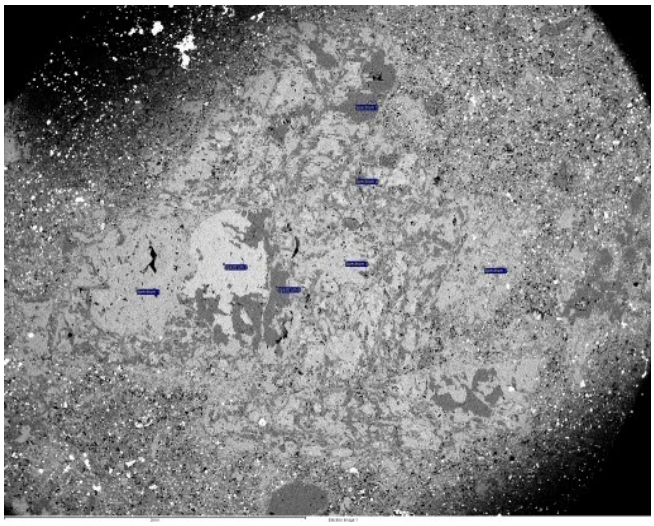

Spectrum	In stats.	Na	Al	Si	S	K	Ca	Fe	Total	Mineral
Spectrum 1	Yes	0	17.44	65.55	0	17.01	0	0	100	Adularia
Spectrum 2	Yes	0	0	0	0	0.54	99.46	0	100	Calcite
Spectrum 3	Yes	0	17.6	64.76	0	16.04	1.6	0	100	Adularia
Spectrum 4	Yes	11.01	18.84	69.74	0	0	0.41	0	100	Albite
Spectrum 5	Yes	11.71	19.49	68.79	0	0	0	0	100	Albite
Spectrum 6	Yes	0	1.05	98.95	0	0	0	0	100	Quartz
Spectrum 7	Yes	0	17.53	63.58	2.05	15.99	0	0.86	100	Adularia + Minor Pyrite

High Resolution EDS Image

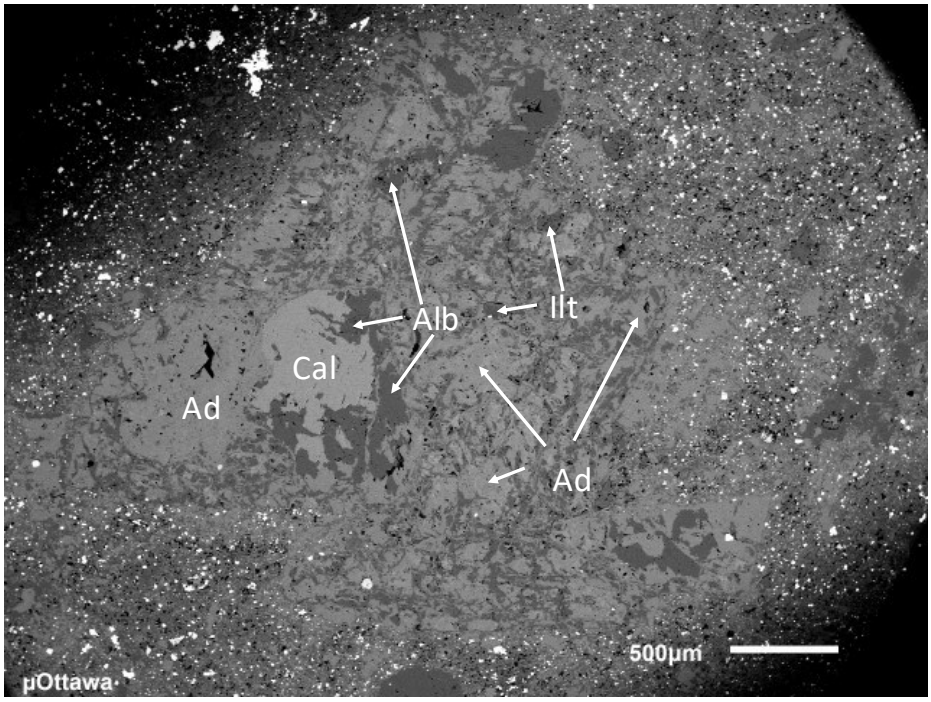

SEM-EDS (Groundmass)

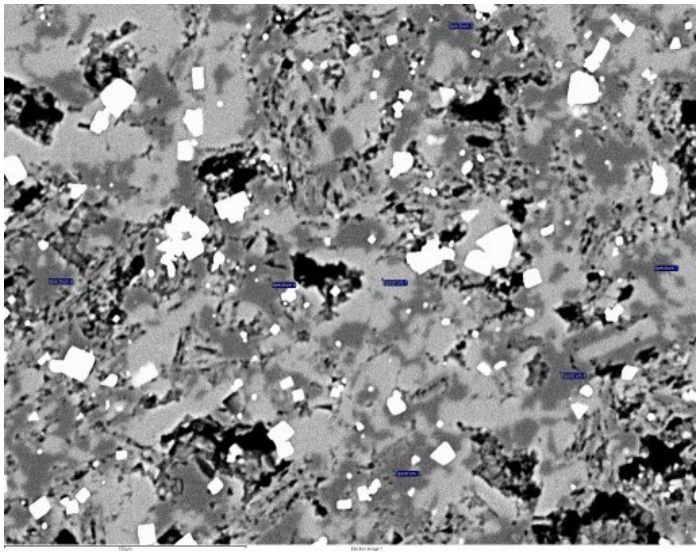

Spectrum	In stats.	Na	Mg	Al	Si	K	Fe	Total	Mineral
Spectrum 1	Yes	0.41	0.44	18.31	65.18	15.65	0	100	Adularia
Spectrum 2	Yes	0	0	1.82	97.71	0.46	0	100	Quartz + Adularia
Spectrum 3	Yes	0	0	1.12	98.55	0.33	0	100	Quartz + Adularia
Spectrum 4	Yes	0	1.98	2.55	94.63	0	0.84	100	Quartz
Spectrum 5	Yes	3.2	0	11.63	79.11	6.05	0	100	Quartz + Albite
Spectrum 6	Yes	0	0	1.04	98.96	0	0	100	Quartz
Spectrum 7	Yes	0	0	0.73	99.27	0	0	100	Quartz

No High-Resolution EDS Image

SEM-EDS (unknown grain)

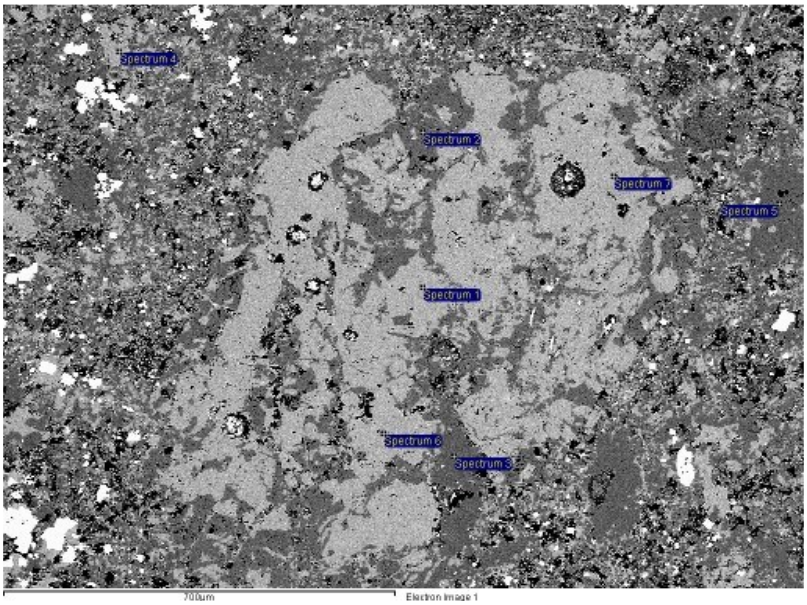

Spectrum	Na	Al	Si	K	Ca	Mineral
Spectrum 1	0	17.69	66.15	16.16	0	Adularia
Spectrum 2	11.24	19.04	69.32	0	0.39	Albite
Spectrum 3	0	0.95	99.05	0	0	Quartz
Spectrum 4	0	18.79	65.17	16.04	0	Adularia
Spectrum 5	0	0.96	99.04	0	0	Quartz
Spectrum 6	0	18.69	65.23	16.08	0	Adularia
Spectrum 7	0	17.82	66.46	15.73	0	Adularia

High Resolution EDS Image

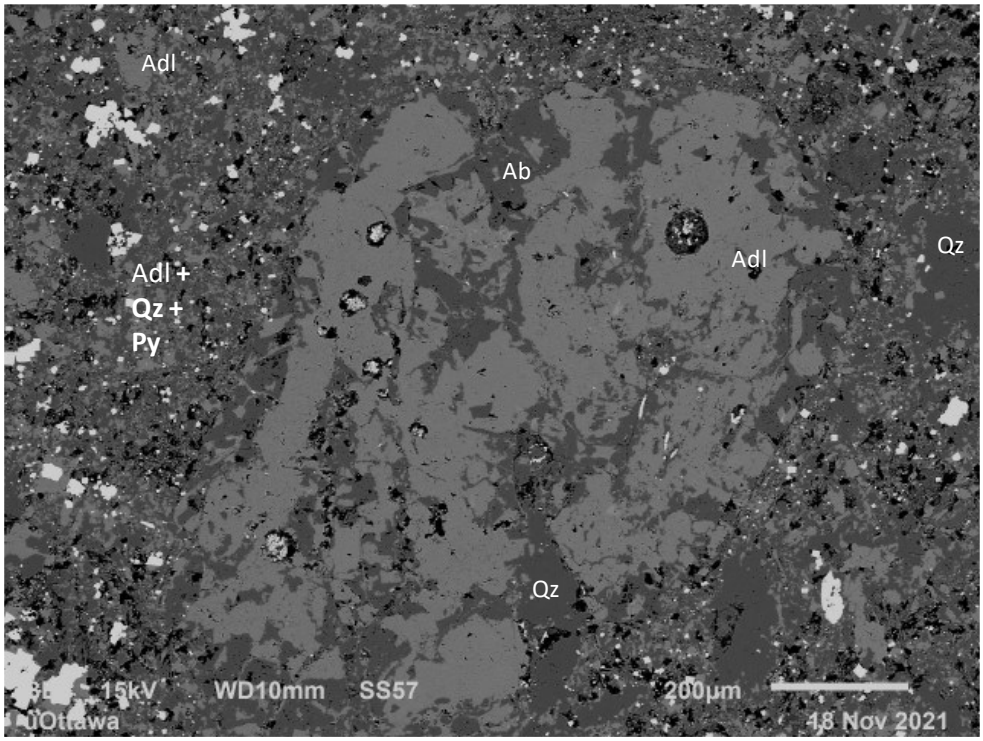

DDH 920SP8MR1496

MTA1496-113

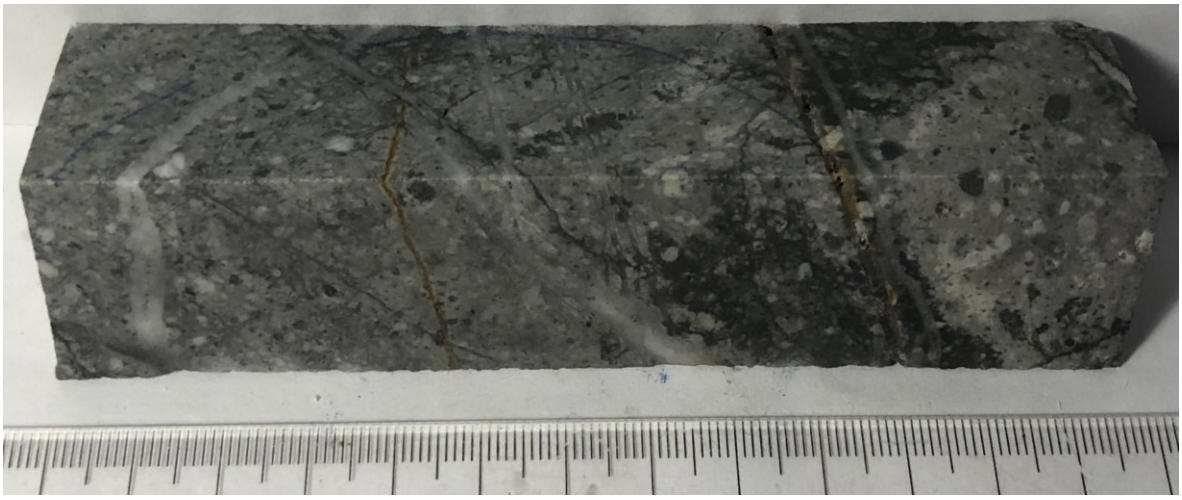

Depth: 113.0m
Sample Desc: Intensely silicified (+minimally clay altered) andesite. 1-5mm plagioclase and hornblende (chlorite altered) phenocrysts throughout. Multiple generations of quartz veinlets. Disseminated pyrite throughout.
XRD Minerals: Not Analyzed
SWIR Minerals: Not Analyzed
LOI: 2.0%
NH4+: 75ppm
δ15N: Too low

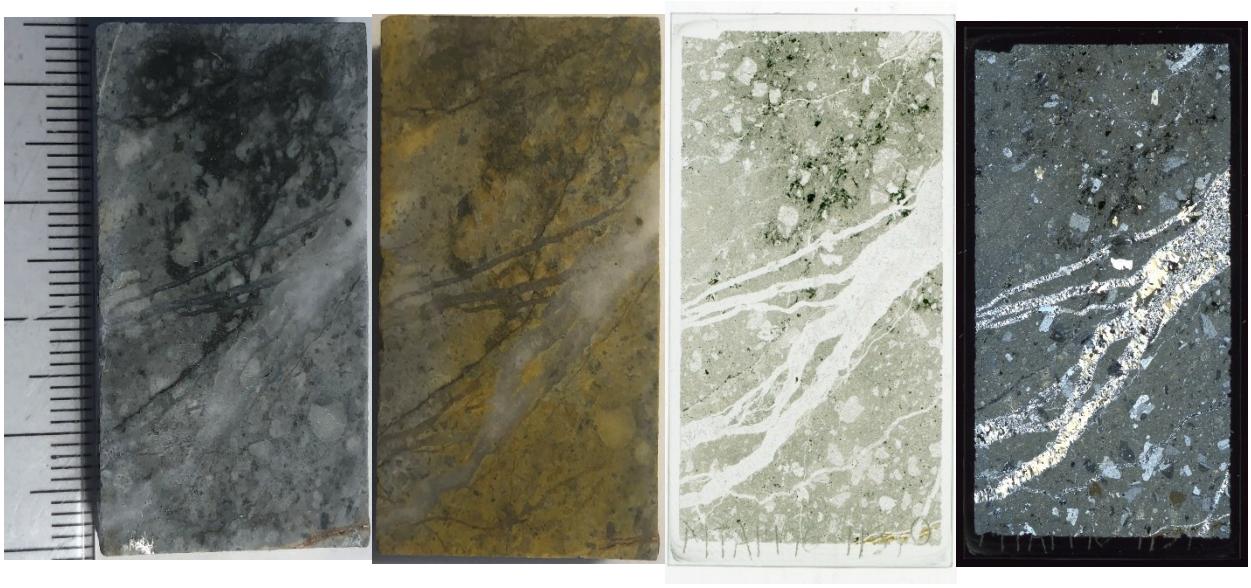

No Thin Section Description

MTA1496-115V

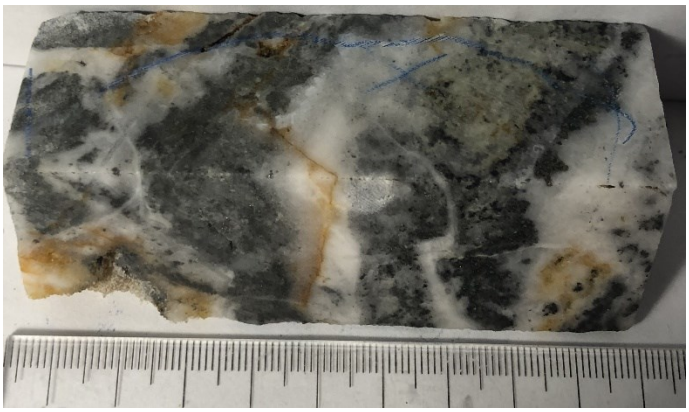

Depth: 115.1m
Sample Desc: Quartz colloform vein breccia. 1-3cm clay rich fragments of altered wallrock. Bands of light coloured and dark quartz. Dark bands contain abundant ore minerals. Rusted quartz patches.
XRD Minerals: Not Analyzed
SWIR Minerals: Not Analyzed
LOI: Not Analyzed
NH4+: Not Analyzed
δ15N: Not Analyzed

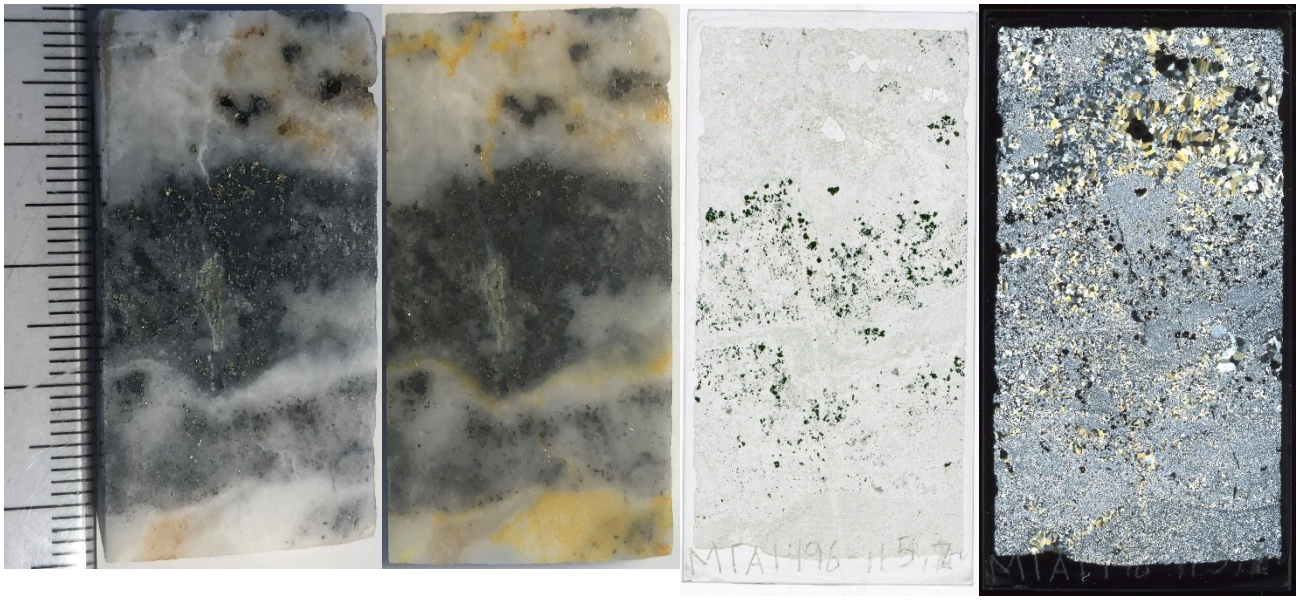

No Thin Section Description

MTA1496-117V

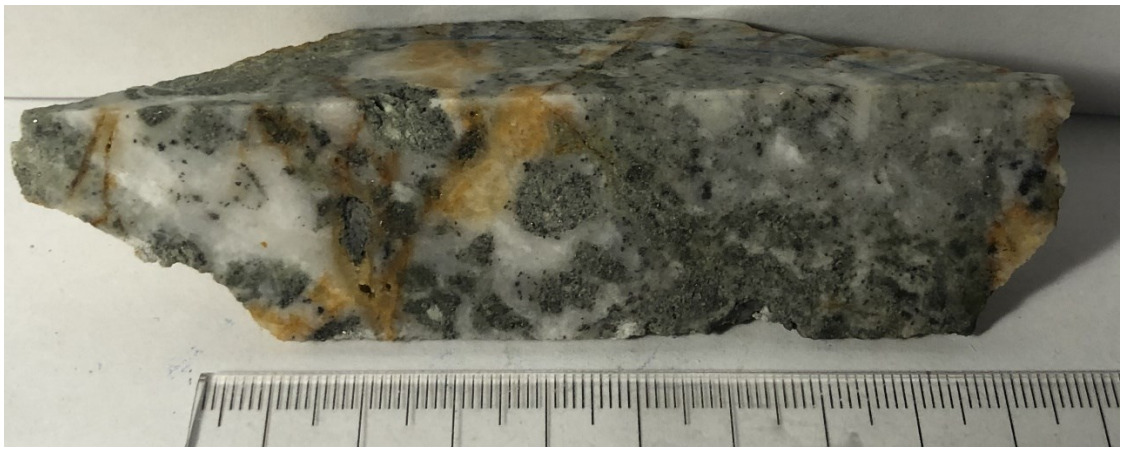

Depth: 117.4m
Sample Desc: Quartz colloform vein breccia. Abundant 0.5 - 3cm patches of sulfides + clays (greenish coloured) which may be brecciated fragments of altered wallrock. Rusted quartz patches.
XRD Minerals: Not Analyzed
SWIR Minerals: Not Analyzed
LOI: Not Analyzed
NH4+: 8ppm
δ15N: Too low

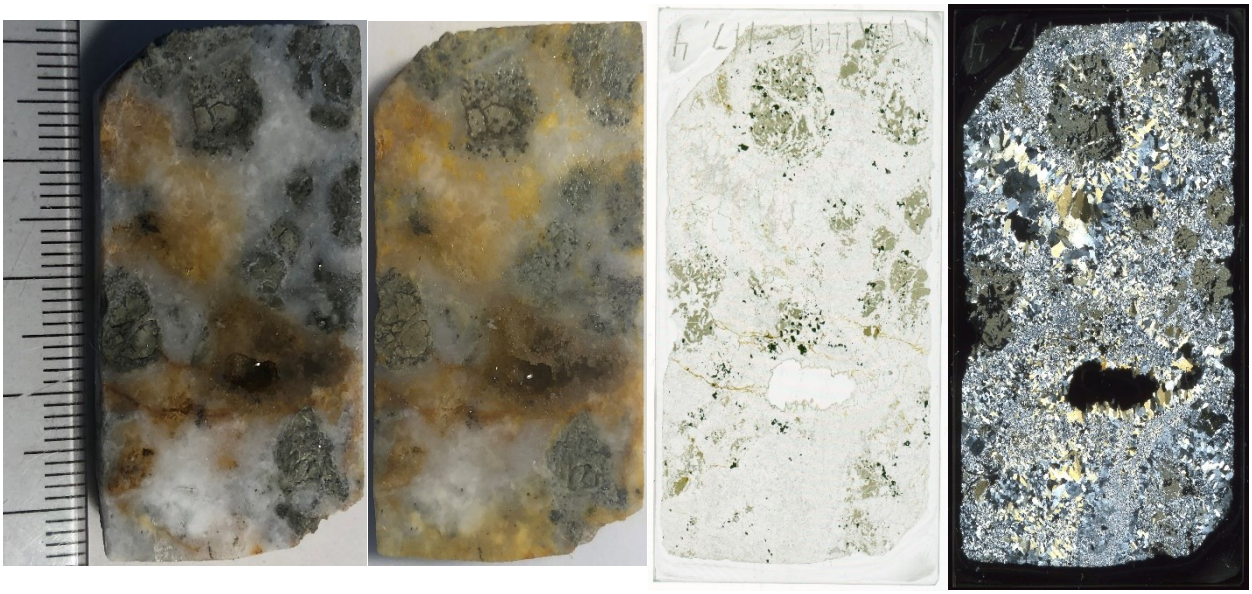

No Thin Section Description

DDH 800SP1MN1203

MTA1203-300V

Depth: 300.0m
Sample Desc: Pink, white, and black brecciated vein sample. Breccia fragments of colloform veins cemented by pinkish microcrystalline quartz or adularia. Dark sulfide rich band near edge of sample.
XRD Minerals: Not Analyzed
SWIR Minerals: Not Analyzed
LOI: 11.2%
NH4+: 12ppm
δ15N: Too low

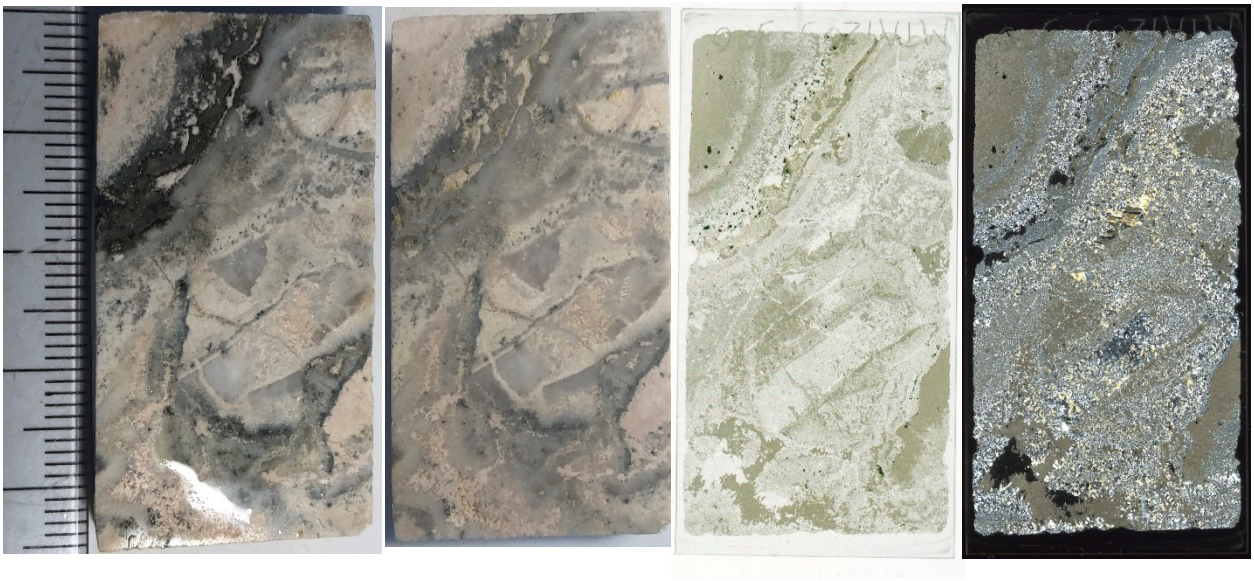

No Thin Section Description

Martha Hill Open Pit

MTA46853V

Depth: N/A
Sample Desc: Colloform banded vein. Microcrystalline Quartz and adularia bands. Comb textures on some bands. Wallrock fragment on right side of sample.
XRD Minerals: Qz (uO)
SWIR Minerals: Not Analyzed
LOI: 1.0%
NH4+: 65ppm
δ15N: Too low

No Petrographic Data

MTA57459V

Depth: N/A
Sample Desc: Vein sample. Significant replaced bladed calcite texture. Quartz adularia rich seen by staining.
XRD Minerals: Qz (uO)
SWIR Minerals: Not Analyzed
LOI: 0.6%
NH4+: 25ppm
δ15N: Too low

No Thin Section Description

MTA57466V

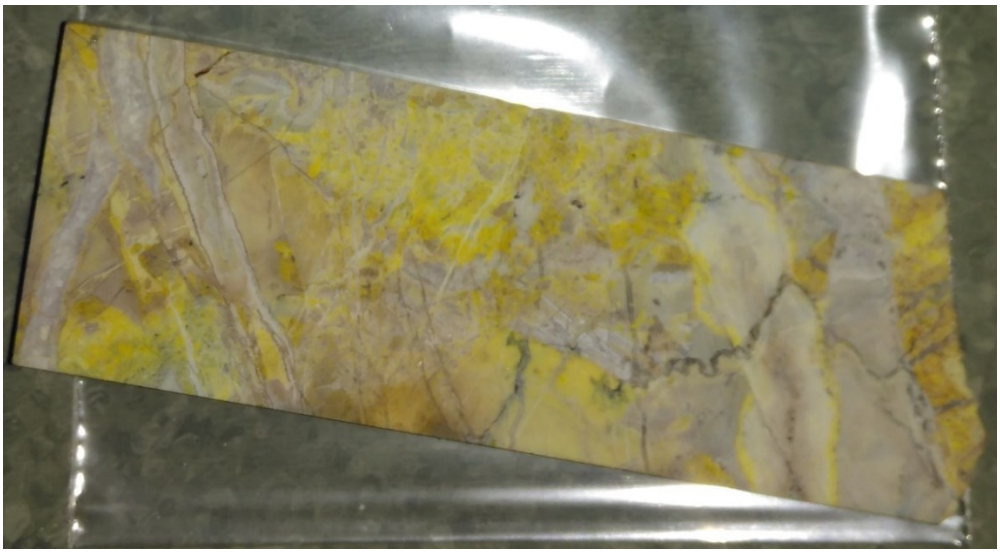

Depth: N/A

Sample Desc: Vein sample. Quartz and adularia rich. Appears brecciated with later colloform veins cutting brecciated portions. Significant adularia staining.

XRD Minerals: Qz (uO)

SWIR Minerals: Not Analyzed

LOI: 0.8%

NH4+: Not Analyzed

δ15N: Not Analyzed

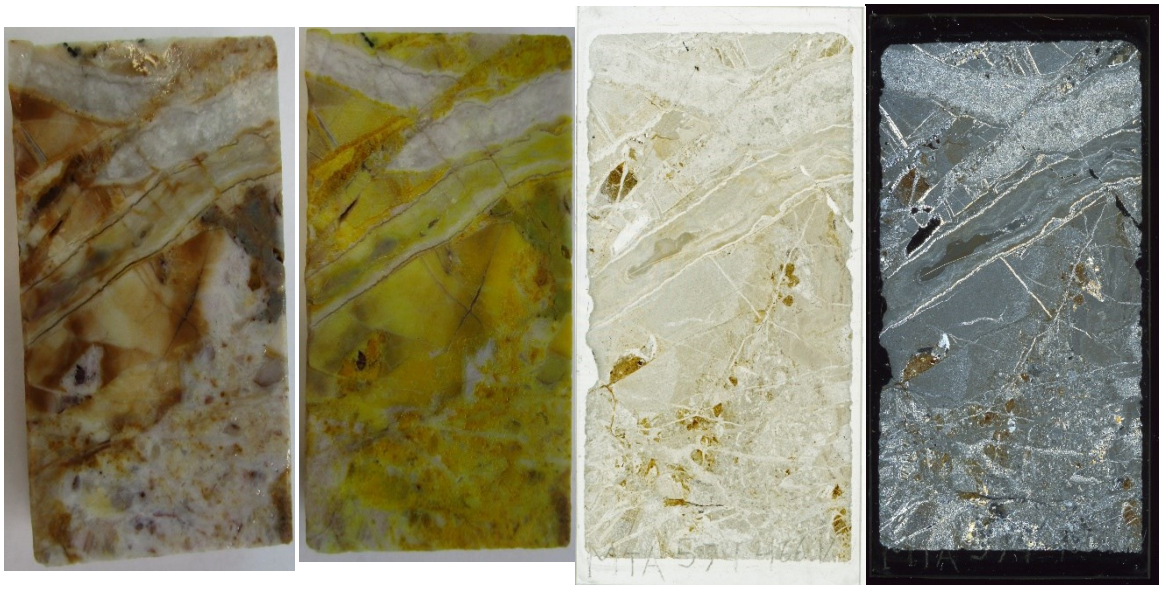

No Thin Section Description

Wharekirauponga (WKP)

DDH WKP42

Spectral Chip Samples

WKP42-26.0

Depth: 26.0m
Sample Desc: Intensely clay altered volcanic rock. Appears as though it is a pyroclastic but is difficult to discern. Dark fragments throughout ranging from 0.5-3mm alter green. Disseminated pyrite throughout.
XRD Minerals: Qz, Ilt, Sm, Chl (uO)
SWIR Minerals : Illite-smectite (Provided by Mark Simpson)
LOI: Not Analyzed
NH4+: Not Analyzed
δ15N: Not Analyzed

No polished thin section

WKP42-46.0

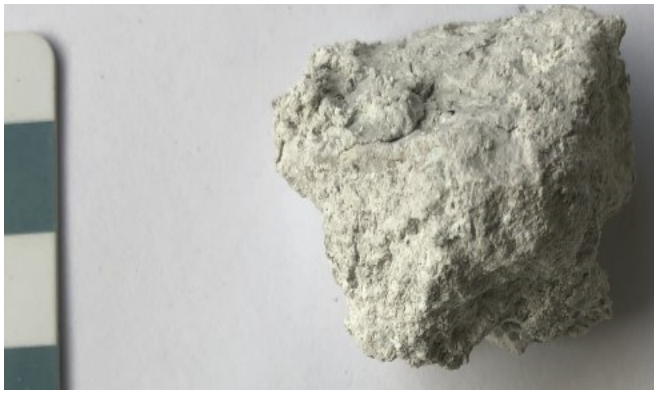

Depth: 46.0m
Sample Desc: Intensely clay altered rhyolitic pyroclastic rock. Appears to be entirely composed of very fine grained, dull white clay minerals. No discernable fragments or clasts.
XRD Minerals: Not Analyzed
SWIR Minerals : Illite (Provided by Mark Simpson)
LOI: 5.8%
NH4+: 740ppm
δ15N: +7.6‰

No polished thin section

WKP42-51.7

Depth: 51.7m
Sample Desc: Strongly altered rhyolite pyroclastic rock or lava sample. Original composition is difficult to discern due to intense alteration. Small 1mm fragments / phenocrysts throughout. More coherent than above samples. Matrix / groundmass is bright white and glittery.
XRD Minerals: Not Analyzed
SWIR Minerals : NH4-Feldspar (Provided by Mark Simpson)
LOI: Not Analyzed
NH4+: Not Analyzed
δ15N: Not Analyzed

No polished thin section

WKP42-56.3

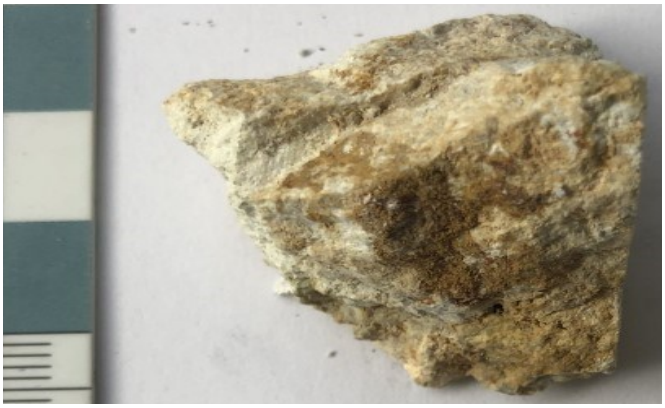

Depth: 56.3m
Sample Desc: Strongly altered rhyolite pyroclastic rock. Original composition is difficult to discern due to intense alteration. More coherent than above tuff samples. Matrix / groundmass is bright white and glittery but is coated in brownish red oxidation.
XRD Minerals: Not Analyzed
SWIR Minerals : NH4-Feldspar (Provided by Mark Simpson)
LOI: 5.3%
NH4+: 734ppm
δ15N: +6.3‰

No polished thin section

WKP42-59.0

Depth: 59.0m
Sample Desc: Intensely clay altered rhyolite pyroclastic rock. Appears to contain small ash or lapilli fragments suggesting tuff. Has been entirely replaced by clay minerals and is very friable. Has a dull greenish white colour.
XRD Minerals: Not Analyzed
SWIR Minerals : NH4-Feldspar (Provided by Mark Simpson)
LOI: 5.3%
NH4+: 658ppm
δ15N: +6.8‰

No polished thin section

WKP42-68.0

Depth: 68.0m
Sample Desc: Intensely clay altered rhyolite pyroclastic rock or lava sample. Difficult to discern original rock type. Reddish fragments throughout ~1mm. Powders easily.
XRD Minerals: Not Analyzed
SWIR Minerals : Illite +/- Kaolinite (Provided by Mark Simpson)
LOI: Not analyzed
NH4+: Not Analyzed
δ15N: Not Analyzed

No polished thin section

WKP42-74.2

Depth: 74.2m
Sample Desc: Clay altered quartz phyric rhyolite or pyroclastic. Groundmass is light gray coloured with rusted patches. Is almost entirely clay altered with ~1mm quartz phenocrysts. Small 3mm veinlet cutting sample at top left.
XRD Minerals: Not Analyzed
SWIR Minerals : Illite, Kaolinite (Provided by Mark Simpson)
LOI: 1.8%
NH4+: 800ppm
δ15N: +3.9‰

No polished thin section

WKP42-75.5

Depth: 75.5m
Sample Desc: Clay altered rhyolite pyroclastic. Groundmass is light gray coloured, coherent, and almost completely coated with rusty brown residue. Is almost entirely composed of clay minerals.
XRD Minerals: Not Analyzed
SWIR Minerals : NH4-Illite, Kaolinite (Provided by Mark Simpson)
LOI: 3.5%
NH4+: 679ppm
δ15N: +5.3‰

No polished thin section

WKP42-80.3

Depth: 80.3m
Sample Desc: Altered rhyolite flow or pyroclastic sample. Groundmass appears strongly silicified. Appears bright white and very coherent. Patches of clay minerals. Possible quartz eyes.
XRD Minerals: Not Analyzed
SWIR Minerals : NH4-Illite, NH4-Feldspar (Provided by Mark Simpson)
LOI: 0.9%
NH4+: 245ppm
δ15N: +6.6‰

No polished thin section

WKP42-103.9

Depth: 103.9m
Sample Desc: Highly silicified rhyolite flow or pyroclastic. Appears dark gray with lighter areas. Dark patches / clasts of chlorite. Clay minerals in the light-coloured areas.
XRD Minerals: Not Analyzed
SWIR Minerals : NH4-Illite (Provided by Mark Simpson)
LOI: Not Analyzed
NH4+: 306ppm
δ15N: +7.3‰

No polished thin section

WKP42-118.2

Depth: 118.2m
Sample Desc: Clay altered pyroclastic rock. Sample is highly rust coated though inside appears to have a white coherent groundmass cementing 1-3mm euhedral quartz crystals. Possible other fragment types though rust coating masks them.
XRD Minerals: Not Analyzed
SWIR Minerals : NH4-Illite (Provided by Mark Simpson)
LOI: Not Analyzed
NH4+: Not Analyzed
δ15N: Not Analyzed

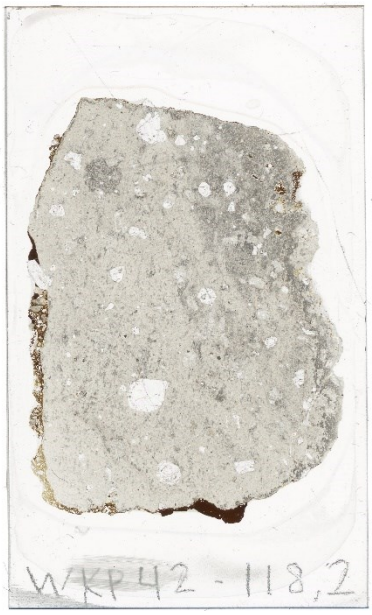

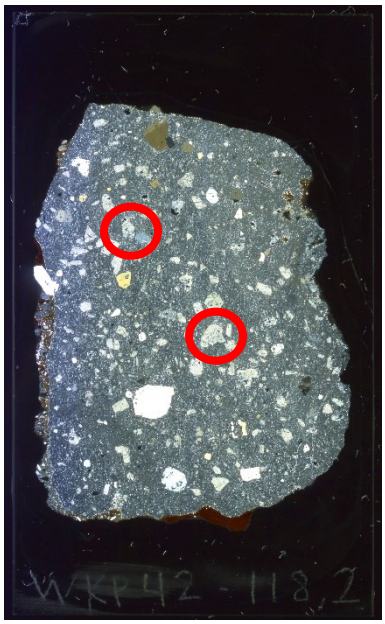

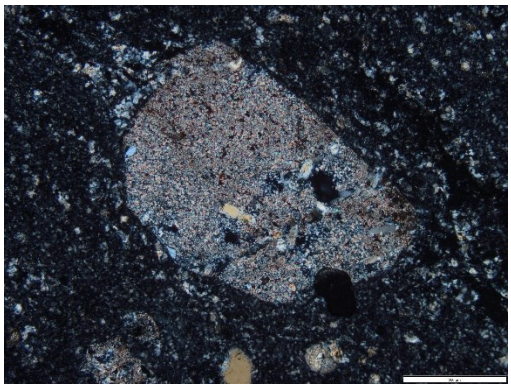

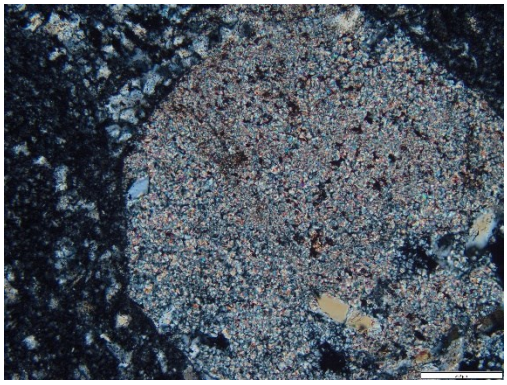

Thin Section Description:

Feldspar and quartz pyric rhyolite. 10% 0.5-2.5mm euhedral quartz phenocrysts. 15% 0.5-1mm Feldspar phenocrysts. Feldspar phenocrysts are completely to almost completely altered to fine grained white mica with minor quartz and / or adularia. Groundmass is very fine grained and composed of interlocking quartz and feldspar (Kfeld?) crystals. No visible white mica in the groundmass.

WKP42-119.8V

Depth: 119.8m
Sample Desc: Colloform microcrystalline quartz vein sample. Quartz appears very clean containing very little sulfides or other minerals. May be part of a small vein system close to surface. Top of sample has clay minerals.
XRD Minerals: Not Analyzed
SWIR Minerals : Kaolinite (Provided by Mark Simpson)
LOI: 1.0%
NH4+: Not Analyzed
δ15N: Not Analyzed

No polished thin section

WKP42-124.0

Depth: 124.0m
Sample Desc: Altered rhyolite sample. Light gray coloured mottled with purple gray. Sample contains ~1mm pits throughout. Either weathered out plagioclase phenocrysts or vesicles.
XRD Minerals: Not Analyzed
SWIR Minerals : NH4-Feldspar (Provided by Mark Simpson)
LOI: Not Analyzed
NH4+: Not Analyzed
δ15N: Not Analyzed

Thin Section Description:

Feldspar and quartz pyric rhyolite. 20% 0.1-1mm feldspar phenocrysts which have been replaced by adularia and overprinted by variable amounts of illite+/- mixed layer smectite. Phenocrysts within the lighter areas have been 70-90% overprinted by illite. The darker banded areas have had minimal illite overprint (5-25%). Illite crystallinity also seems to vary between phenocrysts. Many of the illite rich phenocrysts also contain a highly birefringent isometric/cubic mineral which has strong green absorption colours. This mineral also occurs within the adularia rich phenocrysts and in patches within the groundmass. The groundmass is fine grained to aphanitic quartz +/- feldspar. Some rusting throughout the sample but little to no disseminated pyrite.

WKP42-124
Photomicrographs with SEM-EDS Locations

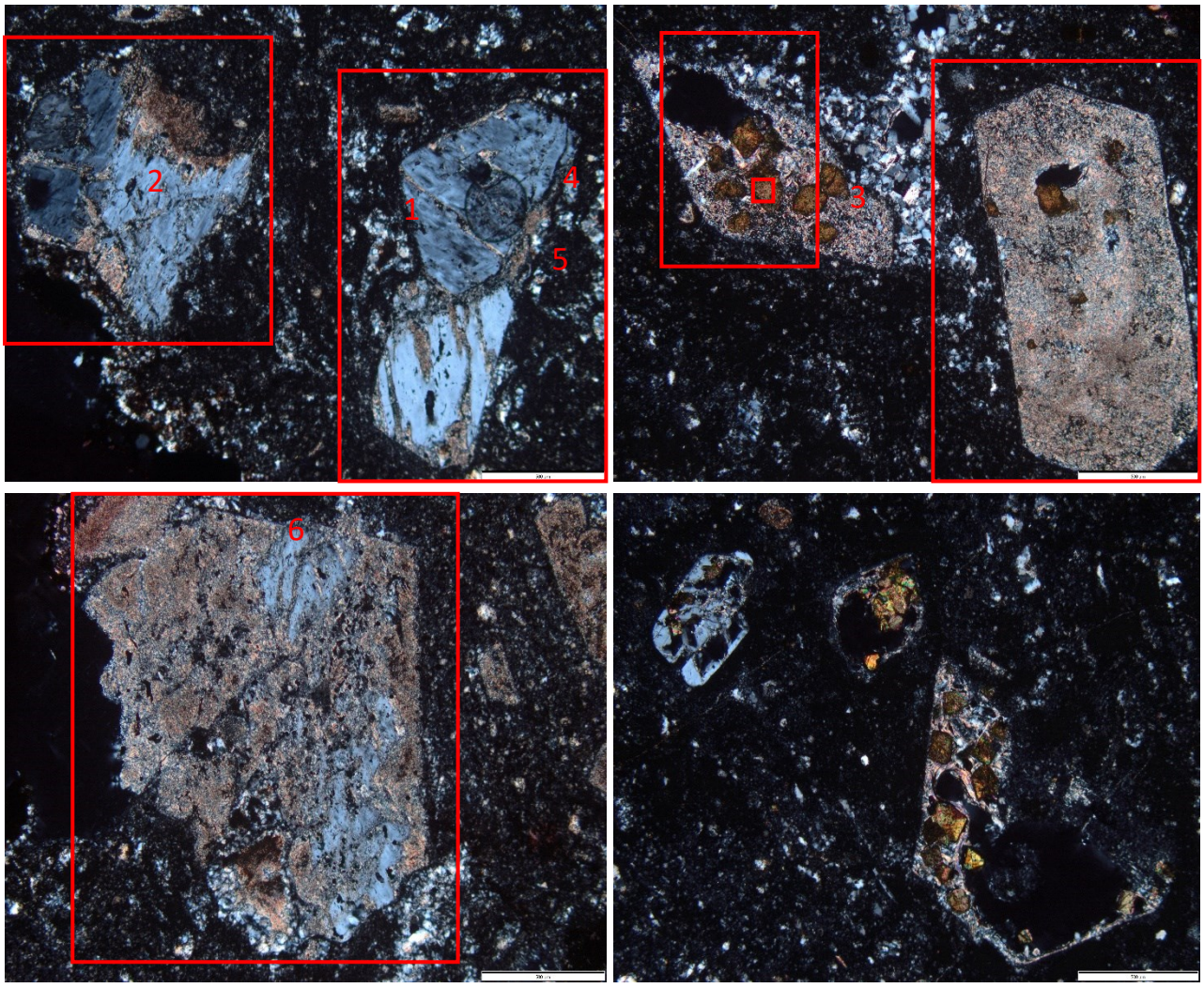

SEM-EDS (1)

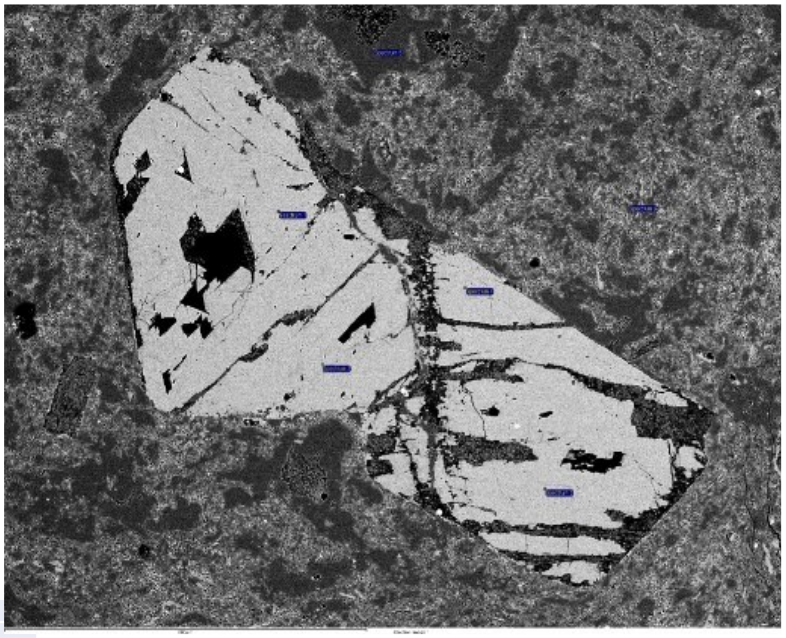

Spectrum	In stats.	Al	Si	K	Total	Mineral	K/Al
Spectrum 1	Yes	18.1	65.67	16.22	100	Adularia	0.90
Spectrum 2	Yes	17.88	65.24	16.88	100	Adularia	0.94
Spectrum 3	Yes	17.64	65.61	16.75	100	Adularia	0.95
Spectrum 4	Yes	17.39	66.05	16.56	100	Adularia	0.95
Spectrum 5	Yes	1.79	97.92	0.29	100	Qz	
Spectrum 6	Yes	11.29	79.27	9.43	100	Qz + Adl	

High Resolution BSE Image

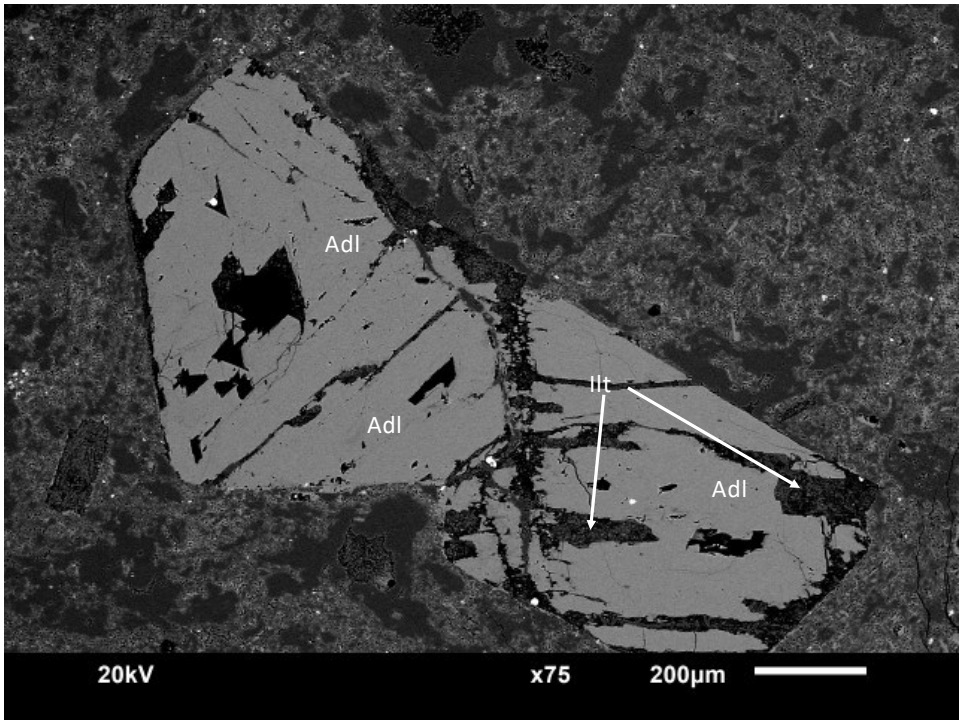

SEM-EDS (2)

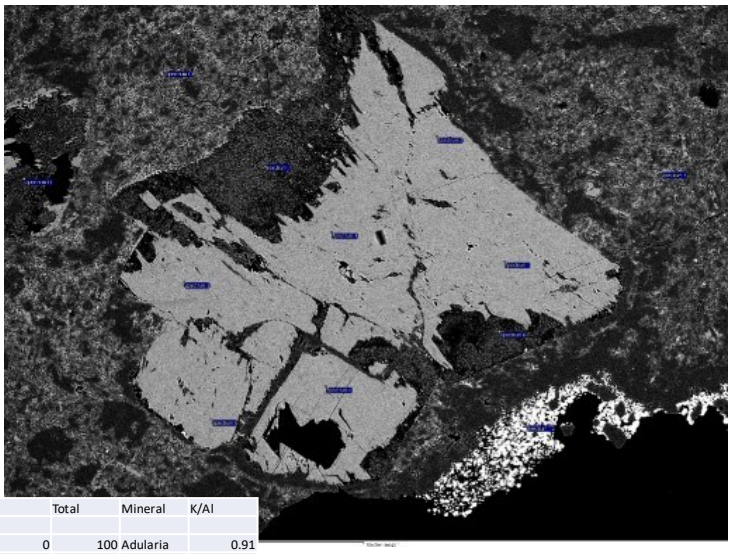

Spectrum	In stats.	Na	Mg	Al	Si	S	K	Fe	Total	Mineral	K/Al
Spectrum 1	Yes	0.48	0	17.43	66.15	0	15.93	0	100	Adularia	0.91
Spectrum 2	Yes	0.32	0	17.84	65.82	0	16.01	0	100	Adularia	0.90
Spectrum 3	Yes	0	0	18.3	65.33	0	16.37	0	100	Adularia	0.89
Spectrum 4	Yes	0	0	17.93	65.69	0	16.38	0	100	Adularia	0.91
Spectrum 5	Yes	0	0	17.89	65.75	0	16.36	0	100	Adularia	0.91
Spectrum 6	Yes	0	0	17.49	66.15	0	16.36	0	100	Adularia	0.94
Spectrum 7	Yes	0	1.65	32.4	55.08	0	9.65	1.21	100	Illite	
Spectrum 8	Yes	0	1.26	33.03	54.36	0	9.92	1.43	100	Illite	
Spectrum 9	Yes	0	0	15.62	70.2	0	14.18	0	100	Qz + Adl	
Spectrum 10	Yes	0	0	19.13	65.29	0	15.58	0	100	Qz + Adl	
Spectrum 11	Yes	0	1.3	24.37	65.09	0	8.31	0.92	100	Illite	
Spectrum 12	Yes	0	0.62	11.08	15.67	1.45	2.22	68.95	100	Jarosite?	

High Resolution BSE Image

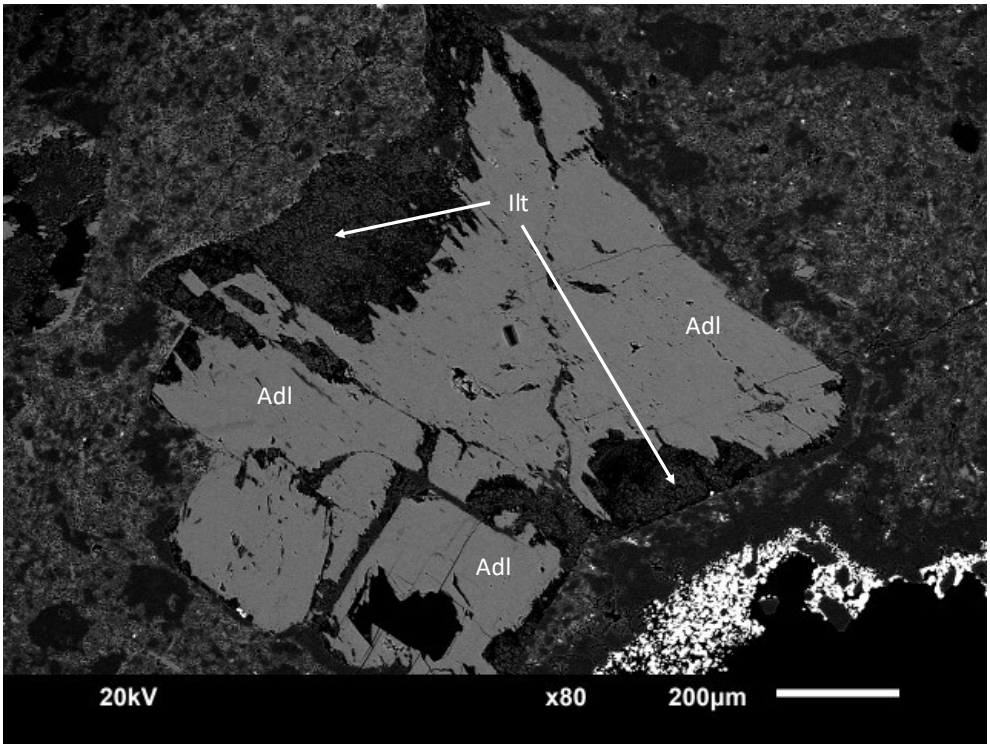

SEM-EDS (3)

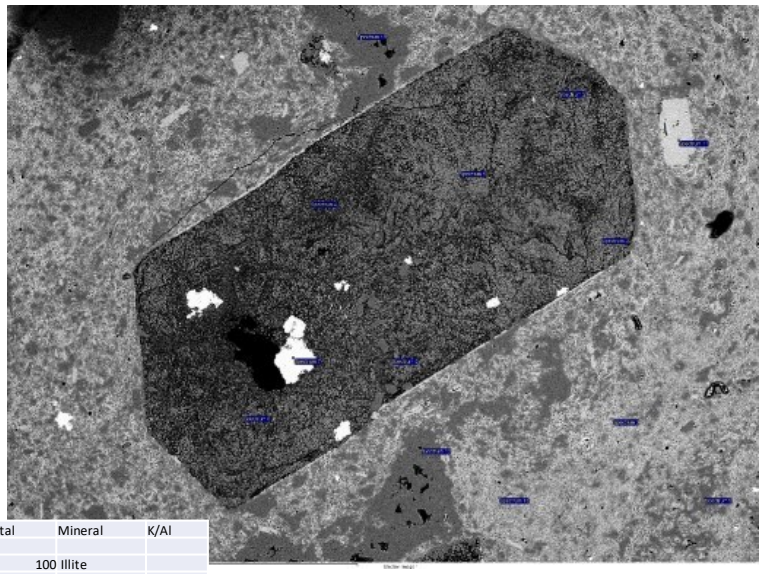

Spectrum	In stats.	Mg	Al	Si	S	K	Fe	Total	Mineral	K/Al
Spectrum 1	Yes	1.39	33.2	53.94	0	10.23	1.24	100	Illite	
Spectrum 2	Yes	1.22	33.18	54.01	0	10.3	1.29	100	Illite	
Spectrum 3	Yes	1.63	32.65	54.75	0	9.83	1.14	100	Illite	
Spectrum 4	Yes	1.16	33.14	54.01	0	10.26	1.43	100	Illite	
Spectrum 5	Yes	1.13	32.76	54.97	0	9.88	1.26	100	Illite	
Spectrum 6	Yes	1.1	33.99	52.76	0	10.45	1.7	100	Illite	
Spectrum 7	Yes	0	8.63	0	37.69	11.35	42.33	100	Jarosite	
Spectrum 8	Yes	0	17.98	66.02	0	15.99	0	100	Adularia (gm)	0.89
Spectrum 9	Yes	0	0.74	99.26	0	0	0	100	Quartz	
Spectrum 10	Yes	0.47	17.82	66.11	0	15.6	0	100	Adl +/- Ilt	
Spectrum 11	Yes	0	17.94	65.34	0	16.72	0	100	Adularia	0.93
Spectrum 12	Yes	0	0.99	99.01	0	0	0	100	Quartz +/- Adl	
Spectrum 13	Yes	0	1.02	98.98	0	0	0	100	Quartz +/- Adl	

High Resolution BSE Image

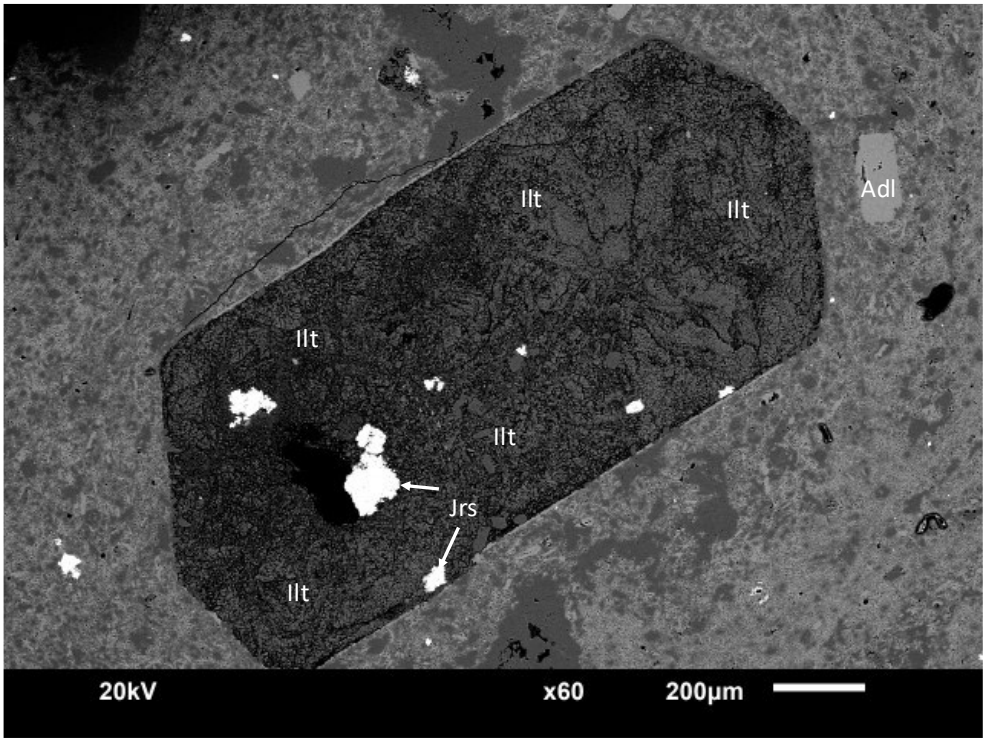

SEM-EDS (4)

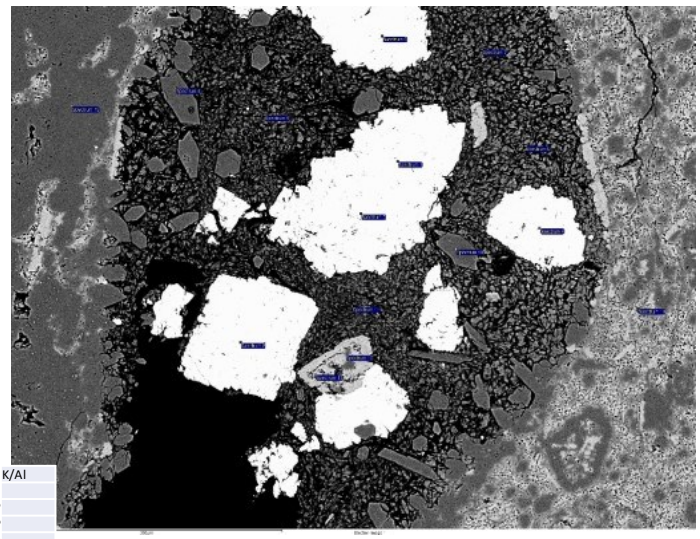

Spectrum	In stats.	Mg	Al	Si	S	K	Fe	Total	Mineral	K/Al
Spectrum 1	Yes	0	8.14	0.49	38.95	10.87	41.55	100	Al Jarosite?	
Spectrum 2	Yes	0	5.96	1.38	36.9	10.31	45.46	100	Al Jarosite?	
Spectrum 3	Yes	0.55	5.32	2.75	35.74	10.23	45.41	100	Al Jarosite?	
Spectrum 4	Yes	0	9.82	0	39.39	11.2	39.6	100	Al Jarosite?	
Spectrum 5	Yes	0	7.4	0.75	38.84	10.89	42.13	100	Al Jarosite?	
Spectrum 6	Yes	0	0.46	99.54	0	0	0	100	Quartz	
Spectrum 7	Yes	1.19	34.22	52.58	0	10.95	1.06	100	Illite	
Spectrum 8	Yes	0.91	34.19	53.5	0	9.93	1.47	100	Illite	
Spectrum 9	Yes	0.72	33.78	54.03	0	10.01	1.45	100	Illite	
Spectrum 10	Yes	0	0.81	99.19	0	0	0	100	Quartz	
Spectrum 11	Yes	1.18	34.04	53.45	0	9.76	1.58	100	Illite	
Spectrum 12	Yes	0	4.93	91.24	0	3.84	0	100	Qz + Ilt	
Spectrum 13	Yes	0	0.9	99.1	0	0	0	100	Quartz	
Spectrum 14	Yes	0	18.09	66.39	0	15.52	0	100	Adularia	0.86
Spectrum 15	Yes	0	17.99	66.25	0	15.76	0	100	Adularia	0.88

High Resolution BSE Image

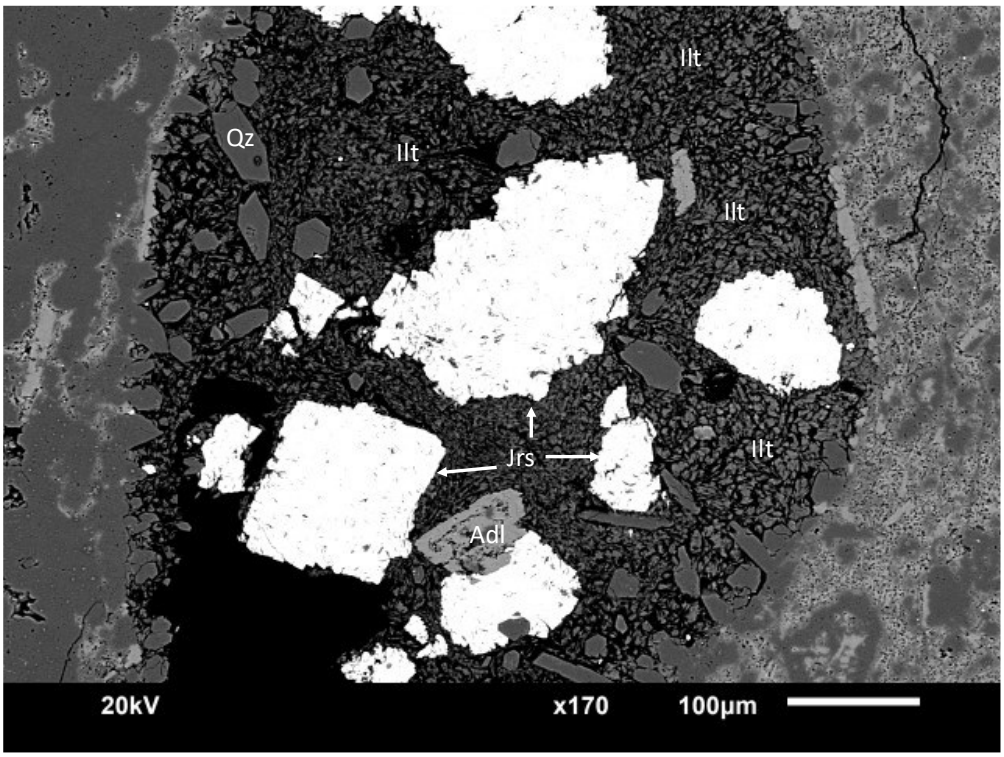

SEM-EDS (5)

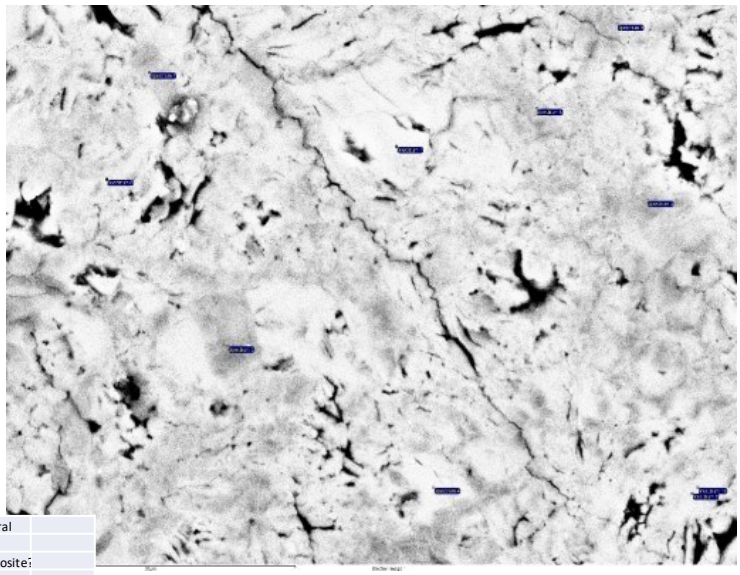

Spectrum	In stats.	Al	Si	S	K	Fe	Total	Mineral
Spectrum 1	Yes	3.43	0.78	37.58	10.46	47.76	100	Al Jarosite?
Spectrum 2	Yes	10.12	0	39.66	10.92	39.3	100	
Spectrum 3	Yes	11.79	0	39.44	10.97	37.8	100	
Spectrum 4	Yes	3.49	0	37.82	9.95	48.74	100	
Spectrum 5	Yes	3.85	0.85	38.11	10.34	46.86	100	
Spectrum 6	Yes	6.13	1.19	37.12	10.56	45	100	
Spectrum 7	Yes	8.97	0.59	38.39	10.31	41.74	100	
Spectrum 8	Yes	8.82	0	39.61	10.42	41.16	100	
Spectrum 9	Yes	8.72	0.59	38.04	10.68	41.97	100	
Spectrum 10	Yes	3.81	0.7	38.16	10.2	47.14	100	

High Resolution BSE Image

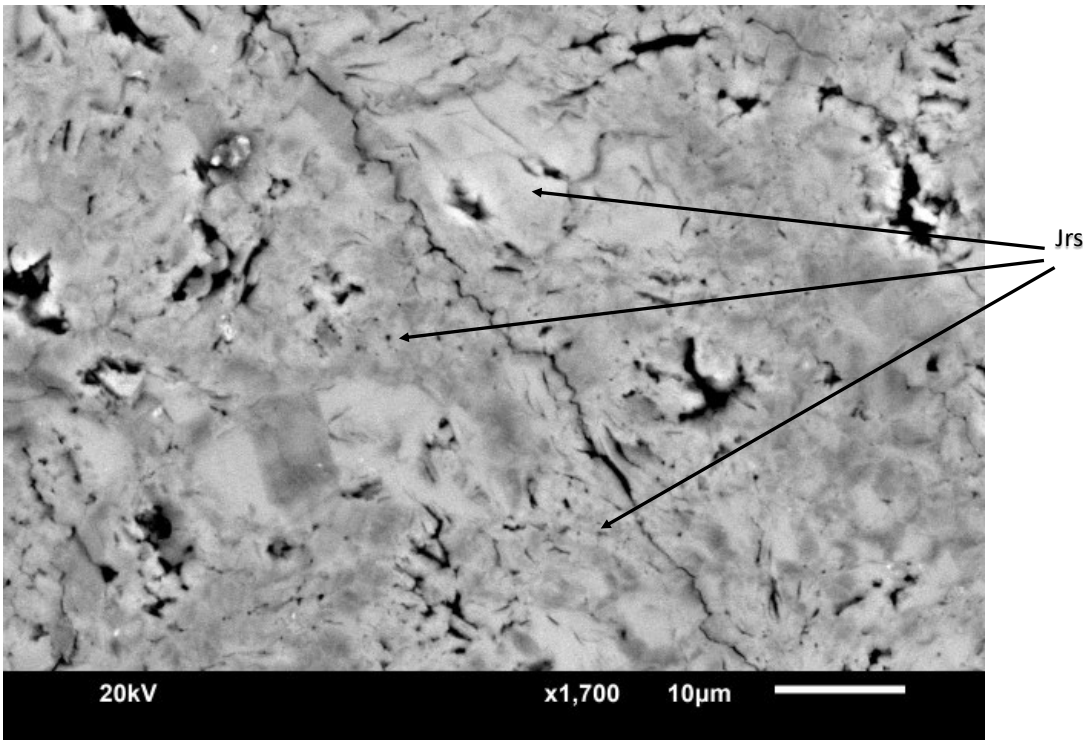

SEM-EDS (6)

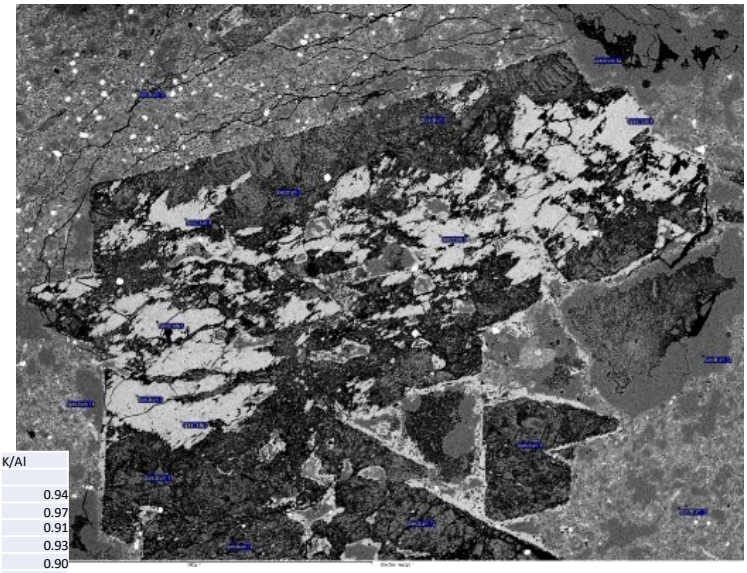

Spectrum	In stats.	Mg	Al	Si	K	Fe	Total	Mineral	K/Al
Spectrum 1	Yes	0	17.71	65.71	16.58	0	100	Adularia	0.94
Spectrum 2	Yes	0	17.52	65.47	17.01	0	100	Adularia	0.97
Spectrum 3	Yes	0	18.08	65.39	16.52	0	100	Adularia	0.91
Spectrum 4	Yes	0	17.79	65.72	16.49	0	100	Adularia	0.93
Spectrum 5	Yes	0	17.92	66	16.09	0	100	Adularia	0.90
Spectrum 6	Yes	0	17.88	65.64	16.48	0	100	Adularia	0.92
Spectrum 7	Yes	1.18	32.62	54.39	10.34	1.48	100	Illite	
Spectrum 8	Yes	1.58	32.49	55.54	9.37	1.01	100	Illite	
Spectrum 9	Yes	1.71	32.41	54.36	10.16	1.36	100	Illite	
Spectrum 10	Yes	1.61	32.12	54.77	10.57	0.92	100	Illite	
Spectrum 11	Yes	0	2.15	97.24	0.62	0	100	Qz + Adl	
Spectrum 12	Yes	1.9	31.94	54.61	9.82	1.72	100	Illite	
Spectrum 13	Yes	0	0.89	98.73	0	0.38	100	Quartz	
Spectrum 14	Yes	0	1.1	98.9	0	0	100	Quartz	
Spectrum 15	Yes	0	5.79	89.95	4.26	0	100	Qz + Adl	
Spectrum 16	Yes	0	14.14	72.31	13.54	0	100	Adularia	0.96
Spectrum 17	Yes	0	2.69	96.62	0.69	0	100	Qz + Adl	

High Resolution BSE Image

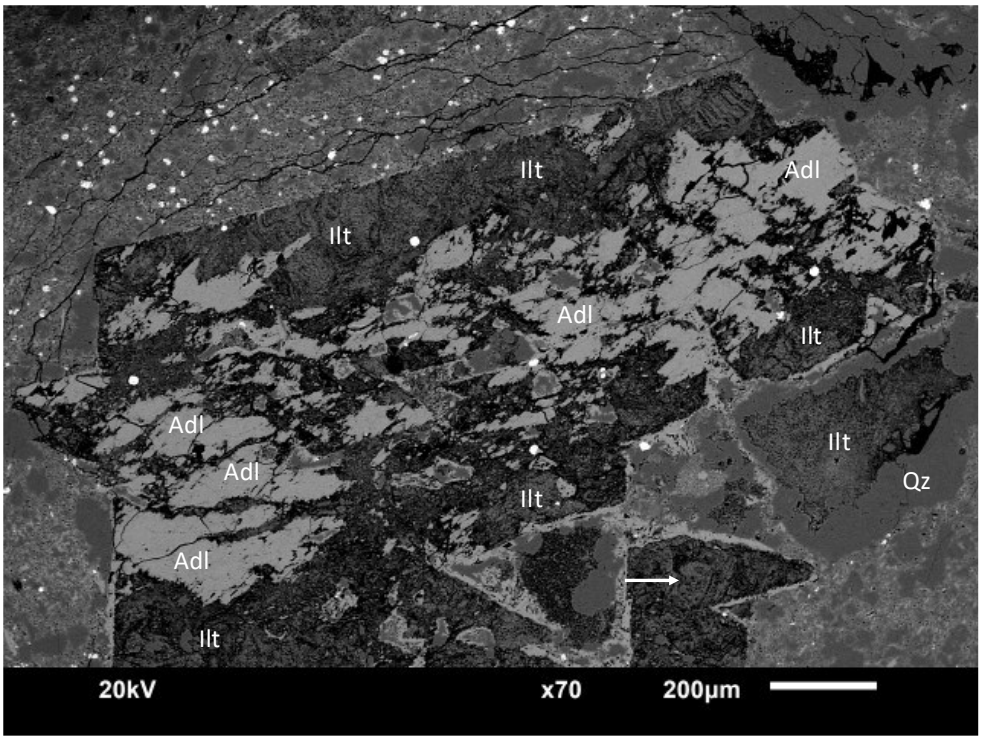

WKP42-142.1

Depth: 142.1m
Sample Desc: Altered flow banded vesicular rhyolite. Quartz eyes (<1%) are <1mm in size. Groundmass is coherent, white, and slightly glittery with dark flow bands.
XRD Minerals: Not Analyzed
SWIR Minerals : Illite, Kaolinite (Provided by Mark Simpson)
LOI: Not Analyzed
NH4+: Not Analyzed
δ15N: Not Analyzed

No polished thin section

WKP42-162.0

Depth: 162.0m
Sample Desc: Clay altered rhyolite. Groundmass is a bright white coloured and has been intensely clay altered. Small <1mm reddish coloured quartz eyes throughout. Minor small rust patches on surface.
XRD Minerals: Not Analyzed
SWIR Minerals : Illite, Kaolinite (Provided by Mark Simpson)
LOI: 3.7%
NH4+: Not Analyzed
δ15N: Not Analyzed

No polished thin section

WKP42-174.0

Depth: 174.0m
Sample Desc: Intensely clay altered rhyolite. Abundant vesicles / excavated crystals. Euhedral <1mm quartz eyes throughout. Minor mafic minerals ~1mm. Groundmass is bright white and glittery.
XRD Minerals: Not Analyzed
SWIR Minerals : Illite (Provided by Mark Simpson)
LOI: Not Analyzed
NH4+: Not Analyzed
δ15N: Not Analyzed

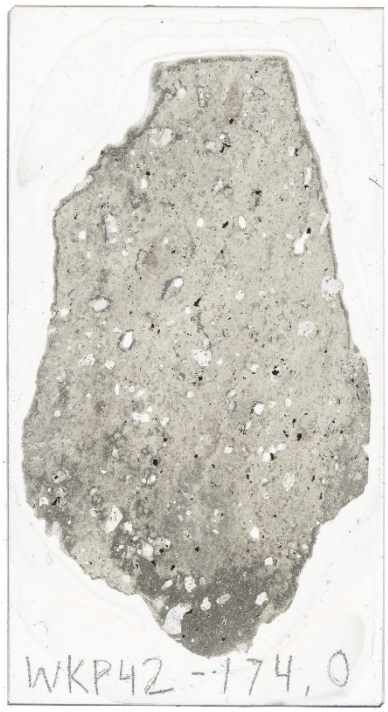

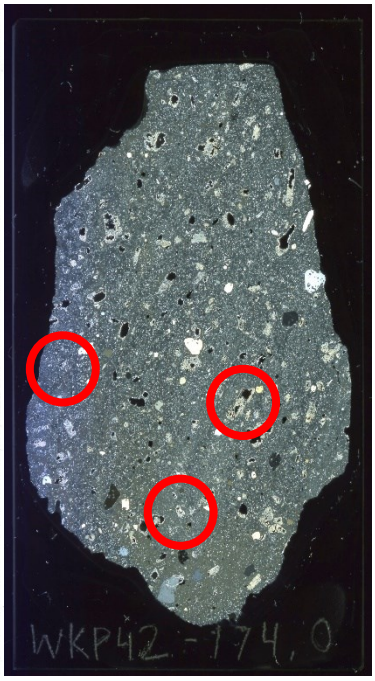

Thin Section Description:

Feldspar quartz phyric rhyolite. 15% subhedral feldspar phenocrysts which range from ~0.1-1mm. Feldspar phenocrysts have been replaced by adularia which has been overprinted by 50-80% illite +/- mixed layer smectite. Much of the illite has been excavated due to polishing but some remains. 5-10% ~0.2-0.5mm subhedral quartz phenocrysts. Groundmass appears to be composed of interlocking quartz and feldspar with little to no clay minerals. Minor disseminated pyrite throughout.

WKP42-174
Photomicrographs with SEM-EDS Locations

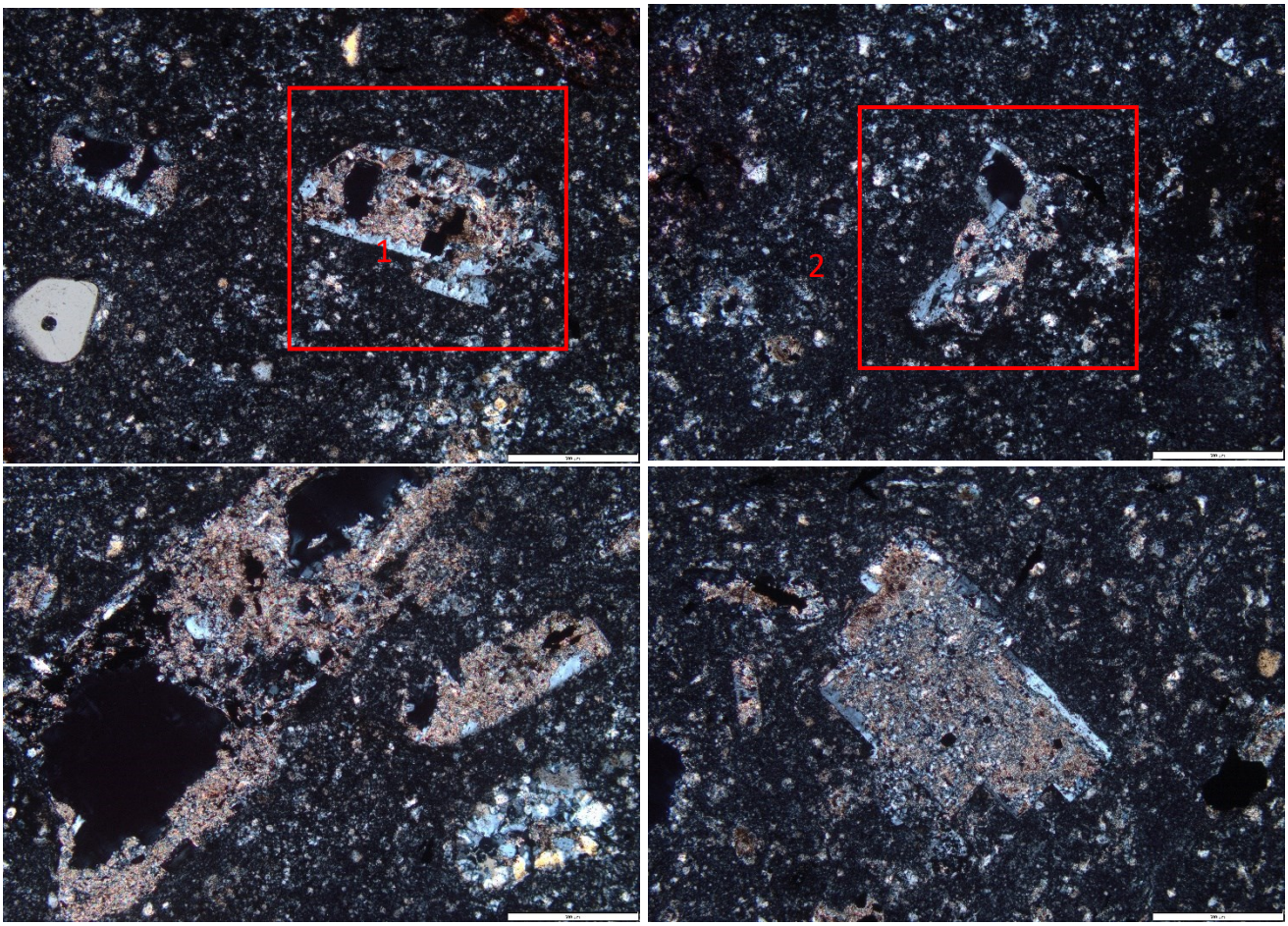

WKP42-174 SEM-EDS

SEM-EDS (1)

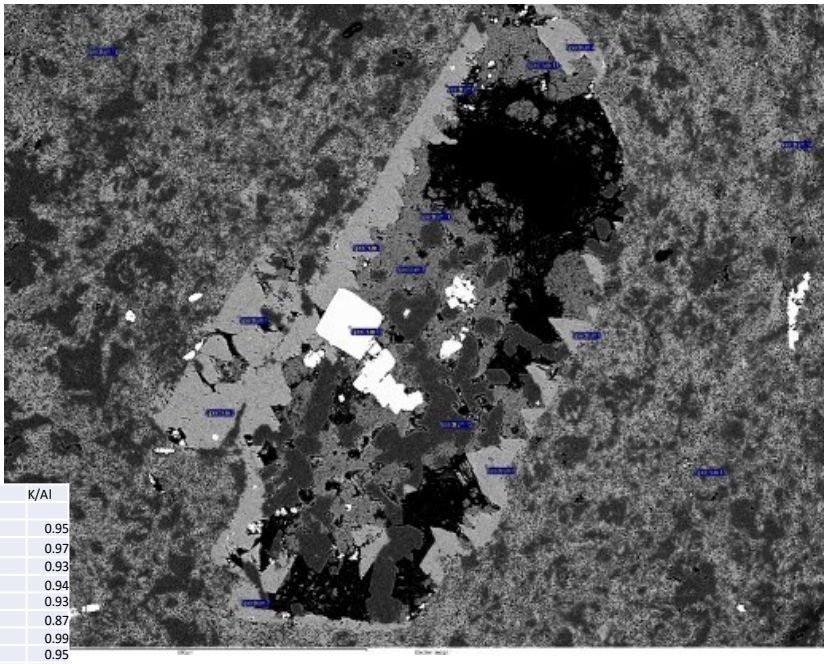

Spectrum	In stats.	Mg	Al	Si	S	K	Ca	Fe	Total	Mineral	K/Al
Spectrum 1	Yes	0	17.51	65.82	0	16.67	0	0	100	Adularia	0.95
Spectrum 2	Yes	0	17.85	64.79	0	17.36	0	0	100	Adularia	0.97
Spectrum 3	Yes	0	17.95	65.36	0	16.69	0	0	100	Adularia	0.93
Spectrum 4	Yes	0	17.96	65.16	0	16.88	0	0	100	Adularia	0.94
Spectrum 5	Yes	0	17.69	65.91	0	16.4	0	0	100	Adularia	0.93
Spectrum 6	Yes	0	18.63	65.24	0	16.13	0	0	100	Adularia	0.87
Spectrum 7	Yes	0	17.15	65.84	0	17.02	0	0	100	Adularia	0.99
Spectrum 8	Yes	0	17.65	65.58	0	16.77	0	0	100	Adularia	0.95
Spectrum 9	Yes	1.24	33.16	52.84	0	10.27	0	2.49	100	Illite	
Spectrum 10	Yes	0.72	33.14	53.07	0	10.61	0	2.46	100	Illite	
Spectrum 11	Yes	1.38	32.48	53.76	0	10.23	0	2.15	100	Illite	
Spectrum 12	Yes	0	0.62	99.38	0	0	0	0	100	Quartz	
Spectrum 13	Yes	0	8.53	84.4	0	7.08	0	0	100	Qz + Adl (gm)	
Spectrum 14	Yes	0.34	21.06	60.89	1.52	14.69	0.83	0.66	100	Qz + Al + Ilt (gm)	
Spectrum 15	Yes	0	17.91	65.42	0	16.67	0	0	100	Qz + Adl (gm)	
Spectrum 16	Yes	0	0	0	65.53	0	0	34.47	100	Pyrite	

High Resolution BSE Image

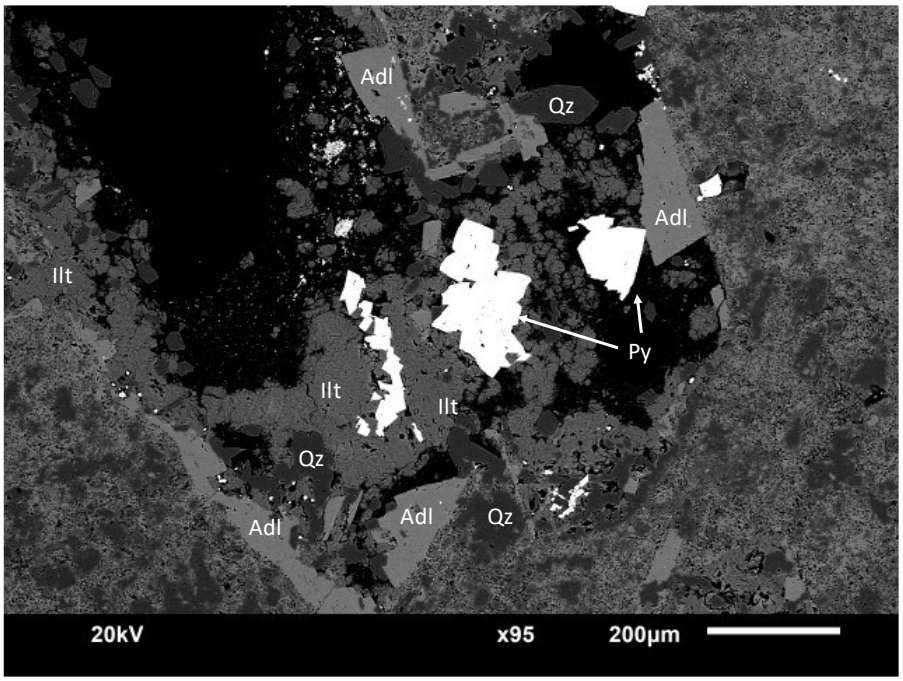

SEM-EDS (2)

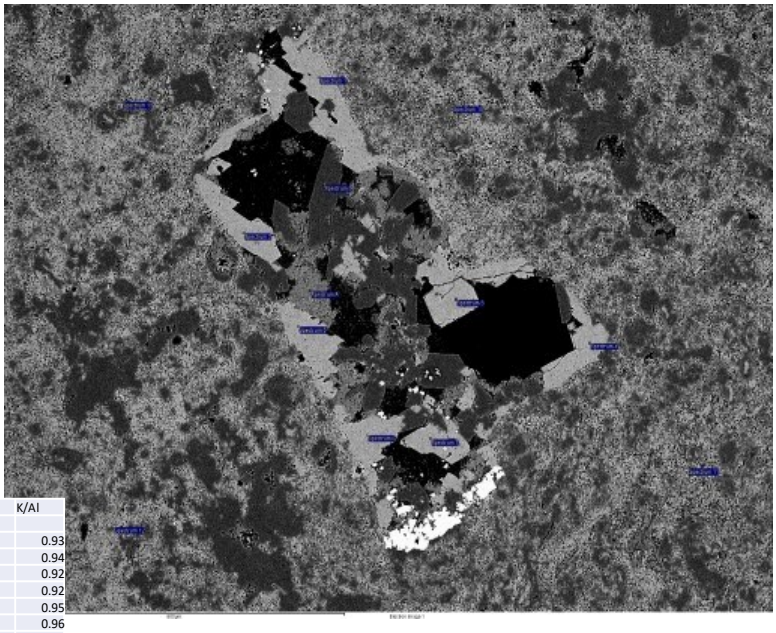

Spectrum	In stats.	Mg	Al	Si	K	Fe	Total	Mineral	K/Al
Spectrum 1	Yes	0	17.47	66.24	16.29	0	100	Adularia	0.93
Spectrum 2	Yes	0	17.9	65.31	16.79	0	100	Adularia	0.94
Spectrum 3	Yes	0	17.72	65.96	16.32	0	100	Adularia	0.92
Spectrum 4	Yes	0	17.87	65.72	16.4	0	100	Adularia	0.92
Spectrum 5	Yes	0	17.52	65.85	16.63	0	100	Adularia	0.95
Spectrum 6	Yes	0	17.52	65.69	16.79	0	100	Adularia	0.96
Spectrum 7	Yes	0	17.71	65.27	17.02	0	100	Adularia	0.96
Spectrum 8	Yes	1.41	32.15	53.19	11.05	2.2	100	Illite	
Spectrum 9	Yes	0	0.48	99.52	0	0	100	Quartz	
Spectrum 10	Yes	0	7.72	86.35	5.93	0	100	Qz + Adl (gm)	
Spectrum 11	Yes	0	17.93	65.72	16.35	0	100	Adularia (gm)	0.91
Spectrum 12	Yes	0	4.09	93.49	2.42	0	100	Qz + Adl (gm)	
Spectrum 13	Yes	0	17.92	65.59	16.5	0	100	Adularia (gm)	0.92

High Resolution BSE Image

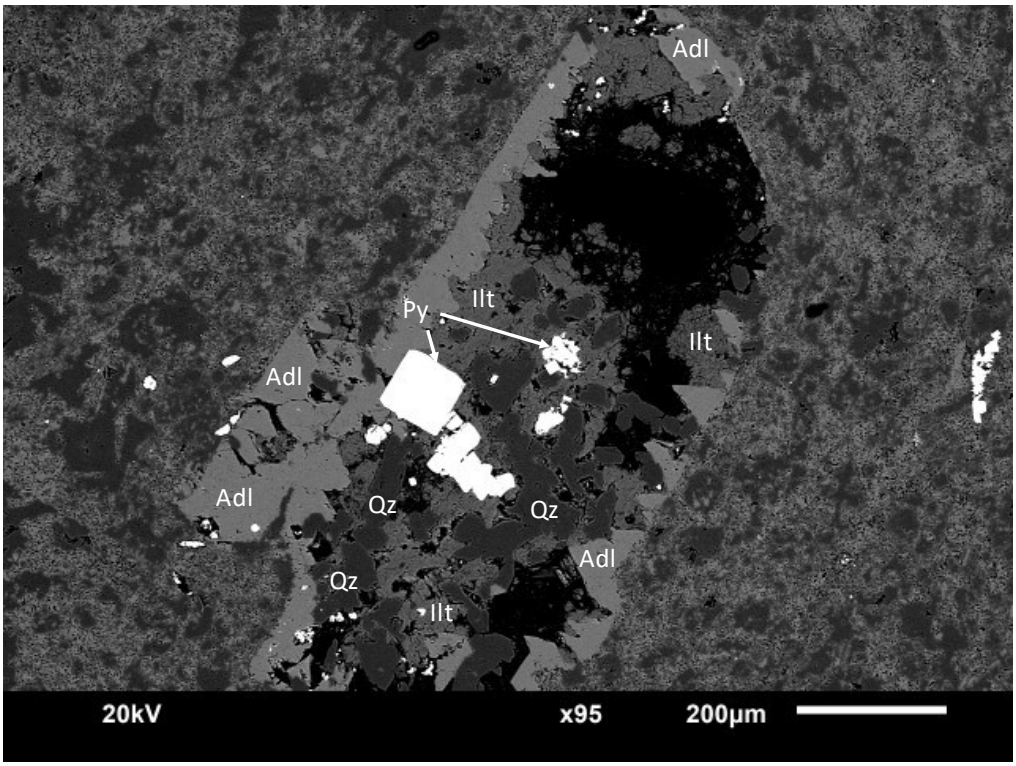

SEM-EDS (3)

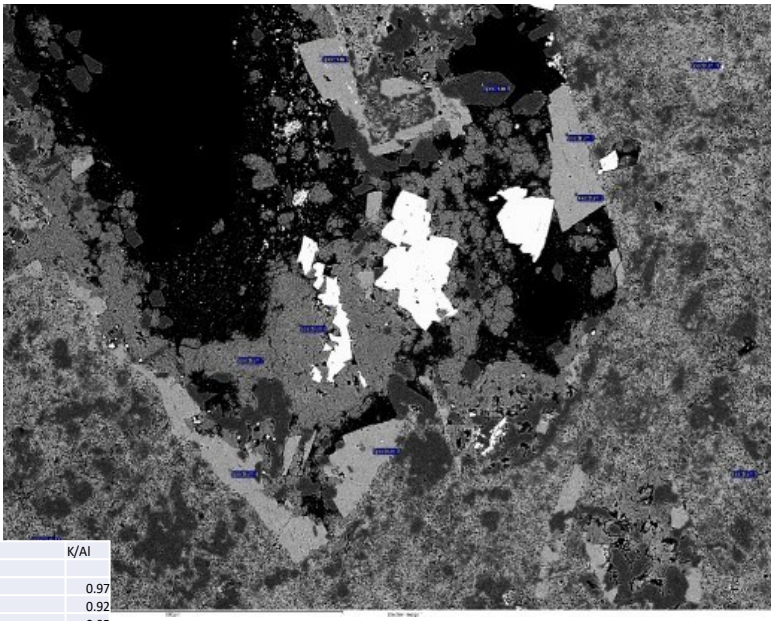

Spectrum	In stats.	Al	Si	K	Fe	Total	Mineral	K/Al
Spectrum 1	Yes	17.57	65.47	16.96	0	100	Adularia	0.97
Spectrum 2	Yes	18.04	65.32	16.65	0	100	Adularia	0.92
Spectrum 3	Yes	18.01	64.87	17.12	0	100	Adularia	0.95
Spectrum 4	Yes	17.6	65.58	16.81	0	100	Adularia	0.96
Spectrum 5	Yes	17.64	65.64	16.72	0	100	Adularia	0.95
Spectrum 6	Yes	33.36	51.71	11.71	3.22	100	Illite	
Spectrum 7	Yes	34.39	52.62	10.6	2.39	100	Illite	
Spectrum 8	Yes	0.43	99.57	0	0	100		
Spectrum 9	Yes	17.9	65.92	16.18	0	100	Adularia (gm)	0.9
Spectrum 10	Yes	17.88	65.73	16.03	0.35	100	Adl + Ilt (gm)	
Spectrum 11	Yes	8.54	83.39	8.07	0	100	Qz + Adl (gm)	

High Resolution BSE Image

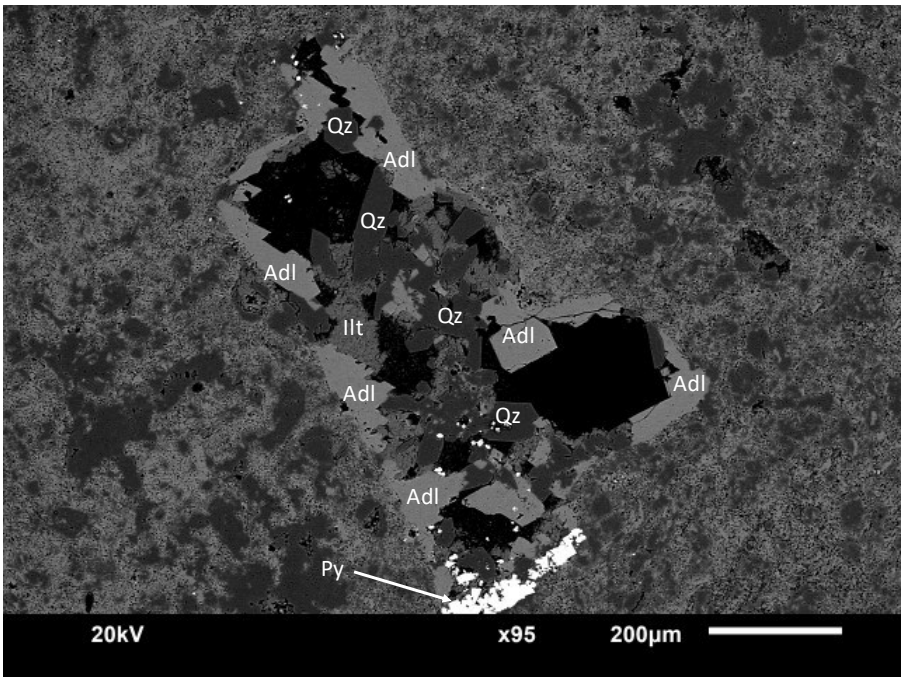

WKP42-196.0

Depth: 196.0m
Sample Desc: Clay altered rhyolite. Groundmass is light gray coloured, coherent, and appears almost silicified. <3mm patches of yellowish white coloured clay minerals. Dark 1mm phenocrysts throughout.
XRD Minerals: Not Analyzed
SWIR Minerals : NH4-Illite (Provided by Mark Simpson)
LOI: 3.5%
NH4+: 421ppm
δ15N: +7.1‰

No polished thin section

WKP42-225.7

Depth: 225.7m
Sample Desc: Medium gray intensely altered rhyolite. Appears irregular and rough textured. Pitted from dissolution of clay mineral patches. Clay minerals within silicified groundmass.
XRD Minerals: Not Analyzed
SWIR Minerals : Illite, Chlorite (Provided by Mark Simpson)
LOI: 3.7%
NH4+: 299ppm
δ15N: +7.7‰

No polished thin section

WKP42-225.7

Depth: 225.7m
Sample Desc: Medium gray intensely altered rhyolite. Appears irregular and rough textured. Pitted from dissolution of clay mineral patches. Clay minerals within silicified groundmass.
XRD Minerals: Not Analyzed
SWIR Minerals : Illite, Chlorite (Provided by Mark Simpson)
LOI: 3.7%
NH4+: 299ppm
δ15N: +7.7‰

No polished thin section

WKP42-245.1

Depth: 245.1m
Sample Desc: Clay altered volcanic rock. Coherent greenish white groundmass cementing minor 1-3mm euhedral quartz crystals and euhedral biotite phenocrysts. Groundmass is earthy not glittery like previous illite samples.
XRD Minerals: Qz, Ad, Ilt, Sm, Chl (uO)
SWIR Minerals : NH4-Illite (Provided by Mark Simpson)
LOI: Not Analyzed
NH4+: Not Analyzed
δ15N: Not Analyzed

No polished thin section

WKP42-277.4

Depth: 277.4m
Sample Desc: Chlorite altered rhyolite. Appears greenish gray with abundant 0.5-2mm dark green patches throughout. Small <1mm white clay patches. Rusted out disseminated sulfides.
XRD Minerals: Not Analyzed
SWIR Minerals : NH4-Illite(Provided by Mark Simpson)
LOI: 1.9%
NH4+: 222ppm
δ15N: +4.8‰

No polished thin section

WKP42-313.5

Depth: 313.5m
Sample Desc: Clay altered rhyolite. Groundmass is mottled bright white and light gray. Small <1mm phenocrysts of reddish quartz Some have been removed leaving a pitted texture. Small phenocrysts and a dark 5mm patch of chlorite in the center of the sample.
XRD Minerals: Not Analyzed
SWIR Minerals : NH4-Illite, Chlorite (Provided by Mark Simpson)
LOI: 1.0%
NH4+: 203ppm
δ15N: +7.7‰

No polished thin section

WKP42-397.0

Depth: 397.0m
Sample Desc: Mottled dark and light gray altered rhyolite sample. Small 1mm phenocrysts of reddish coloured mineral.
XRD Minerals: Not Analyzed
SWIR Minerals : Illite(Provided by Mark Simpson)
LOI: 0.8%
NH4+: Not Analyzed
δ15N: Not Analyzed

No polished thin section

WKP42-407

Depth: 407.9m

Sample Desc: Altered quartz and plagioclase phyric flow banded rhyolite. White ~1mm clay altered plagioclase phenocrysts. Reddish brown coloured translucent 1-4mm phenocrysts. Groundmass near right side is brownish gray while groundmass near left side is yellowish gray. Probably alteration halo of vein off left side. Red hematite alteration along some flow bands. Small 1-3mm quartz veinlets throughout.

XRD Minerals: Qz, Ad, Ilt, Chl {analyzed at uOttawa (uO)}

SWIR Minerals: Not Analyzed

LOI: 2.7%

NH4+: 158ppm

δ15N: +5.9‰

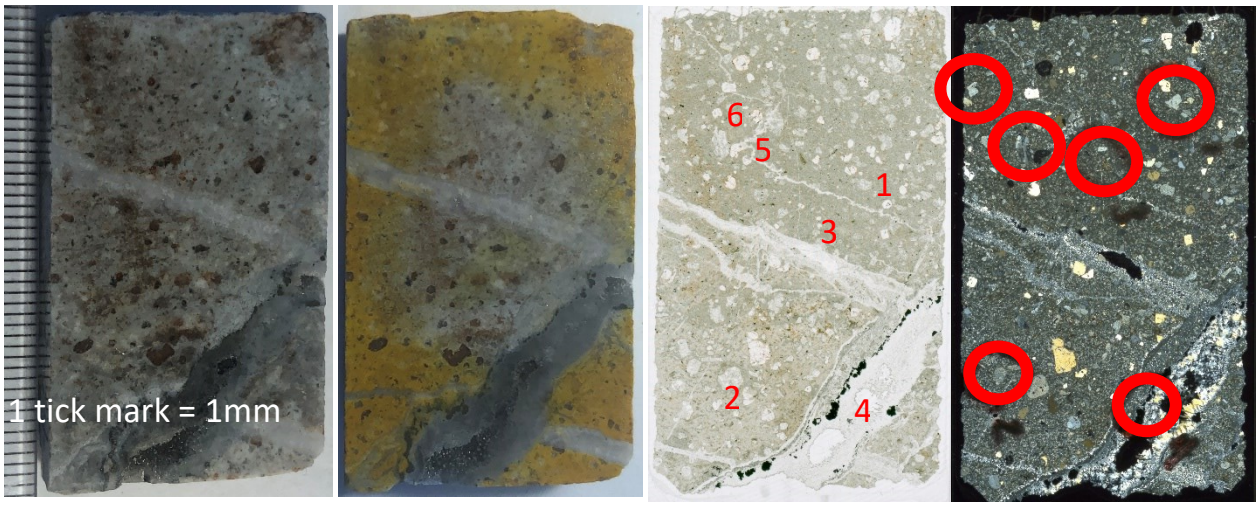

Thin Section Description:

Altered rhyolite flow dome. 20% 0.5-2mm quartz phenocrysts throughout. 15% 0.1-1mm feldspar phenocrysts which have been intensely altered. Feldspar grains are Carlsbad twinned however grains appear to have been strongly adulariatized and original composition is unidentifiable. Most likely originally K-Feldspar. Feldspars are commonly overprinted by white mica covering about 30-70% of the grains. Some white mica overprint is high birefringence (image 2) but some appears brown (photo 1) and is possibly smectite. Minor (5%) chlorite altered mafic mineral grains throughout (image 3). The matrix is very fine grained containing abundant k-feldspar (strong staining), white mica, and quartz. Disseminated euhedral pyrite throughout and “framboidal?” elongated pyrite in veinlet (image 4).

WKP42-407 Photomicrographs

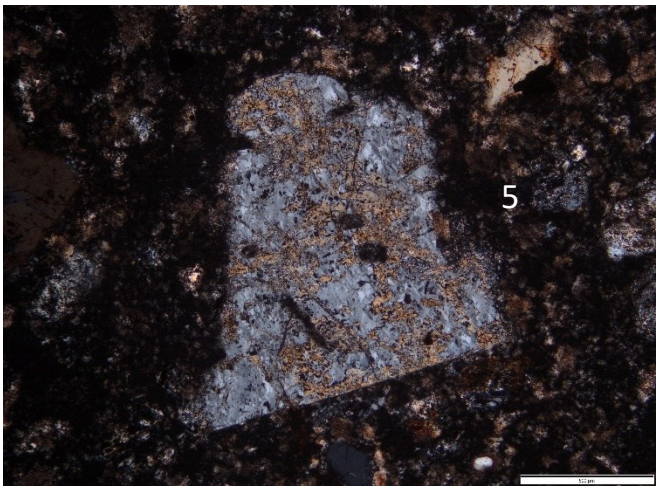

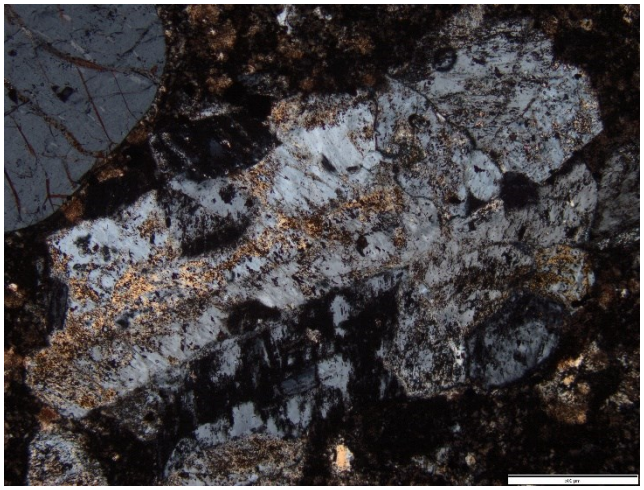

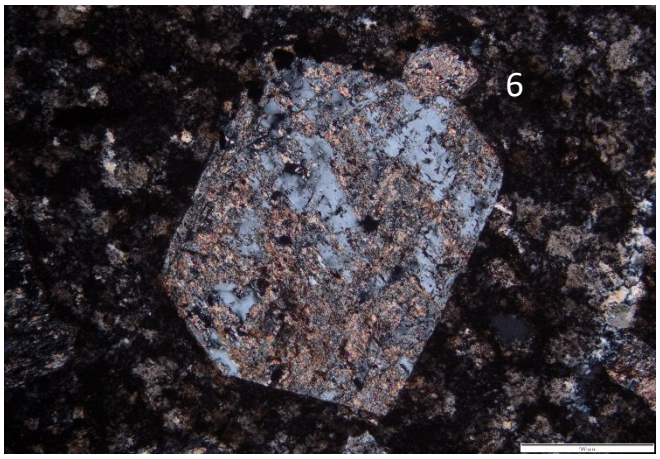

SEM-EDS (1)

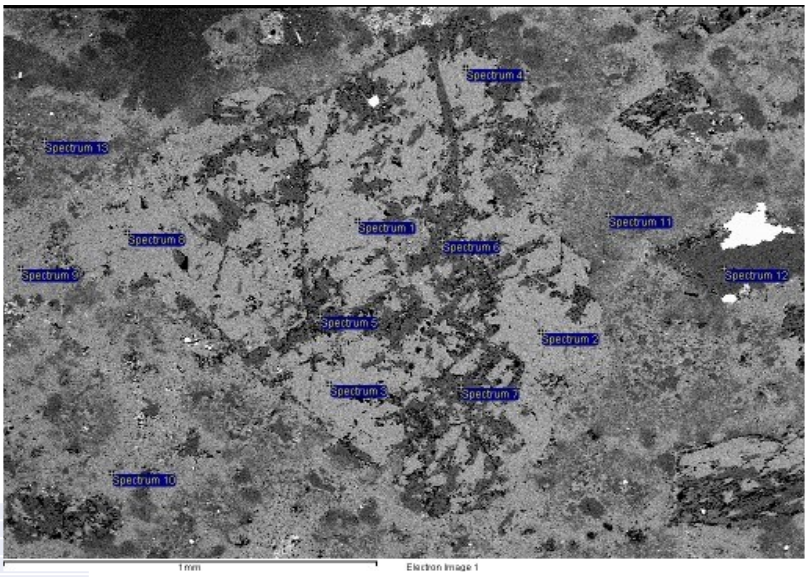

Spectrum	Na	Al	Si	K	Ca	Mineral
Spectrum 1	0.39	17.62	66.09	15.9	0	Adularia
Spectrum 2	0	17.11	66.88	16.02	0	Adularia
Spectrum 3	0	17.85	65.58	16.58	0	Adularia
Spectrum 4	0	17.52	66.34	16.14	0	Adularia
Spectrum 5	11.29	19.71	67.92	0.52	0.57	Albite or maybe smectite?
Spectrum 6	10.76	19.27	69.97	0	0	Albite
Spectrum 7	10.44	19.19	69.54	0.83	0	Albite
Spectrum 8	0	17.74	65.89	16.37	0	Adularia
Spectrum 9	0	17.82	65.45	16.73	0	Adularia
Spectrum 10	0.81	18.07	65.6	15.52	0	Adularia + Albite (Groundmass)
Spectrum 11	0.68	10.7	79.63	8.99	0	Quartz + Adularia (Groundmass)
Spectrum 12	0	0	100	0	0	Quartz (Groundmass)
Spectrum 13	0	3.31	94.82	1.87	0	Quartz + Adularia (Groundmass)

High Resolution BSE Image

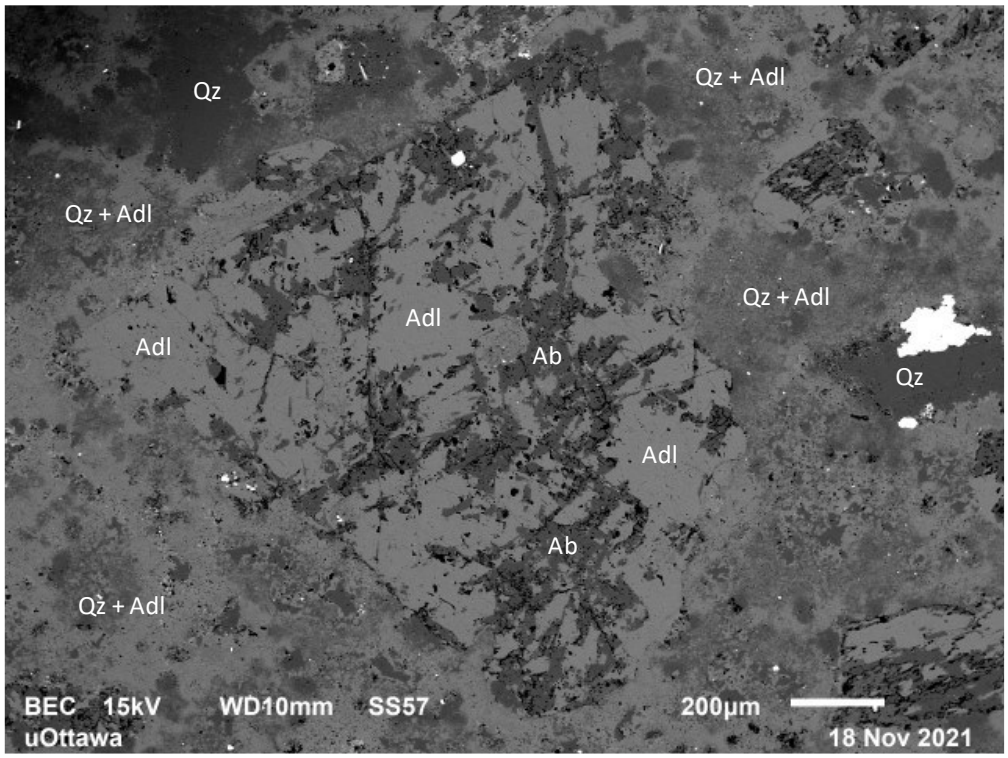

SEM-EDS (2)

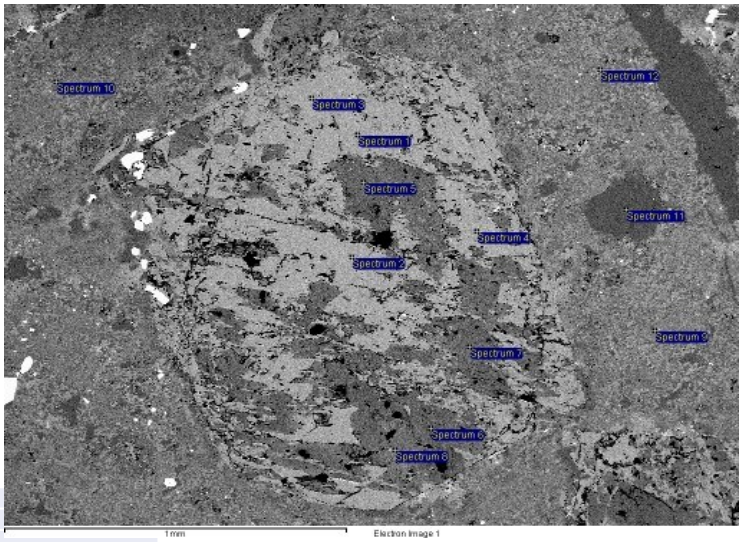

Spectrum	Na	Mg	Al	Si	K	Ti	Fe	Mineral
Spectrum 1	0	0	17.56	66.25	16.19	0	0	Adularia
Spectrum 2	0	0	17.89	66.28	15.84	0	0	Adularia
Spectrum 3	0	0	18.37	65.91	15.73	0	0	Adularia
Spectrum 4	0.49	0	18.2	65.31	16	0	0	Adularia + minor Na
Spectrum 5	0	0.98	33.62	54.45	10.05	0	0.9	Illite
Spectrum 6	0	1.82	31.83	56.07	9.15	0	1.13	Illite
Spectrum 7	0	1.76	33.54	55.24	8.66	0	0.8	Illite
Spectrum 8	0	1.08	33.54	54.65	9.63	0	1.09	Illite
Spectrum 9	0.57	0	6.61	88.3	4.51	0	0	Quartz + Adularia? (Groundmass)
Spectrum 10	0.45	0	9.53	82.1	7.91	0	0	Quartz + Adularia? (Groundmass)
Spectrum 11	0	0	0	100	0	0	0	Quartz (Groundmass)
Spectrum 12	0.68	0	13.56	65.62	7.14	4.24	8.76	Quartz +Adularia+ Rutile + Pyrite?(Groundmass)

High Resolution BSE Image

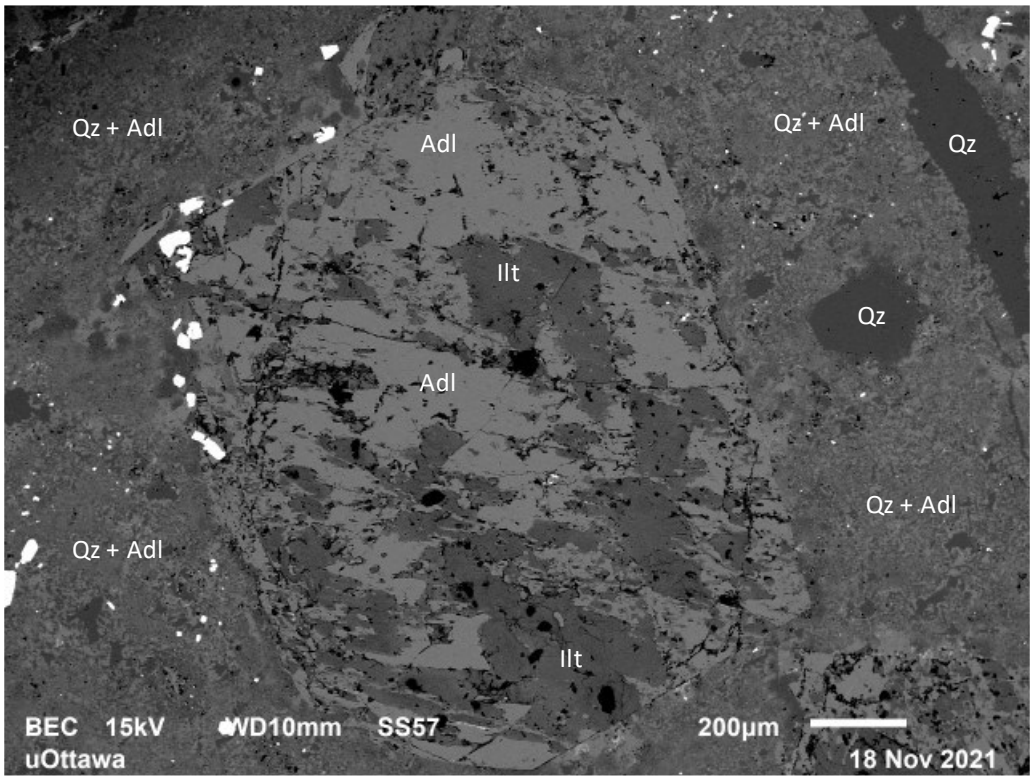

SEM-EDS (5)

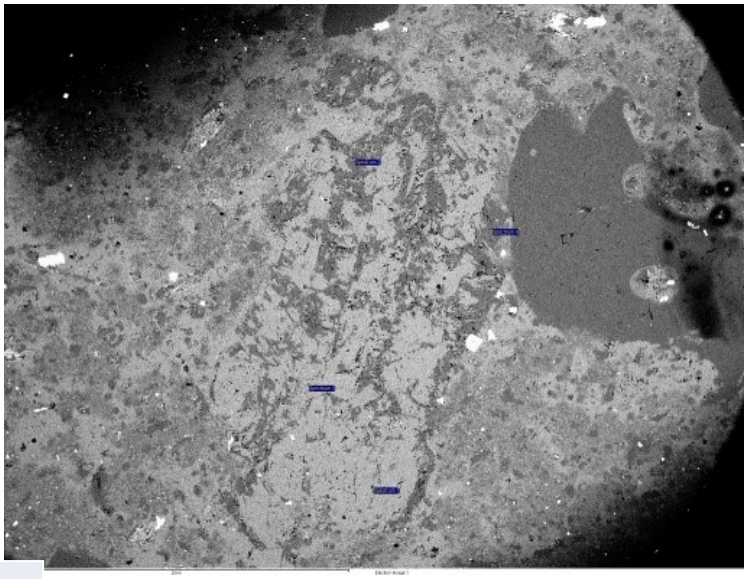

Spectrum	In stats.	Na	Al	Si	K	Total	Mineral
Spectrum 1	Yes	0.95	17.22	65.89	15.94	100	Albite
Spectrum 2	Yes	1.36	4.86	93.78	0	100	Quartz + Albite
Spectrum 3	Yes	0	18.62	64.96	16.42	100	Adularia
Spectrum 4	Yes	7.1	19.06	68.66	5.18	100	Adularia + albite

SEM-EDS (5 zoom)

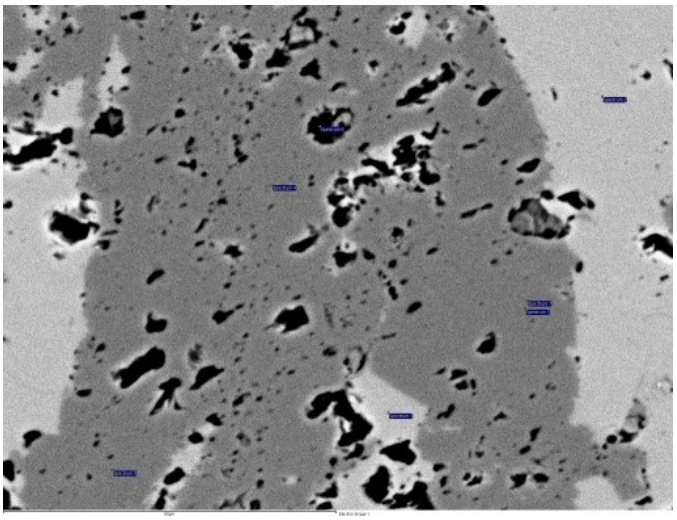

Spectrum	In stats.	Na	Al	Si	K	Ca	Total	Mineral
Spectrum 1	Yes	10.54	19.11	69.92	0	0.43	100	Albite
Spectrum 2	Yes	0	17.41	66.32	16.26	0	100	Adularia
Spectrum 3	Yes	0	17.01	66.9	16.09	0	100	Adularia
Spectrum 4	Yes	11.07	19.27	69.12	0	0.53	100	Albite
Spectrum 5	Yes	11.34	19.76	68.9	0	0	100	Albite
Spectrum 6	Yes	6.13	18.22	73.58	1.34	0.73	100	Hole
Spectrum 7	Yes	11.06	19.17	69.19	0	0.58	100	Albite

SEM-EDS (6)

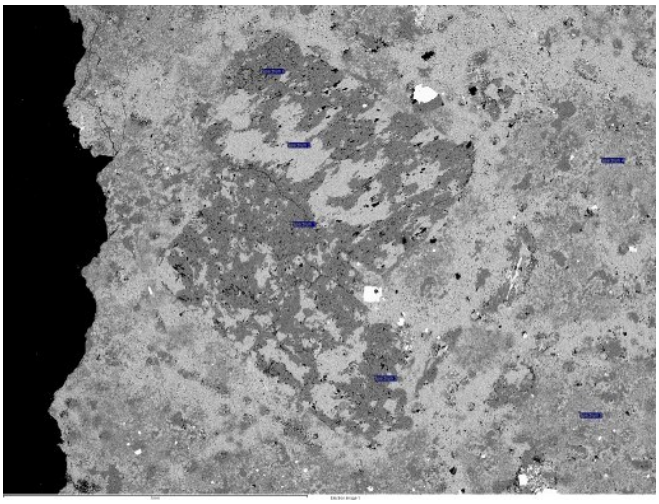

Spectrum	In stats.	Na	Al	Si	K	Fe	Total	Mineral
Spectrum 1	Yes	10.84	19.3	69.57	0.28	0	100	Albite
Spectrum 2	Yes	0	17.15	65.4	17.46	0	100	Adularia
Spectrum 3	Yes	3.59	32.85	61.32	2.25	0	100	Illite + Albite?
Spectrum 4	Yes	0.86	7.79	85.54	5.81	0	100	Quartz + Adularia + Albite
Spectrum 5	Yes	0.56	12.14	77.07	10.23	0	100	Quartz + Adularia + Albite
Spectrum 6	Yes	0.77	34.33	53.79	9.63	1.48	100	Illite

High Resolution BSE Image

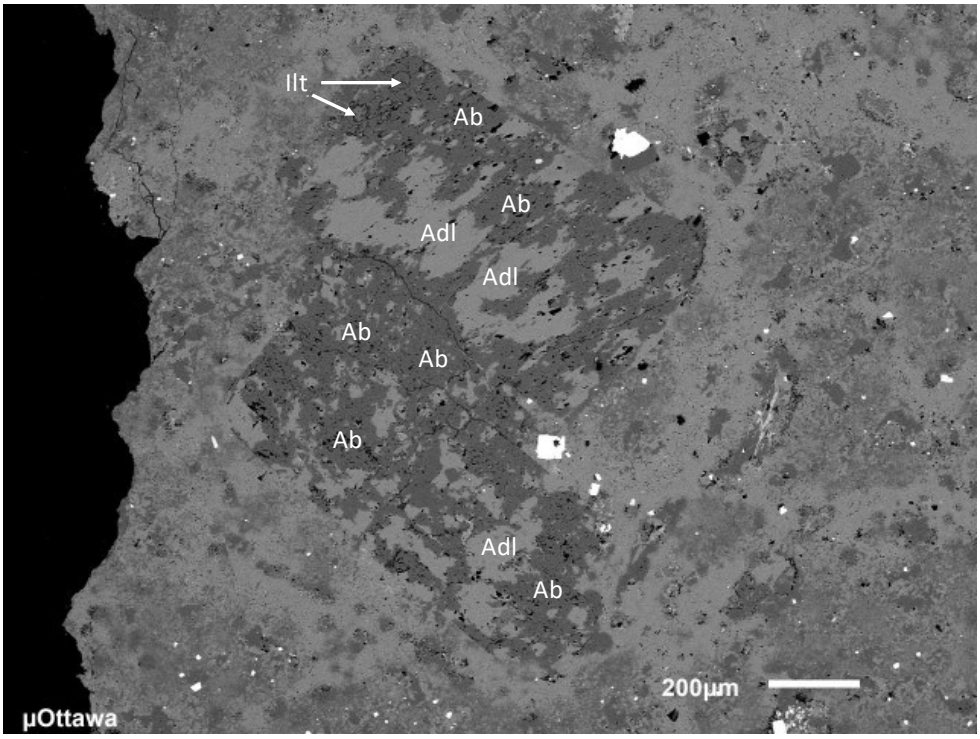

SEM-EDS (6 zoom)

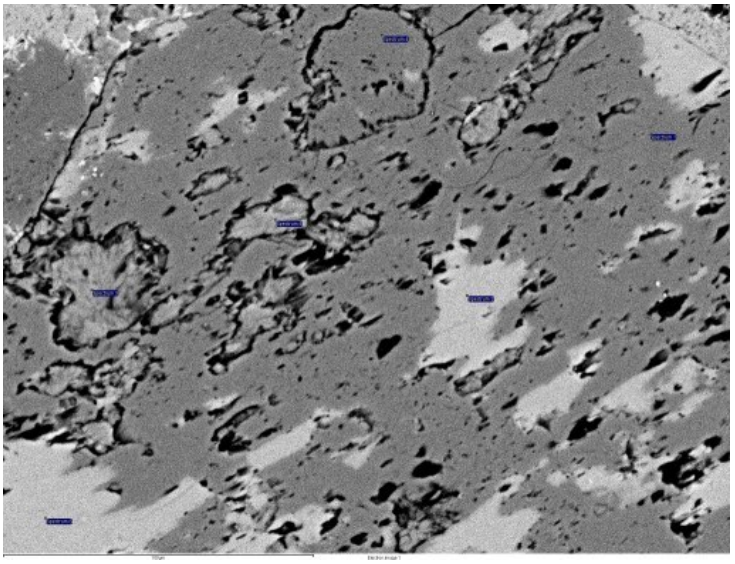

Spectrum	In stats.	Na	Al	Si	K	Ca	Ti	Fe	Total	Mineral
Spectrum 1	Yes	10.58	20.41	67.67	1	0.33	0	0	100	Albite
Spectrum 2	Yes	0	17.26	65.43	16.71	0	0.6	0	100	Adularia
Spectrum 3	Yes	0	33.83	52.99	11.92	0	0	1.26	100	Illite
Spectrum 4	Yes	10.72	20.12	68.4	0	0.76	0	0	100	Albite
Spectrum 5	Yes	0	34.23	53.07	11.37	0	0	1.33	100	Adularia
Spectrum 6	Yes	0	17.34	65.75	16.91	0	0	0	100	Adularia

High Resolution BSE Image

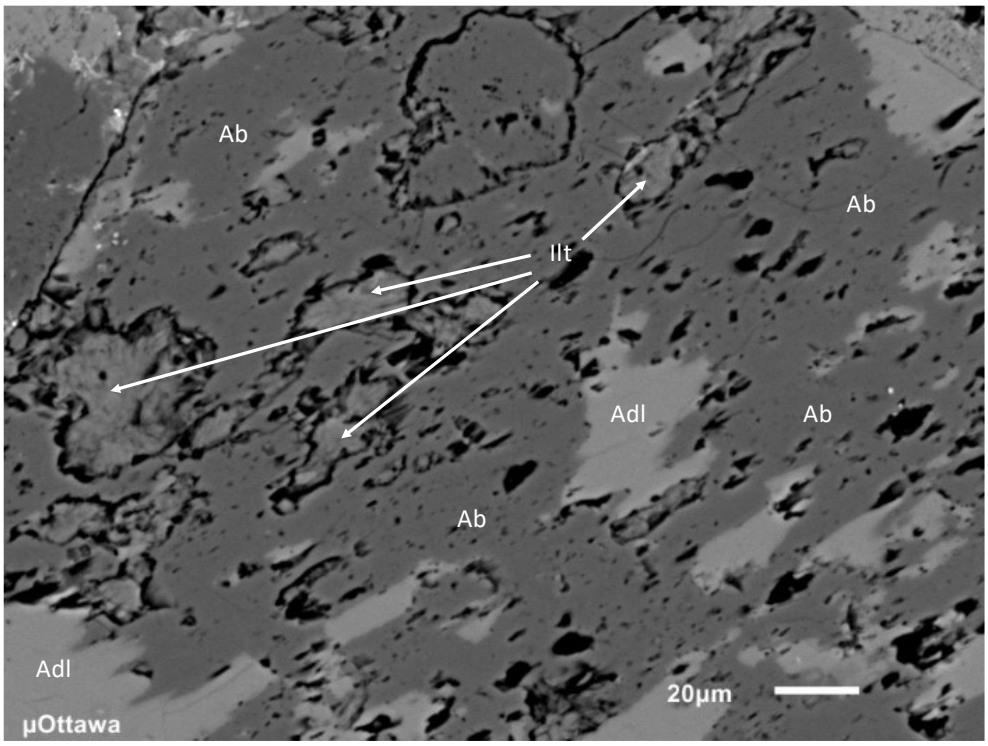

SEM-EDS (Groundmass)

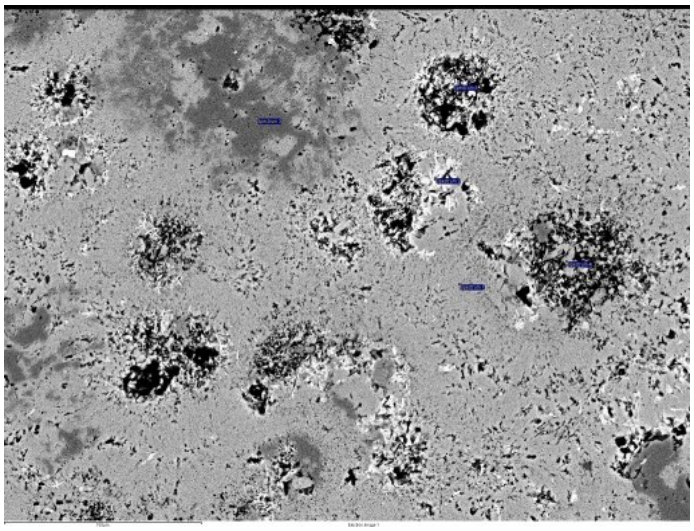

Spectrum	In stats.	Mg	Al	Si	K	Mn	Fe	Total	Mineral
Spectrum 1	Yes	0	17.73	66.41	15.4	0	0.46	100	Adularia
Spectrum 2	Yes	6.7	22.27	33.01	2.11	1.38	34.53	100	Chlorite
Spectrum 3	Yes	0	1.27	98.26	0.47	0	0	100	Quartz
Spectrum 4	Yes	0	17.64	66.59	15.76	0	0	100	Adularia
Spectrum 5	Yes	0	18.26	65.84	15.44	0	0.46	100	Adularia

High Resolution BSE Image

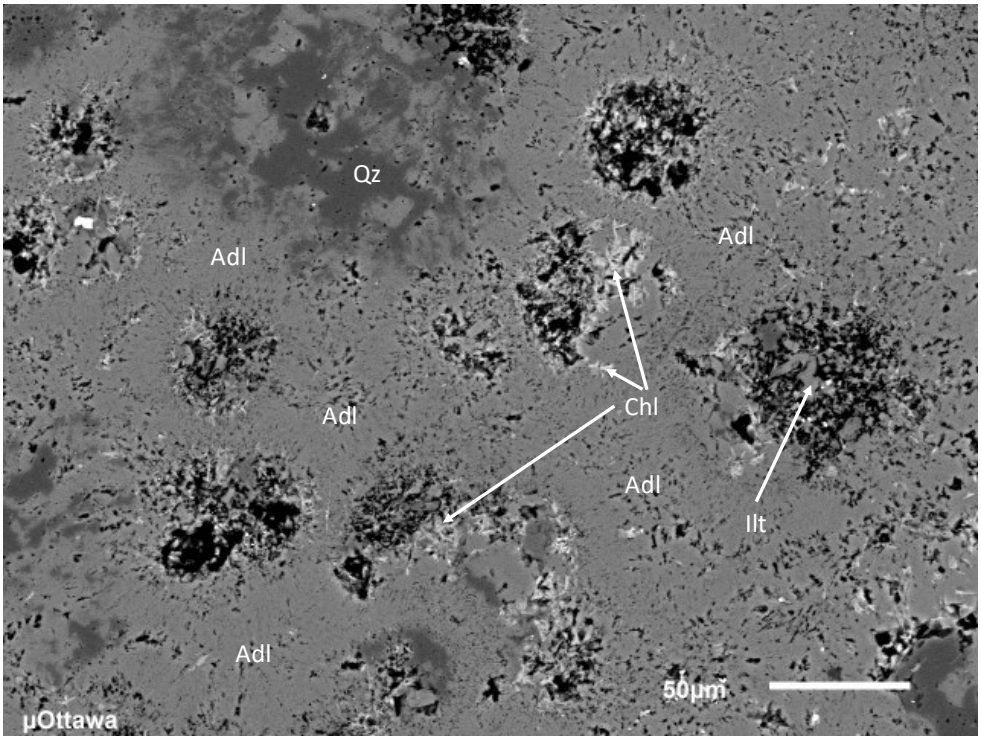

WKP42-409

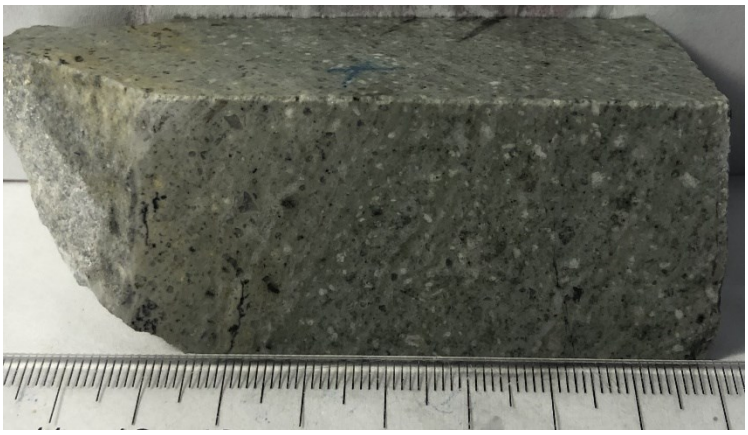

Depth: 409.3m
Sample Desc: Plagioclase and quartz phyric rhyolite. Minimal clay alteration. Highly siliceous. Groundmass is greenish gray. Patches of possible clay minerals throughout groundmass. Minor flow banding.
XRD Minerals: Qz, Ad, Ilt, Chl (uO)
SWIR Minerals: Not Analyzed
LOI: 0.9%
NH4+: 200ppm
δ15N: +6.2‰

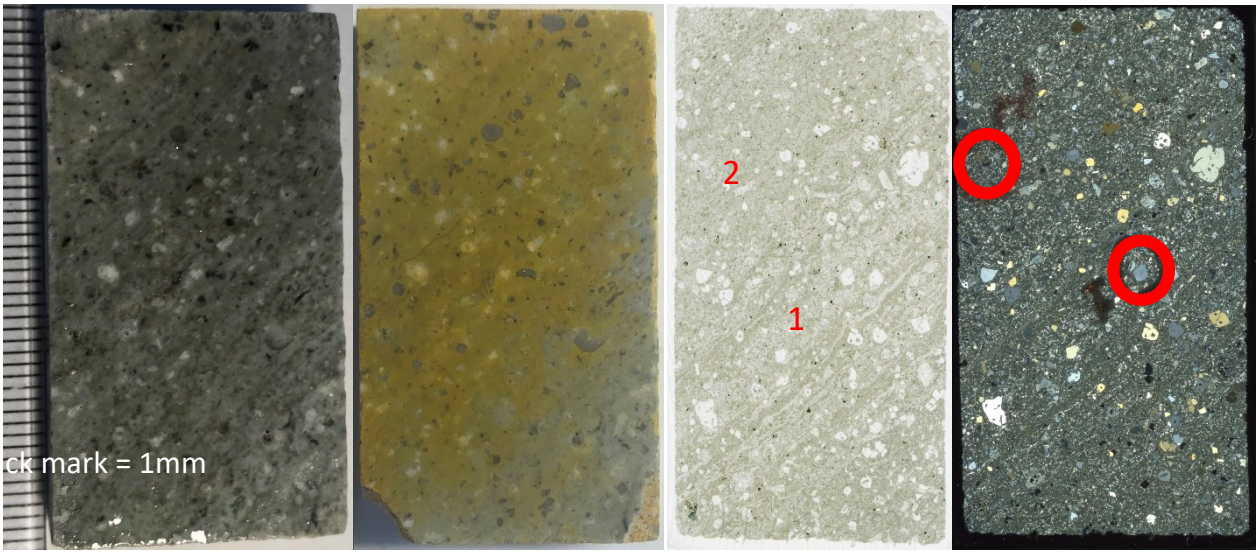

Thin Section Description:
Altered flow banded rhyolite. 15% 0.2-3mm quartz phenocrysts throughout. Euhedral though some dissolution along margin of the quartz phenocrysts. 0.1-2mm feldspar phenocrysts which have been adularia altered and overprinted by 10-60% white mica. Image 1 showing strong white mica alteration and image 2 with low white mica. Both are strongly adulariatized. White mica alteration of some phenocrysts again appears brown while some are strongly birefringent. The matrix is very fine grained with abundant quartz / adularia with moderate amounts of clay sized minerals and minor disseminated pyrite throughout.

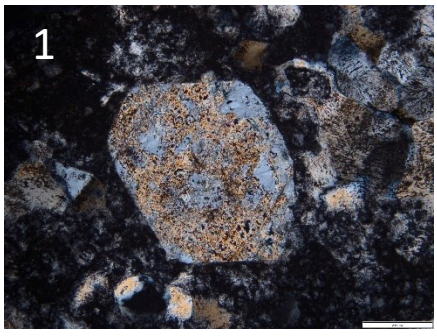

SEM-EDS (1)

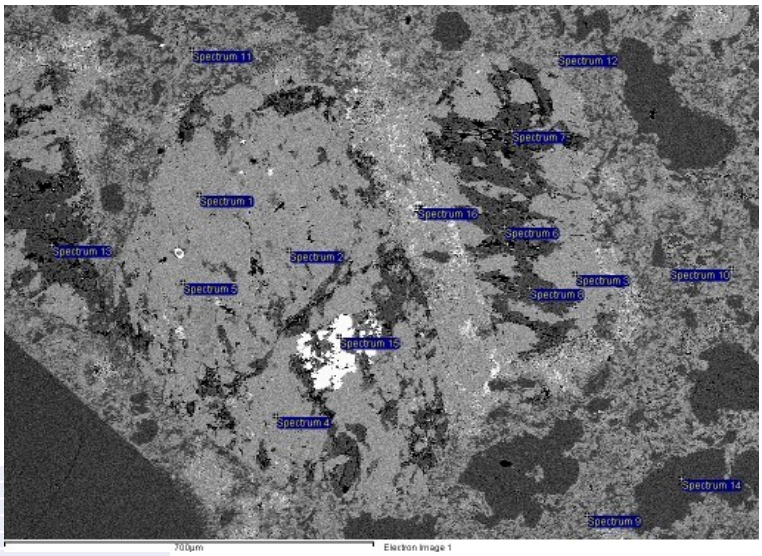

Spectrum	Na	Mg	Al	Si	S	K	Ca	Fe	Mineral
Spectrum 1	0	0	17.6	65.87	0	16.53	0	0	Adularia
Spectrum 2	0	0	18.34	65.7	0	15.96	0	0	Adularia
Spectrum 3	0	0	17.59	66.65	0	15.76	0	0	Adularia
Spectrum 4	0	0	19.46	64.62	0	15.91	0	0	Adularia
Spectrum 5	0	0	17.34	66.29	0	16.37	0	0	Adularia
Spectrum 6	10.18	0	19.01	70.81	0	0	0	0	Albite
Spectrum 7	11.25	0	19.52	68.79	0	0	0.45	0	Albite
Spectrum 8	10.97	0	18.94	69.19	0	0.32	0.57	0	Albite
Spectrum 9	0.6	0	16.03	69.06	0	14.31	0	0	Adularia + Albite (Groundmass)
Spectrum 10	0.32	0	11.12	79.18	0	9.39	0	0	Adularia + Albite + Quartz (Groundmass
Spectrum 11	1.06	0	16.92	67.35	0	14.66	0	0	Adularia + Albite (Groundmass)
Spectrum 12	1.06	0	13.53	74.55	0	10.87	0	0	Adularia + Albite (Groundmass)
Spectrum 13	11.07	0	19.04	69.9	0	0	0	0	Albite (Groundmass)
Spectrum 14	0	0	0.52	99.48	0	0	0	0	Quartz
Spectrum 15	0	0	0	0	65.87	0	0	34.13	Pyrite
Spectrum 16	0	10.09	21.28	38.95	0	1.28	0	28.41	Chlorite? In Adularia

High Resolution BSE Image

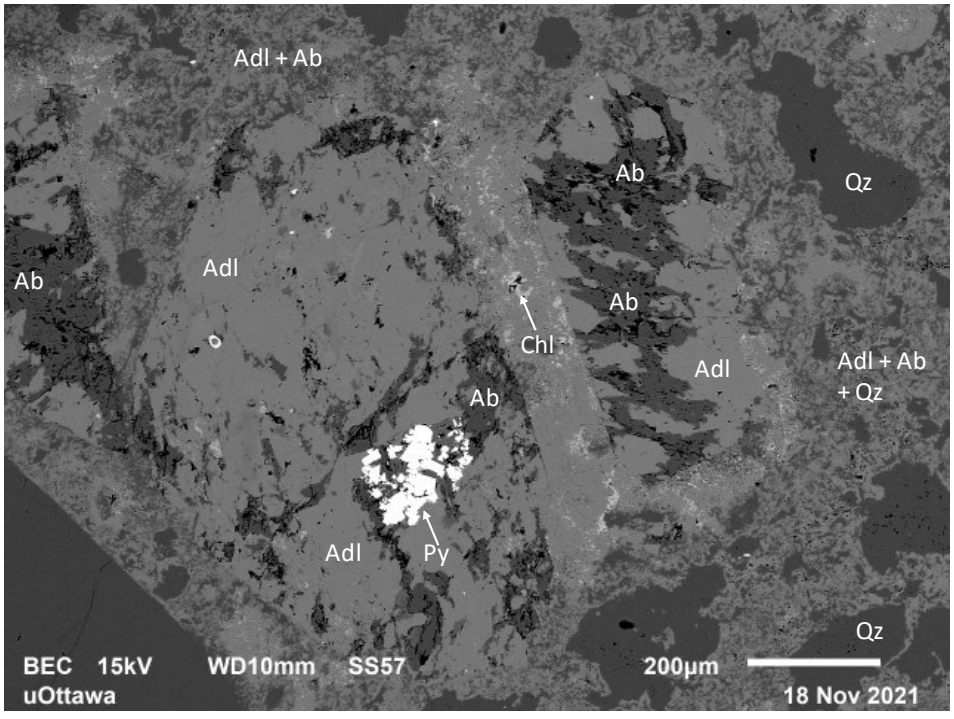

SEM-EDS (2)

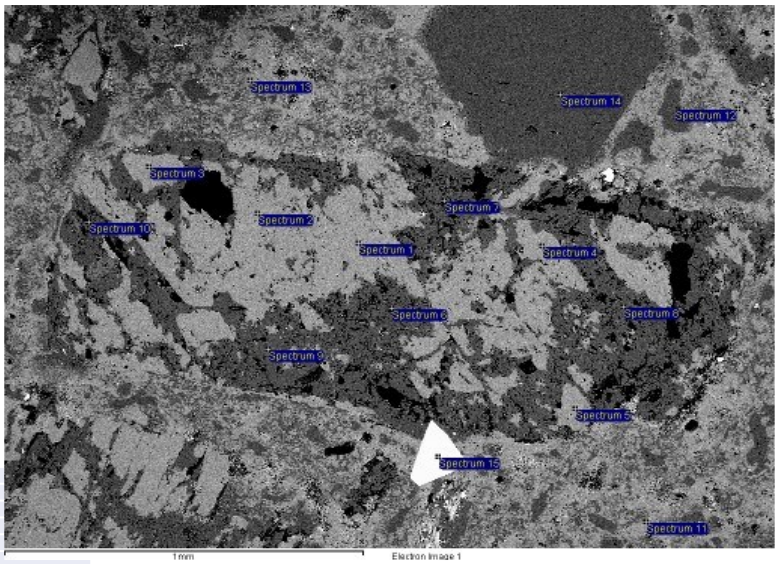

Spectrum	Na	Al	Si	S	K	Ca	Fe	Mineral
Spectrum 1	0	17.49	66.39	0	16.12	0	0	Adularia
Spectrum 2	0	17.97	65.6	0	16.43	0	0	Adularia
Spectrum 3	0	17.81	66.24	0	15.95	0	0	Adularia
Spectrum 4	0.31	17.74	65.66	0	16.29	0	0	Adularia
Spectrum 5	0	17.52	66.22	0	16.26	0	0	Adularia
Spectrum 6	10.91	19.69	69.4	0	0	0	0	Albite
Spectrum 7	11.12	19.14	69.02	0	0	0.72	0	Albite
Spectrum 8	11.24	19.31	68.93	0	0	0.52	0	Albite
Spectrum 9	11.17	19.14	69.22	0	0	0.47	0	Albite
Spectrum 10	11.57	19.36	68.61	0	0	0.47	0	Albite
Spectrum 11	0.72	18.12	65.89	0	15.26	0	0	Adularia (Groundmass)
Spectrum 12	0	10.33	80.04	0	8.15	0	1.49	Quartz + Adularia (Groundmass)
Spectrum 13	0.52	17.74	66.2	0	15.55	0	0	Adularia (Groundmass)
Spectrum 14	0	0.59	99.41	0	0	0	0	Quartz
Spectrum 15	0	0	0	66.78	0	0	33.22	Pyrite

High Resolution BSE Image (left) and Corresponding Photomicrograph (Right)

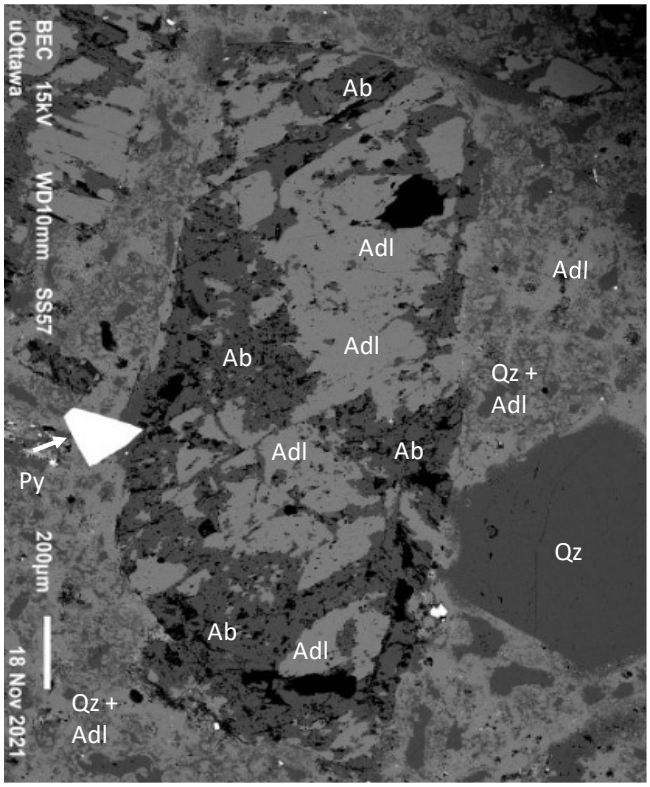

WKP42-412

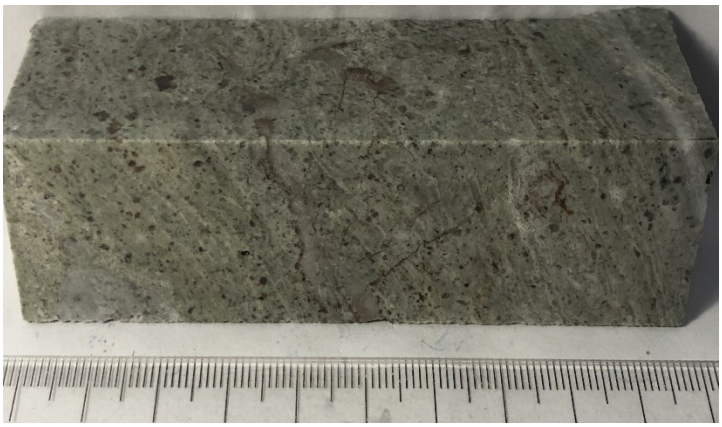

Depth: 412.0m
Sample Desc: Quartz phyric flow banded rhyolite. Translucent 0.5-6mm reddish brown quartz eyes. Banding is well defined alternating green and white. Small chlorite patches in groundmass. Some white bands contain large plagioclase crystals.
XRD Minerals: Qz, Ad, Chl (uO)
SWIR Minerals: Not Analyzed
LOI: 1.8%
NH4+: 236ppm
δ15N: +8.1‰

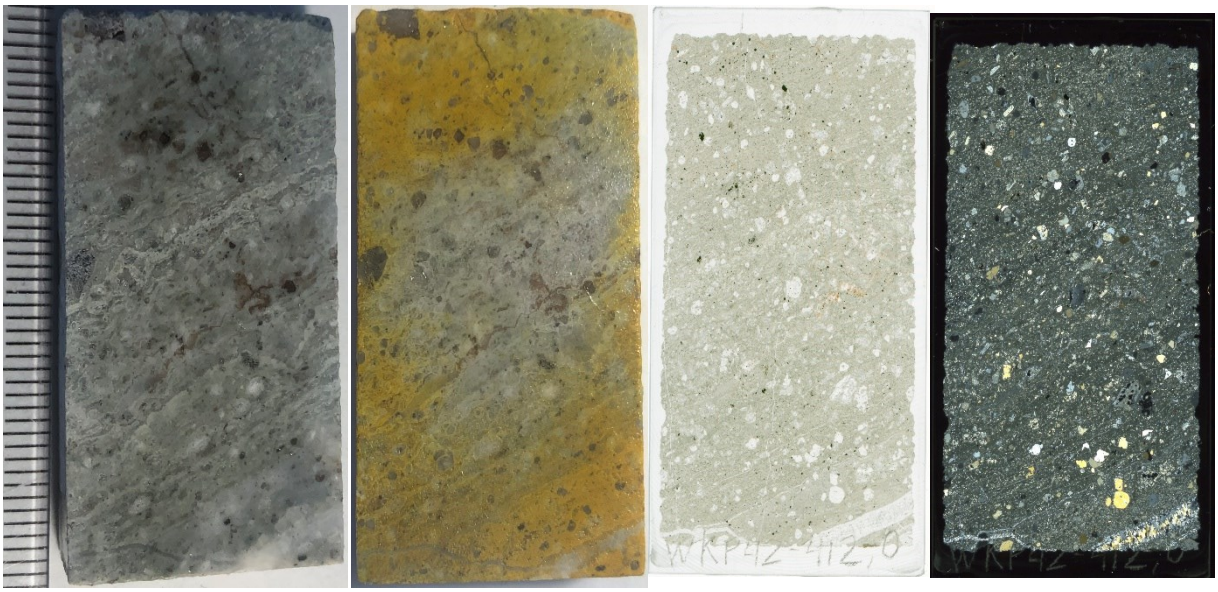

Thin Section Description:
Altered flow banded rhyolite. Abundant (20%) 0.1-1mm subrounded quartz phenocrysts. 20% feldspar phenocrysts (0.1-0.5mm) which have been strongly adularia altered. White mica alteration of the feldspar is less abundant (<10%) and only alters some feldspar phenocrysts. There appears to be quartz (it is yellow and not cross hatched like adularia) alteration overprinting many of the feldspar phenocrysts (image 1). The groundmass is minimally clay altered showing the interlocking crystals (maybe kfeldspar, check in SEM) quite well. Matrix grain size varies along flow bands from 0.1mm to 0.01mm.

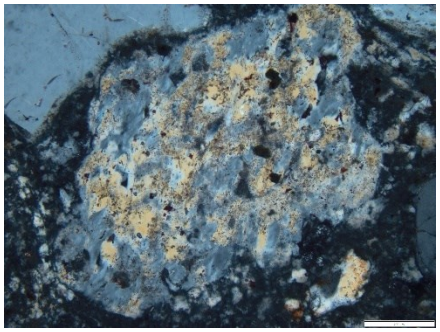

WKP42-416

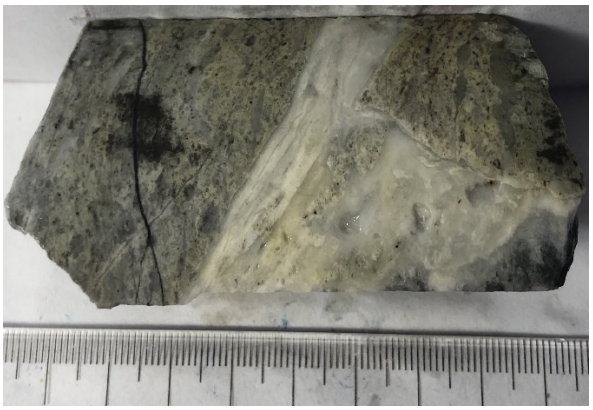

Depth: 416.2m
Sample Desc: Irregular sheeted quartz vein in host quartz phyric flow banded rhyolite. Rhyolite appears like above rhyolites. Groundmass is yellowish closest to veins. Quartz eyes are larger and more irregular closer to vein. Vein appears sheeted near left side. Brecciated and vuggy at right side. Clasts of wallrock throughout. Top right rhyolite may be large 5cm clasts of wallrock.
XRD Minerals: Not Analyzed
SWIR Minerals: Not Analyzed
LOI: 1.6%
NH4+: 149ppm
δ15N: +7.9‰

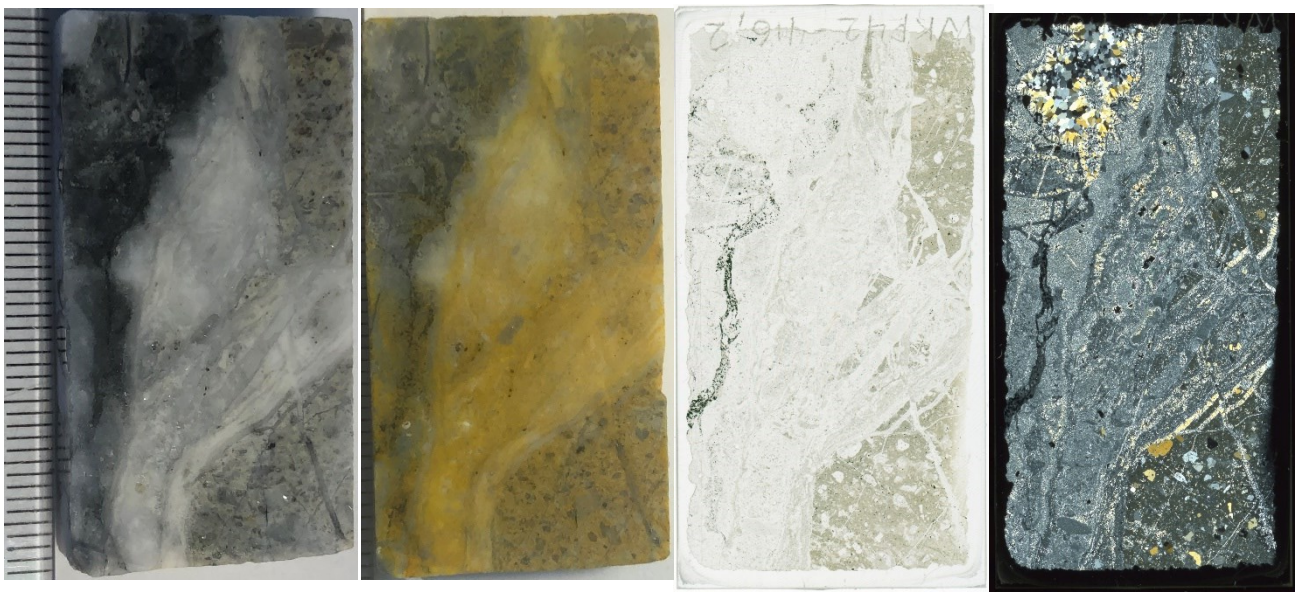

Thin Section Description:
Rhyolite flow with quartz adularia vein. Wallrock portion contains 0.3-2mm subrounded quartz phenocrysts. Feldspar phenocrysts are 0.05-1mm and appear to be completely adulariatized with little (<5%) to no white mica alteration (Photomicrograph 1). The matrix is very fine grained to aphanitic and unidentifiable though it stains indicating adularia. The veinlet shows multiple generations of fluids ranging in grain size from microcrystalline to locally <2mm in vugs. Composed of adularia and quartz. Abundant unidentifiable (tarnished, polish and reevaulate) euhedral sulfides in quartz adularia vein near vug area.

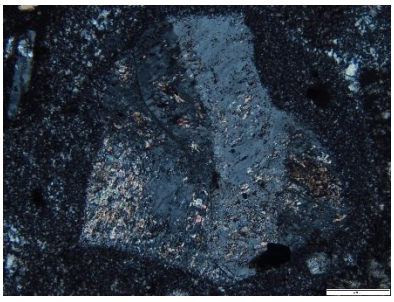

WKP42-421

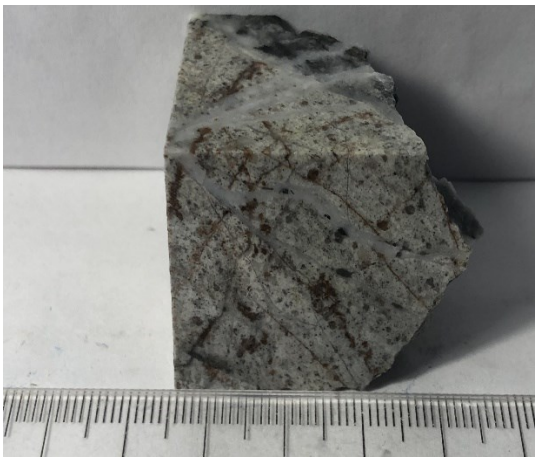

Depth: 421.2m
Sample Desc: Clay altered quartz phyric rhyolite. 0.5-1mm quartz eyes throughout some of which have a reddish brown colour (might not be quartz). Groundmass is bright white and glittery (illite?). Multiple generations of <1mm quartz veinlets; some rusted.
XRD Minerals: Not Analyzed
SWIR Minerals: Not Analyzed
LOI: 0.1%
NH4+: 182ppm
δ15N: +7.5‰

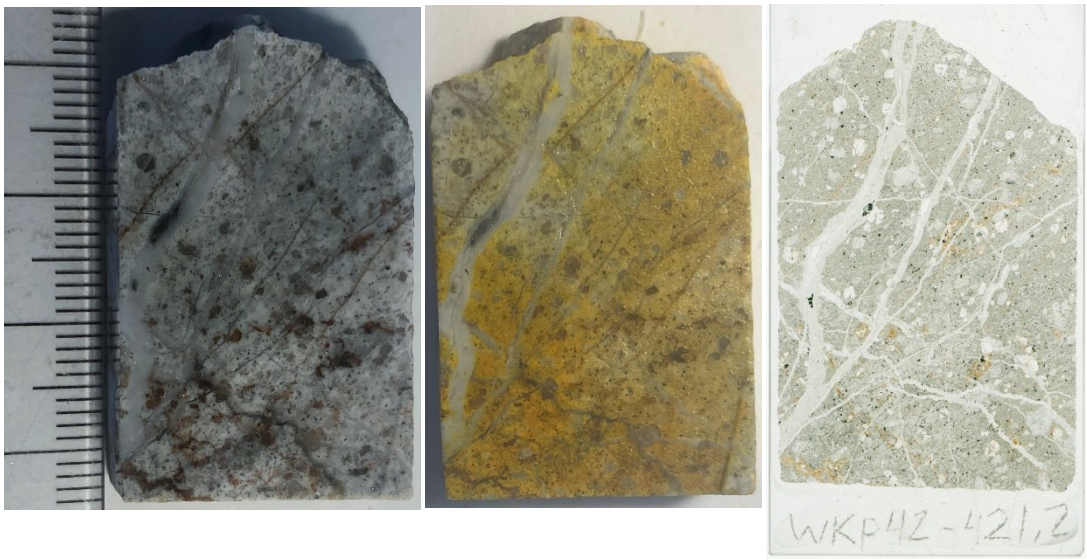

Thin Section Description:
Altered rhyolite dome sample. 5-10% 0.2-1mm quartz phenocrysts. 10% 0.1-0.5mm feldspar phenocrysts which seem to be altered to equal amounts quartz and adularia. Illite tends to overprint the adularia altered portions of the phenocrysts composing ~10-40% of the phenocryst. Illite tends to be quite coarse relative to previous sample and is locally radiating. The groundmass is composed of fine grained to aphanitic quartz and adularia.

WKP42-422

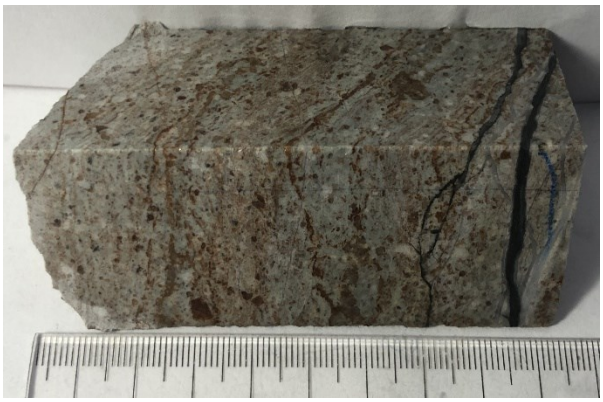

Depth: 422.3m
Sample Desc: Altered quartz and plagioclase phyric flow banded rhyolite. White ~1mm clay altered plagioclase phenocrysts throughout. Reddish brown coloured translucent 1-4mm phenocrysts (quartz?). Red oxidation localized along flow band margins. Intense clay alteration of groundmass and plag phenocrysts at left side of sample. Groundmass is green near right side. 1mm veinlets of visible sulfides.
XRD Minerals: Qz, Ad, Ilt, Chl (uO)
SWIR Minerals: Not Analyzed
LOI: 2.8%
NH4+: 221ppm
δ15N: 6.5‰

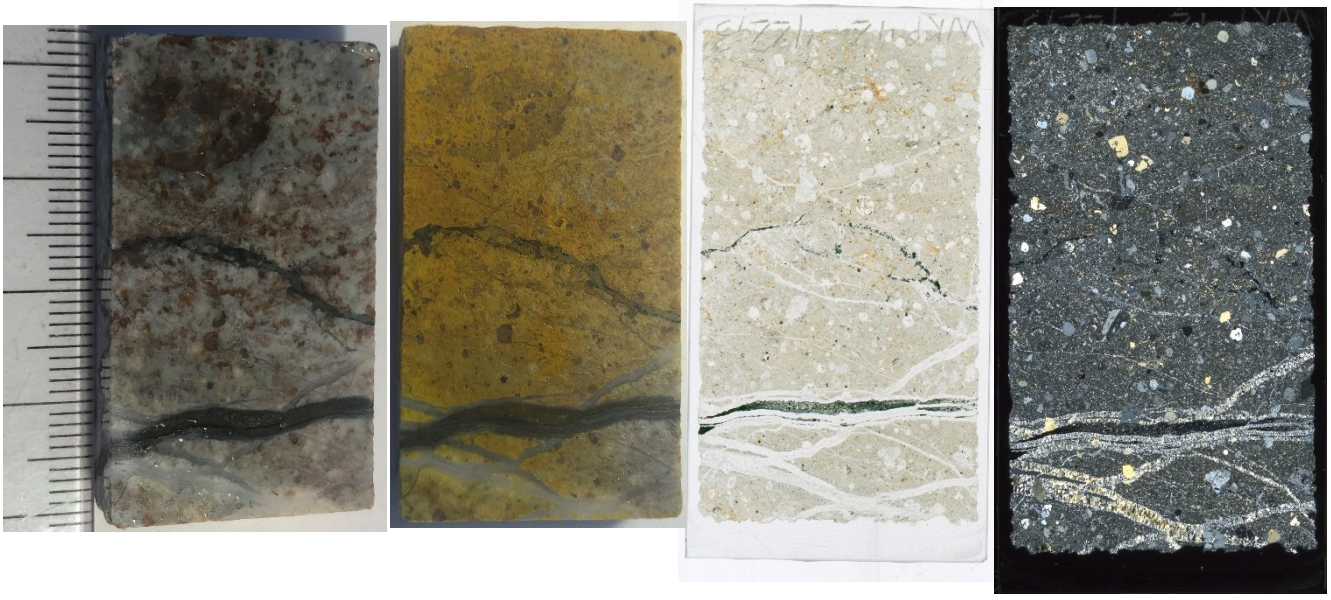

Thin Section Description:
Altered rhyolite dome sample with cross cutting quartz veinlets. 5-10% 0.1-2mm Quartz phenocrysts. 10% 0.1-2mm Feldspar phenocrysts which have been completely altered to adularia. Some show carlsbad twinning. Phenocrysts are minimally overprinted by illite (~5%). A total of ~1% illite. Groundmass is composed of interlocking fine grained quartz and adularia.

WKP42-423V

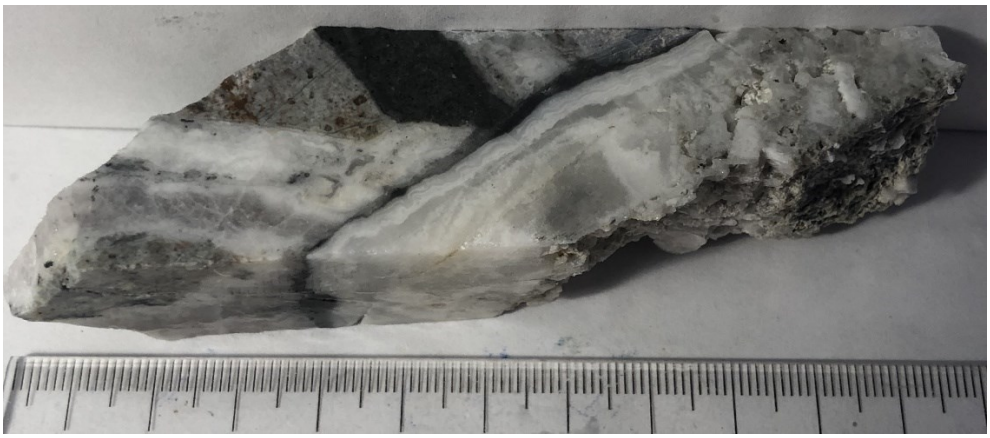

Depth: 423.2m

Sample Desc: Brecciated vein sample. Colloform banded quartz on right side of sample becoming crystalline outwards. Brecciated at top left contain altered rhyolite wallrock and black aphanitic clast. Whole left side could be wallrock + sheeted vein (like WKP42-416.2) with colloform vein in contact diagonally.

XRD Minerals: Not Analyzed

SWIR Minerals: Not Analyzed

LOI: 1.8%

NH4+: Not Analyzed

δ15N: Not Analyzed

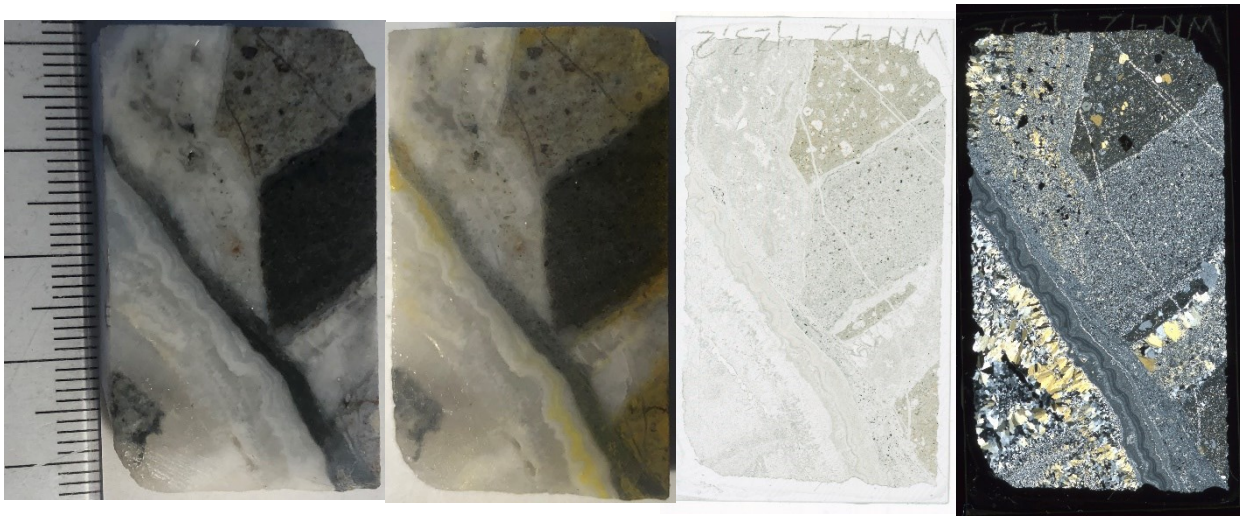

No Thin Section Description

WKP42-430V

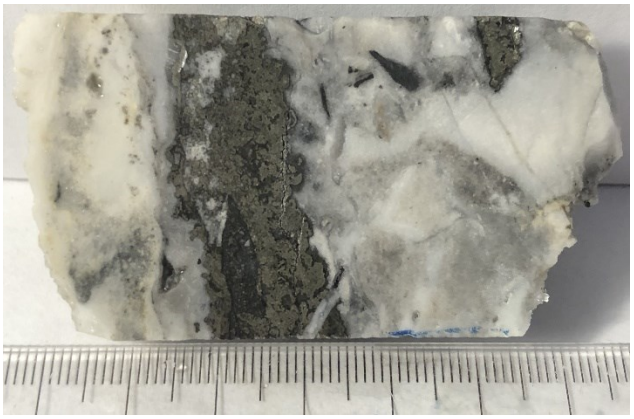

Depth: 430.7m
Sample Desc: Brecciated quartz crustiform vein. Bulk of sample is microcrystalline quartz with dark sulfide rich fragments. Dark band / clasts containing abundant visible sulfides.
XRD Minerals: Not Analyzed
SWIR Minerals: Not Analyzed
LOI: 5.4%
NH4+: 67ppm
δ15N: +5.7‰

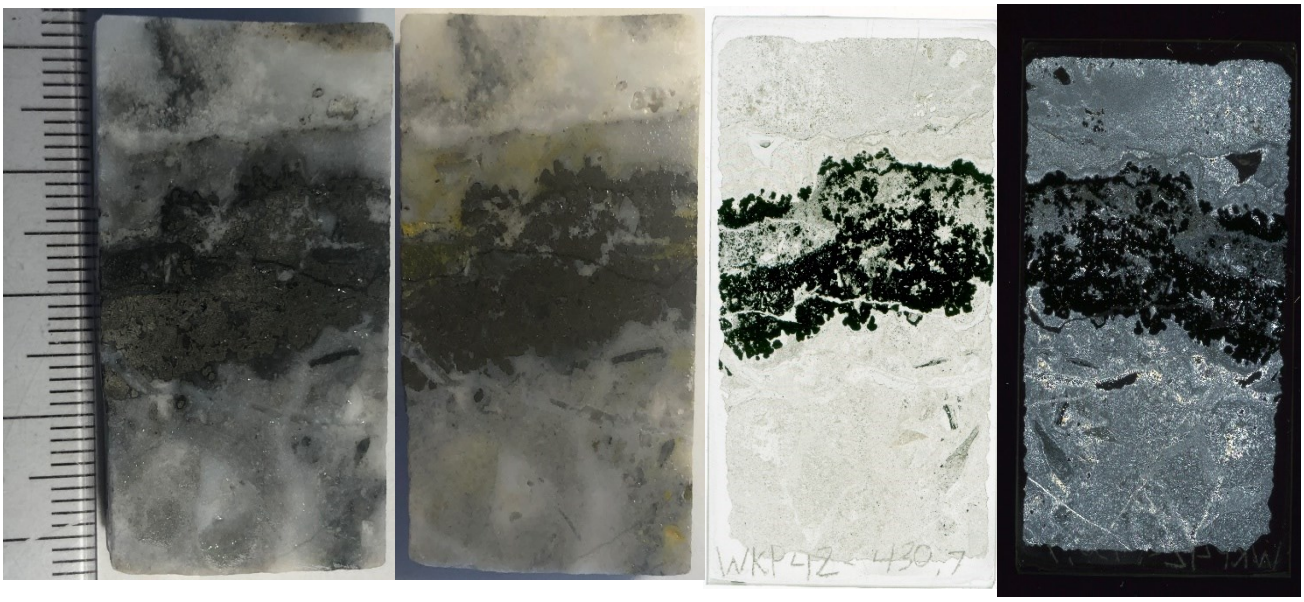

Thin Section Description:
Quartz vein sample. Large 2cm dark sulfide rich band. Very fine to microcrystalline quartz +/- adularia. Minor staining indicates little adularia. No visible illite. Greenish clay mineral (chlorite, corrensite?) mixed in with sulfide rich band.

WKP42-435V

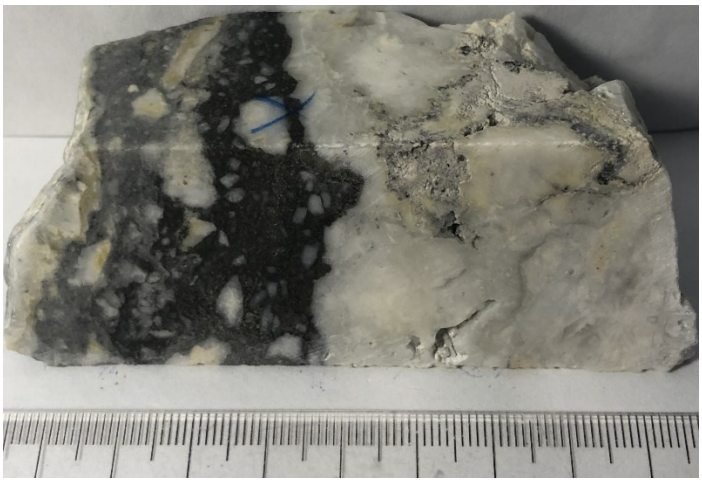

Depth: 435.8m
Sample Desc: Brecciated vein sample. Microcrystalline quartz rich section on right side of sample. No apparent banding. Patches of what appear to be clay minerals. Dark areas are composed of visible sulfides with white 0.3-2cm brecciated quartz vein clasts throughout.
XRD Minerals: Qz, Ad (uO)
SWIR Minerals: Not Analyzed
LOI: 0.0%
NH4+: 62ppm
δ15N: Too low

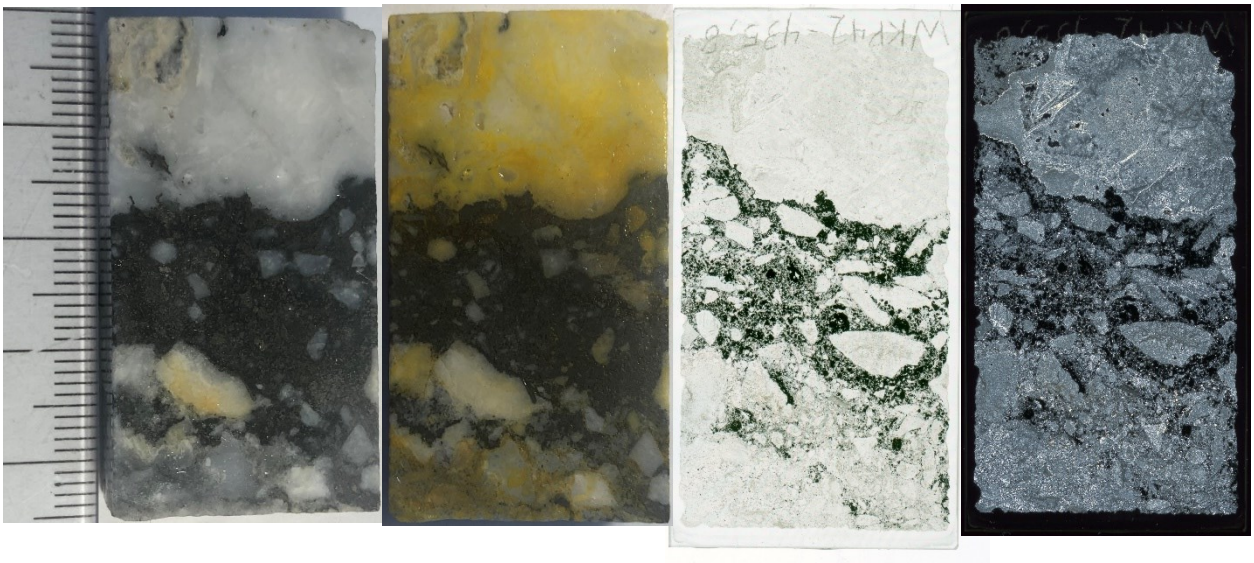

Thin Section Description:
Microcrystalline quartz adularia vein. Primarily composed of very fine to microcrystalline (gel) quartz +/- adularia. Brecciated sulfide rich 3cm section in the center. Brownish red coloured dusty very fine grained coloured mineral near sulfide rich area. May be a clay mineral or rusting from sulfides.

WKP42-438.7V

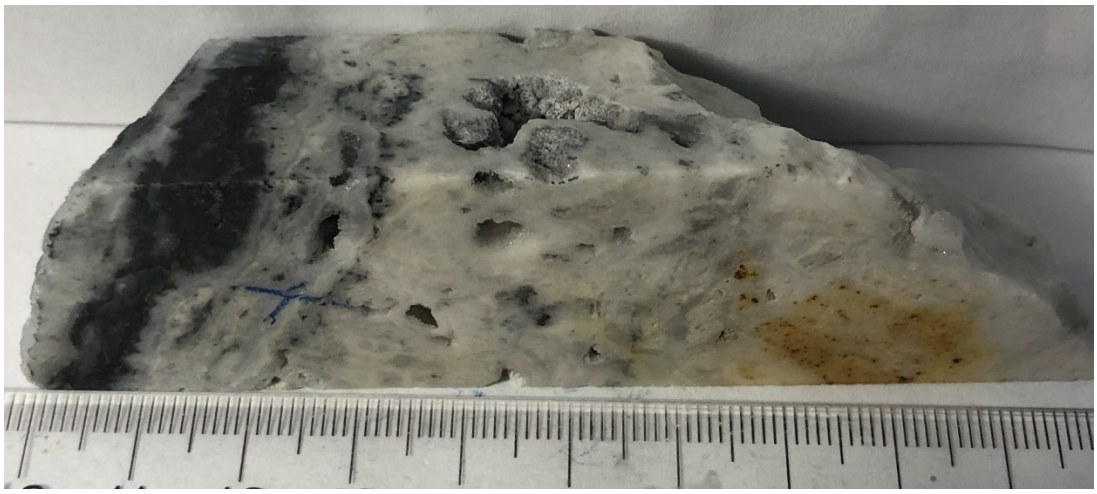

Depth: 438.7m
Sample Desc: Crustiform / colloform vein sample. Left side shows colloform banding with 1-5mm bands. Dark band contains visible sulfides. Right of the colloform banding is massive microcrystalline quartz (+/- adularia) with large 2-15mm vugs.
XRD Minerals: Not Analyzed
SWIR Minerals: Not Analyzed
LOI: 0.9%
NH4+: Not Analyzed
δ15N: Not Analyzed

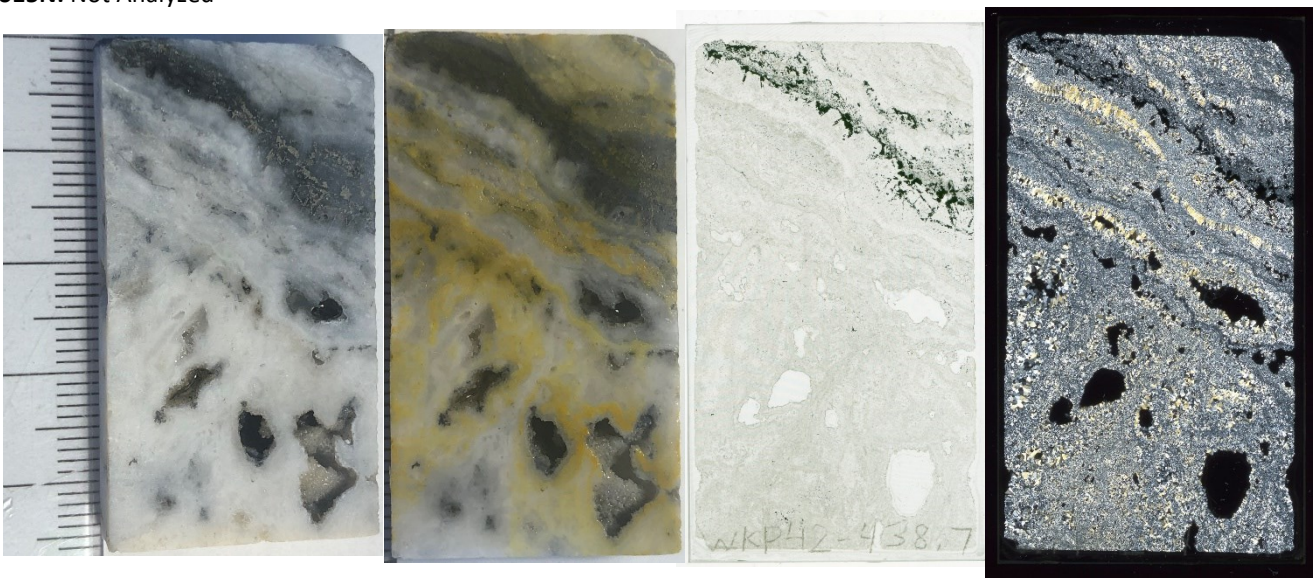

No Thin Section Description

WKP42-438.9V

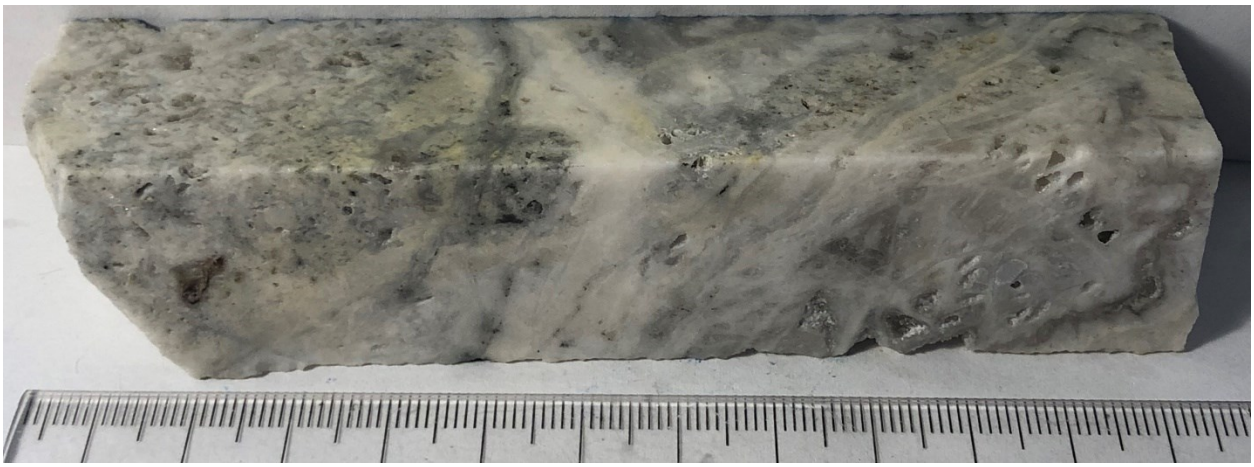

Depth: 438.9m
Sample Desc: Quartz vein sample. Massive vuggy microcrystalline quartz (+/- adularia) which appears to be cut by sheeted veinlets. Could also be brecciated. Yellowish clay minerals at margins of sheeted veinlets.
XRD Minerals: Not Analyzed
SWIR Minerals: Not Analyzed
LOI: 0.0%
NH4+: Not Analyzed
δ15N: Not Analyzed

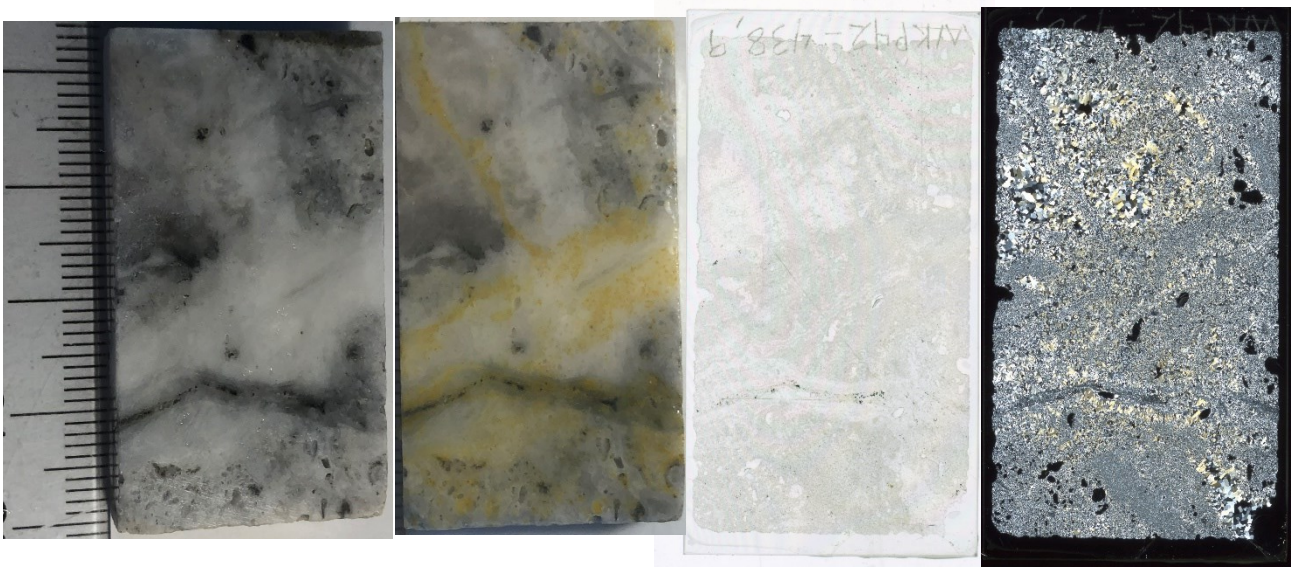

No Thin Section Description

WKP42-489

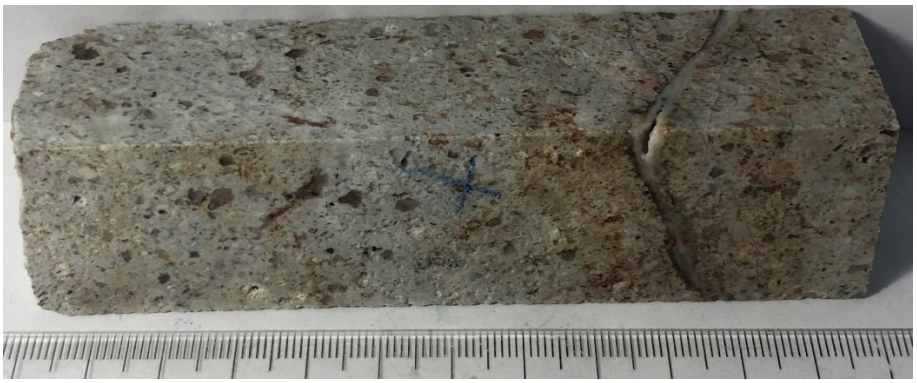

Depth: 489.2m
Sample Desc: Clay altered quartz and plagioclase phyric rhyolite. Abundant 0.5-1mm quartz eyes throughout. Relict or completely altered and dissolved 0.5-2mm plagioclase phenocrysts. Groundmass is bleached white and clay altered. Rusted patches especially near the small 1mm quartz veinlet. Disseminated sulfides.
XRD Minerals: Not Analyzed
SWIR Minerals: Not Analyzed
LOI: 1.8%
NH4+: 187ppm
δ15N: +7.5‰

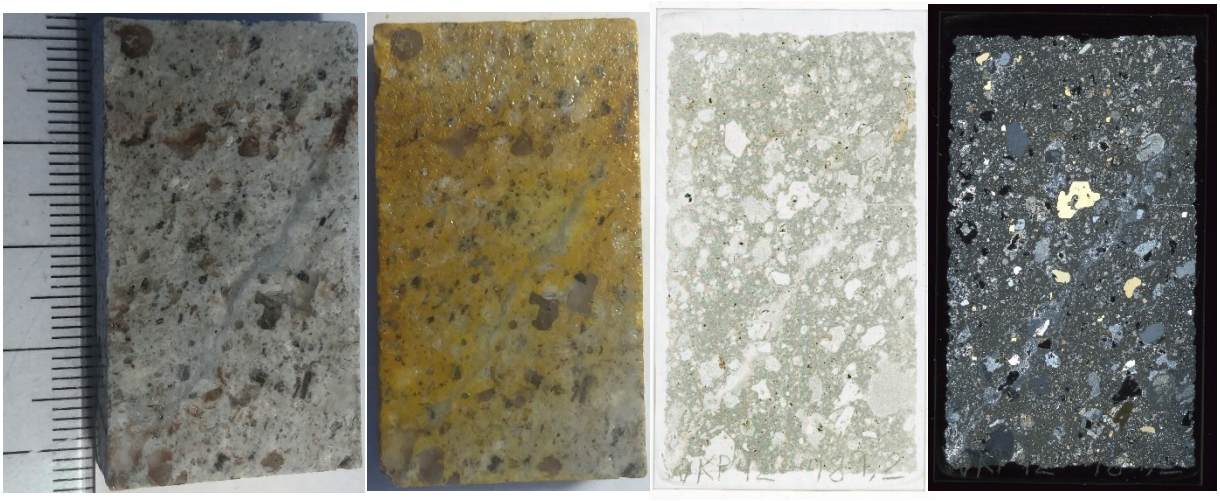

Thin Section Description:
Altered rhyolite dome. 10-15% 0.2-4mm quartz phenocrysts. 15% 1-2mm feldspar phenocrysts are completely adularia altered and overprinted by 10-60% illite. Illite is well developed, radiating, and relatively coarse compared to previous sections. Illite makes up ~5-10% of the sample. Minor chlorite altered patches throughout (~2-3%). Groundmass is composed of very fine grained to aphanitic quartz and adularia.

WKP42-509

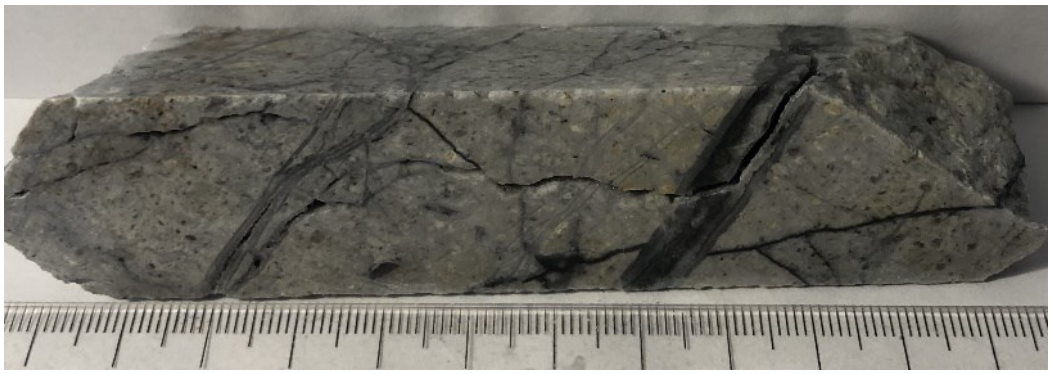

Depth: 509.0m
Sample Desc: Altered quartz phyric rhyolite. Quartz eyes are 1-3mm. Possible plagioclase phenocrysts. Groundmass appears highly silicified. Multiple generations of veinlets / stringers. Disseminated sulfides.
XRD Minerals: Not Analyzed
SWIR Minerals: Not Analyzed
LOI: 0.9%
NH4+: 162ppm
δ15N: +6.0‰

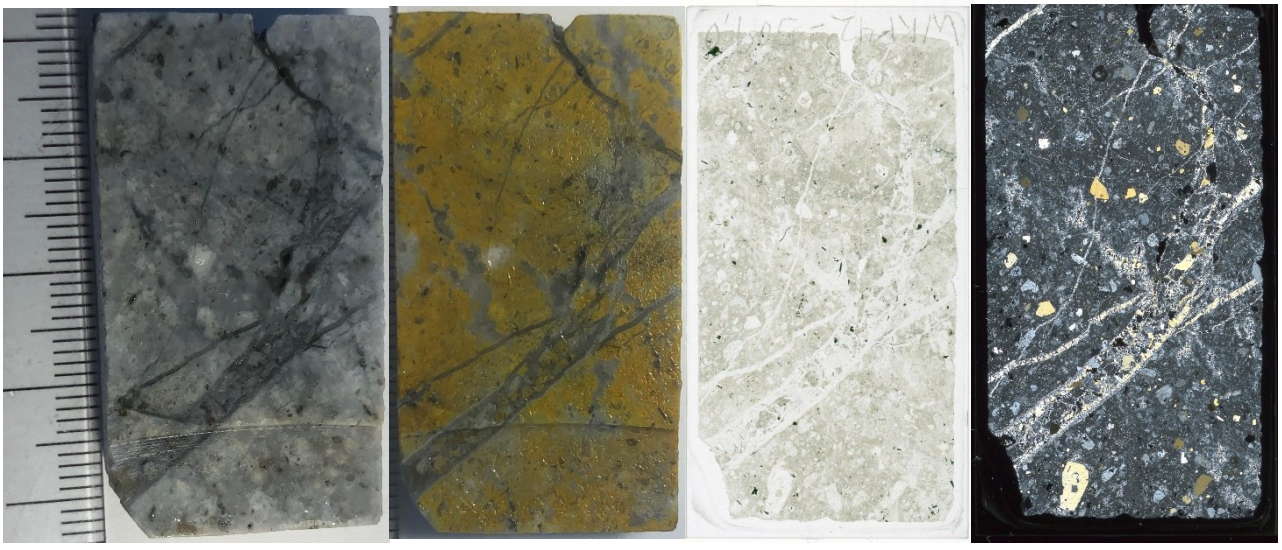

Thin Section Description:
Adularia altered rhyolite dome sample with minor quartz veinlets. Sample contains ~10% 0.1-3mm quartz phenocrysts. 15% 0.1-2mm Feldspar phenocrysts which are completely altered to adularia and quartz. Very minor (1-5%) illite overprinting some feldspar phenocrysts. Total of <1% illite. Groundmass is composed of fine grained to aphanitic quartz and adularia.

WKP42 Spectral Chip Samples continued

WKP42-522.5

Depth: 522.5m
Sample Desc: Light gray coloured clay altered rhyolite. 1 3mm phenocrysts of dark coloured mineral (Chlorite). Groundmass is coherent and appears silicified with small patches of white clay minerals.
XRD Minerals: Not Analyzed
SWIR Minerals : NH4-Feldspar (Provided by Mark Simpson)
LOI: 1.8%
NH4+: 228ppm
δ15N: 6.4‰

No polished thin section

WKP42-553.2

Depth: 553.2m
Sample Desc: Clay + silica altered quartz phyric flow banded rhyolite. Abundant quartz eyes ranging from 0.5-2mm. Groundmass is bright white and coherent. Appears glittery possibly due to illite content. Vuggy botryoidal quartz on backside.
XRD Minerals: Not Analyzed
SWIR Minerals : NH4-Illite (Provided by Mark Simpson)
LOI: Not Analyzed
NH4+: Not Analyzed
δ15N: Not Analyzed

No polished thin section

WKP42-573.6

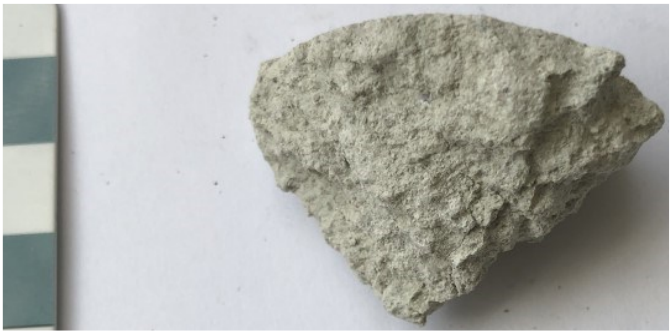

Depth: 573.6m
Sample Desc: Clay altered volcanic rock. Difficult to discern original rock composition as it has been intensely clay altered. Possible quartz eyes suggesting rhyolite. Groundmass is friable and earthy.
XRD Minerals: Qz, Ad, Ilt, Chl (uO)
SWIR Minerals : Illite (Provided by Mark Simpson)
LOI: Not Analyzed
NH4+: Not Analyzed
δ15N: Not Analyzed

No polished thin section

WKP42-604.8

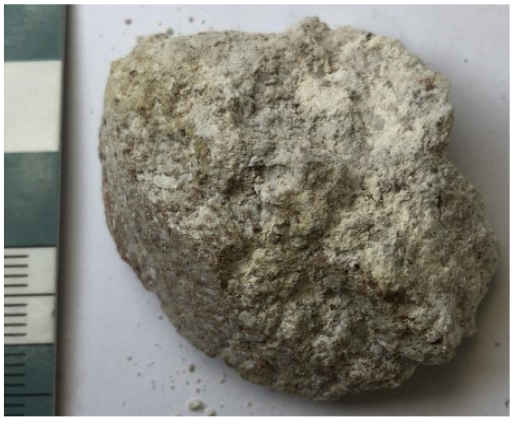

Depth: 604.8m
Sample Desc: Clay altered rhyolite or tuff. Sample is brittle and not coherent suggesting either intense clay alteration of rhyolite or rather clay alteration of an ash layer. Contains what look like small lightercoloured clasts / lapilli throughout.
XRD Minerals: Not Analyzed
SWIR Minerals : Illite (Provided by Mark Simpson)
LOI: 2.8%
NH4+: 218ppm
δ15N: +4.3‰

No polished thin section

DDH WKP44

WKP44-540.0

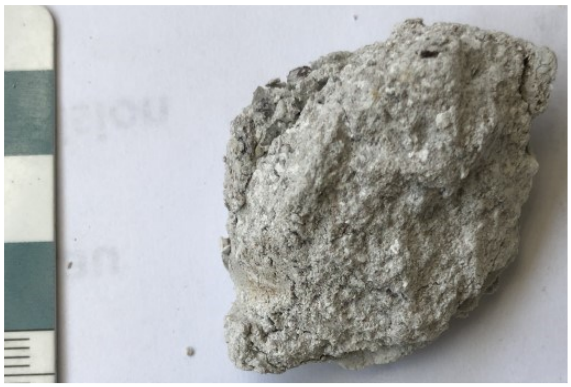

Depth: 540.0m
Sample Desc: Clay altered rhyolite pyroclastic. Small 0.5 3mm light gray-coloured lapilli throughout. Groundmass is a darker greenish gray. Sample is very brittle and not coherent.
XRD Minerals: Not Analyzed
SWIR Minerals : Not acquired
LOI: 6.6%
NH4+: 443ppm
δ15N: 5.1‰

No polished thin section

WKP44-554.0

Depth: 554.0m
Sample Desc: Clay altered rhyolite pyroclastic sample. Small 0.5-3mm light gray-coloured lapilli throughout. Groundmass is a darker greenish gray. Sample is more coherent than above sample. Dark patches coating the sample.
XRD Minerals: Not Analyzed
SWIR Minerals : Not acquired
LOI: 1.8%
NH4+: 298ppm
δ15N: +4.8‰

No polished thin section

WKP44-564.0

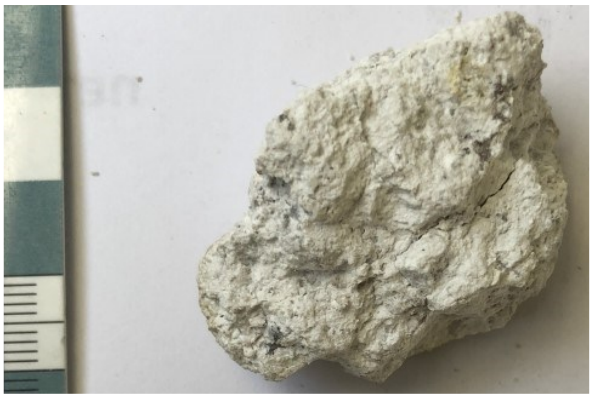

Depth: 564.0m
Sample Desc: Yellowish gray clay altered rhyolite pyroclastic sample. Contains very small <0.1mm light-coloured grains visible in the bottom left of sample photo. Sporadic dark patches throughout which may be due to a mineral or oxidation.
XRD Minerals: Not Analyzed
SWIR Minerals : Not acquired
LOI: 2.7%
NH4+: 232ppm
δ15N: 5.0‰

No polished thin section

WKP44-607.0

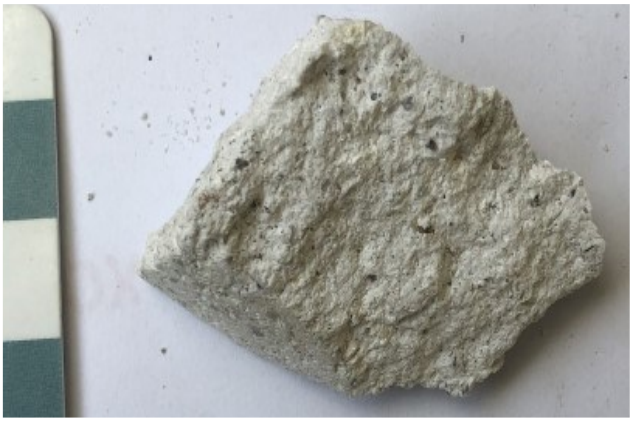

Depth: 607.0m
Sample Desc: Clay altered rhyolite. <1mm quartz eyes throughout. Some appear red (may be a different unidentified mineral). Red phenocrysts are more irregularly shaped than the translucent ones. Groundmass is bright white and coherent containing abundant clay minerals.
XRD Minerals: Not Analyzed
SWIR Minerals : Not acquired
LOI: 1.9%
NH4+: 425ppm
δ15N: 5.8‰

No polished thin section

WKP44-628.0

Depth: 628.0m
Sample Desc: Intensely clay altered volcanic rock. Hard. 1-2mm reddish patches (quartz eyes?). Abundant disseminated sulfides. Groundmass is friable and earthy.
XRD Minerals: Not Analyzed
SWIR Minerals : Not acquired
LOI: Not Analyzed
NH4+: Not Analyzed
δ15N: Not Analyzed

No polished thin section

WKP44-641.0

Depth: 641.0m
Sample Desc: Clay altered rhyolite. Groundmass is bright white and coherent. Appears glittery (illite?). Abundant quartz eyes which are mostly ~1mm but some are ~4mm.
XRD Minerals: Not Analyzed
SWIR Minerals : Not acquired
LOI: 1.0%
NH4+: 401ppm
δ15N: +5.7‰

No polished thin section

WKP44-695.0

Depth: 695.0m
Sample Desc: Clay altered rhyolite. Groundmass is bright white and coherent. Abundant 1mm quartz eyes. Some phenocrysts appear dark / reddish, irregular, and flaky (biotite?). Dark veinlet cutting left side of sample.
XRD Minerals: Not Analyzed
SWIR Minerals : Not acquired
LOI: 2.9%
NH4+: 408ppm
δ15N: +5.0‰

No polished thin section

WKP44-711.0

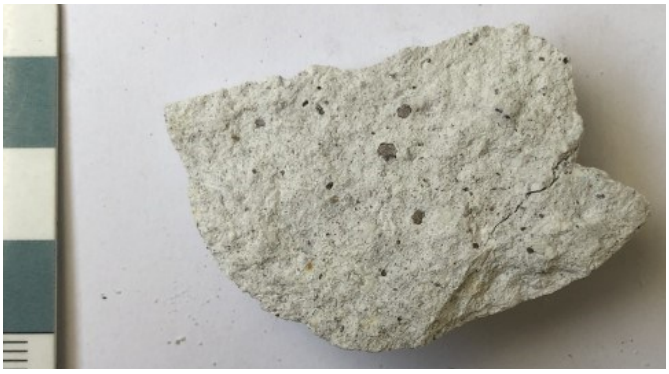

Depth: 711.0m
Sample Desc: Clay altered rhyolite. Groundmass is bright white and coherent. Abundant <1mm phenocrysts some of which appear dark / reddish, irregular, and flaky. Larger 3mm opaque hexagonal phenocrysts at center of sample (biotite?).
XRD Minerals: Not Analyzed
SWIR Minerals : Not acquired
LOI: 3.6%
NH4+: 486ppm
δ15N: 3.4‰

No polished thin section

DDH WKP78

WKP78-332.0

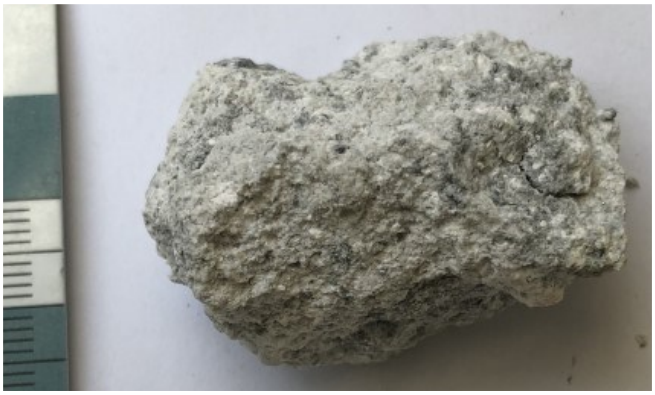

Depth: 332.0m
Sample Desc: Intensely clay altered rhyolite lava or pyroclastic. Small 1mm clay altered irregular white fragments / phenocrysts throughout. Groundmass is greenish white, brittle, and earthy. Abundant sulfides occurring in patches throughout.
XRD Minerals: Not acquired
SWIR Minerals : Not acquired
LOI: Not Analyzed
NH4+: Not Analyzed
δ15N: Not Analyzed

No polished thin section

WKP78-358.0

Depth: 358.0m
Sample Desc: Intensely clay altered rhyolite pyroclastic. Very soft and earthy altered ash with small <0.5mm clay altered white clasts / grains throughout. Clay altered groundmass is very soft and expands with water.
XRD Minerals: Qz, Ilt/Sm (uO)
SWIR Minerals: Not acquired
LOI: 7.2%
NH4+: 1581ppm
δ15N: 1.7‰

No polished thin section

WKP78-372.0

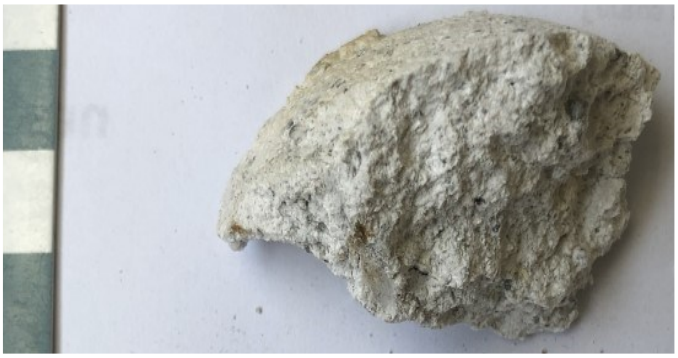

Depth: 372.0m
Sample Desc: Intensely clay altered rhyolite pyroclastic. Groundmass is bright white, brittle, and earthy. Minor disseminated sulfides throughout.
XRD Minerals: Qz, Ilt/Sm (uO)
SWIR Minerals: Not acquired
LOI: Not Analyzed
NH4+: Not Analyzed
δ15N: Not Analyzed

No polished thin section

WKP78-394.0

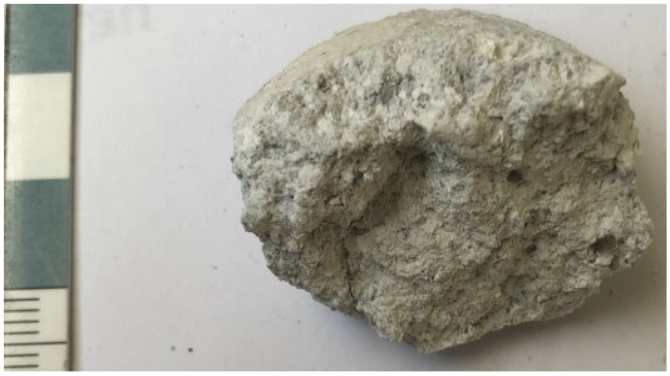

Depth: 394.0m
Sample Desc: Intensely clay altered rhyolite pyroclastic. Groundmass is light gray, soft, and earthy. Some hardly visible 1-3mm whiter coloured clasts / phenocrysts throughout. 1-3mm pits throughout which appears to be due to weathering and excavation of clasts.
XRD Minerals: Not Analyzed
SWIR Minerals : Not acquired
LOI: 7.8%
NH4+: 2783ppm
δ15N: 0.5‰

No polished thin section

DDH WKP81

WKP81-437V

Depth: 437.5m
Sample Desc: Crustiform colloform banded vein sample. Microcrystalline quartz bands appear to be separated by clay rich bands which have dissolved leaving vugs. Comb texture quartz at right side of sample. Gray bands containing sulfide minerals.
XRD Minerals: Not Analyzed
SWIR Minerals: Not Analyzed
LOI: 1.0%
NH4+: 38ppm
δ15N: Too low

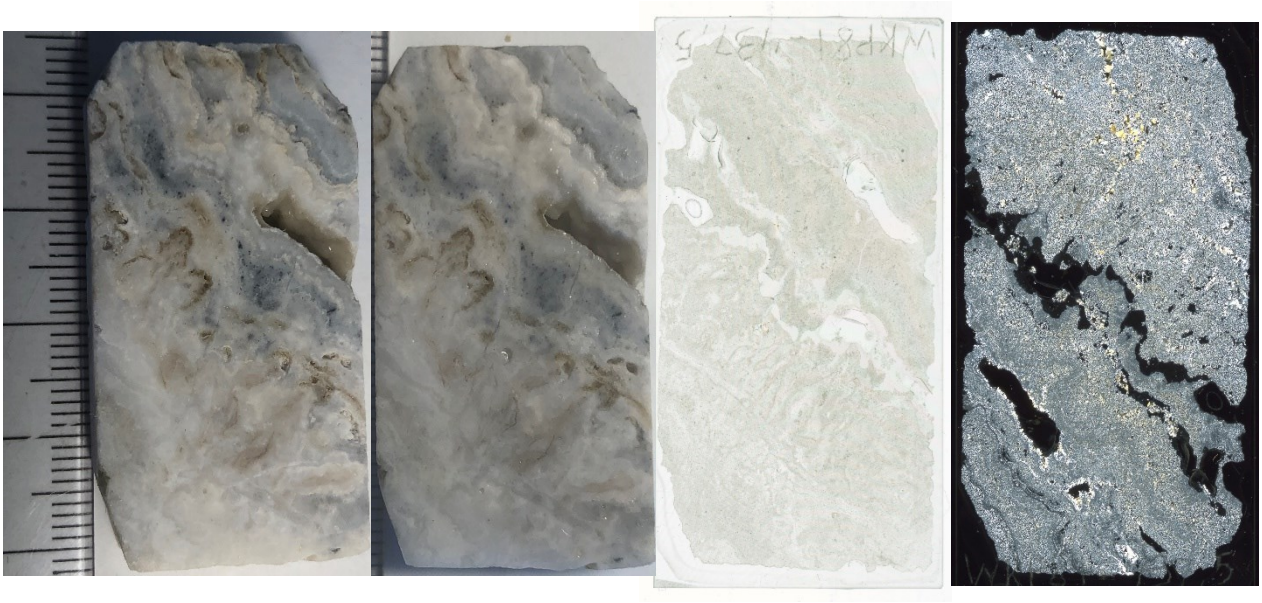

No Thin Section Description

WKP81-448V

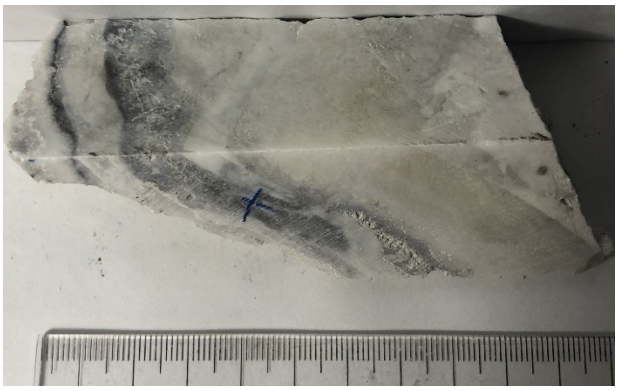

Depth: 448.6m
Sample Desc: Crustiform vein sample. Bands are irregularly shaped and are ~1cm. Primarily composed of microcrystalline quartz. Dark bands of sulfide rich areas. Whiter area at end is potentially adularia. Small patch of clay minerals at bottom of photo.
XRD Minerals: Not Analyzed
SWIR Minerals: Not Analyzed
LOI: Not Analyzed
NH4+: Not Analyzed
δ15N: Not Analyzed

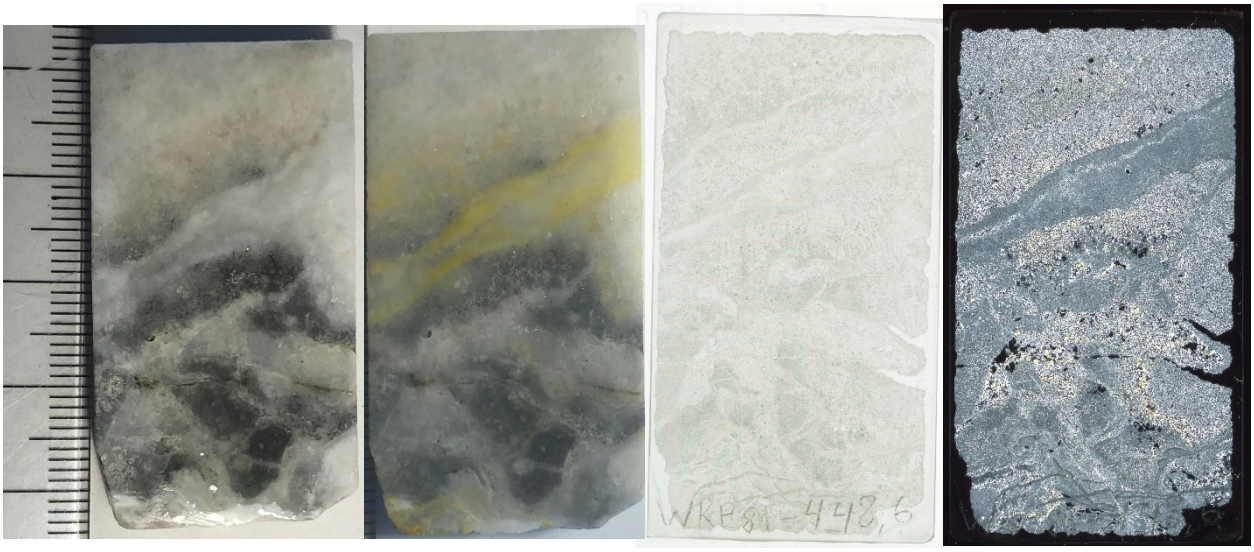

No Thin Section Description

WKP81-455V

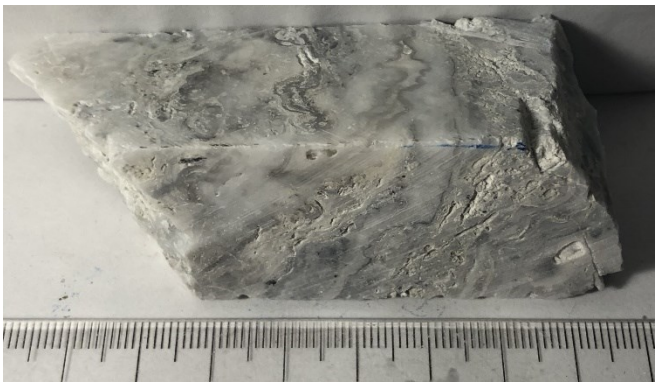

Depth: 455.3m
Sample Desc: Crustiform / colloform vein sample. Bands alternate colloform microcrystalline quartz and clay rich bands. Clay rich bands are slightly dissolved and irregular. Vugs throughout sample.
XRD Minerals: Not Analyzed
SWIR Minerals: Not Analyzed
LOI: 0.8%
NH4+: 37ppm
δ15N: Too low

No Thin Section Description

WKP81-456V

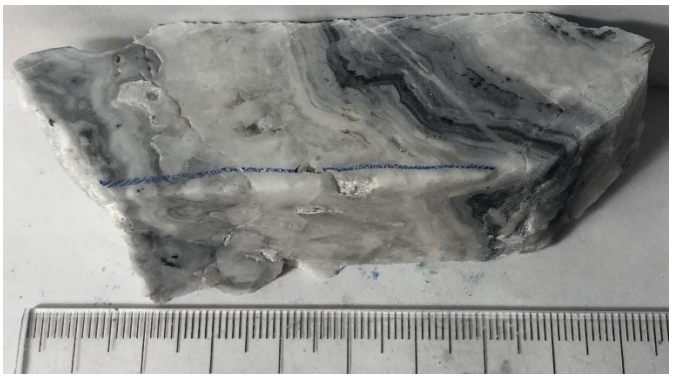

Depth: 456.5m
Sample Desc: Colloform / crustiform vein sample. Bands range from 2cm - 0.1cm. Thin colloform bands <1mm surround dark sulfide rich band near right side of sample. Contains visible 0.5mm ore minerals. Left side of sample is irregularly banded / brecciated and contains calcite or crystalline quartz.
XRD Minerals: Not Analyzed
SWIR Minerals: Not Analyzed
LOI: Not Analyzed
NH4+: Not Analyzed
δ15N: Not Analyzed

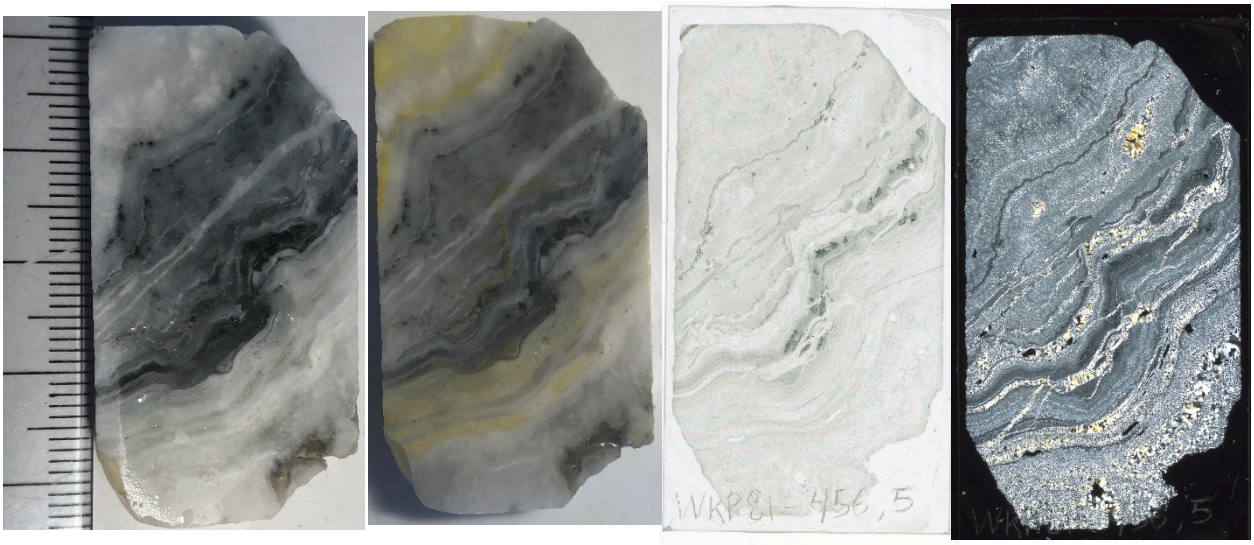

No Thin Section Description

WKP81-459V

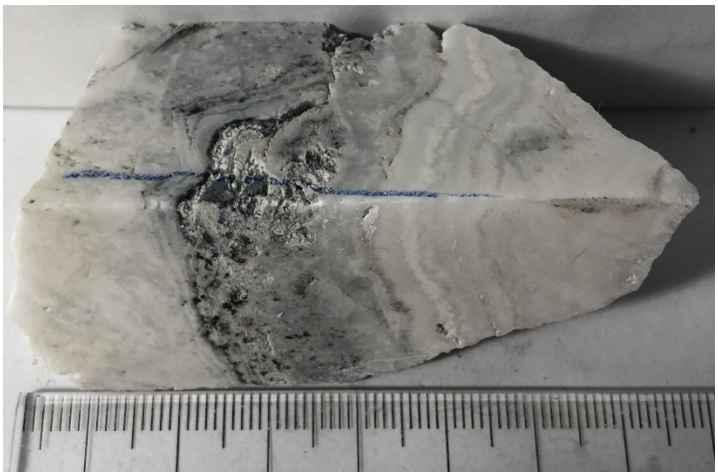

Depth: 459.6m
Sample Desc: Colloform banded microcrystalline quartz vein sample. Bands composed of primarily quartz though patch near center appears to contain clay minerals. Dark band containing sulfide minerals.
XRD Minerals: Not Analyzed
SWIR Minerals: Not Analyzed
LOI: Not Analyzed
NH4+: Not Analyzed
δ15N: Not Analyzed

No Thin Section Description

WKP81-475V

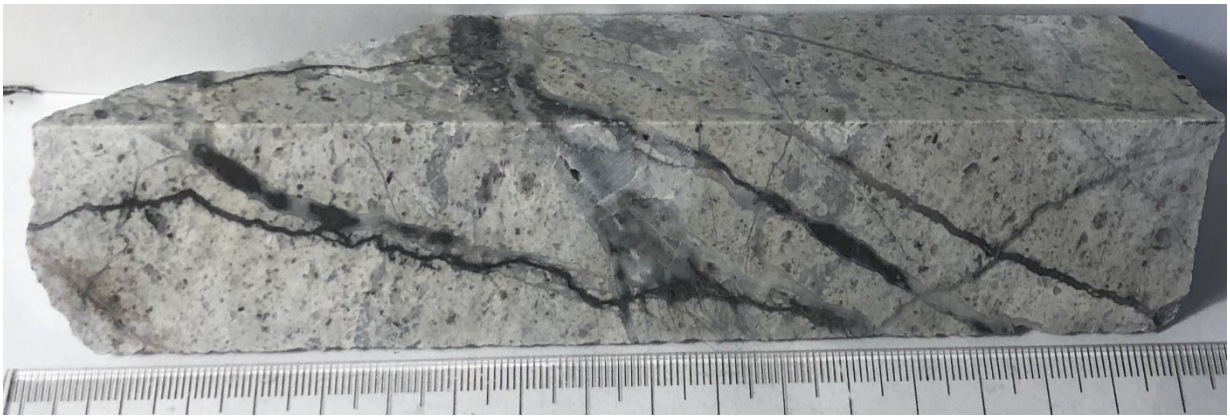

Depth: 475.1m
Sample Desc: Clay altered quartz phyric rhyolite. Abundant 0.5-1mm quartz eyes throughout. Multiple generations of small 1-4mm quartz veinlets many containing significant number of sulfides. Vugs near veinlets.
XRD Minerals: Not Analyzed
SWIR Minerals: Not Analyzed
LOI: 1.9%
NH4+: 170ppm
δ15N: +8.1‰

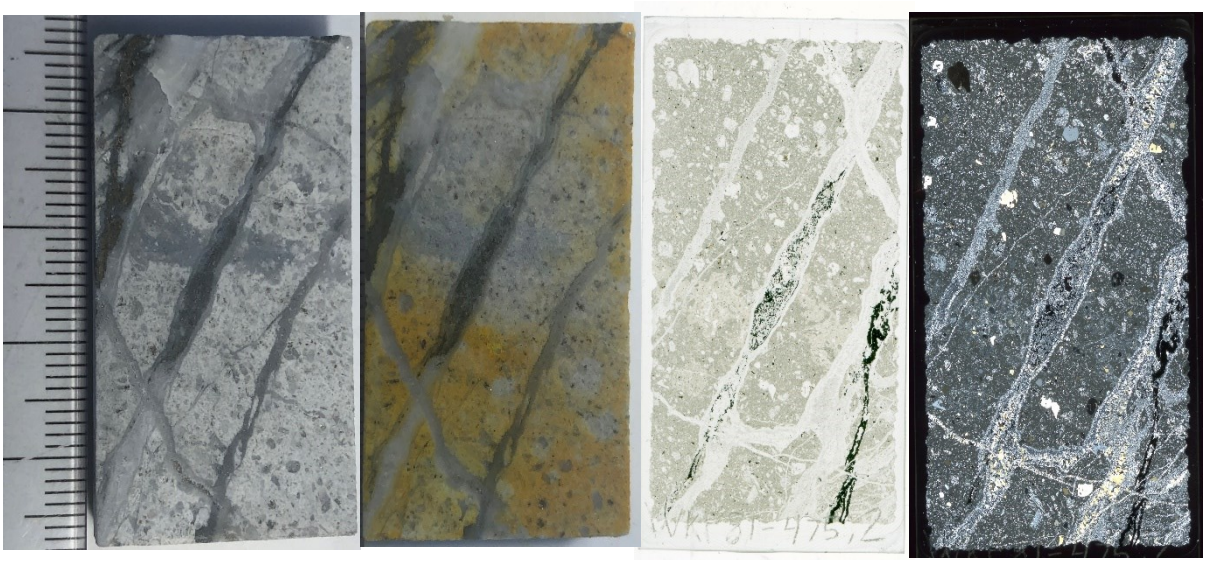

No Thin Section Description

Appendix C | SWIR Spectra

*Reflectance patterns were provided by Mark Simpson. Reflectance patterns are available for Favona DDH63, 87, and 104 as well as WKP42-124 and WKP42-174. A mineral ID results table (Table 8) is available for the WKP42 spectral chip samples which was provided by Mark Simpson.

FVN63-12

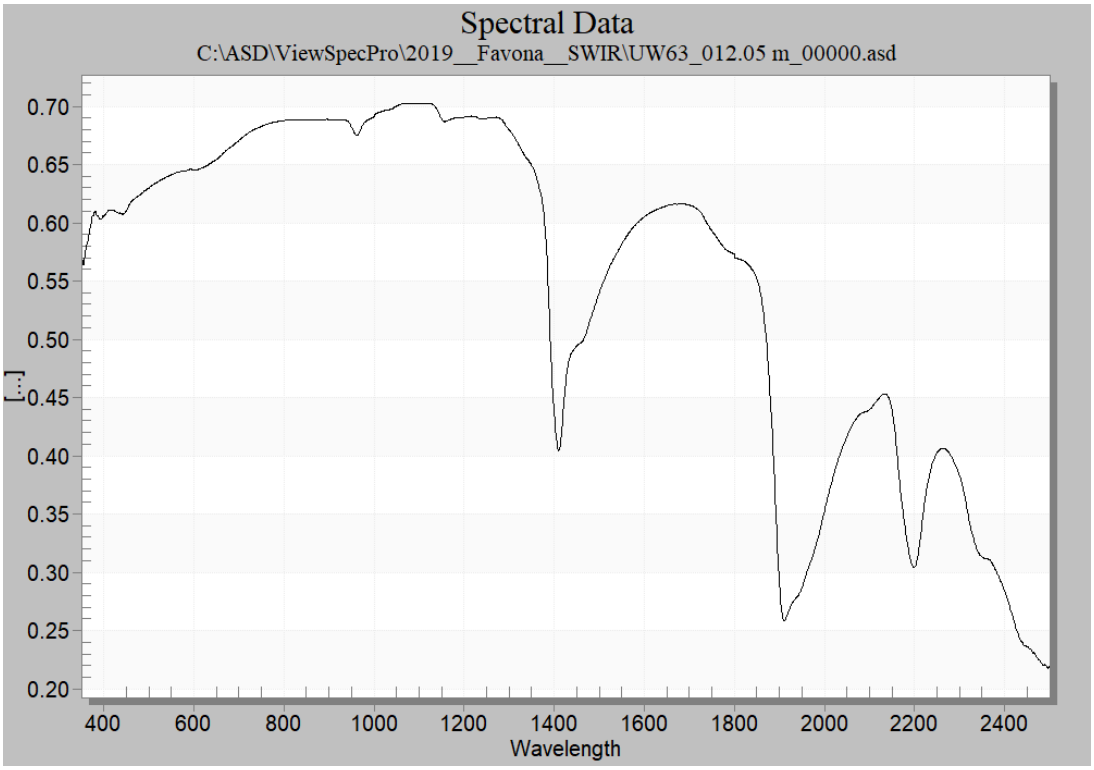

FVN63-80

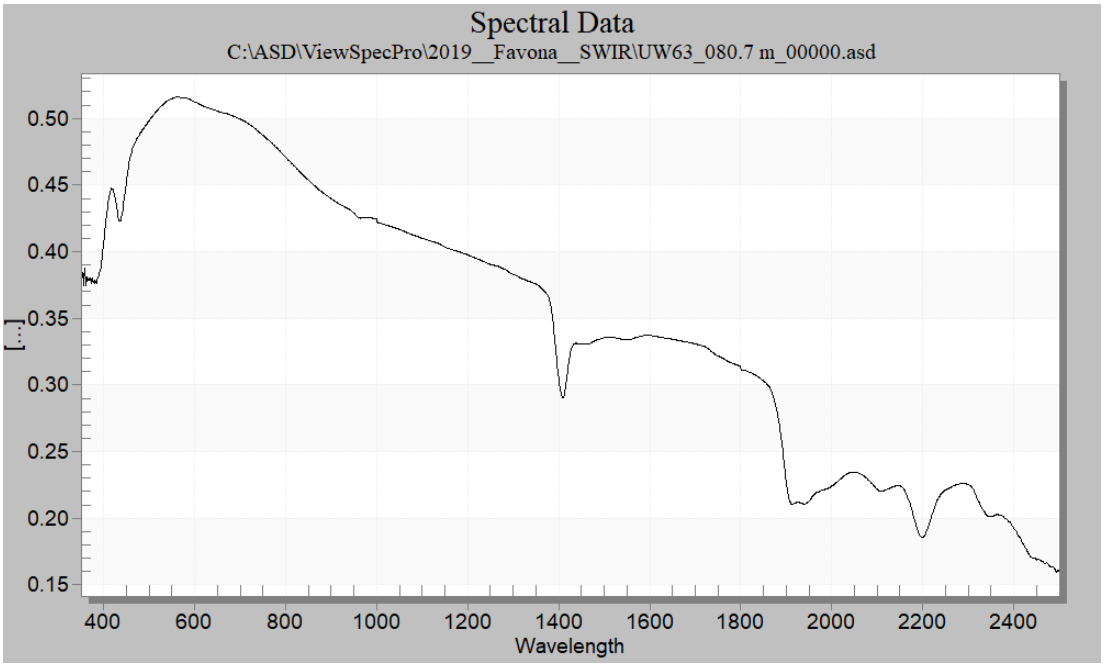

FVN63-135

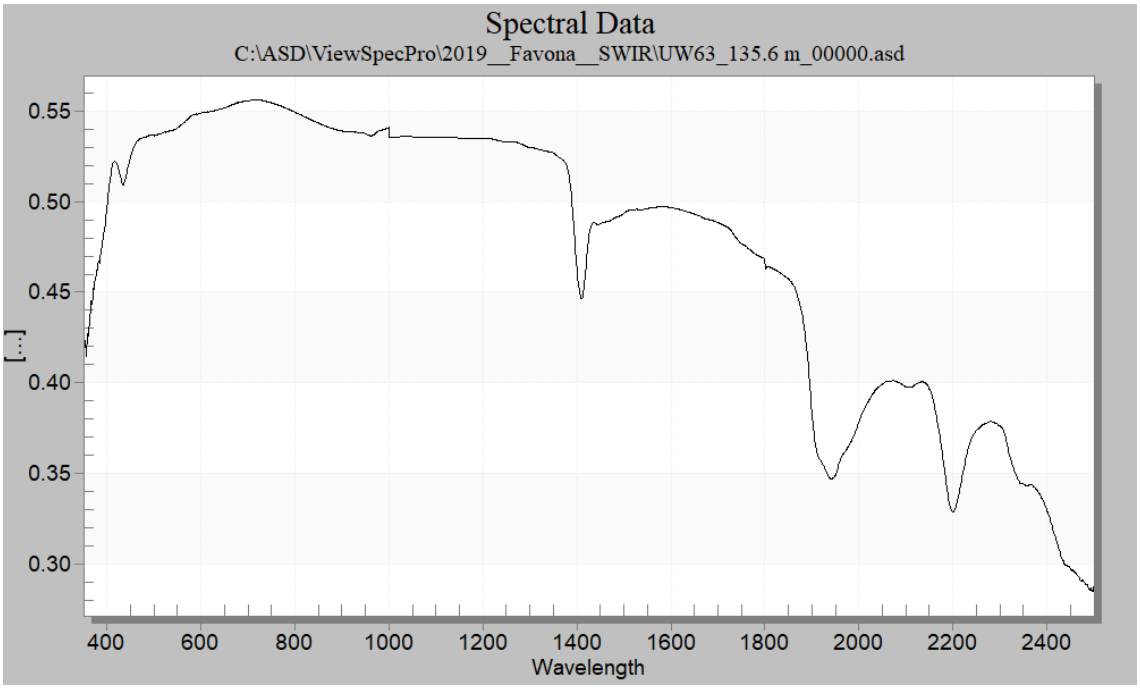

FVN63-180

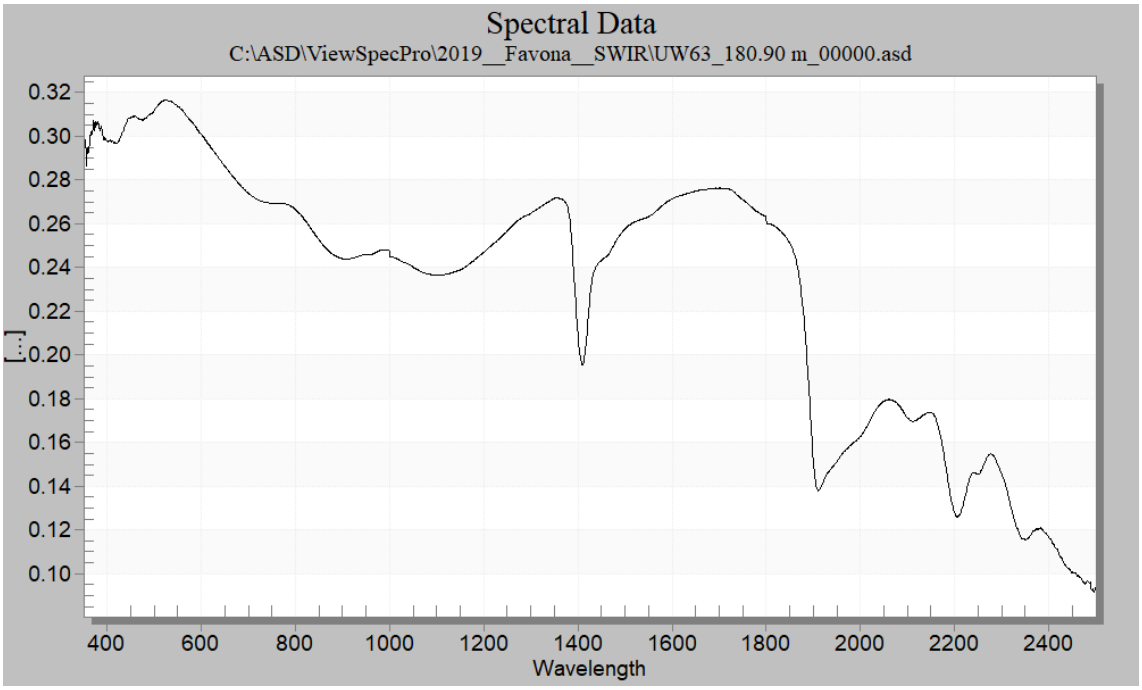

FVN87-211

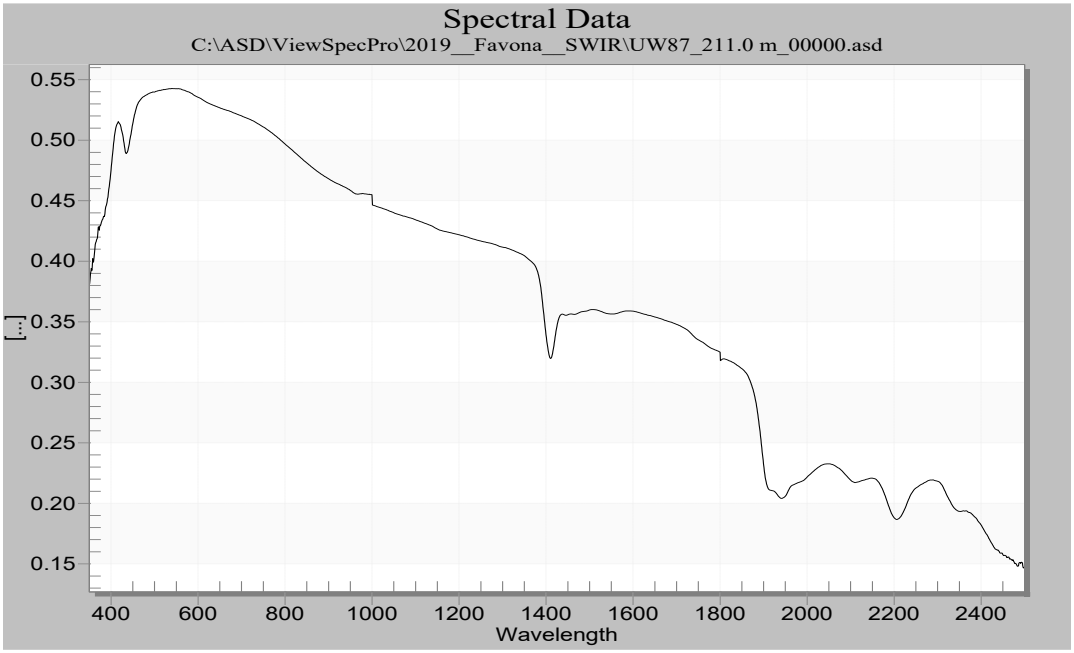

FVN87-251

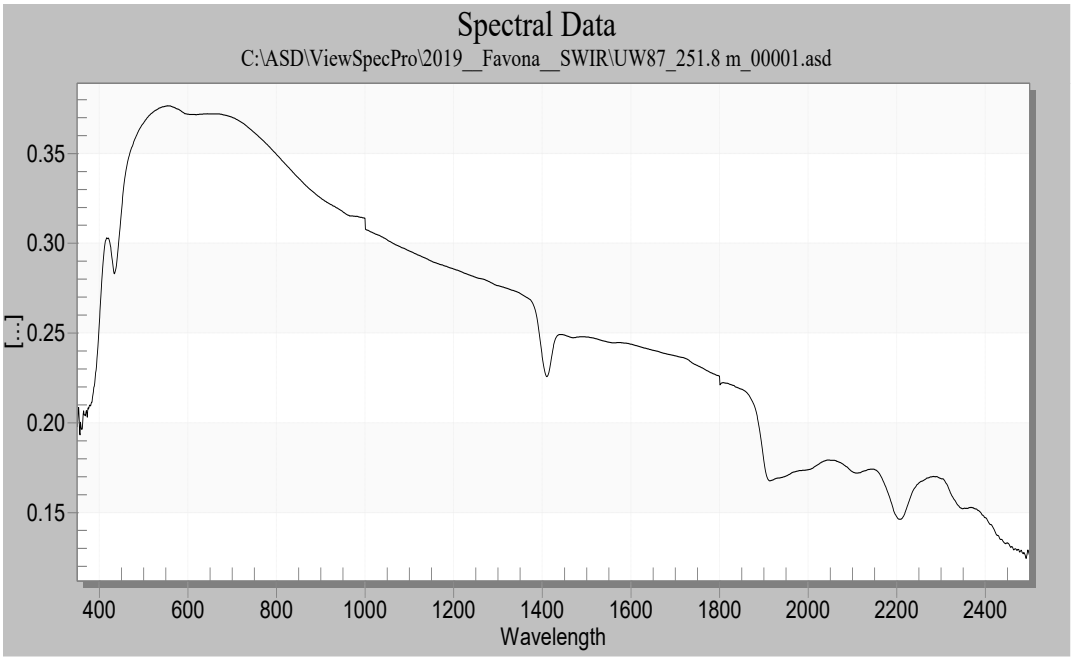

FVN87-299

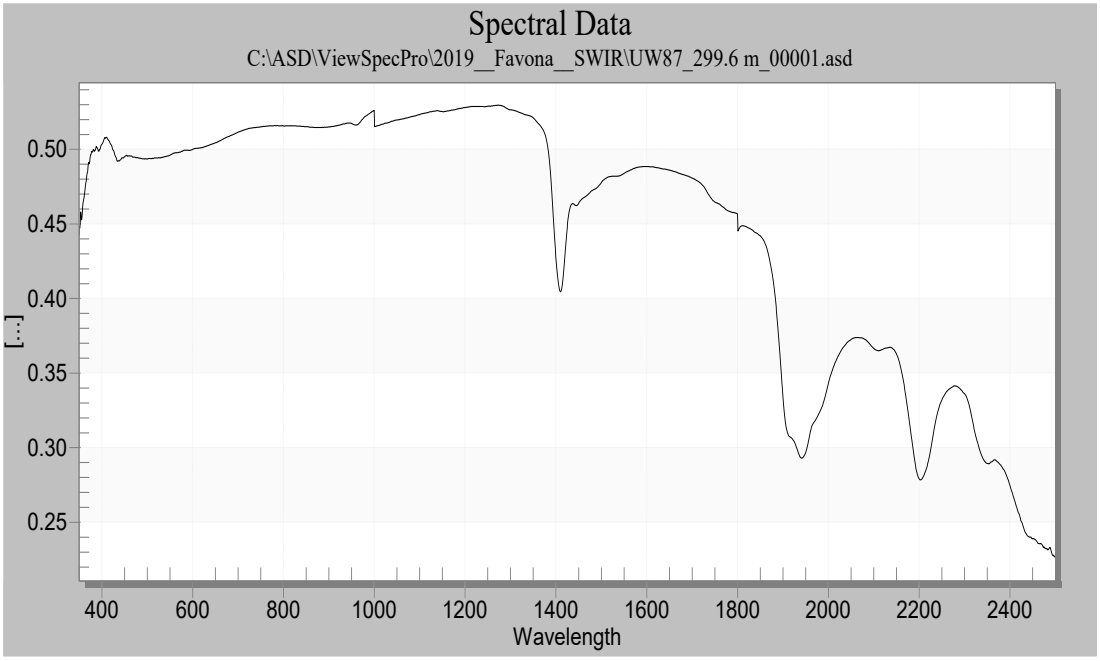

FVN87-337

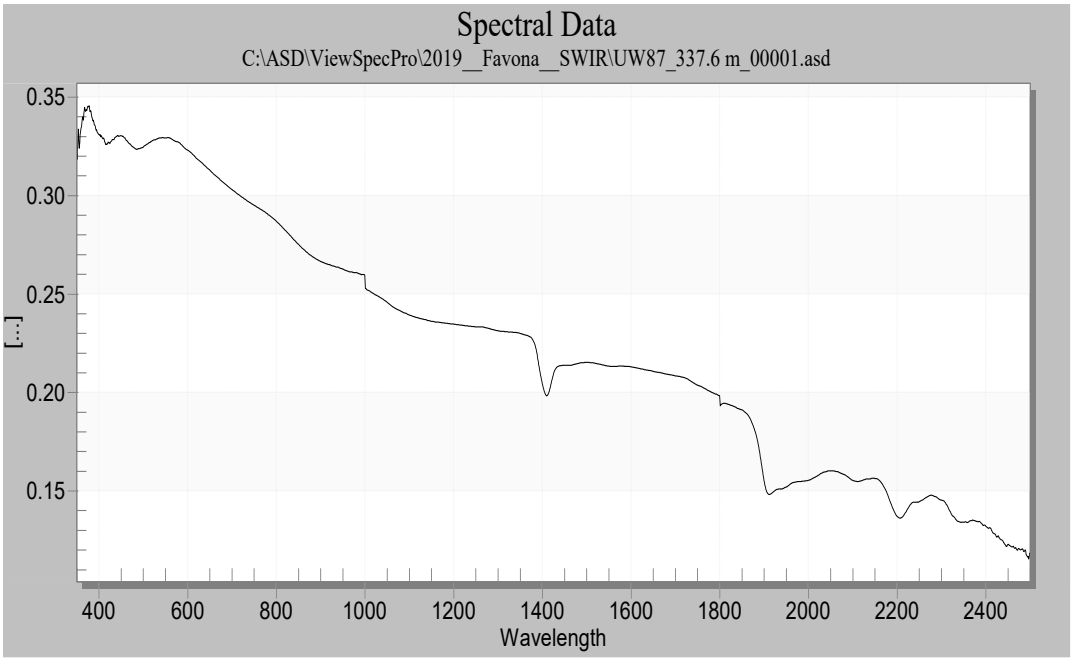

FVN104-103

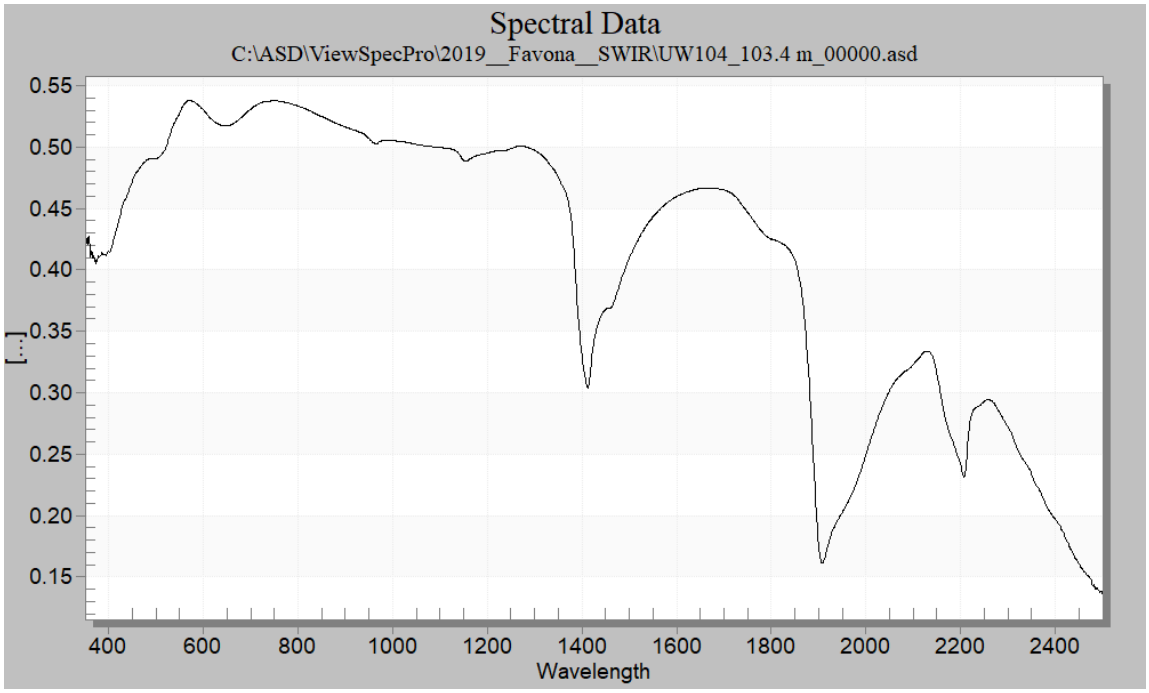

FVN104-188

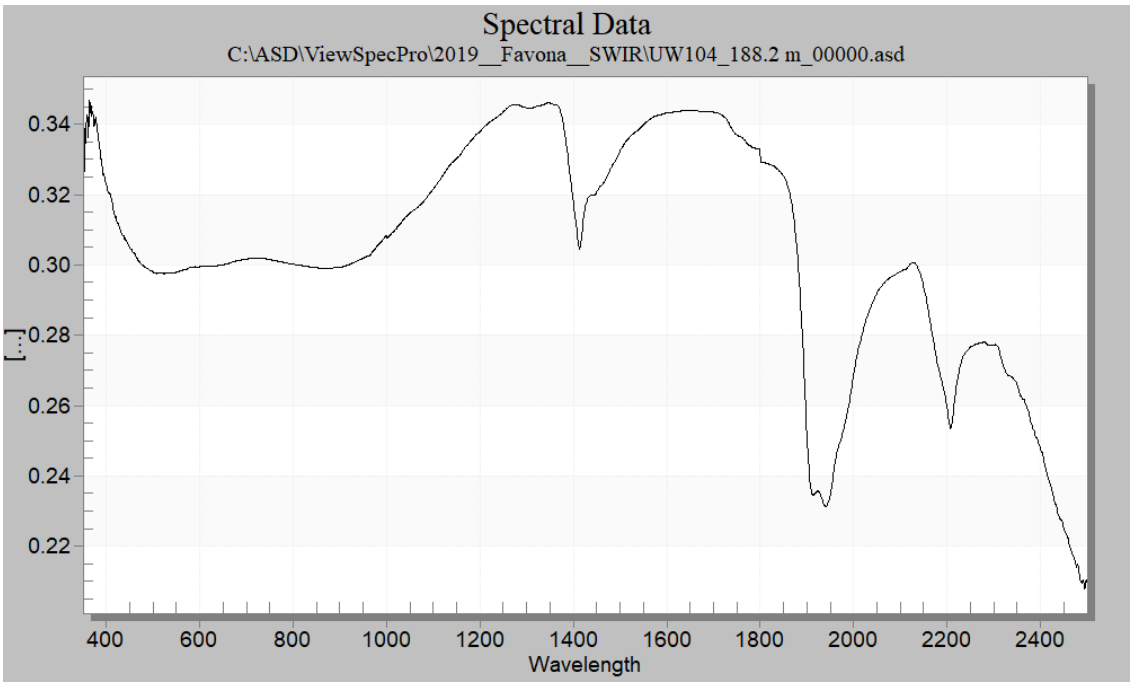

FVN104-270

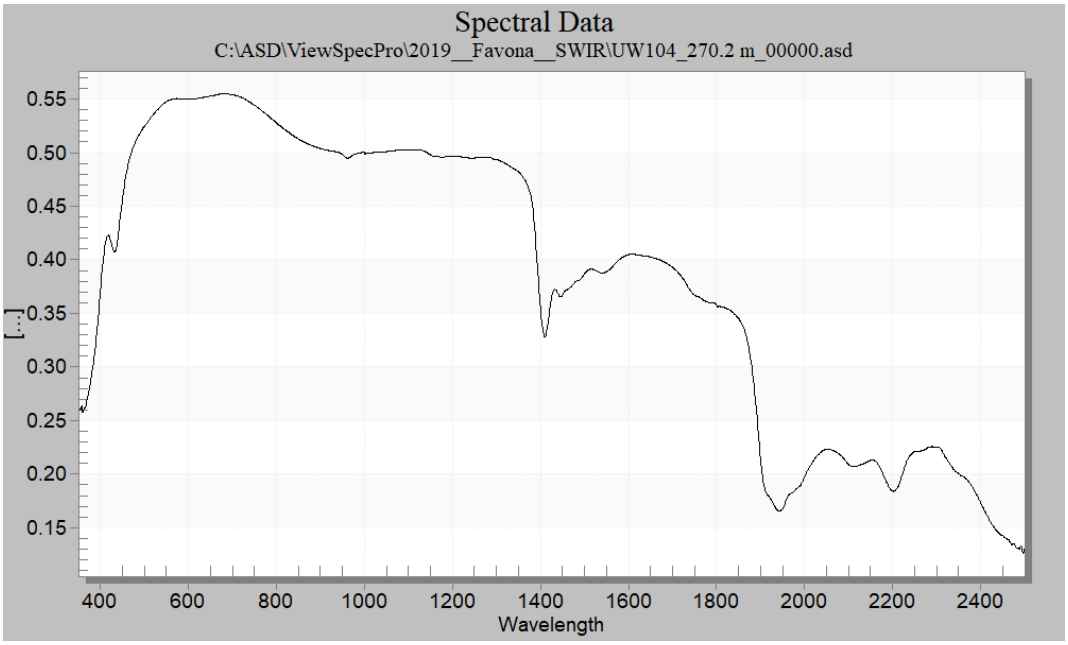

FVN104-312

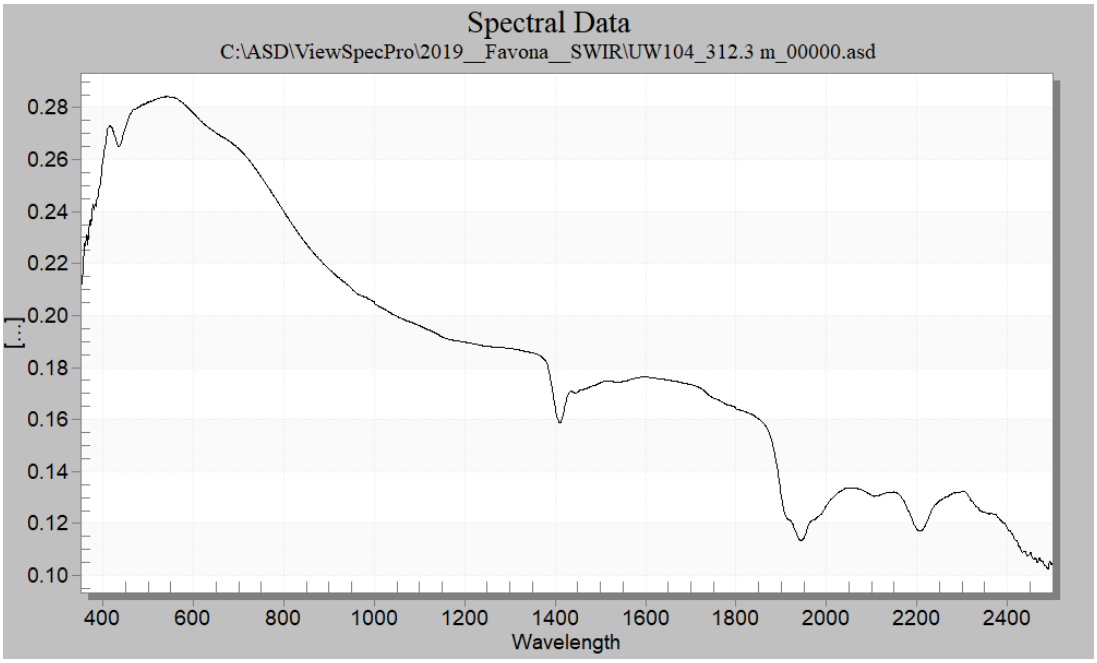

FVN104-340

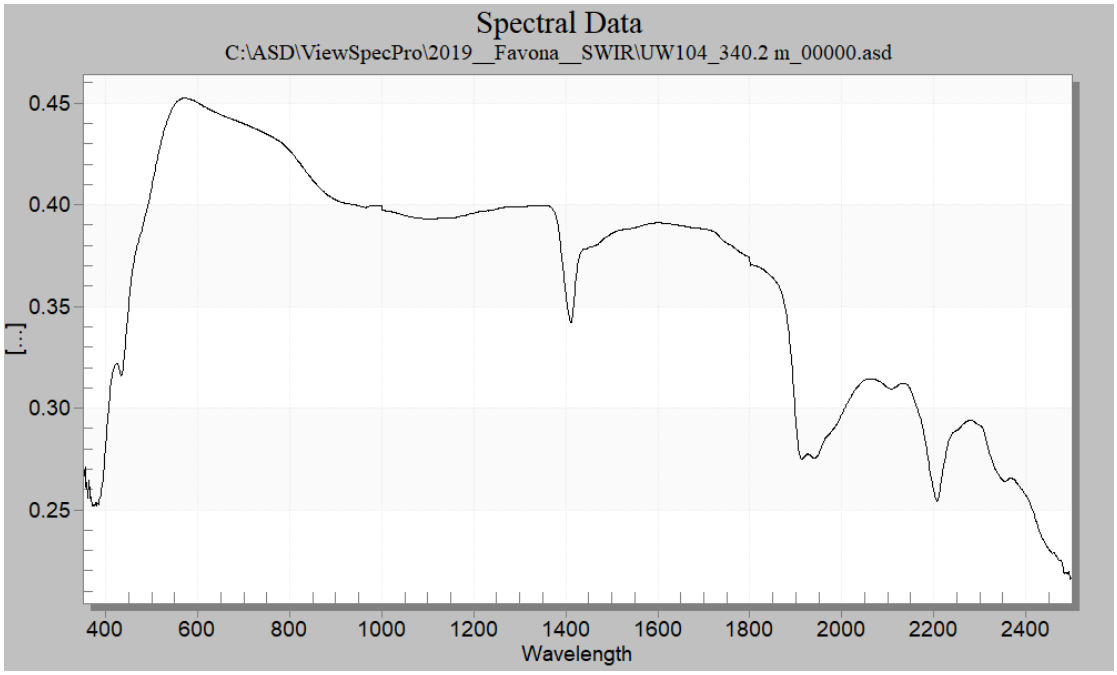

FVN104-374

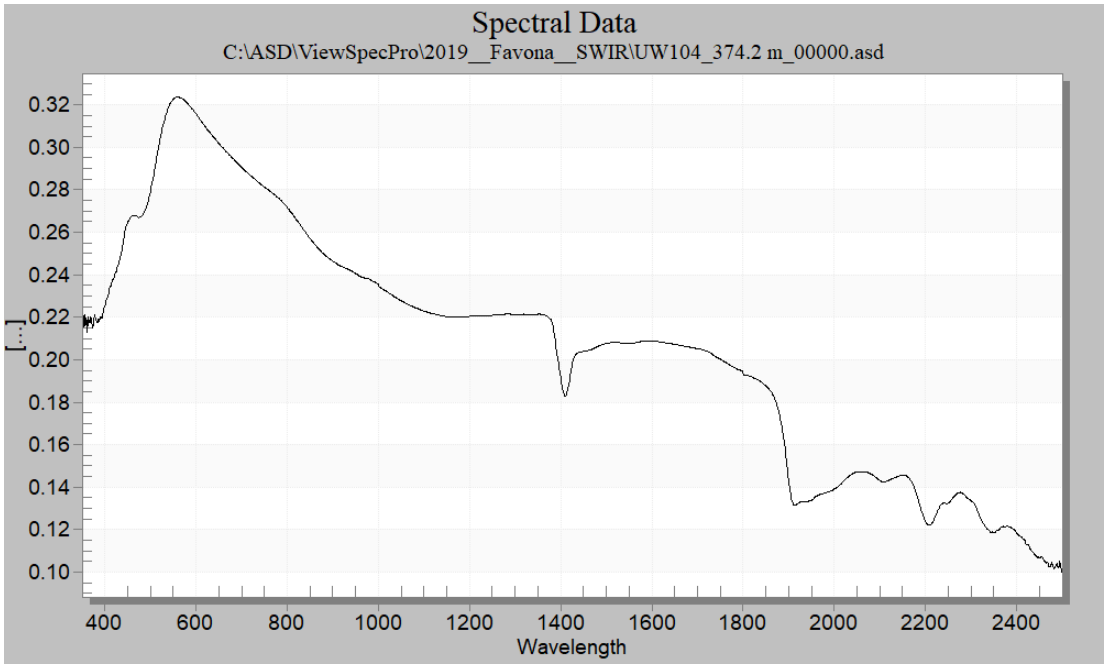

FVN104-417

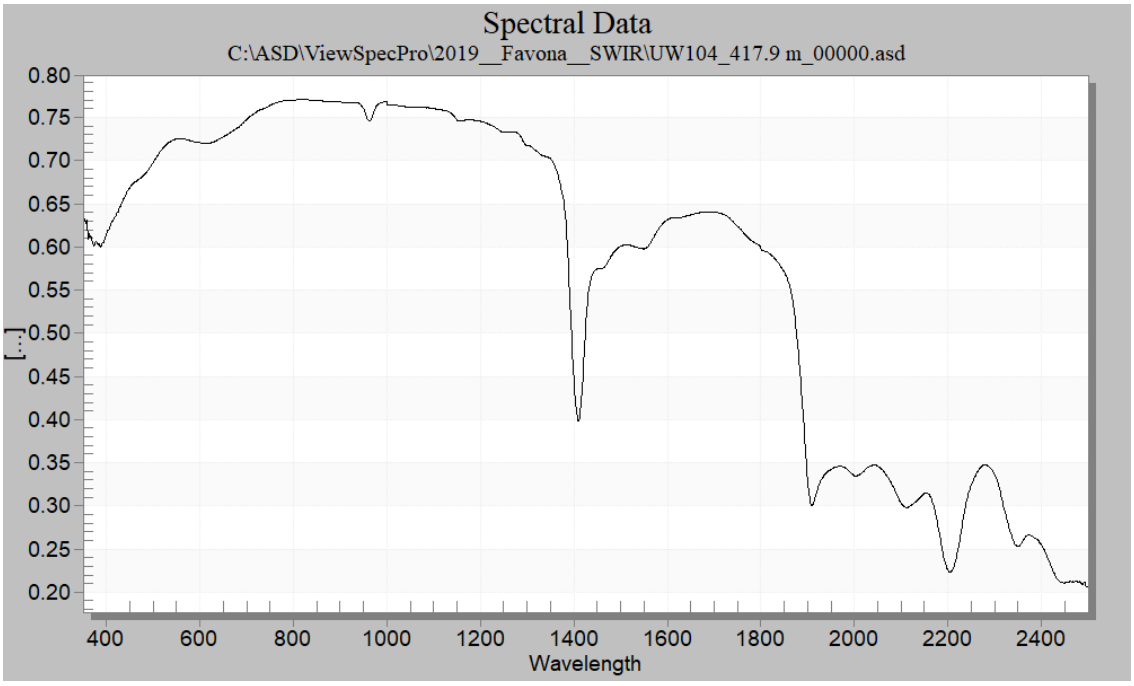
Spectral Data
C:\ASD\ViewSpecPro\2019__Favona__SWIR\UW104_417.9 m_00000.asd
[...]
0.80
0.75
0.70
0.65
0.60
0.55
0.50
0.45
0.40
0.35
0.30
0.25
0.20
400
600
800
1000
1200
1400
1600
1800
2000
2200
2400
Wavelength

WKP

WKP42-124

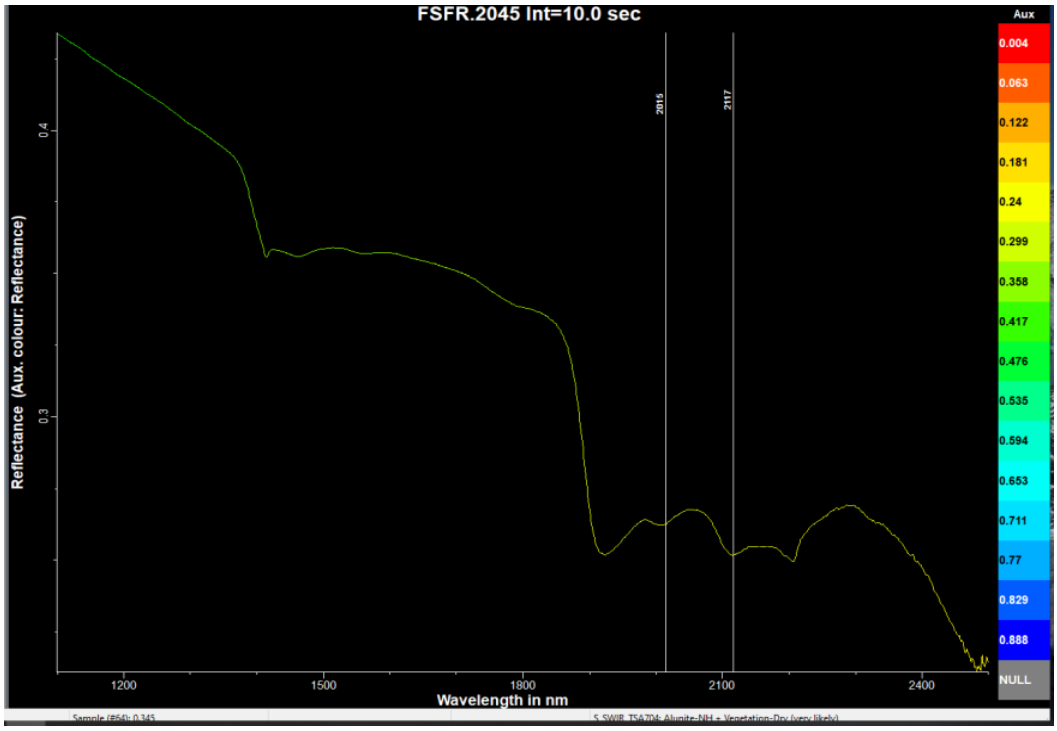

WKP42-174

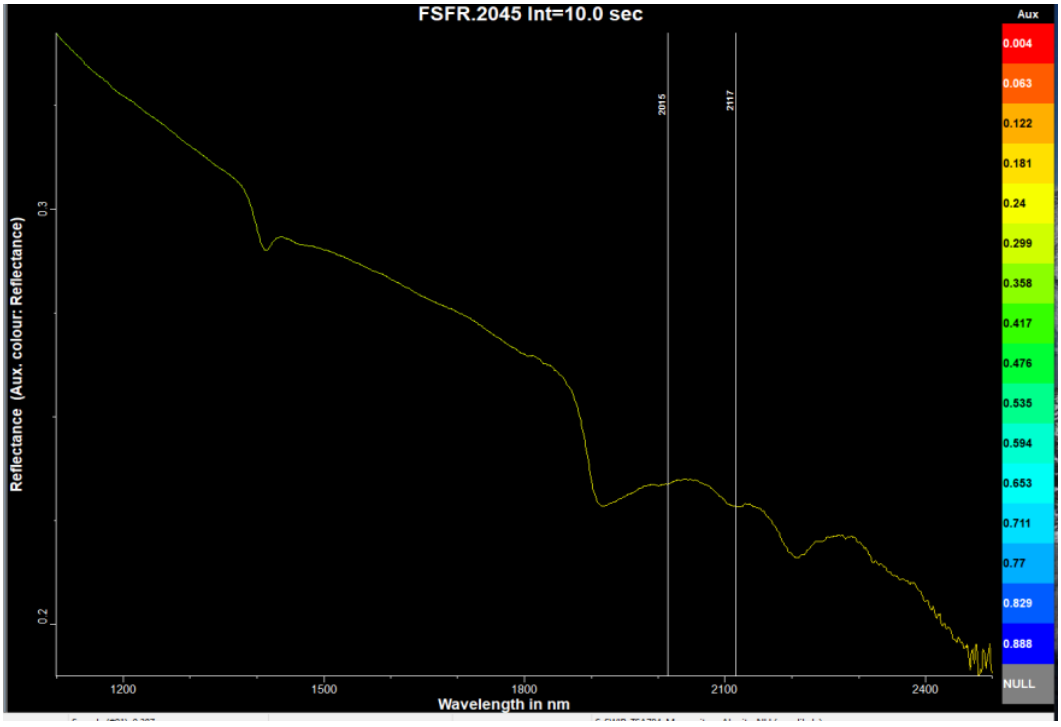

Table 9. *Summary of WKP42 spectral chip SWIR reflectance spectroscopy results provided by Mark Simpson. Spectra were acquired by OceanaGold and interpreted by Mark Simpson.*

Sample ID	NH_4-illite	NH_4-IS	NH_4-feldspar	Illite	Illite-smectite	Smectite	Kaolinite	Chlorite	Calcite	Gypsum	Jarosite
WKP42-26.0					1						
WKP42-46.0				1							
WKP42-51.7			1								
WKP42-56.3			1								
WKP42-59.0			1								
WKP42-68.0				1			??				
WKP42-74.2				1			1				
WKP42-75.5	1						1				
WKP42-80.3	1		1								
WKP42-103.9	1										
WKP42-118.2	1										
WKP42-119.8							1				
WKP42-124			1								
WKP42-142.1				1			1				
WKP42-162.0				1			1				
WKP42-174.0				1							
WKP42-196.0	1										
WKP42-225.7				1				1			
WKP42-245.1	1										
WKP42-277.4	1										
WKP42-313.5	1							1			
WKP42-397.0				1							
WKP42-522.5			1								
WKP42-553.2	1										
WKP42-573.6				1							
WKP42-604.8				1							

Appendix D | XRD

*Includes XRD patterns with labeled peaks for various Favona, Martha, and WKP samples. Also includes a table (Table 9) provided by Mark Simpson which summarizes the results of the XRD analysis of Favona wallrock samples from Simpson & Mauk, 2007.

Favona Vein Samples

FVN63-88V

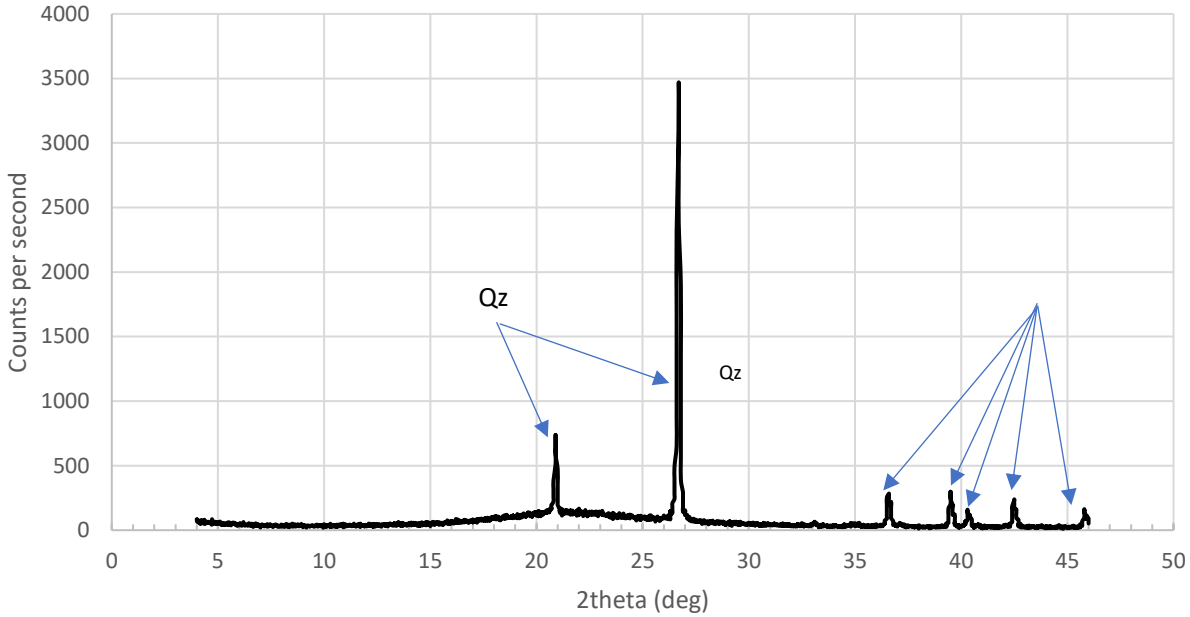

FVN63-117V

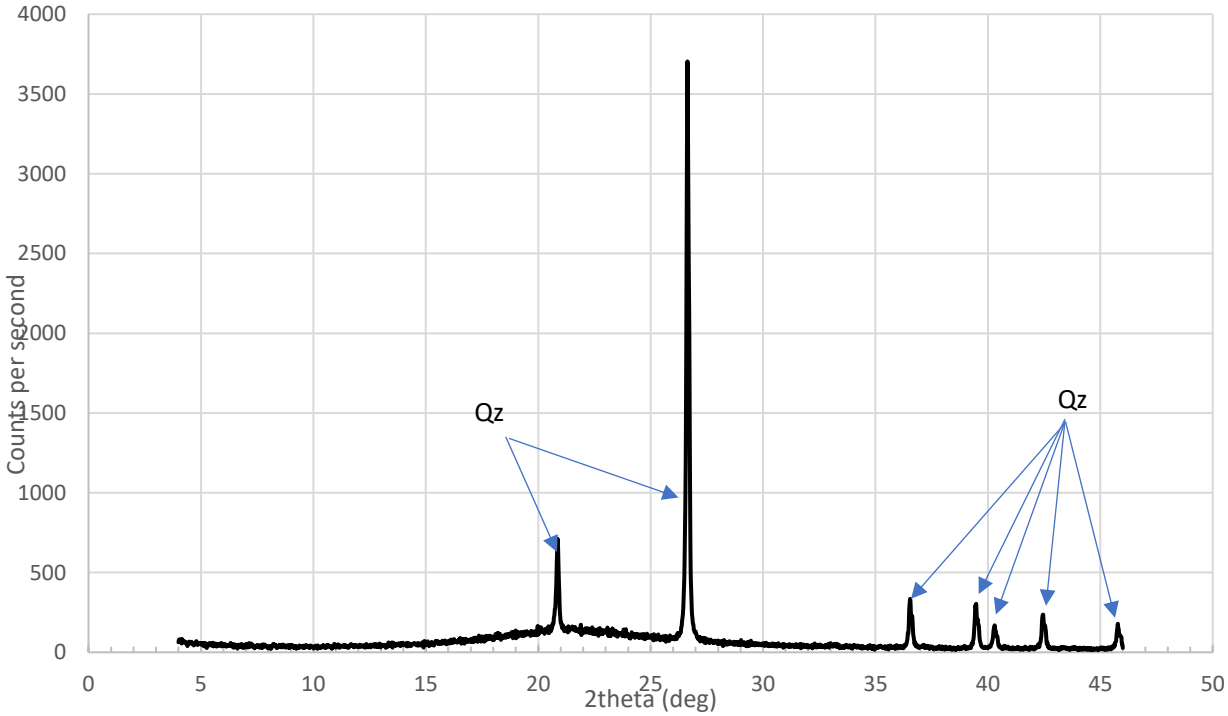

FVN63-185V

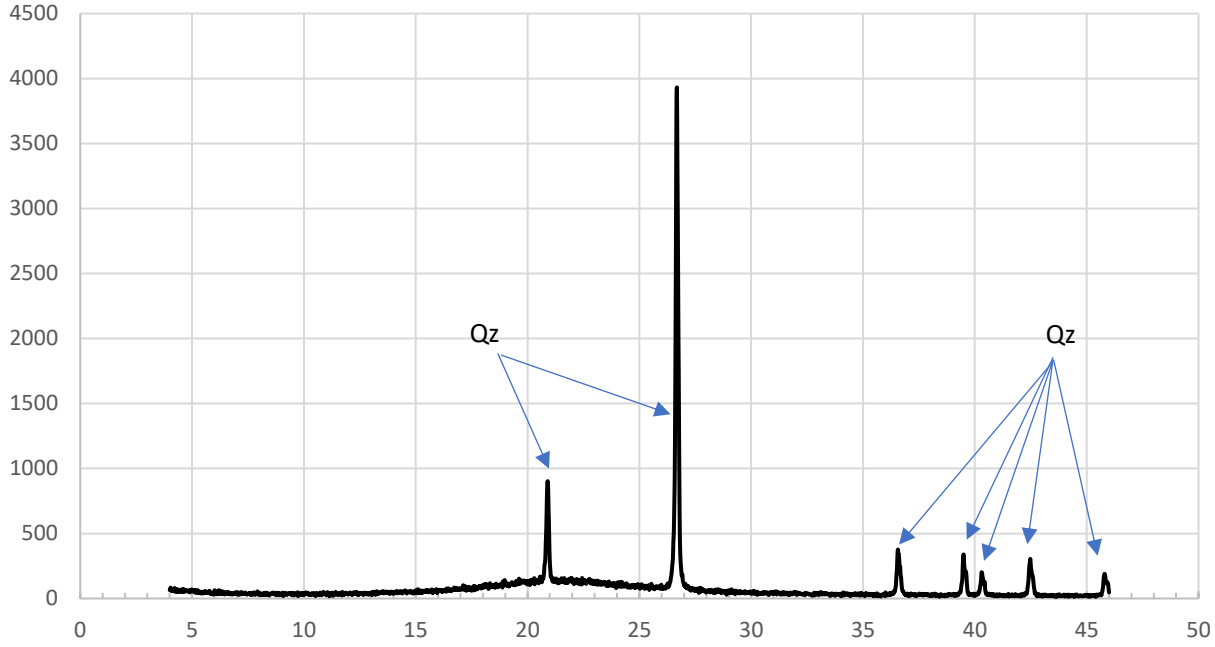

FVN58180V

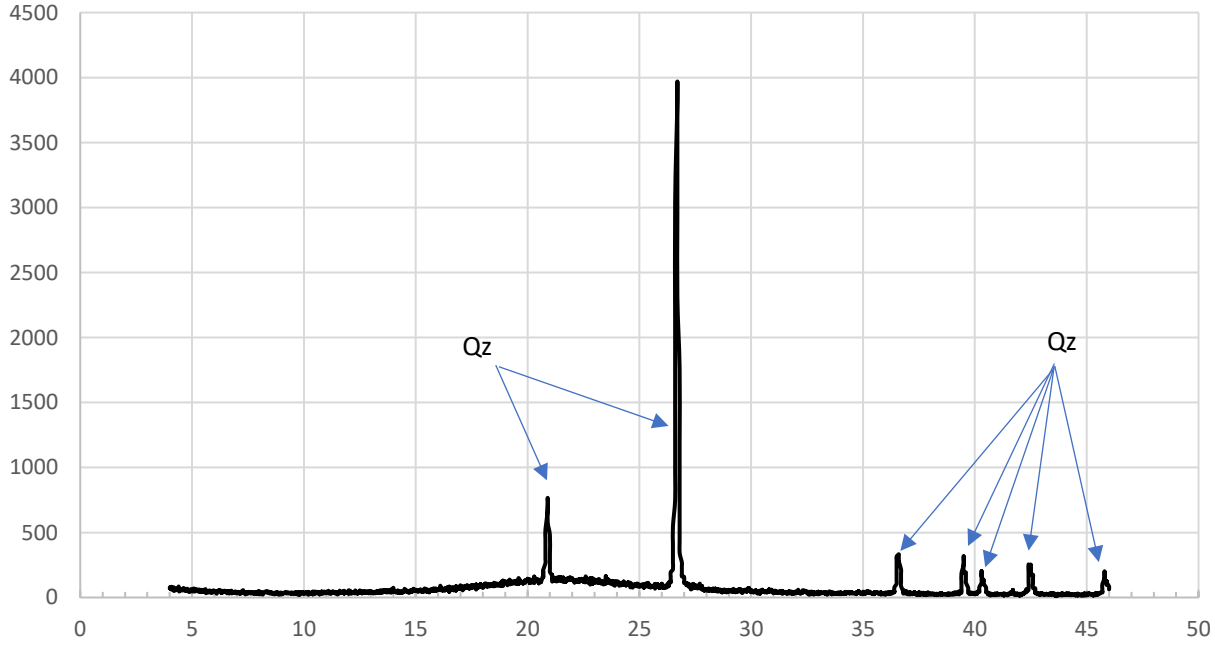

FVN60248V

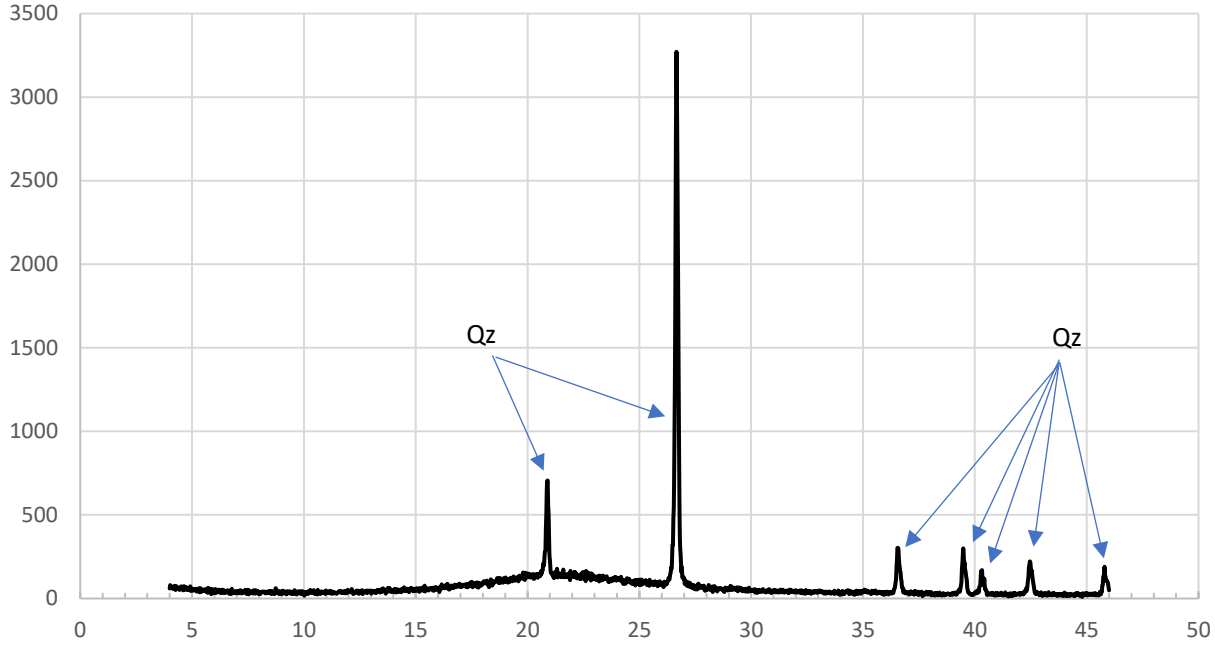

Martha Vein Samples

MTA46853V

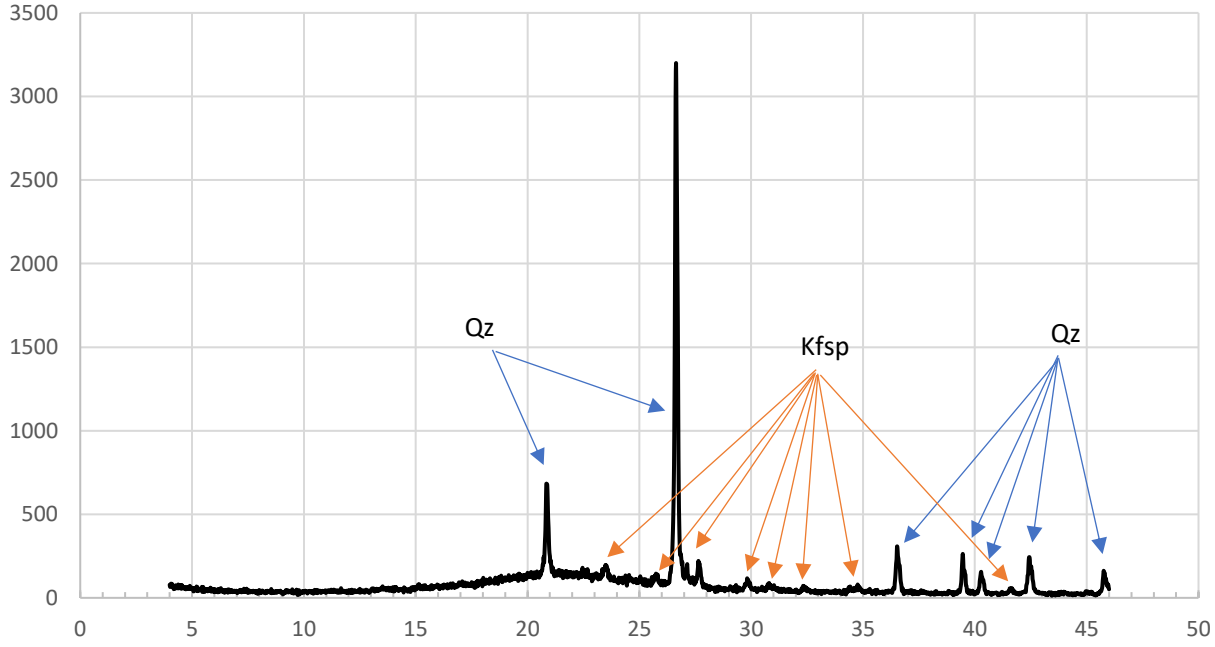

MTA57459V

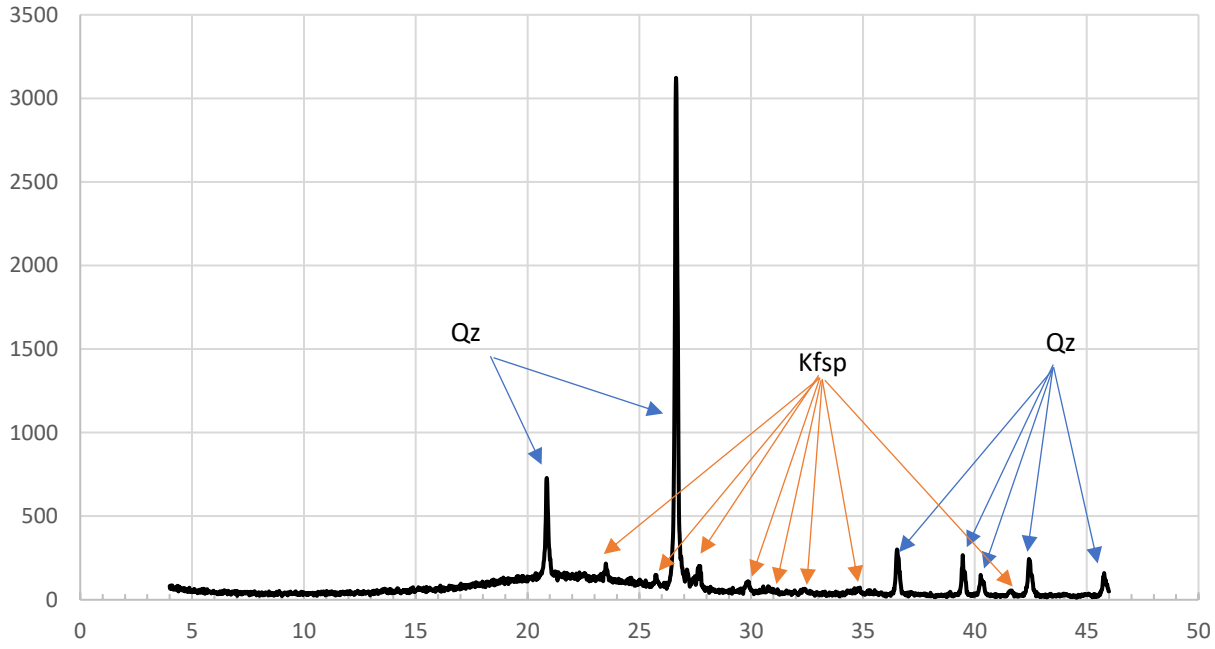

MTA57466V

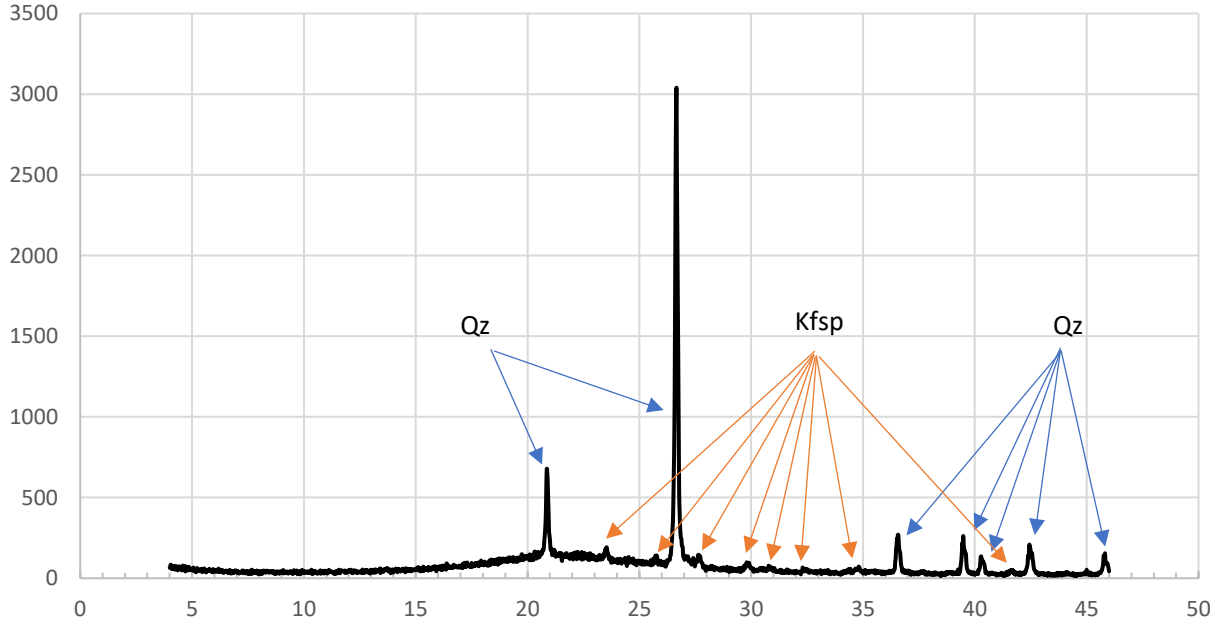

Martha Wallrock Samples

MTA1460-204 Bulk

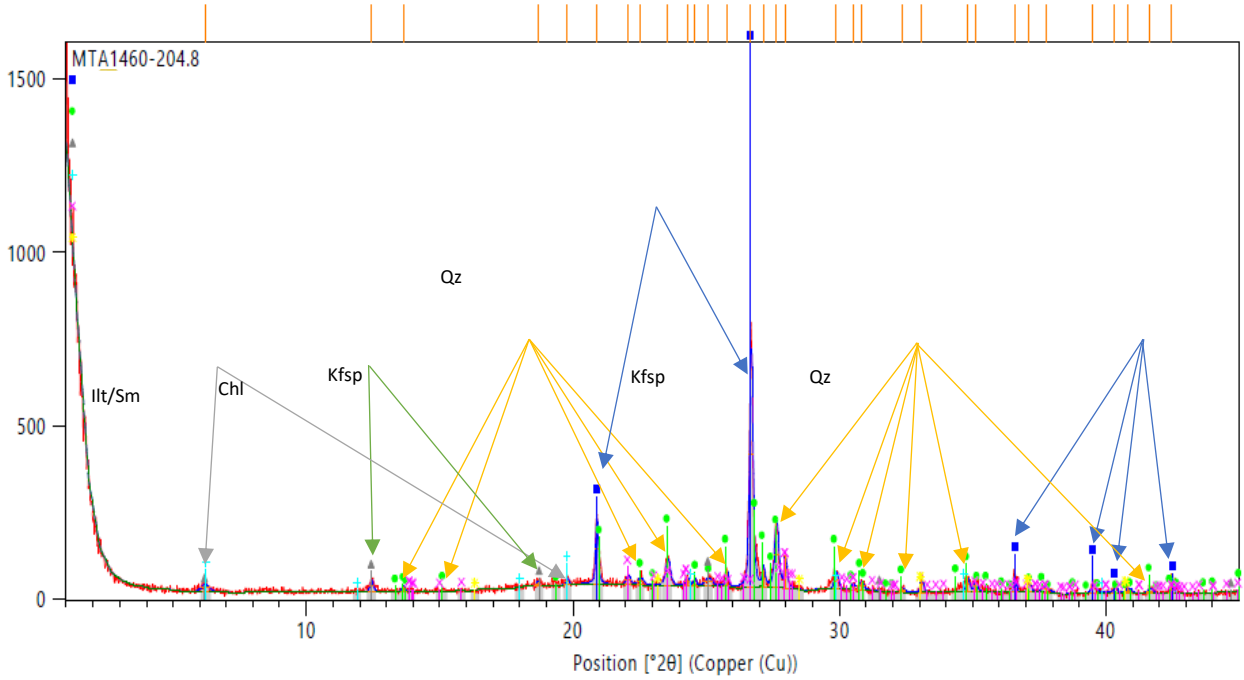

MTA1460-204 <10µm Separate

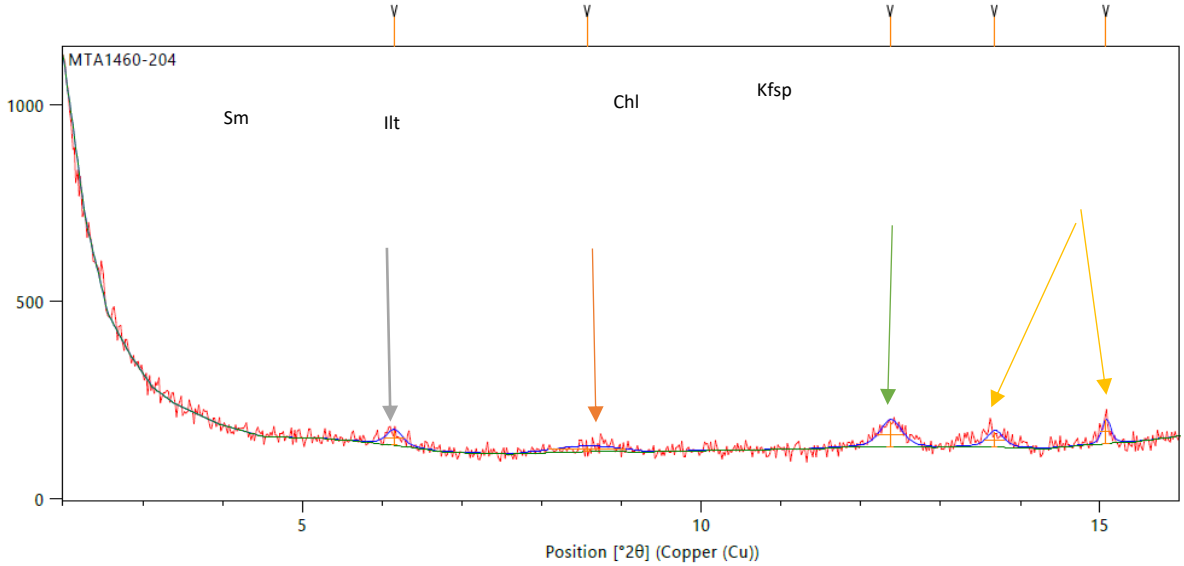

WKP Wallrock Samples

WKP42-26 <10µm Separate

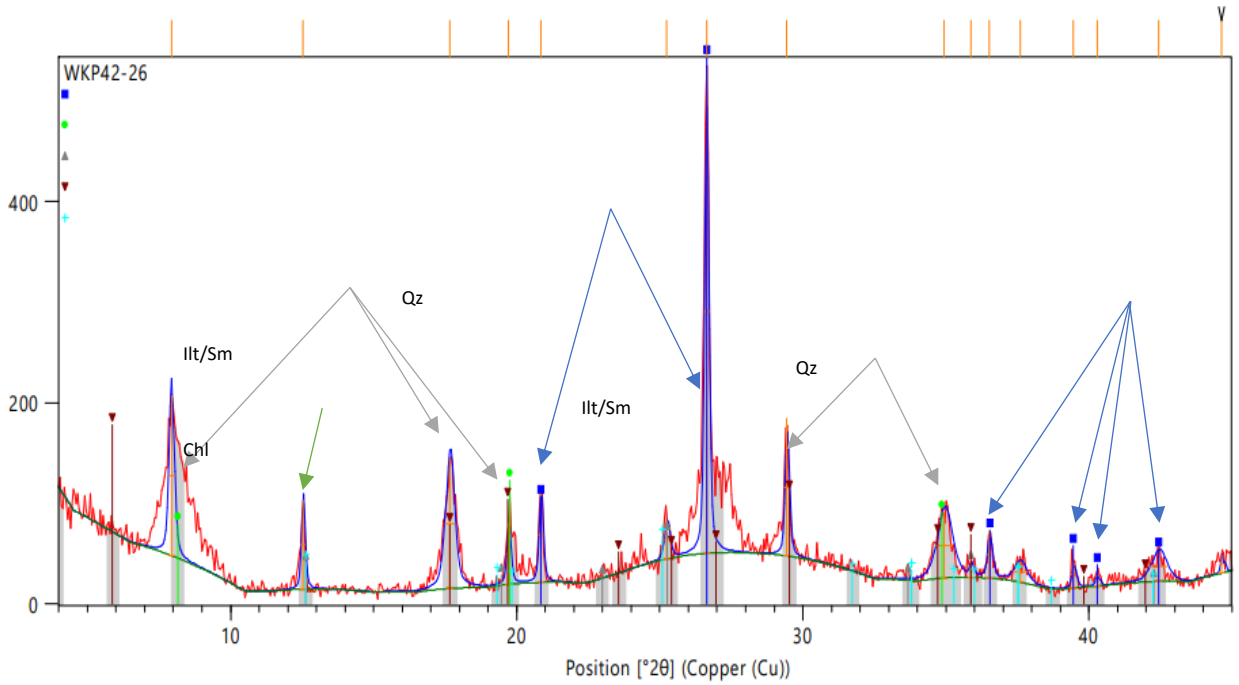

WKP42-26 <10µm Separate Glycolated

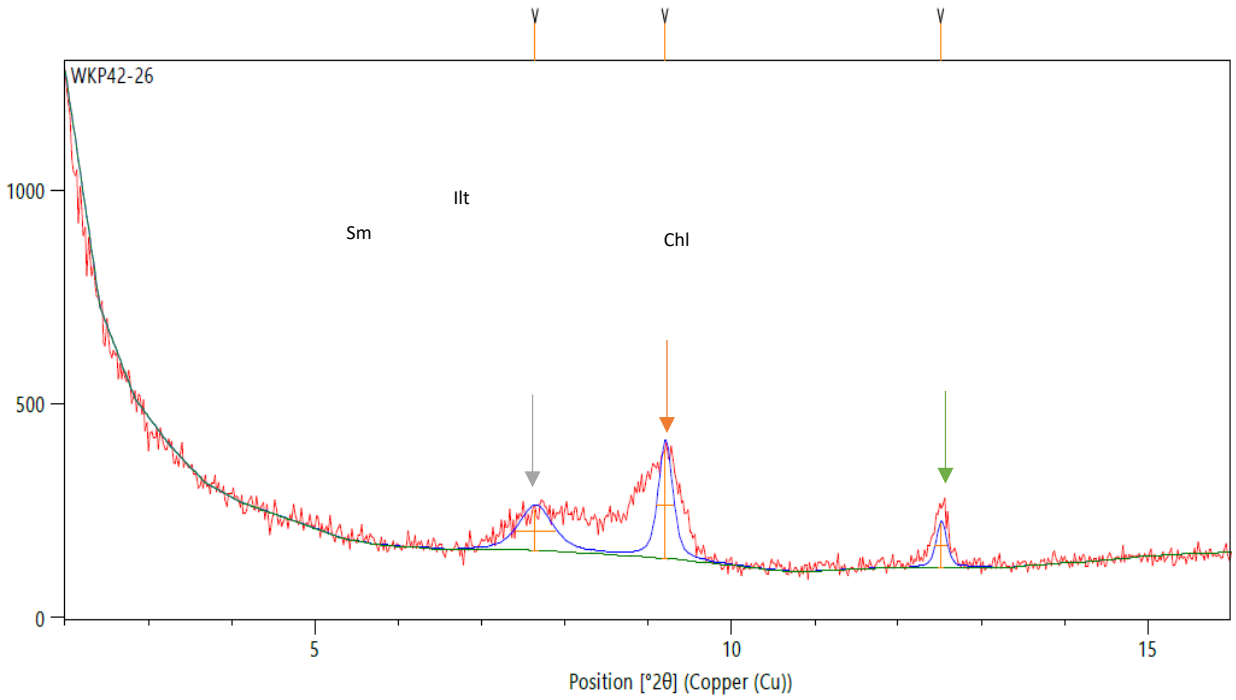

WKP42-245 <10µm Separate

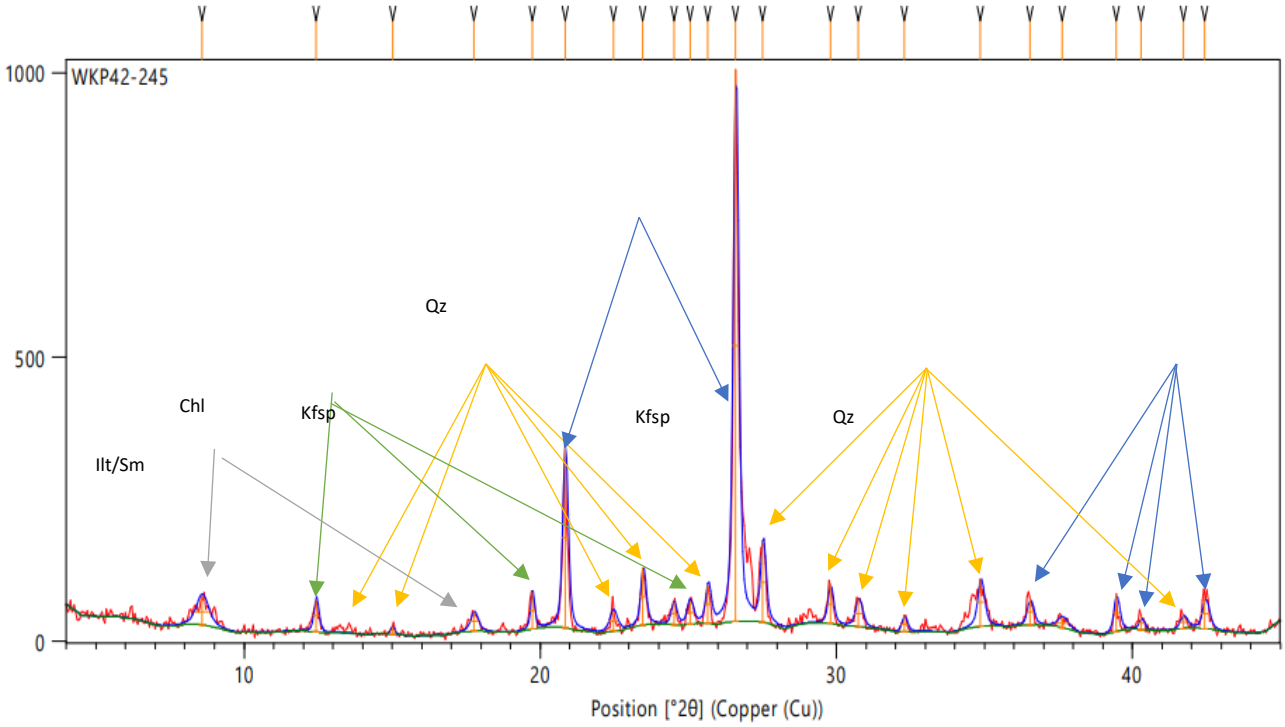

WKP42-245 <10µm Separate Glycolated

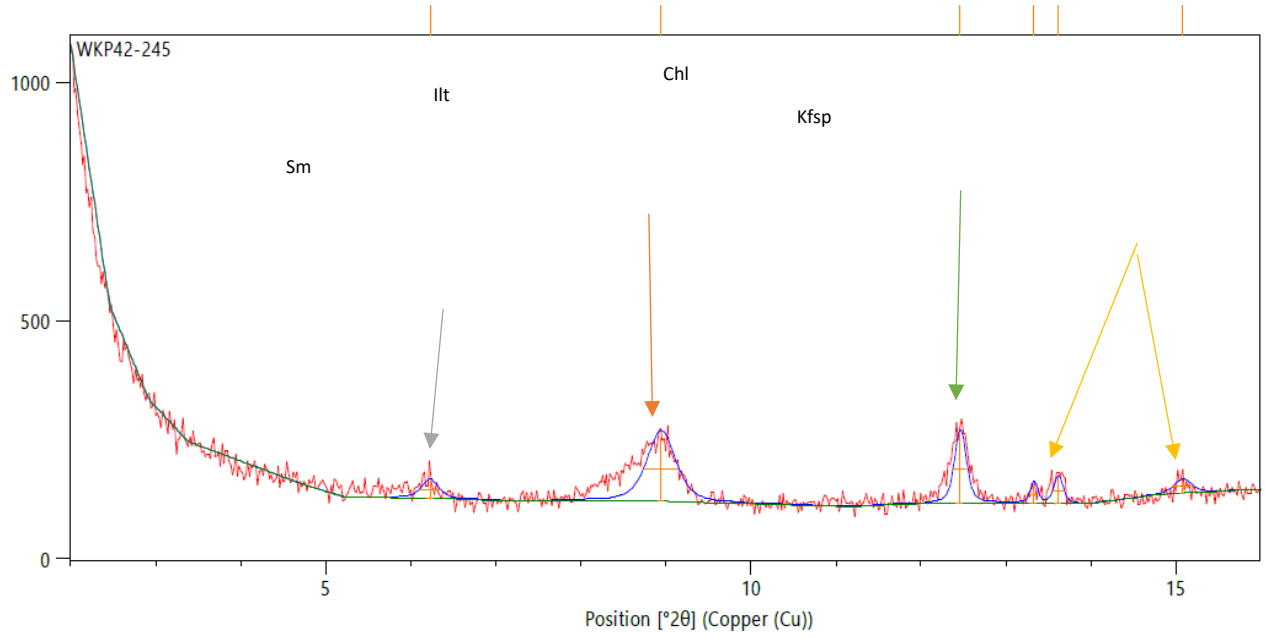

WKP42-407 <10µm Separate

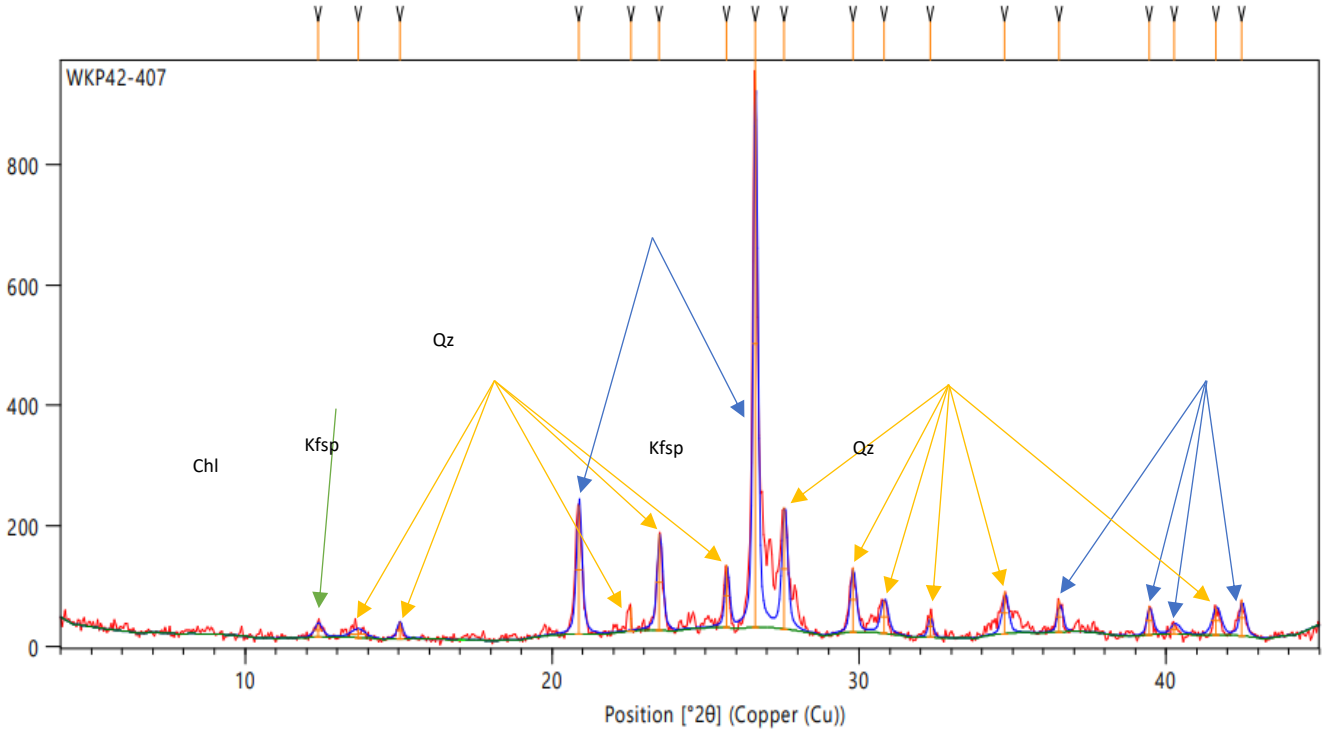

WKP42-407 <10µm Separate Glycolated

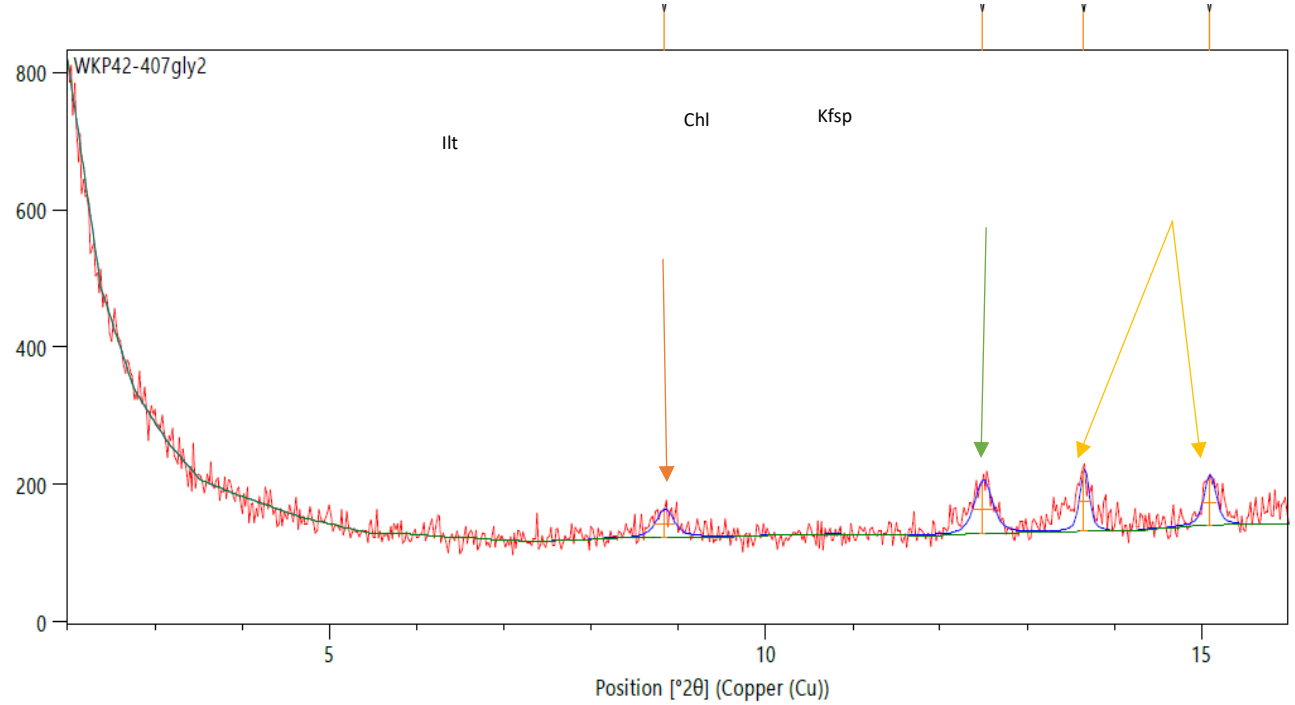

WKP42-409 <10µm Separate

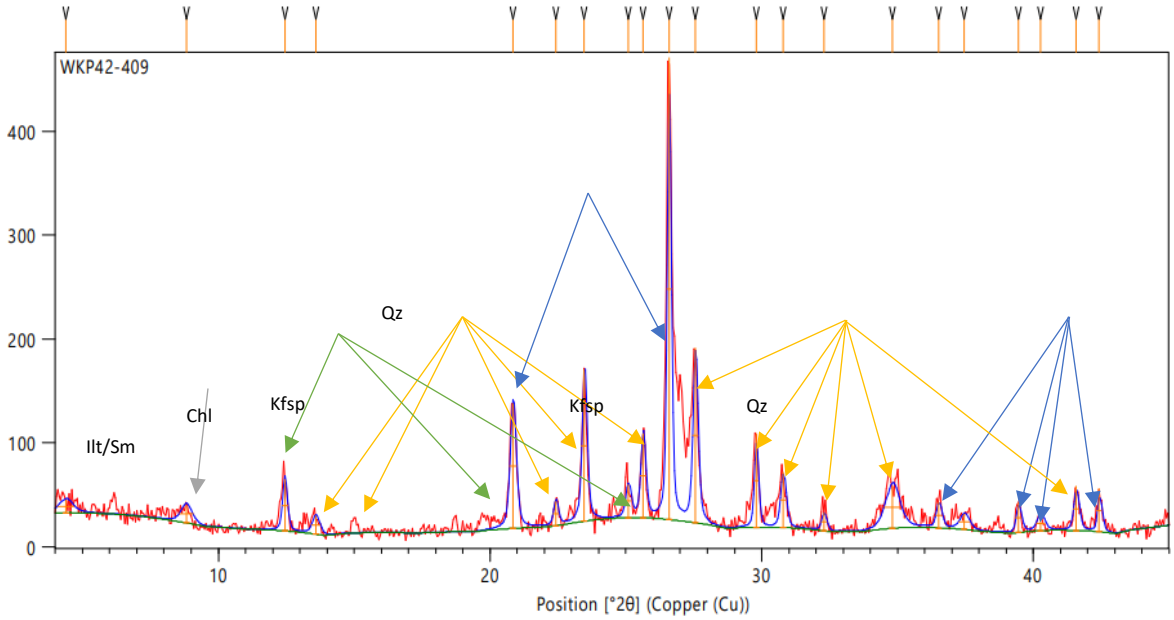

WKP42-409 <10µm Separate Glycolated

Not Analyzed

WKP42-412 <10µm Separate

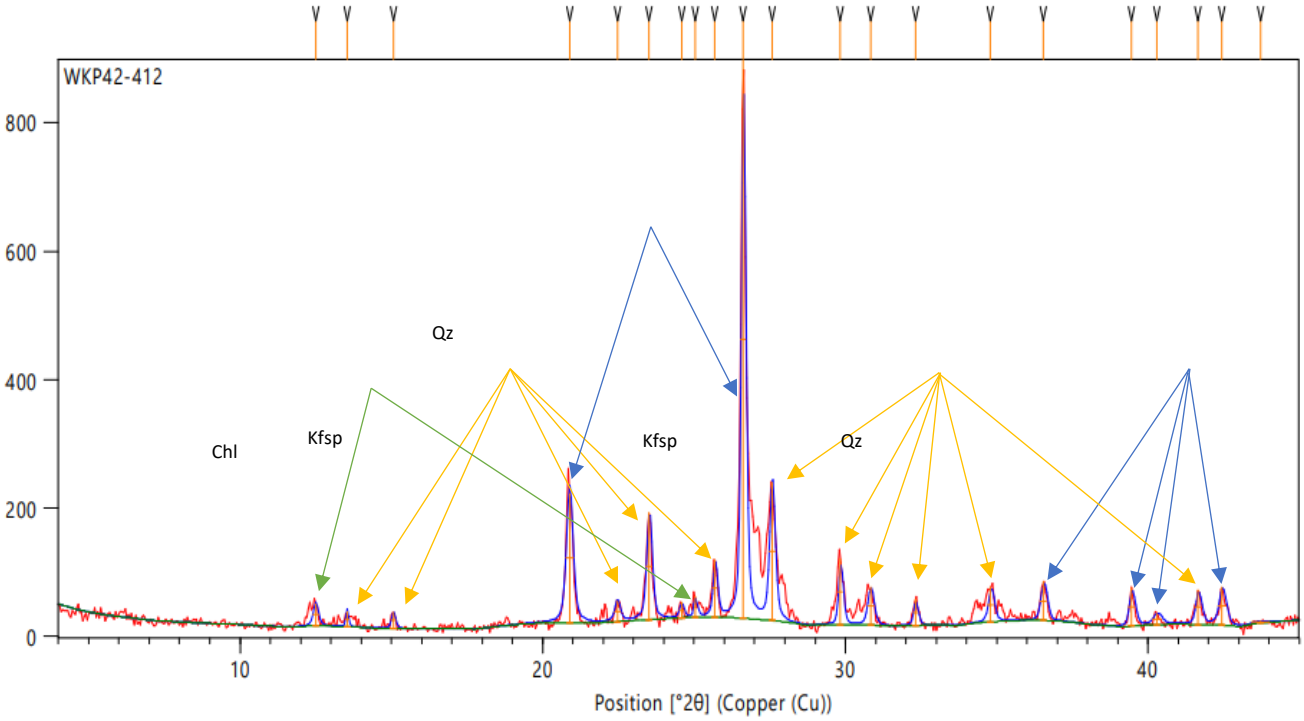

WKP42-412 <10µm Separate Glycolated

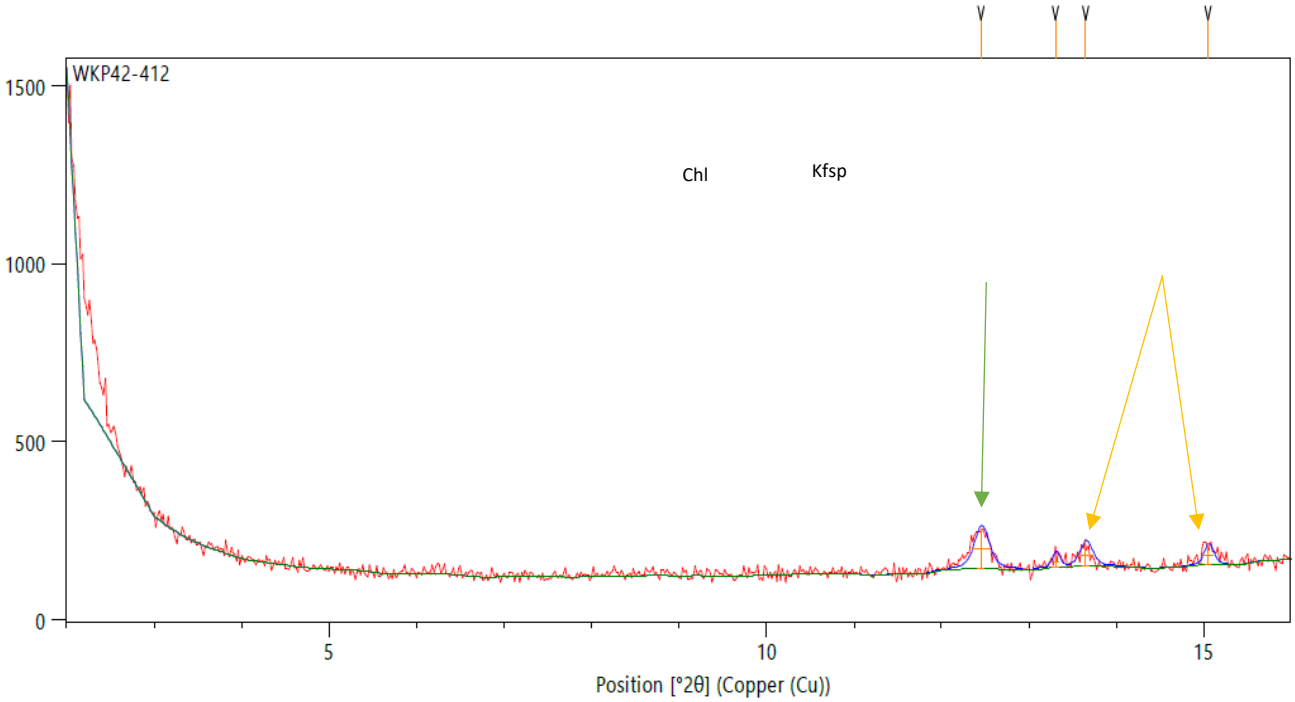

WKP42-422 <10µm Separate

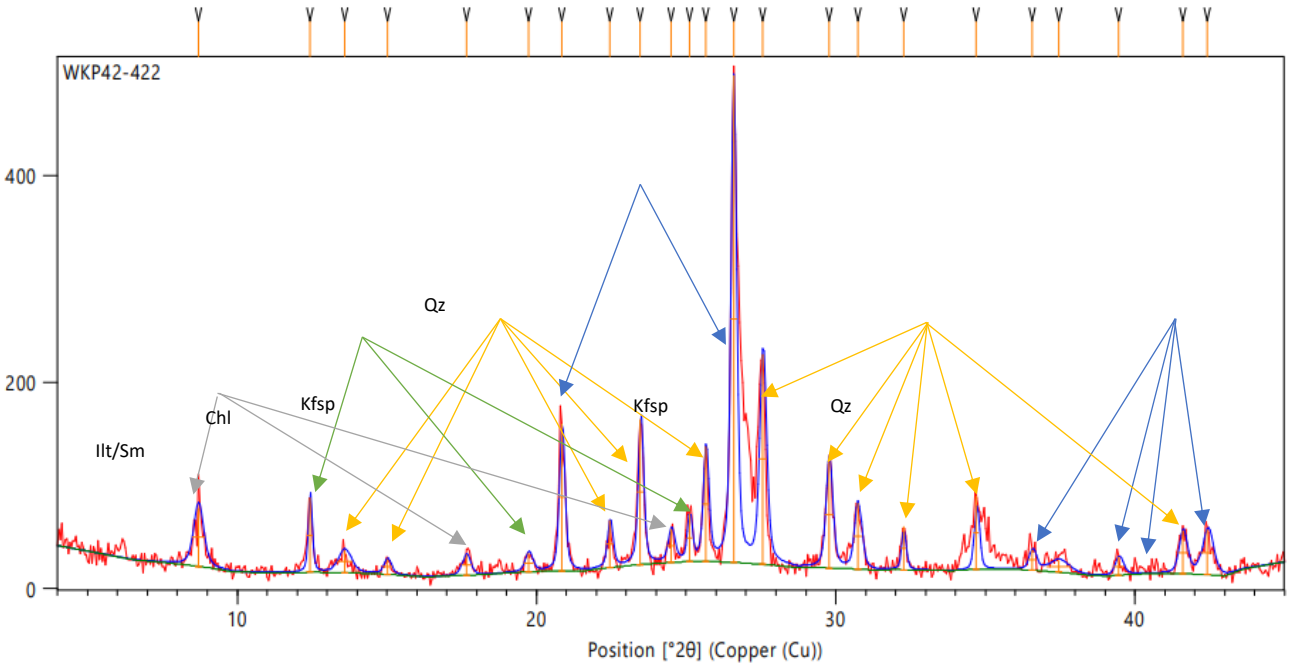

WKP42-422 <10µm Separate Glycolated

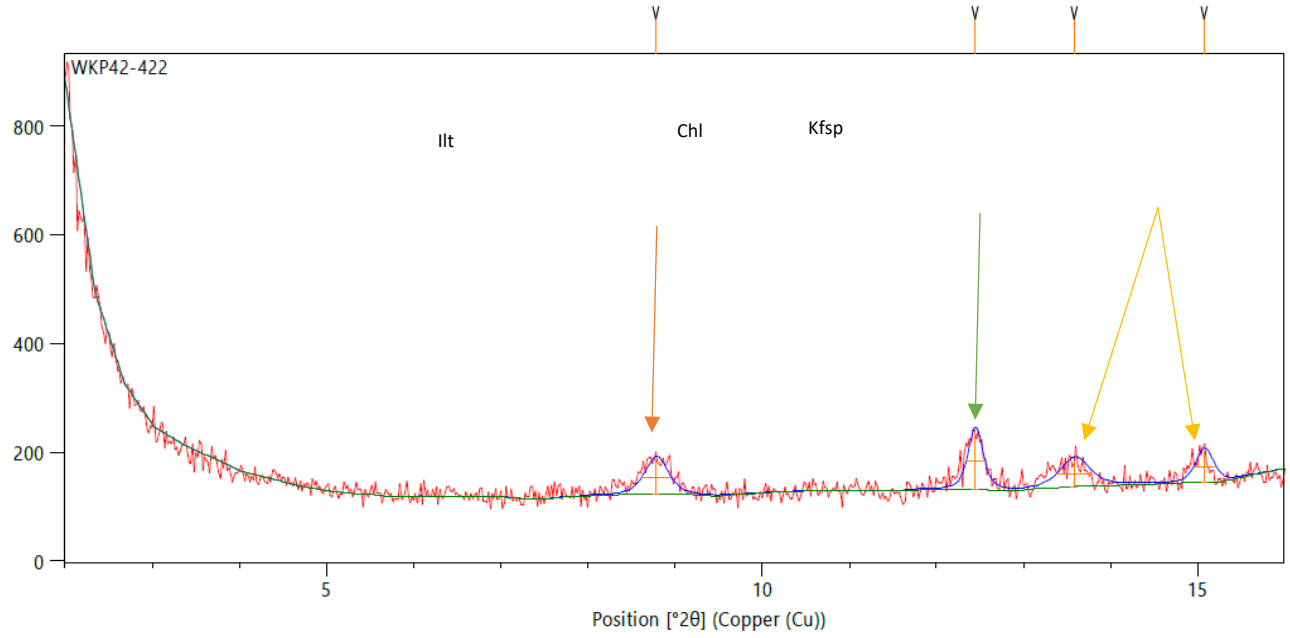

WKP42-435V <10µm Separate

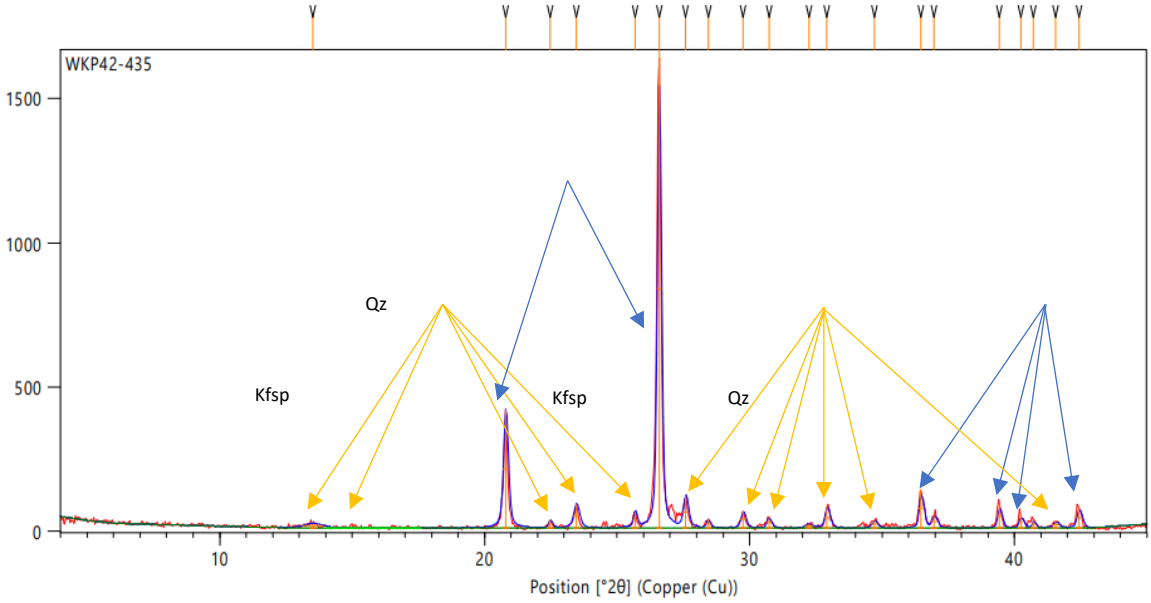

WKP42-435V <10µm Separate Glycolated

Not Analyzed

WKP42-573 <10µm Separate

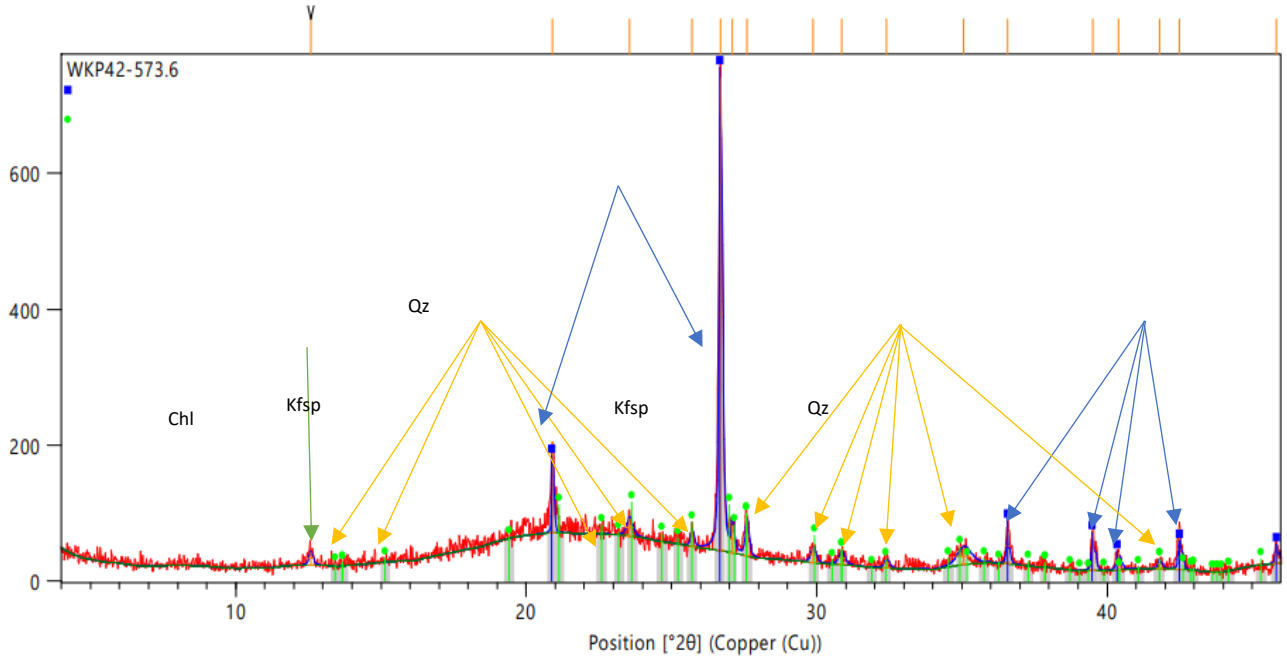

WKP42-573 <10µm Separate Glycolated

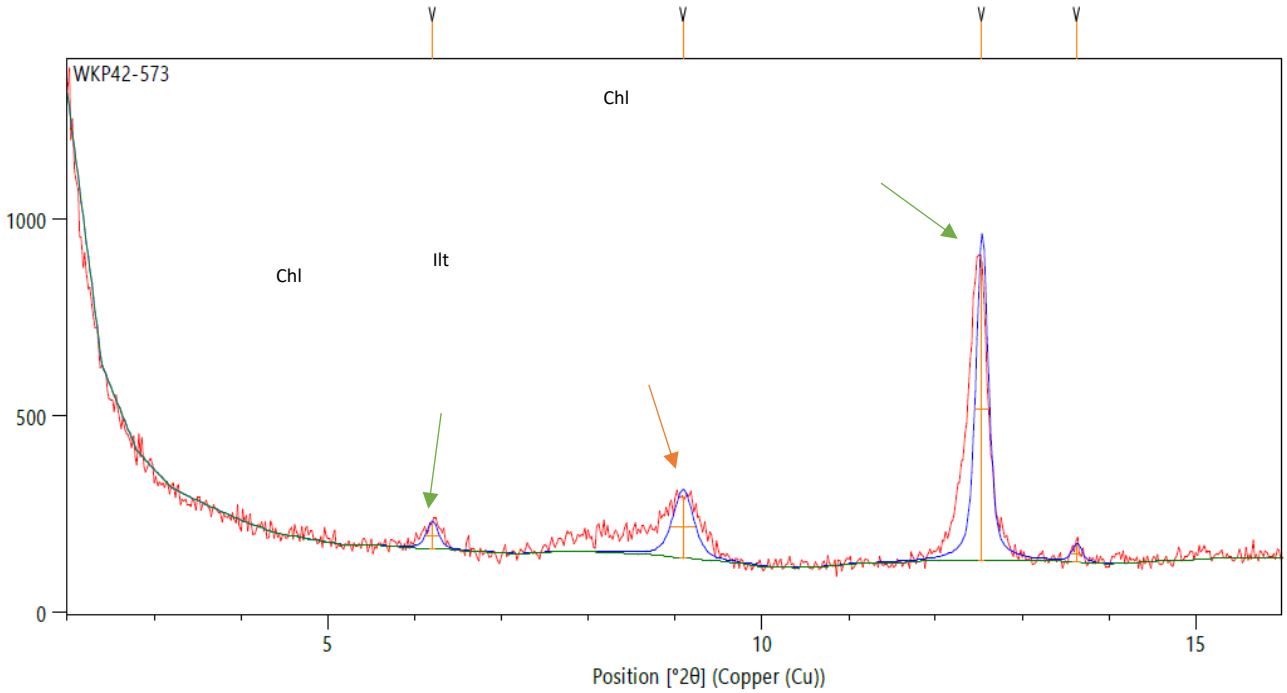

WKP78-358 <10µm Separate

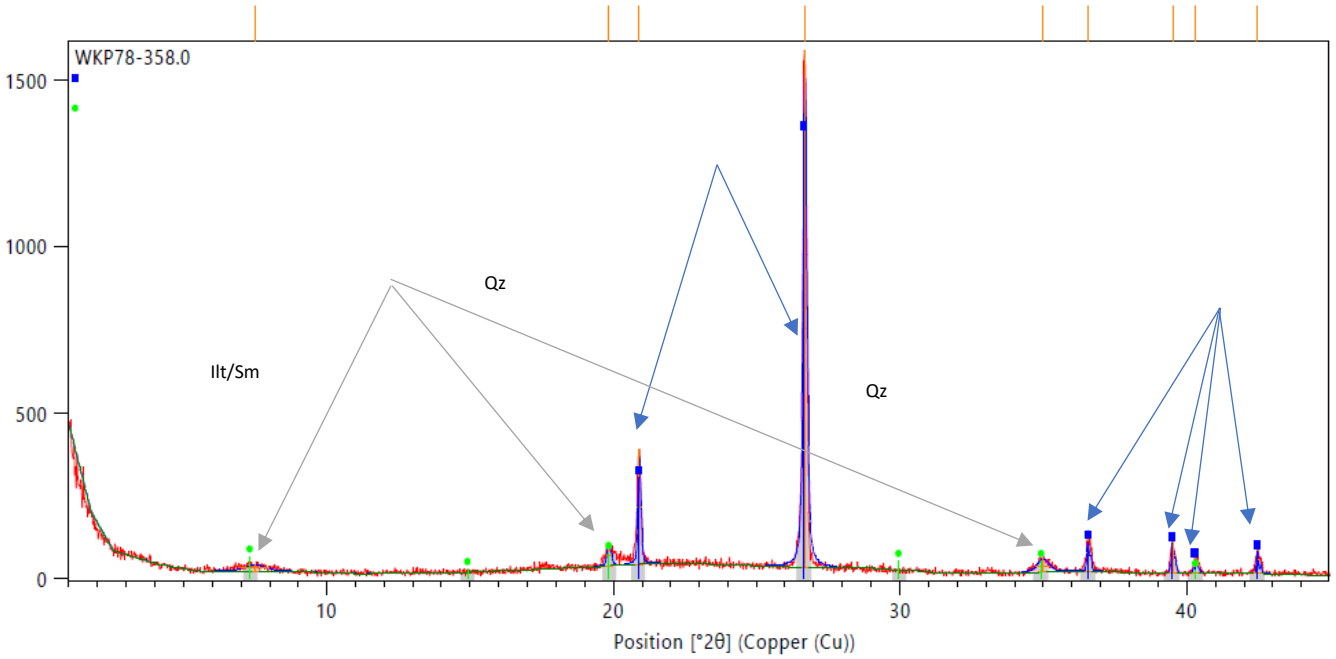

WKP78-372 <10µm Separate

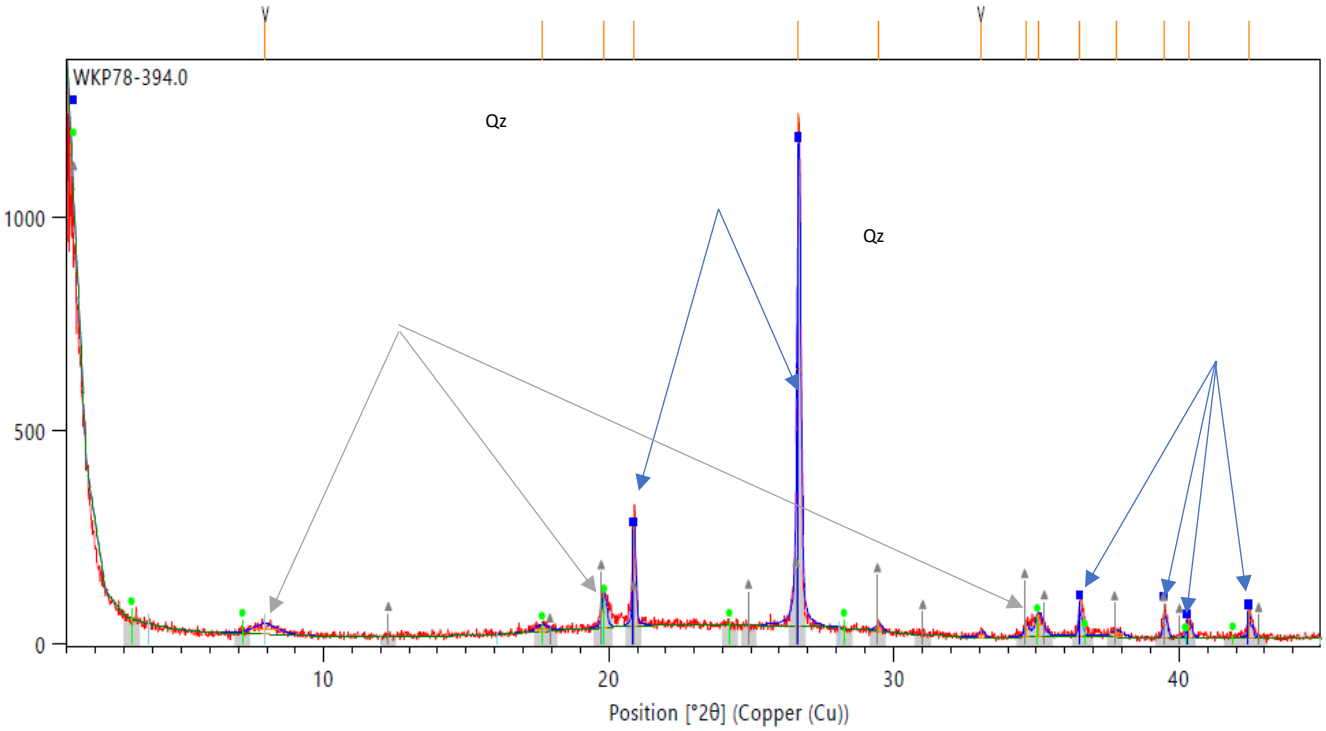

Table 10. Selected XRD results table from Simpson & Mauk, 2007. Summary of alteration minerals identified from whole rock and clay separate XRD analysis at the Favona deposit. Ab = albite, Ad = adularia, Ank = ankerite, Chl = chlorite, Chl-S = interlayered chlorite-smectite, Corren = corrensite, Crist = cristobalite, Cal = calcite, Haly = halloysite = I = illite, I-S = interlayered illite-smectite, K = kaolinite, Mt = magnetite, Plag = plagioclase, Py = pyrite, Q = quartz, Sid = siderite, Sm = smectite. [1]Depth in meters down hole. Depths in italics indicate samples with thin sections. [2]Interlayered clays, I0.9S is an interlayered illite-smectite with 90 percent illite

Drill	Depth[1]	Hydrothermal minerals													Igneous
hole	(m)	Q	Ad	Ab	Chl	Chl-Sm[2]	I	I-S[2]	Sm	K	Cal	Ank	Sid	Py	Plag
UW63	12.05	X						$I_{0.8}S$							
	36.05	X						$I_{0.85}S$						X	
	80.70	X	X					$I_{0.9}S$						?	
	101.80	X	X					$I_{0.9}S$						X	
	135.6	X	X				X							X	
	180.9	X	X		X		X								
	226.8	X	?		X			$I_{0.9}S$						X	
	62.10	X	X			Corren				X				X	
UW87	99.90	X						$I_{0.7}S$		X				X	
	149.10	X	X					$I_{0.8}S$						?	
	183.50	X						$I_{0.8}S$						X	
	211.00	X	X					$I_{0.85}S$						X	
	251.80	X	X				X							X	
	299.60	X					X							X	
	337.60	X	X		X			$I_{0.95}S$						X	
	379.30	X	X	?	X		X							X	?
	422.00	X	X	?	X		X							X	
UW104	103.40	Crist	X						X	X				X	
	128.60	X							X	X				X	
	160.30	X Crist	X						X	X				X	
	188.20	X	X					$I_{0.3}S$		X					
	222.80	X	?			Chl-Sm		$I_{0.6}S$						X	
	270.20	X	?					$I_{0.75}S$						X	
	312.30	X	?		?			$I_{0.9}S$						X	
	340.20	X	X	X	X		X							X	
	374.20	X	X		X		X							X	
	417.90	X	X				X							X	
	455.20	X	X		X		X								
UW69	194.00	X	X		X		X								
UW84	161.70	X						$I_{0.8}S$						X	
UW85	*85.70*	X	X					?						X	

Appendix E | Conference Abstracts

AMMONIUM MINERALS IN THE ALTERATION HALOS OF EPITHERMAL GOLD-SILVER DEPOSITS IN THE HAURAKI GOLDFIELD, NEW ZEALAND

N. Kieran Kristoffersen[1], Keiko Hattori[1], Mark P. Simpson[2]

[1] Dept. Earth and Env. Sciences, University of Ottawa, Ottawa, ON, Canada
[2] GNS Science-Wairakei Research Centre, 114 Karetoto Road-RD4, Taupo 3377, New Zealand

Ammonium has been detected in some epithermal Au-Ag deposits, including in Nevada, Japan, Argentina, Mexico, and New Zealand, using short-wave infrared (SWIR) spectrometry. When ammonium is present, it is concentrated around veins. This study examined the distribution and occurrence of ammonium in three epithermal low-sulfidation vein-type deposits in the Hauraki goldfield of New Zealand: Martha (>6.7Moz Au, >42.1Moz Ag), Favona (>0.6Moz Au, >2.36Moz Ag), and the recently discovered Wharekirauponga (WKP; 0.42Moz Au, 0.8Moz Ag) deposit. The Martha and Favona auriferous quartz-adularia veins are hosted by late Miocene to Pliocene andesite, whereas auriferous veins at WKP are hosted by late Miocene to Pliocene rhyolite. SWIR spectrometry identified ammonium at Favona and WKP but not at Martha. The wallrock is altered to form quartz, illite, mixed layer illite/smectite, adularia, chlorite, and pyrite. Kaolinite occurs at WKP. Ammonium contents are low in veins (<94 ppm) but are commonly high in the altered wallrocks. The wallrock ammonium values at Favona (<10,117 ppm) are much higher than at both Martha (<192 ppm) and WKP (<982 ppm). Leaching experiments using a 2N KCl solution shows that over 90% of ammonium is in mineral structures. Samples with high ammonium (>1,000 ppm) show significant absorption at 1980 nm and 2100 nm in the SWIR spectra, suggesting hydrous alteration minerals as the major host of ammonium. This is supported by a positive correlation of ammonium concentrations with LOI (0.6-16.3 wt%) and with K_2O (1.3-8.0 wt%), Buddingtonite (ammonium feldspar) was identified in a few samples at WKP. At Favona, SWIR identified a halo of ammonium minerals extending ~100m from veins which corresponds to a zone of high ammonium (990-10117 ppm). The footwall illite altered zone contains 990-4301 ppm ammonium. In the hanging wall, within 100 m of the mineralization in the mixed layer illite/smectite alteration zone, ammonium values range from 1827-10117 ppm. Outside of 100 m from the mineralization in the hanging wall, ammonium values range from 107-301 ppm with the smectite-bearing samples being the lowest (107 ppm). $\delta^{15}N$ values for all wallrock samples (n=54) range from +0.5 to +7.9 ‰, suggesting the derivation of nitrogen from the Jurassic greywacke basement or sediments intercalated with volcanic rocks.

Citation:

Kristoffersen, N.K., Hattori, K., Simpson, M.P. (2021). Ammonium Minerals in the Alteration Halos of Epithermal Gold-Silver Deposits in the Hauraki Goldfield, New Zealand. Geological Society of America Abstracts with Programs. Vol 53, No. 6, 2021. DOI: 10.1130/abs/2021AM-366994

AMMONIUM ASSOCIATED WITH THE FAVONA EPITHERMAL GOLD DEPOSIT IN THE COROMANDEL PENINSULA, NEW ZEALAND: ITS DISTRIBUTION AND SOURCE

N. Kieran Kristoffersen[1], Keiko Hattori[1], Mark P. Simpson[2]

[1] Dept. Earth and Env. Sciences, University of Ottawa, Ottawa, ON, Canada
[2] GNS Science-Wairakei Research Centre, 114 Karetoto Road-RD4, Taupo 3377, New Zealand

The Hauraki goldfield in the Coromandel peninsula hosts numerous epithermal low-sulfidation vein-type deposits including Martha (>6.7Moz Au, >42.1Moz Ag), Favona (>0.6Moz Au, >2.36Moz Ag) deposits, and the recently discovered Wharekirauponga (WKP; 0.42Moz Au of indicated and 0.72 Moz Au inferred resource) prospect. The gold deposits occur in extensively altered andesitic to rhyolitic volcanic rocks of late Miocene to Pliocene ages that overlie the basement of Jurassic metasedimentary rocks. Alteration formed adularia, illite, mixed-layered illite-smectite, chlorite, kaolinite, smectite, calcite and albite. Some deposits / prospects also have ammonium minerals based on short-wave infrared (SWIR) reflectance spectroscopy. This study determined the quantity of ammonium in rocks, its distribution, and host minerals, as well as investigated nitrogen isotope compositions to evaluate the source. Leaching experiment using a 2N KCl solution shows that over 90% of ammonium is in mineral structures. Ammonium concentrations show broad positive correlations with LOI (0.6-16.3 wt%), and K2O (1.3 to 8.0 wt%), suggesting it is hosted by hydrous K-bearing minerals. This is consistent with samples with high ammonium showing significant absorption of Al-OH in the SWIR spectra. At Favona, SWIR identified ammonium in wall rocks extending ~100m from veins, which contain ammonium (990-10117 ppm). The footwall illite altered zone contains 990-4301 ppm ammonium. In the hanging wall, within 100 m of the mineralization in the mixed layer illite/smectite alteration zone, ammonium values range from 1827-10117 ppm. Beyond this 100 m zone in the hanging wall, ammonium contents are low, 107-301 ppm, which are too low to be detected with SWIR. δ15N values range from +0.5 to +7.9 ‰(n=54), suggesting that nitrogen in ammonium is sourced / derived from either the metasedimentary basement or sediments intercalated with volcanic rocks.

Citation:

Kristoffersen, N.K., Hattori, K., Simpson, M.P. (2021). Ammonium associated with the Favona epithermal gold deposit in the Coromandel peninsula, New Zealand: its distribution and source. Society of Geology Applied to Mineral Deposits 16th Biennial Meeting Rotorua.